School of Civil and Mechanical Engineering

Investigation of the properties of geopolymers using ground ferronickel slag as a source material

Jhutan Chandra Kuri
0000-0002-6012-3219

This thesis is presented for the Degree of
Doctor of Philosophy
of
Curtin University

April 2022

DECLARATION

To the best of my knowledge and belief, this thesis contains no material previously published by any other person except where due acknowledgement has been made.

This thesis contains no material which has been accepted for the award of any other degree or diploma in any university**.**

Signature: (JHUTAN CHANDRA KURI)

Date: 06/07/2022

DEDICATION

To my beloved family

ACKNOWLEDGEMENTS

ABSTRACT

This study focused on the use of ground ferronickel slag (GFNS) as a precursor for geopolymer binder. A mixture of NaOH and Na_2SiO_3 liquids was used as an alkaline activator. Fly ash (FA) was replaced by 0, 25, 50, 75 and 100% GFNS to evaluate the effect of GFNS on the characteristics of geopolymer. The fresh, mechanical properties and durability performance of the geopolymer paste and mortar mixtures using GFNS were studied. Various microstructural investigations were conducted to interpret the effect of GFNS on the geopolymerisation process and properties of the reaction product. Based on the fresh, mechanical and durability test results, optimal level of ferronickel slag was recommended for manufacturing of geopolymers.

It was found that setting time and workability of fresh geopolymer paste decreased with the increase of GFNS content. Soundness test results showed expansion of geopolymer product well below the acceptable limit. Maximum compressive strength of the geopolymer mortar was achieved for 75% replacement of fly ash by GFNS. Microstructural analysis revealed the formation of amorphous sodium magnesium alumino-silicate hydrate (N-M-A-S-H) gel as a reaction product of FA-FNS based geopolymer.

It is important to investigate the interaction of GFNS binder with aggregates. Therefore, fresh, mechanical and durability properties of geopolymer mortar made with sand, different percentages of GFNS and fly ash were investigated. It was also found that workability of geopolymer mortar reduced with the increase of GFNS as a substitute of fly ash. The reduction of workability due to the increase of GFNS is ascribed to the angular shape and higher fineness of GFNS particles. For the same GFNS content, flow of mortar increased as the liquid content increased from 40% to 45%. The increase of workability is ascribed to the increase of water to binder ratio as the liquid content increased. Compressive strength of mortar was found to maximize at GFNS content of 75%. The 28-day and 90-day compressive strengths of geopolymer mortar using 40% alkaline liquid were 75 and 96 MPa, respectively. The use of GFNS decreased the porosity and sorptivity of the geopolymer mortar by providing denser structures due to the improvement of reaction mechanism.

The use of GFNS improved the resistance of geopolymer mortar against elevated temperature exposures. Geopolymer mortar having 50% GFNS showed maximum residual compressive strength at exposure to elevated temperature. The crystalline phases of the geopolymer did not change significantly until 600 °C. The number of crystalline peaks increased and amorphousity decreased significantly at 1000 °C. The N-M-A-S-H gel produced in fly ash-GFNS geopolymer provided a higher thermal stability than neat fly ash geopolymer. Besides, non-destructive ultrasonic results revealed that the lower frequency component dominates across all temperature exposures in the neat fly ash geopolymer mortar, which indicates the presence of more voids and cracks in the neat fly ash geopolymer than fly ash-GFNS geopolymer. Furthermore, it was found that geopolymer mortar containing 75% GFNS showed better acid and sulphate resistance than the neat fly ash geopolymer mortar. The N-M-A-S-H gel and lower calcium content of GFNS made the fly ash-GFNS blended geopolymer less susceptible in acid and sulphate solution than neat fly ash geopolymer.

Overall, the use of GFNS as a source material in geopolymer was found a promising option to produce green construction materials.

LIST OF PUBLISHED WORKS AND WORK PREPARED FOR PUBLICATION

Journal:

1. **Kuri, J. C.**, Khan, M. N. N., & Sarker, P. K. (2021). Fresh and hardened properties of geopolymer binder using ground high magnesium ferronickel slag with fly ash. *Construction and Building Materials*, 272, 121877, https://doi.org/10.1016/j.conbuildmat.2020.121877.

2. **Kuri, J. C.**, Khan, M. N. N., & Sarker, P. K. (2020). Workability, strength and microstructural properties of ground ferronickel slag blended fly ash geopolymer mortar. *Journal of Sustainable Cement-Based Materials*, https://doi.org/10.1080/21650373.2020.1823905.

3. **Kuri, J. C.**, Majhi, S., Sarker, P. K., & Mukherjee, A. (2021). Microstructural and non-destructive investigation of the effect of high temperature exposure on ground ferronickel slag blended fly ash geopolymer mortars. *Journal of Building Engineering*, 43, 103099, https://doi.org/10.1016/j.jobe.2021.103099.

4. **Kuri, J. C.**, Shaikh, F. U. A., & Sarker, P. K. (2021). Sulphuric acid resistance of ground ferronickel slag blended fly ash geopolymer mortar. *Construction and Building Materials, 313, 125505,* https://doi.org/10.1016/j.conbuildmat.2021.125505.

5. **Kuri, J. C.**, Nuruzzaman, M., & Sarker, P. K. (2022). Sulphate resistance of geopolymer mortar produced using ground ferronickel slag with fly ash. *Structural Concrete* (*under review*).

6. **Kuri, J. C.**, & Sarker, P. K. (2022). Effects of alkali activator and ground ferronickel slag on the workability and strength of fly ash geopolymer mortar. *Concrete in Australia, 48(1), 40-45*.

Conference:

1. **Kuri, J. C.**, Khan, M. N. N., & Sarker, P. K. (2020). Compressive strength of geopolymer mortar using ground ferronickel slag and fly ash. Third European and Mediterranean Structural Engineering and Construction Conference, EURO-MED-SEC-3, Limassol, Cyprus, August 3-8, 2020, *Proceedings of International Structural Engineering and Construction,* 7(1), MAT-05, https://doi.org/10.14455/isec.res.2020.7(1).mat-05.

TABLE OF CONTENTS

ix

LIST OF FIGURES

LIST OF TABLES

LIST OF ABBREVIATIONS

ACI	American Concrete Institute
AS	Australian Standards
ASTM	American Society for Testing and Materials
C-A-S-H	Calcium aluminosilicate hydrate
EDS/EDX	Energy Dispersive X-ray Spectroscopy
ICDD	International Centre for Diffraction Data
FA	Fly Ash
FNS	Ferronickel slag
GFNS	Ground ferronickel slag
GGBFS	Ground Granulated Blast Furnace Slag
LOI	Loss on Ignition
M-A-S-H	Magnesium aluminosilicate hydrate
N-A-S-H	Sodium aluminosilicate hydrate
N-M-A-S-H	Sodium magnesium aluminosilicate hydrate
OPC	Ordinary Portland Cement
PDF	Powder Diffraction File
QXRD	Quantitative X-Ray Diffraction
RH	Relative Humidity
SCM	Supplementary Cementitious Materials
SEM	Scanning Electron Microscopy
SH	Sodium Hydroxide (NaOH)
SS	Sodium Silicate (Na_2SiO_3)
SSD	Saturated Surface Dry
TGA	Thermogravimetric Analysis
UPV	Ultrasonic Pulse Velocity
VPV	Volume of Permeable Voids
XRD	X-Ray Diffraction
XRF	X-Ray Florescence

CHAPTER 1: INTRODUCTION

1.1 Background

Concrete is one of the most widely used building materials in the world. Usually cement is used as the binding material for conventional concrete production. Due to the high demand of cement, the annual world cement production is predicted to increase from around 2540 million tonnes in 2006 to between 3680 million tonnes and 4380 million tonnes in 2050, as shown in Fig. 1.1 [1, 2]. On the other hand, the production of Portland cement is considered as a very energy intensive as well as greenhouse gas emitting material due to the limestone decomposition and flaming of fossil fuels during its manufacturing process [3-5]. A significant quantity of CO_2 is released to the environment in the manufacturing process of the cement. Approximately 5-7% of the global anthropogenic CO_2 emission is caused by the cement industry [6, 7]. One ton of CO_2 is emitted for the production of one ton of cement. In addition, around 105 kWh electricity and about 60 to 130 kg fuel oil or its equivalent is required for the production of one ton of cement [3, 8].
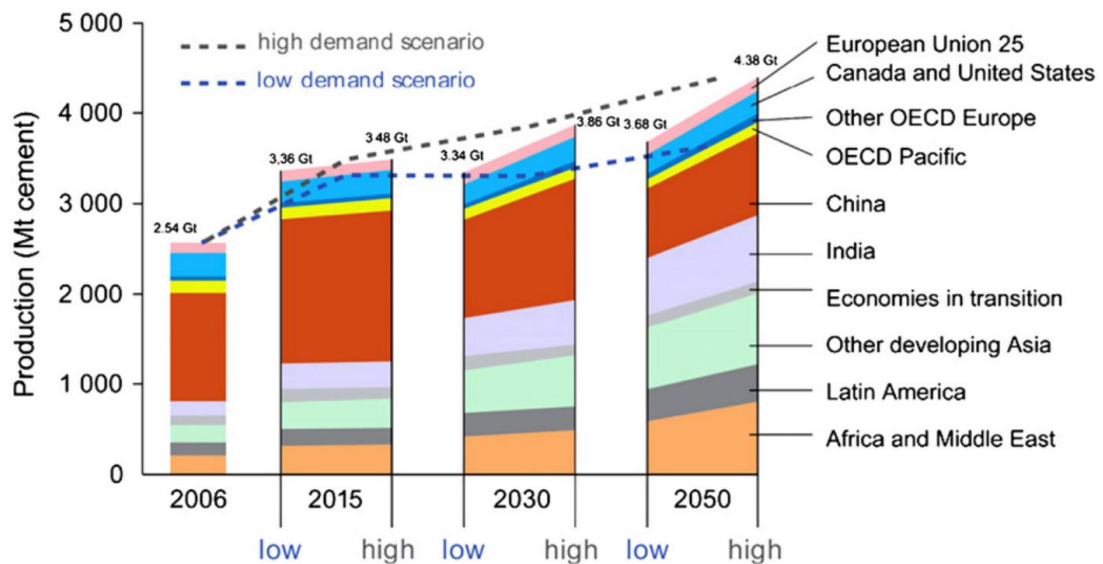
Fig. 1.1 Annual world cement production [1, 2]. Note: OECD = Organization for Economic Co-operation and Development

Therefore, the investigation of alternative binders to cement is one of the primary fields of research concerning energy and greenhouse gas emission for the manufacturing of Portland cement. In this connection, geopolymer is an alternate binder that utilizes industrial by-products as a replacement for cement. Geopolymers are inorganic polymers where a heterogeneous chemical reaction takes place between alkali metal silicate solutions and aluminosilicate solid materials under very alkaline conditions [9-11]. Geopolymers are manufactured from the reaction of a variety of aluminosilicate source materials which comprises industrial by-products such as ground granulated blast furnace slag (GGBFS) and fly ash, which are generous in Aluminium (Al) and Silicon (Si). The general formula to express the chemical constitution of geopolymer is $M_n[-(SiO_2)_z-AlO_2]_n.wH_2O$, where M is the cations of alkali, n is polymerization degree, and z is Si/Al ratio [12, 13]. The formation of geopolymers can be shown by the following schematic reactions [14, 15]:

$$(Si_2O_5, Al_2O_2)_n + nSiO_2 + 4nH_2O \xrightarrow{\text{NaOH or KOH}} n(OH)_3 - Si - O - Al^{(-)} - (OH)_3$$
$$|$$
$$(OH)_2$$

$$n(OH)_3 - Si - O - Al^{(-)} - (OH)_3 \xrightarrow{\text{NaOH or KOH}} (Na, K) - (- Si - O - Al^{(-)} - O - Si - O -)_n + 4nH_2O$$
$$|$$
$$(OH)_2$$

Ortho(sialate-siloxo)   (Na, K)-poly(sialate-siloxo)
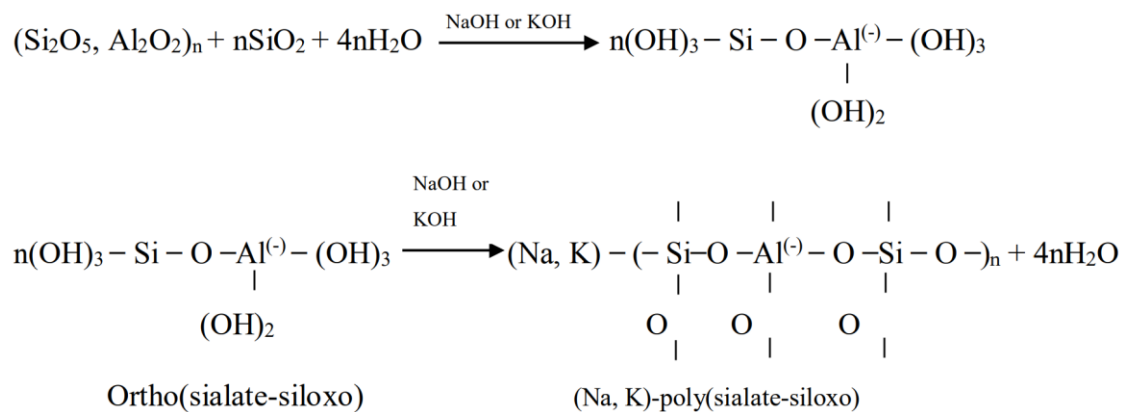
The geopolymerization mechanism follows four stages: a) dissolution of silicon and aluminum from the rigid aluminosilicate materials, b) formation of Si-O-Si or/and Si-O-Al oligomers species, c) polycondensation of the oligomers, and d) bonding of the undissolved solid molecules to get the final solid polymeric structure; although it is very difficult to isolate each stage separately [9, 16]. Duxson et al. [17] presented these stages in a conceptual model as given in Fig. 1.2.
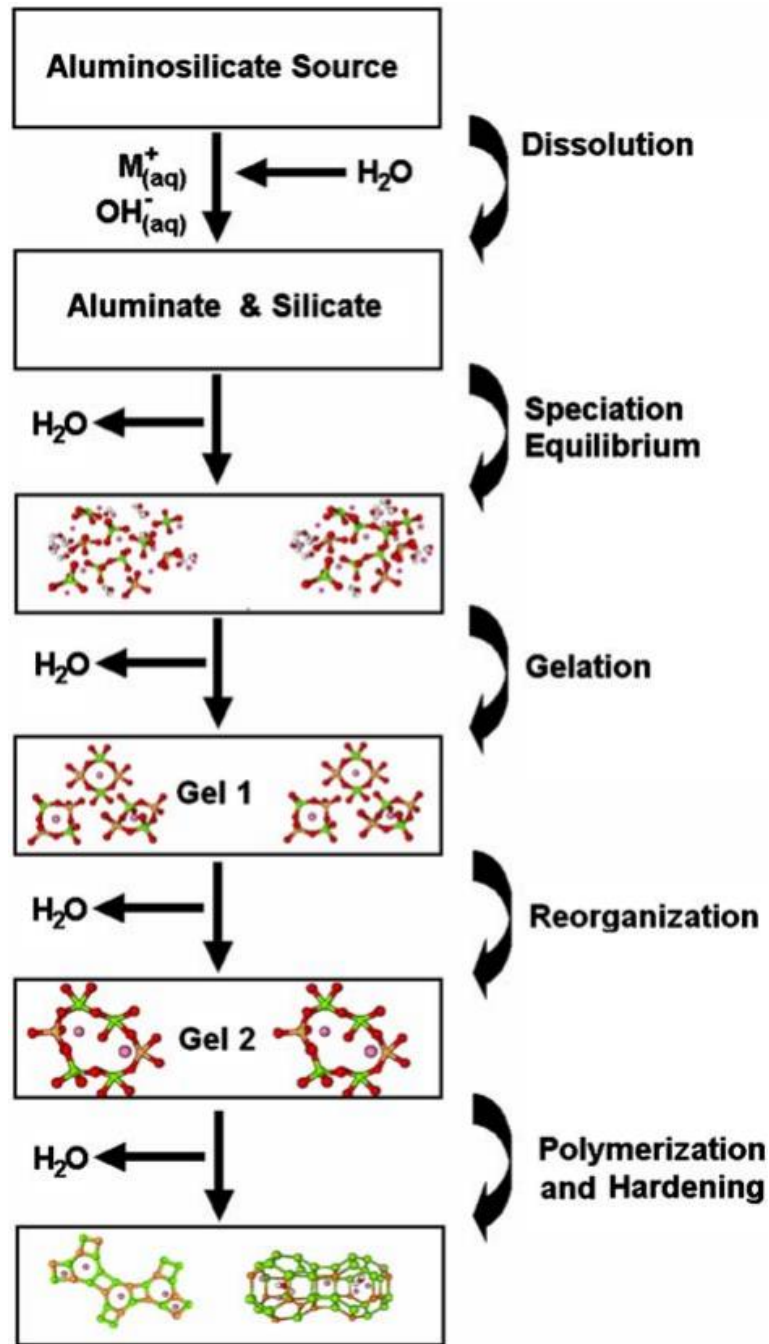
Fig. 1.2 Conceptual model of geopolymerisation process [17]

Ferronickel slag (FNS) is an industrial residue discharged during the manufacturing of ferronickel alloys [18-20]. Principle constituents of FNS are SiO_2, FeO, and MgO, which are present in crystalline and non-crystalline mineral form [21-23]. As FNS has a notable proportion of amorphous silica [24-26], ground FNS (GFNS) has shown reactivity when utilized with an alkaline solution in geopolymers [9, 12]. In this study, FNS was collected from the smelting of garnierite ores of New Caledonia. The aim of

the study is to investigate the properties of geopolymers using ground ferronickel slag as a precursor. Finely ground FNS was used with fly ash to produce geopolymer.

1.2 Research objectives

The main objective of the study is to investigate the behavior of geopolymers using ground ferronickel slag as a precursor. The following points describe the sub objectives to achieve the main objective:

- Evaluate the physical, chemical and microstructural characteristics of ground ferronickel slag as a source material for geopolymer binder.
- Assess the fresh properties, hardened properties and durability performance of the geopolymer pastes and mortars incorporating GFNS.
- Investigate the microstructural properties of geopolymer binder by using different advanced techniques such as QXRD, SEM, EDS and TGA in order to explain the strength development and properties observed in large specimens.

1.3 Research significance

It has been known from recent studies that geopolymers have promising mechanical, chemical and physical properties in with good durability performance in terms of porosity, water absorption, permeability and shrinkage and resistance to fire and other aggressive chemicals [27-29]. The properties of geopolymer are comparable to the properties of ordinary Portland cement (OPC) binders. Besides, the manufacturing of geopolymer needs lower amount of energy as well as it utilizes industrial by-products. Therefore, geopolymer not only can decrease the carbon footprints, but also it can contribute to lower the pollution of environment by utilizing industrial by-products.

Utilization of industrial by-products has become one of the major subjects of interest among the scientific community and the industry owners. Safe disposal of these by-products is a matter of great concern. Disposal of these industrial by-products needs a huge volume of land and energy. As discussed earlier, FNS is an industrial by-product of ferronickel production process. This study was conducted using ferronickel slag of the garnierite ores produced by Société Le Nickel (SLN) New Caledonia, which is one of the world's largest nickel producers. The ore is smelted at the temperature range of

1500 °C to 1600 °C and a water cooling method is used to granulate the molten slag. For the manufacturing of one ton of ferronickel alloy, around 14 tonnes of slag is produced as a by-product. At the present time, over 25 million tonnes of FNS is staked in that site [30]. Therefore, utilization of GFNS as a binder in the construction field will benefit the environment and ease the safe disposal of the by-product. Consequently, the utilization of this material in geopolymer will give numerous economic, environmental and technical advantages.

1.4 Thesis structure

The thesis is organised in eight chapters as outlined below:

Chapter 1 presents the background, research objectives and significance of the study.

Chapter 2 entitled "Literature Review" provides the past study of the use of ferronickel slag as construction materials.

Chapter 3 describes the synthesis of geopolymer binder using GFNS with fly ash. Fresh and hardened properties of geopolymer paste were investigated at varying SS/SH ratio and curing conditions.

Chapter 4 presents the fresh, mechanical and durability properties of geopolymer mortar made with sand, different percentages of GFNS and fly ash.

Chapter 5 discusses the thermal resistance of geopolymer mortar produced from GFNS and fly ash.

Chapter 6 presents the sulphuric acid resistance of GFNS blended fly ash geopolymer mortar.

Chapter 7 describes the durability of geopolymer mortar made from GFNS and fly ash after exposure to the 5% sodium sulphate solution for up to 1.5 years.

Chapter 8 presents the conclusions of this research and recommendations for future studies.

1.5 References

[1]   A. Hasanbeigi, L. Price, E. Lin, Emerging energy-efficiency and CO_2 emission reduction technologies for cement and concrete production: A technical review, Renew. Sust. Energ. Rev. 16 (2012) 6220-6238.

[2]   World Business Council for Sustainable Development (WBCSD)/International Energy Agency (IEA), Cement roadmap targets, 2009. Available from: /www.iea. org/papers/2009/Cement_Roadmap_targets_viewing.pdfS.

[3]   N. Lemonis, P.E. Tsakiridis, N.S. Katsiotis, S. Antiohos, D. Papageorgiou, M.S. Katsiotis, M. Beazi-Katsioti, Hydration study of ternary blended cements containing ferronickel slag and natural pozzolan, Constr. Build. Mater. 81 (2015) 130–139.

[4]   A. Wongsa, A. Wongkvanklom, D. Tanangteerapong, P. Chindaprasirt, Comparative study of fire-resistant behaviors of high-calcium fly ash geopolymer mortar containing zeolite and mullite, J. Sustain. Cem. Mater. 9 (2020) 307-321.

[5]   M. Khalifeh, A. Saasen, T. Vrålstad, H.B. Larsen, H. Hodne, Experimental study on the synthesis and characterization of aplite rock-based geopolymers, J. Sustain. Cem. Mater. 5 (2016) 233-246.

[6]   E. Benhelal, G. Zahedi, E. Shamsaei, A. Bahadori, Global strategies and potentials to curb CO_2 emissions in cement industry, J. Clean. Prod. 51 (2013) 142-161.

[7]   World Business Council for Sustainable Development (WBCSD)/International Energy Agency (IEA). Cement Technology Roadmap 2009—Carbon emissions reductions up to 2050, 2009.
Available from: /www.iea.org/papers/2009/Cement_Roadmap.pdfS.

[8]   P.K. Mehta, P.J.M. Monteiro, Concrete microstructure, properties, and materials, 3rd ed., New York: McGraw-Hill, 2006.

[9]   I. Maragkos, I.P. Giannopoulou, D. Panias, Synthesis of ferronickel slag based geopolymers, Minerals Eng. 22 (2009) 196–203.

[10]   P. Zhang, K. Wang, Q. Li, J. Wang, Y. Ling, Fabrication and engineering properties of concretes based on geopolymers/alkali-activated binders – A review, J. Clean. Prod. 258 (2020), 120896.

[11]   Z. Zhang, H. Wang, J.L. Provis, Quantitative study of the reactivity of fly ash in geopolymerization by FTIR, J. Sustain. Cem. Mater. 1(2012) 154–166.

[12] Z. Zhang, Y. Zhu, T. Yang, L. Li, H. Zhu, H. Wang, Conversion of local industrial wastes into greener cement through geopolymer technology: a case study of high magnesium nickel slag, J. Clean. Prod. 141 (2017) 463–471.

[13] E. Alvarez-Ayuso, X. Querol, F. Plana, A. Alastuey, N. Moreno, M. Izquierdo, O. Font, T. Moreno, S. Diez, E.Vazquez, M. Barra, Environmental, physical and structural characterisation of geopolymer matrixes synthesised from coal (co-)combustion fly ashes. J. Hazard. Mater. 154 (2008) 175–183.

[14] J.G.S. van Jaarsveld, J.S.J. van Deventer, L. Lorenzen, The potential use of geopolymeric materials to immobilise toxic metals: Part I. Theory and applications, Miner. Eng. 10 (1997) 659-669.

[15] J. Davidovits, Geopolymers and geopolymeric materials, Journal of Thermal Analysis, 35 (1989) 429-441.

[16] D. Panias, I. Giannopoulou, The geopolymerization technology for the utilization of mining and metallurgical solid wastes. In: GDMB (Ed.), Proceedings of the European Metallurgical Conference EMC, 2007, vol. 2, Düsseldorf, Germany, June 11–14, pp. 625–640.

[17] P. Duxson, A. Fernández-Jiménez, J.L. Provis, G.C. Lukey, A. Palomo, J.S.J. van Deventer, Geopolymer technology: the current state of the art. J. Mater. Sci. 42 (2007) 2917–2933.

[18] M. Bouasria, L. Babouri, F. Khadraoui, D. Chateigner, S. Gascoin, V. Pralong, M. Benzaama, B. Orberger, Y.E. Mendili, Insight into the partial replacement of cement by ferronickel slags from New Caledonia, Eur. J. Environ. Civ. Eng. (2020), https://doi.org/10.1080/19648189.2020.1814421.

[19] Y.C. Choi, S. Choi, Alkali-silica reactivity of cementitious materials using ferro- nickel slag fine aggregates produced in different cooling conditions, Constr. Build. Mater. 99 (2015) 279–287.

[20] A.K. Saha, M.N.N. Khan, P.K. Sarker, Value added utilization of by-product electric furnace ferronickel slag as construction materials: a review, Resour. Conserv. Recycl. 134 (2018) 10–24.

[21] Y. Huang, Q. Wang, M. Shi, Characteristics and reactivity of ferronickel slag powder, Constr. Build. Mater. 156 (2017) 773–789.

[22] D. Wang, Q. Wang, S. Zhuang, J. Yang, Evaluation of alkali-activated blast furnace ferronickel slag as a cementitious material: reaction mechanism,

engineering properties and leaching behaviors, Constr. Build. Mater. 188 (2018) 860–873.

[23] Q. Wu, S. Wang, T. Yang, H. Zhu, S. Li, Effect of high-magnesium nickel slag on hydration characteristics of Portland cement, J. Mater. Civ. Eng. 31 (2019), 04019051.

[24] A.K. Saha, P.K. Sarker, Mechanical properties of concrete using ferronickel slag and fine aggregate and supplementary cementitious material, Concr. Australia. 44 (2018) 40–44.

[25] H. Kim, C.H. Lee, K.Y. Ann, Feasibility of ferronickel slag powder for cementitious binder in concrete mix, Constr. Build. Mater. 207 (2019) 693–705.

[26] Y. Chen, T. Ji, Z. Yang, W. Zhan, Y. Zhang, Sustainable use of ferronickel slag in cementitious composites and the effect on chloride penetration resistance. Constr. Build. Mater. 240 (2020) 117969.

[27] A. Fernández-Jiménez, J.G. Palomo, F. Puertas, Alkali-activated slag mortars mechanical strength behaviour, Cem. Concr. Res. 33 (1999) 1313–1321.

[28] P. Duan, C. Yan, W. Zhou, D. Ren, Fresh properties, compressive strength and microstructure of fly ash geopolymer paste blended with iron ore tailing under thermal cycle, Constr. Build. Mater. 118 (2016) 76–88.

[29] M. Vafaei, A. Allahverdi, Durability of geopolymer mortar based on waste-glass powder and calcium aluminate cement in acid solutions, J. Mater. Civ. Eng. 29 (2017) 04017196.

[30] A.K. Saha, P.K. Sarker, Sustainable use of ferronickel slag fine aggregate and fly ash in structural concrete: mechanical properties and leaching study, J. Clean. Prod. 162 (2017) 438–448.

CHAPTER 2: LITERATURE REVIEW

2.1 Overview

Though every chapter contained detailed literature review on the specific studies, this chapter reviews the use of ferronickel slag as a construction material. The production process and properties of ferronickel slag are discussed on the basis of existing literature. Besides, previous findings of the use of granulated ferronickel slag as aggregates and use of ground ferronickel slag as SCMs in OPC or source materials in geopolymer are discussed.

2.2 Ferronickel Slag

Ferronickel slag (FNS) is a by-product which is discharged in the refinement process of ferronickel alloys from nickel ores, as shown in Fig. 2.1 [1]. Based on cooling speed, two types of ferronickel slag are available. One of them is air-cooled FNS, which looks gray and lumpy after cooling. Another type is water-cooled FNS, which is a sphere-like shape and looks dark after cooling, as shown in Fig. 2.2 [2, 3].

(a)
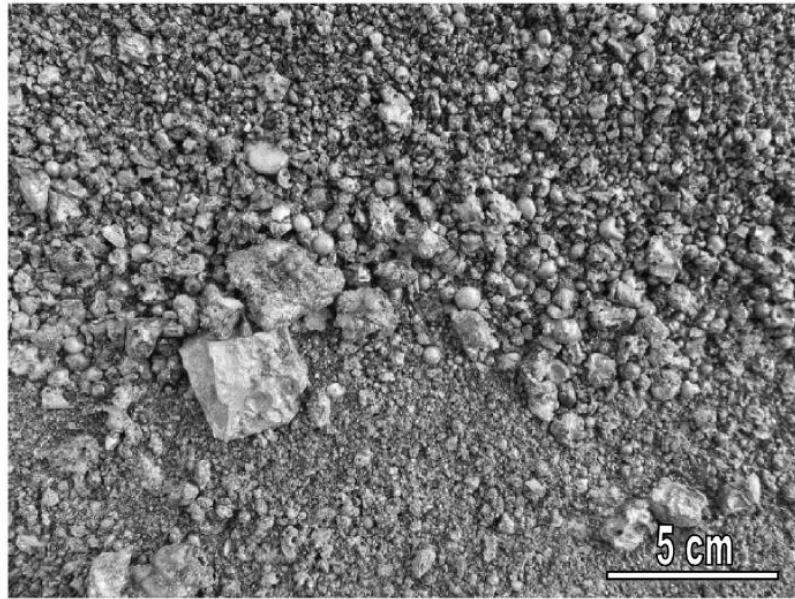
(b)

Fig. 2.1 Ferronickel slag: (a) Far view of stockpiled ferronickel slag, (b) Close view [1].
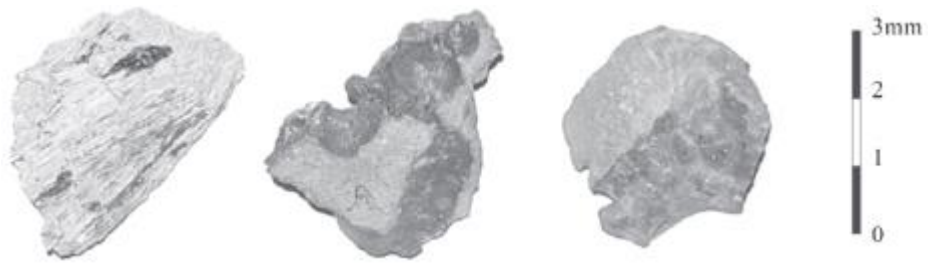
(a)
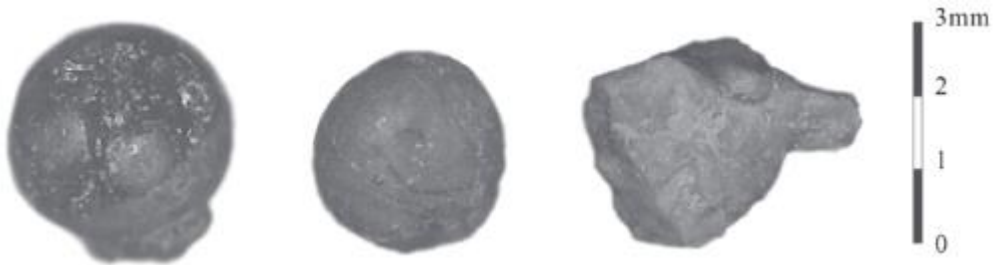
(b)

Fig. 2.2 Optical microscopy of (a) Air-cooled FNS, (b) Water-cooled FNS [2].

Table 2.1 Physical properties of ferronickel slag [4]

	Specific gravity (g/cm^3)	Water absorption (%)
A-FNS [2]	3.11	1.64
W-FNS [2]	2.81	0.71
W-FNS [5]	2.85	0.42
A-FNS [6]	2.93	1.87
W-FNS [6]	3.08	0.13
W-FNS [7]	2.84	1.98
W-FNS [8]	2.97	1.20
A-FNS [9]	3.02	2.20
W-FNS [9]	2.84	0.73

Note: A-FNS = air-cooled ferronickel slag, W-FNS = water cooled ferronickel slag

The physical properties and chemical constituents of FNS highly depend on the source of ore and the smelting process and cooling methods. Table 2.1 shows the physical properties of FNS obtained from different sources. It can be noticed that in general air-cooled ferronickel slag showed higher specific gravity and water absorption compared to water-cooled ferronickel slag [2, 9].

Table 2.2 shows the chemical compositions of FNS obtained from different sources. It can be seen that principal constituents of FNS are SiO_2, Fe_2O_3, and MgO. In general, ferronickel slag from laterite ore contained high proportions of Fe_2O_3 and low proportions of MgO. On the other hand, the ferronickel slag generated from garnierite ore contained high amounts of MgO and low amount of Fe_2O_3 [2, 9].

Table 2.2 Chemical constituents of ferronickel slag [4]

	A-FNS [6]	W-FNS [6]	W-FNS [10-12]	W-FNS [13]	W-FNS [14]	A-FNS [2]	W-FNS [2]	W-FNS [15-17]	FNS [18]
SiO_2	55.6	52.7	32.74	40.29	41.18	62.80	58.1	53.29	19.8
Al_2O_3	--	--	8.32	10.11	5.98	1.95	2.29	2.67	12.25
Fe_2O_3	7.57	6.70	43.83	37.69	40.02	7.13	11.10	11.9	17.62
MgO	27.8	34.0	2.76	5.43	7.79	24.70	26.50	31.6	9.66
SO_3	0.06	0.04	0.18	--	0.64	0.03	0.04	--	0.87
CaO	5.18	2.30	3.73	3.65	4.12	2.07	0.29	0.42	4.48
Na_2O	--	--	--	--	0.09	0.13	0.09	0.11	0.33
K_2O	--	--	--	--	0.37	0.02	0.06	--	0.04
Cr_2O_3	--	--	3.07	2.58	2.75	--	--	1.08	2.48
NiO	--	--	0.1	0.09	0.13	--	--	0.1	0.30
Co_3O_4	--	--	0.02	--	0.02	--	--	0.01	0.14
LOI^a	--	--	--	--	--	0.94	1.24	0.83	--
Types of ores	--	--	Laterites	Laterites	Laterites	--	--	Garnierite	--
Source	Japan	Japan	LARCO Greece	LARCO Greece	LARCO Greece	SNNC, South Korea	SNNC, South Korea	SLN New Caledonia	--

Fig. 2.3 Ground ferronickel slag (GFNS) [19].

Fig. 2.3 shows the photograph of ferronickel slag after grinding. As ferronickel has a notable proportion of amorphous silica, ground ferronickel slag (GFNS) showed reactivity when utilized with conventional cement as a supplementary cementitious material [14, 20-22] or with an alkaline liquid as a precursor [23-25] to produce geopolymers.

2.3 Use of ferronickel slag as aggregate

The physical characteristics of FNS are suitable for utilization as aggregate in concrete. Several investigations were carried out regarding utilization of FNS as an aggregate. Togawa et al. [9] investigated the features of bleeding, water tightness and freeze-thaw resistance of concrete with ferronickel slag fine aggregate. The authors found that the incorporations of limestone powder, blast furnace slag and silica fume noticeably enhanced the bleeding and the compressive strength of ferronickel slag concrete. The authors recommended that the utilization of limestone powder can

enhance the freeze-thaw resistance of FNS concrete. It was noticed that the water tightness of ferronickel slag concretes was the identical to that of the reference concrete using natural sand [9]. Shoya et al. [8] suggested that ferronickel slag can be a promising fine aggregate for the manufacturing of high performance concrete with self compactability and high durability.

Tomosawa et al. [26] studied alkali-silica reactivity of ferronickel slag aggregate concrete. They suggested that addition of GGBFS, inclusion of fly ash and use of low alkali cement are the potential measures to restrain the reactivity of FNS aggregates. After that, several studies were conducted to mitigate alkali-aggregate reaction of FNS aggregate concrete. Choi and Choi [2] noticed that the water cooled FNS appeared higher alkali–silica reactivity than air cooled FNS. They also found that the partial replacement of cements with GGBFS or fly ash, and of FNS with sea sand decreased the alkali–silica reactivity (ASR) of FNS aggregate concrete. Saha and Sarker [15] reported that the application of GGBFS was not enough to minimize expansion up to the requirement. On the other hand, the utilization of class F fly ash as a supplementary cementing material was found effective in decreasing the ASR expansion. Recently, several studies were conducted by researchers to evaluate the fresh, hardened, and durability related properties of mortar and concrete where FNS was used as a fine aggregate [27-31]. In addition, fresh, mechanical and durability properties of concrete were investigated where ferronickel slag was used as coarse aggregate [6, 7, 32].

2.4 Use of ground ferronickel slag (GFNS) as supplementary cementitious materials

As ferronickel slag has a notable proportion of amorphous silica, ground ferronickel slag (GFNS) has shown reactivity when used with Portland cement. Lemonis et al. [14] conducted a study on the hydration of ternary blended cements consisting of a natural pozzolan and GFNS. It was seen that the rate of strength development of GFNS blended cements were lower compared to the reference control sample. At the early ages, the hydration rate of the mixture was delayed due to the addition of the natural pozzolan and GFNS. However, the pozzolanic reaction contributed to progress of strength at the late ages. The amorphous silicate matrix was dissolved and reacted with Portlandite to produce a secondary CSH gel and enhanced the density [14]. In addition, Katsiotis et al. [33] utilized GFNS as a supplementary material with Portland cement.

They also reported identical results. Rahman et al. [21] studied the fresh and hardened characteristics of mortars and cement pastes blended with GFNS and GGBFS. The authors reported that the water demand and setting times were not notably changed due to the use of the GFNS as a cement substitution up to 50%. The compressive strengths of mortar were slightly lower than that of the reference mixture. From the microstructural analysis, it was observed that as Mg was in stable forsterite ferroan form, and it did not participate in the hydration process. Therefore, in soundness test, there was no significant expansion despite the high Mg content of GFNS [21]. Recently, several studies were conducted by other researchers to evaluate the properties of the paste, mortar and concrete where GFNS was used as a supplementary binder [20, 22, 34-36]. Li et al. [20] found that the use of 20% GFNS as a replacement of cement improved the sulphate resistance of the mortar. Zhai et al. [22] reported that the use of high magnesium ferronickel slag as a supplementary cementitious material did not provide volume expansion. Kim et al. [35] noticed that GFNS concrete provided lower strength compared to OPC concrete at an early age. However, the strength of GFNS concrete substantially increased in a long-term period due to the latent hydration. Chen et al. [36] found that the pore structure of concrete was refined by the use of GFNS, which provided higher corrosion resistance and lower electrical conductivity of concrete.

2.5 Use of GFNS as precursor in geopolymers

Due to the presence of a high proportion of amorphous silica, GFNS has shown reactivity as a precursor in geopolymers. Komnitsas et al. [10] investigated the suitability of geopolymer synthesis from low Ca electric arc furnace GFNS where kaolinite, sodium hydroxide, sodium silicate and water were used as additives. The 2^3 factorial design method was applied to evaluate the influence of the age, heating time and temperature on the compressive strength of the geopolymers. The authors found that only aging period was effective for the compressive strength development, while heating temperature and time had an insignificant influence on the compressive strength. They also found some new phases such as thermonatrite, sodalite, calcite, trona and maghemite from XRD and FTIR analysis. It was seen that when samples were exposed to freeze-thaw cycles and distilled water for 4 months, the durability of the produced geopolymers was insignificantly affected. On the other hand, when the geopolymer specimens were exposed to an acid solution, a significant strength loss

was observed [10].

Komnitsas et al. [11] reported that as the size of K^+ is larger than Na^+, K^+ is more useful for the formation of larger silicate oligomers. Thus, KOH supplied higher amount of inorganic polymer precursors than NaOH. Consequently, better compressive strength and setting were obtained from KOH activator solution. They also observed that the existence of kaolin in the initial paste increased porosity. Thus, the compressive strength was reduced due to the increased porosity of the new structure. They suggested that short-term pre-curing has a positive effect on the compressive strength. However, longer pre-curing enhance the compressive strength insignificantly [11]. In another study, Komnitsas et al. [12] analysed the impact of nitrate and sulphate ions on GFNS based geopolymer. They noticed that nitrate and sulphate ions reduced the compressive strength of geopolymers. These ions consumed greater amounts of moles from alkali activator solution. Thus, geopolymerisation process was hampered and lower amount of gel was produced. It was also shown that heavy metals were confined in the geopolymer matrix, although the characteristics of developed gel enhance the level of encapsulation. The authors also found that the rise of the molarity of KOH decreased some drawbacks due to the increased participation of KOH in geopolymeric reactions [12].

Moreover, Maragkos et al. [13] observed that the properties of GFNS geopolymer controlled by the solid to liquid (S/L) ratio and the initial NaOH and initial SiO_2 concentration. The optimum amount of S/L ratio, initial NaOH and initial SiO_2 concentration for the synthesis of FNS geopolymers were 5.4 g/mL, 7 M and 4 M, respectively [13]. Yang et al. [37] studied the impacts of high-magnesium nickel slag (HMNS) on fly ash based geopolymer considering the microstructural and mechanical analysis. They found that the sodium magnesium aluminosilicate gel was the prime constituent of the binder. It was seen that the HMNS substitution provided a greater amount of silicate constituents which ultimately increased Si/Al ratio. It was observed that for 20% GFNS geopolymer samples, the volume of pores was lower than those of the other samples. On the other hand, higher amount of GFNS such as 40% or 60% GFNS reduced Si/Al ratio and increased porosity. Thus, the compressive strength decreased due to the use of higher amount of GFNS. The authors found that for 1.2 to 2.0 molar ratio of alkali activator solutions, the optimum amount of HMNS was 20%

where higher compressive strength and lower drying shrinkage were obtained compared to other proportions of HMNS. They also pointed out that the HMNS is not as reactive as usual MgO-based expansive agents. As a result, the volume stability problem of fly ash-based geopolymers was not noticeable due to the addition of HMNS [37].

Besides, Zhang et al. [1] reported high compressive strength for 20 and 40% HMNS compared to 100% fly ash geopolymer. They found that this improvement was because of the reactivity of glassy forms of HMNS. It was reported that the production of geopolymer needs lower amount of energy as well as the emission of lower CO_2 compared to conventional cement paste [1]. In addition, Sakkas et al. [38] examined the thermal and mechanical performances of GFNS based geopolymers. They found that the geopolymers had low water absorption, low thermal conductivity, and high compressive strength which are identical or even better compared to other fire-resistant substances such as fire barrier 135, meyco fireshield 1350, promatect board, cyc feu 6 and pyrocrete 241. Giannopoulou and Panias [39] found that the thermal insulation of GFNS geopolymers was comparable with that of calcium silicate board, which is one of the marketable insulation materials.

Recently, Bian et al. [40] investigated the effect of Na_2O equivalent on the fresh and hardened properties of GFNS geopolymer. The authors reported that the optimum Na_2O equivalent is 5% in GFNS geopolymer considering workability and strength. Cao et al. [23] evaluated the leaching kinetics and reactivity of GFNS in NaOH solutions. It was found that dissolved magnesium was primarily involved in the development of N-M-S-H gels and hydrotalcite. Chromium was not detected at the time of leaching process. Bouaissi et al. [41] found that the use of HMNS in fly ash-GGBFS geopolymer concrete increased the intermolecular bond of geopolymer matrix. Thus, a highly compacted matrix with less pores was found in the FA-GGBFS-HMNS geopolymer concrete. Cao et al. [42] evaluated the feasibility of using GFNS blended with GGBFS to produce geopolymers. The authors found that for the Na_2SiO_3 activated geopolymer, the drying and autogenous shrinkage increased with the increase of GFNS. On the other hand, the drying and autogenous shrinkage decreases with the increase of GFNS for the NaOH activated geopolymer.

17

2.6 Summary

From the above review, it is noticed that GFNS is a feasible source material for the production of geopolymer binder. However, GFNS as a precursor in geopolymer has not been studied extensively by the scientific community unlike fly ash or ground granulated blast furnace slag. Moreover, properties of GFNS based geopolymers also depend on the source of the GFNS. In this study, GFNS was collected from the smelting of garnierite ores of New Caledonia, which should be properly analysed prior to use as a source material of geopolymer. Therefore, the aim of the study was to investigate the properties of geopolymers using GFNS as a source material. A solution of NaOH and Na$_2$SiO$_3$ was utilized as an alkaline activator. Binary mixes of GFNS with fly ash were investigated at different curing conditions. The fresh properties and mechanical and durability properties of the hardened geopolymer paste and mortar using GFNS was studied. Various microstructural studies were performed in order to interpret the effect of GFNS on the geopolymerisation process and the reaction product. Based on the fresh, mechanical and durability test results, optimal level of GFNS was recommended for manufacturing geopolymers.

2.7 References

[1] Z. Zhang, Y. Zhu, T. Yang, L. Li, H. Zhu, H. Wang, Conversion of local industrial wastes into greener cement through geopolymer technology: A case study of high-magnesium nickel slag, J. Clean. Prod. 141 (2017) 463–471.

[2] Y.C. Choi, S. Choi, 2015, Alkali-silica reactivity of cementitious materials using ferro-nickel slag fine aggregates produced in different cooling conditions, Constr. Build. Mater. 99 (2015) 279–287.

[3] JMIA, Research of Ferronickel Slag Fine Aggregate for Concrete, Japan Mining Industry Association, 1991.

[4] A.K. Saha, M.N.N. Khan, P.K. Sarker, Value added utilization of by-product electric furnace ferronickel slag as construction materials: A review, Resour. Conserv. Recycl. 134 (2018) 10-24.

[5] A.K. Saha, P.K. Sarker, Sustainable use of ferronickel slag fine aggregate and fly ash in structural concrete: Mechanical properties and leaching study, J. Clean. Prod. 162 (2017) 438–448.

[6] T. Sato, K. Watanabe, A. Ota, M. Aba, Y. Sakoi, Influence of excessive bleeding on frost susceptibility of concrete incorporating ferronickel slag as

aggregates, 36th Conference on Our World in Concrete & Structures, Singapore (2011).

[7] Y. Sakoi, M. Aba, Y. Tsukinaga, S. Nagataki, Properties of concrete used in ferronickel slag aggregate, Proceedings of the 3rd International Conference on Sustainable Construction Materials and Technologies, Tokyo, Japan (2013) 1-6.

[8]   M. Shoya, S. Sugita, T. Tsukinaga, M. Aba, K. Tokuhasi, Properties of self-compacting concrete with slag fine aggregates, Exploiting Wastes in Concrete, University of Dundee, Scotland (1999), 121-130.

[9]   K. Togawa, M. Shoya, K. Kokubu, Characteristics of bleeding, freeze-thaw resistance and watertightness of concrete with ferro-nickel slag fine aggregates, J. Socie. Mater. Sci. Jpn., 45 (1) (1996), 101-109, 10.2472/jsms.45.101.

[10] K. Komnitsas, D. Zaharaki, V. Perdikatsis, Geopolymerisation of low calcium ferronickel slags, J. Mater. Sci. 42 (2007) 3073–3082.

[11] K. Komnitsas, D. Zaharaki, V. Perdikatsis, Effect of synthesis parameters on the compressive strength of low-calcium ferronickel slag inorganic polymers, J. Hazard. Mater. 161 (2009) 760–768.

[12] K. Komnitsas, D. Zaharaki, G. Bartzas, Effect of sulphate and nitrate anions on heavy metal immobilisation in ferronickel slag geopolymers, Appl. Clay Sci. 73 (2013) 103–109.

[13] I. Maragkos, I.P. Giannopoulou, D. Panias, Synthesis of ferronickel slag-based geopolymers, Miner. Eng. 22 (2009) 196–203.

[14] N. Lemonis, P.E. Tsakiridis, N.S. Katsiotis, S. Antiohos, D. Papageorgiou, M.S. Katsiotis, M. Beazi-Katsioti, Hydration study of ternary blended cements containing ferronickel slag and natural pozzolan, Constr. Build. Mater. 81 (2015) 130–139.

[15]   A.K. Saha, P.K. Sarker, Expansion due to alkali-silica reaction of ferronickel slag fine aggregate in OPC and blended cement mortars, Constr. Build. Mater. 123 (2016) 135-142.

[16] A.K. Saha, P.K. Sarker, Durability characteristics of concrete using ferronickel slag fine aggregate and fly ash, Magaz. Concr. Res. 70 (2017) 865-874.

[17] A.K. Saha, P.K. Sarker, Durability of mortar incorporating ferronickel slag aggregate and supplementary cementitious materials subjected to wet-dry cycles, Inter. J. Concr. Struc. Mater. 12 (2018) 29.

[18] E. Fidancevska, B. Mangutova, D. Milosevski, M. Milosevski, J. Bossert, Obtaining of dense and highly porous ceramic materials from metallurgical slag, Sci. Sinter. 35 (2003), 85-91.

[19] S.J. Choi, J.H. Kim, S.H. Bae, T.G. Oh, Effect of fly ash on compressive strength, drying shrinkage, and carbonation depth of mortar with ferronickel-slag powder, Appl. Sci. 11 (2021) 1037.

[20] B. Li, B. Huo, R. Cao, S. Wang, Y. Zhang, Sulfate resistance of steam cured ferronickel slag blended cement mortar, Cem. Concr. Compos. 96 (2019) 204–211.

[21] M.A. Rahman, P.K. Sarker, F.U.A. Shaikh, A.K. Saha, Soundness and compressive strength of Portland cement blended with ground granulated ferronickel slag, Constr. Build. Mater. 140 (2017) 194–202.

[22] M. Zhai, H. Zhu, G. Liang, Q. Wu, C. Zhang, S. Hua, Z. Zhang, 2020. Enhancing the recyclability of air-cooled high-magnesium ferronickelslag in cement-based materials: A study of assessing soundness through modifying method. Constr. Build. Mater. 261, 120523.

[23] R. Cao, Z. Jia, Z. Zhang, Y. Zhang, N. Banthia, Leaching kinetics and reactivity evaluation of ferronickel slag in alkaline conditions, Cem. Concr. Res. 137 (2020) 106202.

[24] N. You, B. Li, R. Cao, J. Shi, C. Chen, Y. Zhang, The influence of steel slag and ferronickel slag on the properties of alkali-activated slag mortar, Constr. Build. Mater. 227 (2019) 116614.

[25] K. Komnitsas, L. Yurramendi, G. Bartzas, V. Karmali, E. Petrakis, Factors affecting co-valorization of fayalitic and ferronickel slags for the production of alkali activated materials, Sci. Total Environ. 721 (2020) 137753.

[26] F. Tomosawa, S. Nagataki, T. Kajiwara, M. Yokoyama, Alkali-aggregate Reactivity of Ferronickel-Slag Aggregate Concrete, ACI Special Publication 170 (1997) 1591–1602.

[27] J. Sun, J. Feng, Z. Chen, Effect of ferronickel slag as fine aggregate on properties of concrete, Constr. Build. Mater. 206 (2019) 201–209.

[28] Q.D. Nguyen, M.S.H Khan, A. Castel, T. Kim, 2019. Durability and microstructure properties of low-carbon concrete incorporating ferronickel slag sand and fly ash. J. Mater. Civ. Eng. 31(8), 04019152.

[29] J. Bao, Z. Yu, L. Wang, P. Zhang, X. Wan, S. Gao, T. Zhao, Application of ferronickel slag as fine aggregate in recycled aggregate concrete and the effects on transport properties, J. Clean. Prod. 304 (2021), 127149.

[30] A.K. Saha, P.K. Sarker, Effect of sulphate exposure on mortar consisting of ferronickel slag aggregate and supplementary cementitious materials, J. Build. Eng. 28 (2020), 101012.

[31] M. Nuruzzaman, J.O.C. Casimiro, P.K. Sarker, Fresh and hardened properties of high strength self-compacting concrete using by-product ferronickel slag fine aggregate, J. Build. Eng. 32 (2020), 101686.

[32] Aba, M., Sakoi, Y., Shoya, M., Tsukinaga, Y., Nagataki, S., 2010. Properties of concrete incorporating ferronickel slag as coarse aggregate. Concrete Research and Technology. 21(3), 2010.

[33] N.S. Katsiotis, P.E. Tsakiridis, D. Velissariou, M.S. Katsiotis, S.M. Alhassan, M. Beazi, Utilization of ferronickel slag as additive in Portland cement: a hydration leaching study. Waste Biomass Valor. 6 (2015) 177–189.

[34] D. Wang, Q. Wang, S. Zhuang, J. Yang, Evaluation of alkali-activated blast furnace ferronickel slag as a cementitious material: Reaction mechanism, engineering properties and leaching behaviors, Constr. Build. Mater. 188 (2019) 860–873.

[35] H. Kim, C.H. Lee, K.Y. Ann, Feasibility of ferronickel slag powder for cementitious binder in concrete mix, Constr. Build. Mater. 207 (2019) 693–705.

[36] Y. Chen, T. Ji, Z. Yang, W. Zhan, Y. Zhang, Sustainable use of ferronickel slag in cementitious composites and the effect on chloride penetration resistance, Constr. Build. Mater. 240 (2020) 117969.

[37] T. Yang, X. Yao, Z. Zhang, Geopolymer prepared with high-magnesium nickel slag: Characterization of properties and microstructure, Constr. Build. Mater. 59 (2014) 188–194.

[38] K. Sakkas, P. Nomikos, A. Sofianos, D. Panias, Utilisation of FeNi-Slag for the production of inorganic polymeric materials for construction or for passive fire protection, Waste and Biomass Valorization 5 (2014) 403–410.

[39] I. Giannopoulou, D. Panias, Fire resistant geopolymers synthesized from industrial wastes, World Journal of Engineering 5 (2008) 130-131.

[40] Z. Bian, G. Jin, T. Ji, Effect of combined activator of $Ca(OH)_2$ and Na_2CO_3 on workability and compressive strength of alkali-activated ferronickel slag system, Cem. Concr. Compos. 123 (2021) 104179.

[41] A. Bouaissi, L. Li, M.M.A.B. Abdullah, Q. Bui, Mechanical properties and microstructure analysis of FA-GGBS-HMNS based geopolymer concrete, Constr. Build. Mater. 210 (2019) 198–209.

[42] R. Cao, B. Li, N. You, Y. Zhang, Z. Zhang, Properties of alkali-activated ground granulated blast furnace slag blended with ferronickel slag, Constr. Build. Mater. 192 (2018) 123-132.

CHAPTER 3: FRESH AND HARDENED PROPERTIES OF GEOPOLYMER BINDER USING GFNS WITH FLY ASH

The contents presented in this chapter were published in the following paper:

Kuri, J. C., Khan, M. N. N., & Sarker, P. K. (2021). Fresh and hardened properties of geopolymer binder using ground high magnesium ferronickel slag with fly ash. Construction and Building Materials, 272, 121877.

This chapter evaluates the fresh and hardened properties of geopolymer paste containing different percentages of GFNS with fly ash. The setting time, flow time, flow diameter, soundness by Le-Chatelier expansion, compressive strength and microstructural properties were determined. The experimental results were analyzed to evaluate the effect of using GFNS as a geopolymer precursor, understand the behaviour of the geopolymer products and correlations among the properties.

3.1 Overview

Geopolymers are inorganic polymers obtained by synthesis of aluminosilicate source materials with alkaline liquids [1]. Previous studies attempted using various aluminosilicate source materials that comprises industrial by-products as well as natural raw materials, such as fly ash, ground granulated blast furnace slag (GGBFS), metakaolin, silica fume, palm oil fuel ash and rice husk ash, which are abundant in Aluminium (Al) and Silicon (Si). Geopolymers are reported to possess high compressive strength [2, 3], high thermal stability [4-6], low permeability [7], and good resistance to chemical attacks [8] and freeze-thaw cycles [9], which are comparable to the properties of ordinary Portland cement (OPC) binders.

The composition, amorphousness and fineness of the starting materials highly influenced the characteristics of geopolymer [10]. Gao et al. [11] reported that the lower molar ratio of SiO_2/Na_2O provided faster setting time of geopolymer as compared to the higher SiO_2/Na_2O ratio. Chindaprasirt et al. [12] observed an acceleration of setting in high calcium fly ash based geopolymers due to the increase of SiO_2 or Al_2O_3, where the optimum SiO_2/Al_2O_3 ratio was in the range of 3.20 to 3.70. Setting time of geopolymer was also found to be influenced by the liquid to solids (L/S) ratio. Setting time of fly ash geopolymer paste increased with the increase of the

L/S ratio [13]. The ratio of sodium silicate to sodium hydroxide solutions (SS/SH) of the activating liquid influenced fresh [14] and hardened [15] properties of geopolymers. Workability of geopolymer was found to decrease with the increase of SS/SH ratio due to the increase of viscosity [16]. The molar ratio of Si/Al showed a great influence on the formation of geopolymer gel, which also influence the compressive strength. Ozer and Soyer-Uzun [17] reported an increase of compressive strength with the increase of the molar ratio of Si/Al. Besides, it was found that a higher MgO content of alkali activated slag provided faster reaction and better mechanical properties [18,19]. Bernal et al. [20] and Abdalqader et al. [21] reported that the alkali activated slag with higher MgO content produced hydrotalcite as the principal secondary reaction product in addition to calcium aluminosilicate hydrate (C-A-S-H). Moreover, the properties of geopolymer are also influenced by the curing conditions. Usually heat curing accelerates the geopolymerization reaction which provides quick setting and high early strength [22].

Ferronickel slag (FNS) is a by-product which is discharged in the refinement process of ferronickel alloys from nickel ores [23]. The ore is smelted in a rotary kiln or electric furnace to produce ferronickel. The main chemical components of FNS are Si, Mg and Fe, which exist in the forms of crystalline and non-crystalline minerals [24]. Several investigations were conducted by different researchers where FNS was used as aggregate [25, 26]. Besides, owing to high amount of amorphous silica, ground FNS (GFNS) has shown reactivity as a supplementary cementitious material in OPC [27-30] or a source material in geopolymer [31-33].

Komnitsas et al. [34] investigated the properties of kaolinite-GFNS based geopolymer. The authors noticed that the compressive strength of kaolinite-GFNS geopolymer highly depends on the age of specimens. It was also shown that the presence of sulphate and nitrate ions hindered the geopolymer reaction and thus reduced the geopolymer product as well as strength of GFNS geopolymer [35]. In another study, Komnitsas et al. [36] noticed that KOH activated GFNS geopolymer provided higher compressive strength and faster setting as compared to NaOH activated geopolymer due to the larger size of K$^+$. However, Xu and Deventer [37] demonstrated that the small size of Na$^+$ enhanced the ionic pair reaction with the smaller silicate oligomers and thus, higher strength was found for NaOH activated geopolymers compared to KOH activated geopolymers. Maragkos et al. [38] noticed that the optimal conditions

for the synthesis of GFNS geopolymers were 5.4 g/mL solid to liquid (S/L) ratio, 7M initial NaOH concentration and 4M initial SiO$_2$ concentration. At this optimum condition, high compressive strength (120 MPa), high apparent density (2480 kg/m^3) and low water absorption (0.7%) were achieved.

Fly ash contains substantial proportions of Si and Al. On the other hand, GFNS has significant amounts of Si and Mg [24]. Therefore, blending of GFNS with fly ash will make a suitable combination of materials to form sodium magnesium aluminosilicate hydrate (N-M-A-S-H) gel. In the process of FA-GFNS geopolymerization, the Si-O-Si, Si-O-Al and Al-O-Al bonds of fly ash and GFNS particles are first broken in the highly alkaline solution to develop silicate monomers [Si(OH)$_3$$^-$] and aluminium monomers [Al(OH)$_4$$^-$]. In consequence, oligomerization of SiO(OH)3$^-$ and Al(OH)4$^-$ is occurred. In the next stage, Na$^+$ and Mg^{2+} are incorporated into the aluminosilicate structures and geopolymer precursors are formed as per Eq. 3.1 [39-41]. Then, in the polycondensation stage, the geopolymer precursors together form a 3D network according to Eq. 3.2. Finally, a geopolymer gel structure is formed by making bonds with the undissolved solid particles [39, 40].

$$[Si_jO_k(OH)_{3j-2k}]^- + [Al_lO_m(OH)_{4l-2m}]^- + pOH^- + pNa^+ + pMg^{2+} =$$
$$[Si_jAl_lO_{k+m+p}(OH)_{3j-2k+4l-2m-p}]^{p-}.pNa^+.pMg^{2+} + pH_2O \ \ldots\ldots................... (3.1)$$

$$n\left([Si_jAl_lO_{K+m+p}(OH)_{3j-2k+4l-2m-p}]^{p-}.pNa^+.pMg^{2+}\right) =$$
$$[Si_{nj}Al_{nl}O_{n(k+m+p)}(OH)_{n(3j-2k+4l-2m-p)-2w}]^{np-}.npNa^+.npMg^{2+} + wH_2O$$
$$\ldots\ldots\ldots\ldots\ldots\ldots\ldots\ldots\ldots\ldots\ldots\ldots\ldots\ldots\ldots\ldots\ldots\ldots\ldots\ldots\ldots\ldots..\ldots\ldots\ldots (3.2)$$
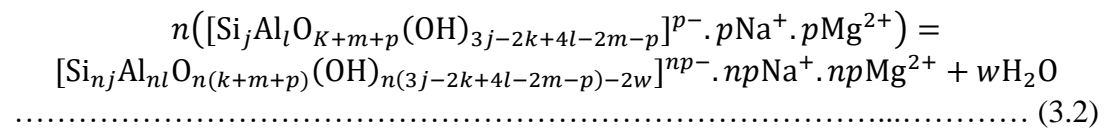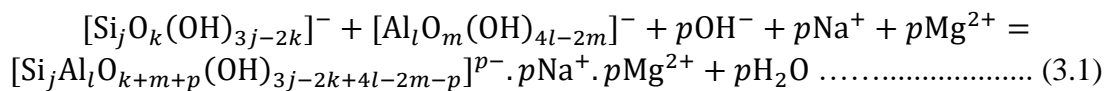
where, the coefficients j, k, l, m and p depend on the alkali solution and chemical constituents of GFNS and fly ash, and n presents the degree of polymerization.

Zhang et al. [42] observed that the application of 20% and 40% GFNS substitution provided higher compressive strength as compared that of 100% fly ash. It was also noticed that the thermal stability of geopolymer increased due to the incorporation of GFNS, which is associated with the formation of sodium magnesium aluminosilicate gel [43, 44]. Moreover, Sakkas et al. [45] found that the GFNS based geopolymer possess low water absorption and low thermal conductivity, which are comparable to that of other fire-resistant materials. Bouaissi et al. [46] observed that the replacement

of fly ash with 10% GFNS and 20% GGBFS in geopolymer concrete increased the 28-day compressive strength and splitting tensile strength by 100% and 58%, respectively.

Pentlandite, garnierite and laterite ores are the main sources of nickel. The FNS used in this study is produced from garnierite ore by Société Le Nickel (SLN) New Caledonia, which is one of the world's largest nickel producers. Since garnierite ore contains a high amount of magnesium [47], the magnesium content of the FNS is also relatively high. Safe disposal of the by-product is a matter of great concern, and its storage is occupying a huge area of land. About 25 million tonnes of this FNS is currently available at one site for potential uses [48]. Therefore, the development of GFNS as a binder for concrete will provide a route for the safe disposal of the by-product FNS and save on the land required for its storage. This will also benefit the environment by reducing the carbon dioxide emission of cement production. As mentioned, the FNS contains a relatively high proportion of Mg unlike the FNS studied by Maragkos et al. [38], Komnitsas et al. [34-36] and Sakkas et al. [45]. The high Mg content limits the use of GFNS as a supplementary cementitious material (SCM) due to the concern over volume stability of concrete. Therefore, it is essential to understand the soundness behaviour of GFNS geopolymers. At present, very little information is available on the fresh properties of fly ash-GFNS geopolymers, with no published results on the setting and soundness properties. Moreover, the properties of geopolymer are significantly influenced by the alkali activator and curing conditions which needs to be studied in detail. Therefore, it is important to understand the effects of high magnesium content of GFNS on the setting, workability and expansion behaviour of geopolymer binders using variable alkali activator. This study investigated the properties of geopolymers using GFNS as a precursor at ambient and heat curing conditions. The setting time, workability, soundness and compressive strength of geopolymer binders produced using different percentages of GFNS with fly ash were evaluated. The influence of silicate to hydroxide ratio of the alkaline activator on fresh and hardened properties of fly ash-GFNS geopolymer was also investigated. Microstructure analysis of the hardened geopolymer binder was conducted by scanning electron microscopy (SEM) images, energy-dispersive X-ray spectroscopy (EDS) and quantitative X-ray diffraction (QXRD) analysis to gain insights into the reaction products.

3.2 Materials and Methods

3.2.1 Materials

Class F fly ash (FA), GFNS and an alkaline activator liquid were used for the production of the geopolymer paste. The SEM images of Fig. 3.1(a) and (b) show the morphology of GFNS and fly ash, respectively. It is seen that the shapes of GFNS and fly ash particles are angular and spherical, respectively. The chemical compositions of GFNS and fly ash, determined by X-ray fluorescence spectrometer, are shown in Table 3.1. It can be noticed that GFNS has substantial amounts of Si, Mg and Fe, whereas fly ash contained notable proportions of Si and Al. The strength activity index of the fly ash was 78%. The maximum size of granulated FNS was about 5 mm which was ground using a laboratory ball mill.

10 µm   EHT = 5.00 kV   Signal A = SE2   Aperture Size = 30.00 µm
WD = 4.9 mm
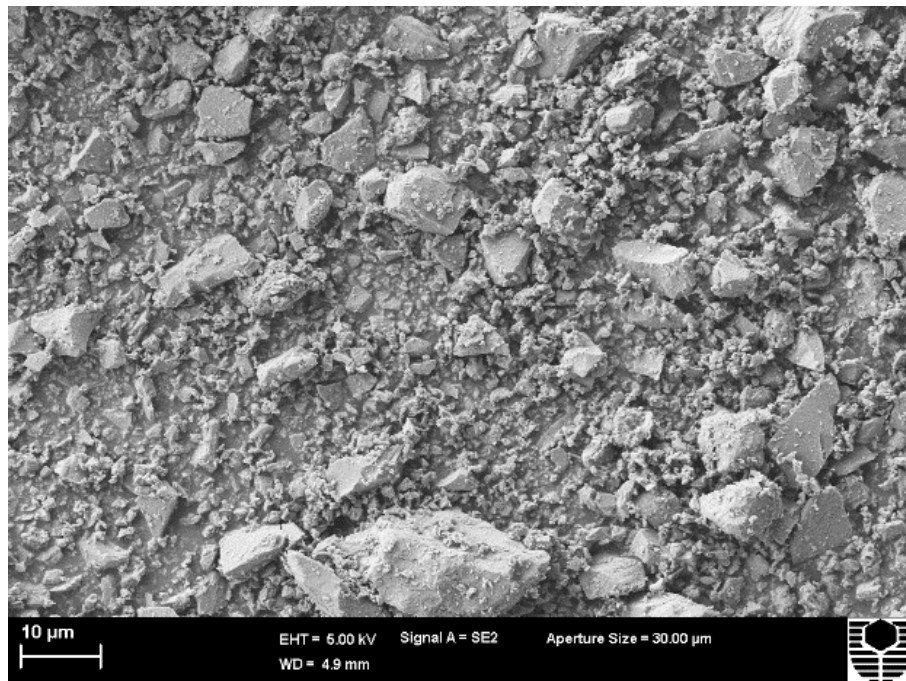
(a)
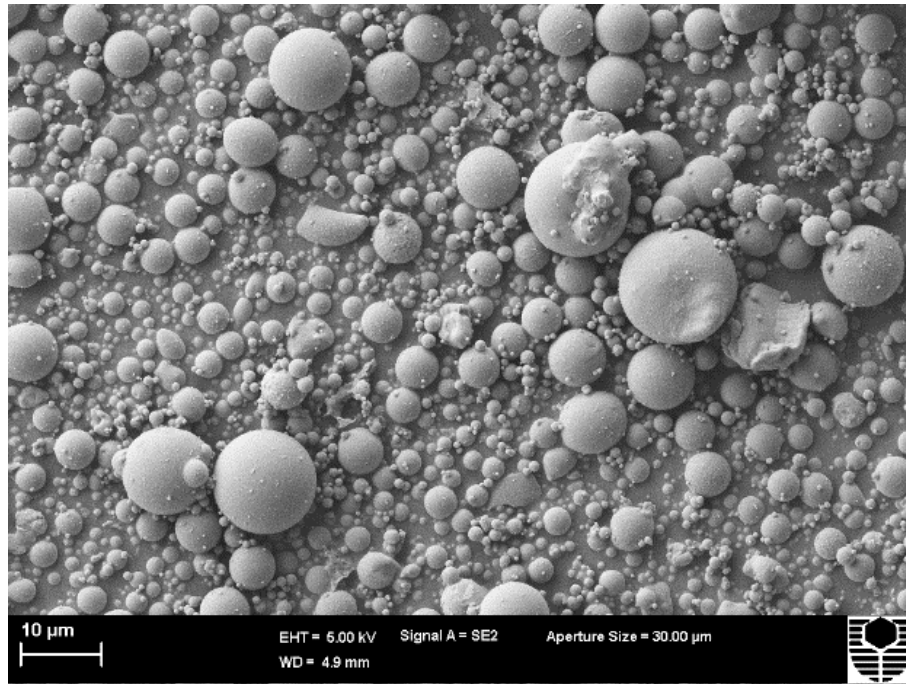
(b)

Fig. 3.1 (a) SEM image of GFNS; and (b) SEM image of fly ash.

Table 3.1 Chemical compositions of GFNS and fly ash

Constituents	GFNS (%)	Fly ash (%)
SiO_2	51.42	60.03
Al_2O_3	2.88	22.75
CaO	0.48	3.80
Fe_2O_3	12.85	6.78
K_2O	0.03	1.28
MgO	30.58	1.29
Na_2O	0.08	0.54
P_2O_5	0.01	0.89
SO_3	0.05	0.25
TiO_2	0.06	1.06
MnO	0.46	0.07
SrO	<0.01	0.05
Cr_2O_3	1.07	0.01
ZnO	0.02	---
Loss on ignition	---	1.15
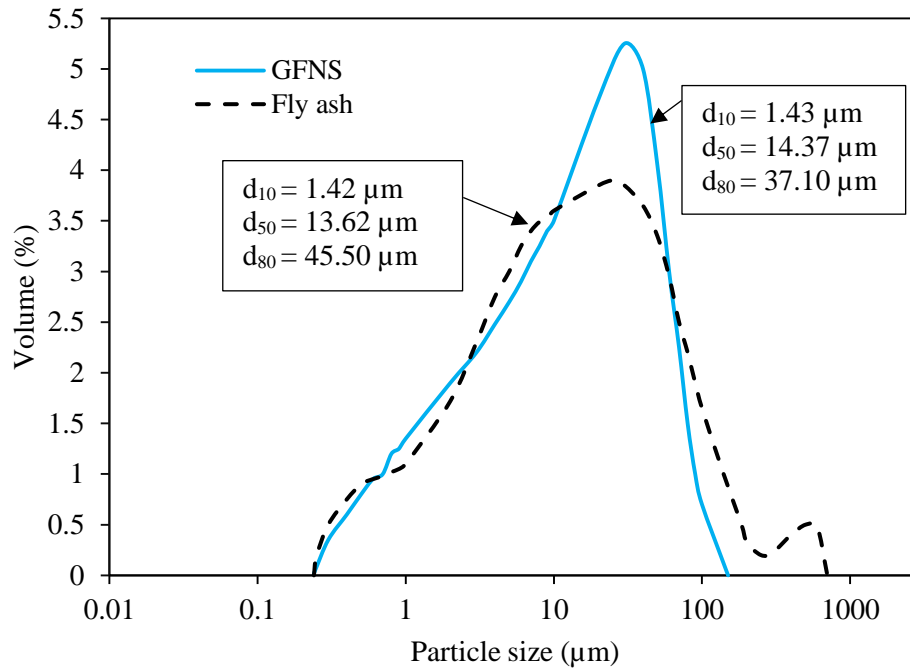
Fig. 3.2 Particle size distributions of GFNS and fly ash.

The GFNS and fly ash particles were went through the laser beam, where the intensity of scattered light was determined and converted to particle size using a Malvern Mastersizer 2000 particle size analyzer. The particle size of GFNS varied from 0.240 to 140 µm and that of fly ash varied from 0.250 to 700 µm, shown in Fig. 3.2. The mean particle size (d_{50}) of GFNS was 14.37 µm, which is similar to that of fly ash (13.62 µm). The Blaine's specific surface area of the fly ash was 3800 cm^2/g and that of GFNS was 4200 cm^2/g. The specific gravity of the fly ash and GFNS were 2.40 and 2.95, respectively.

A mixture of sodium hydroxide (SH) and sodium silicate (SS) solutions was used as the alkali activator. The amount of alkali activator solution was constant as 40% of the total solid binder for all mixtures. The concentration of SH solution was 8M which was also constant for all the mixtures. It was made by mixing 98% pure NaOH pellets and normal water. The Na_2SiO_3 solution was collected from a local commercial source which consists 14.7% Na_2O, 29.4% SiO_2 and 55.9% water. The ratio of the SS/SH solutions varied from 1.5 to 2.5. The amount of activator solution, SS/SH ratio and molarity of NaOH were adopted on the basis of the previous works on geopolymers to achieve workability and strength [13, 14].

3.2.2 Mix proportions

The mixture proportions of geopolymer pastes are presented in Table 3.2, where fly ash was replaced by 0, 25, 50, 75 and 100% GFNS. The molar ratios of the mixtures are also given in Table 3.2. The molar ratios were calculated using the chemical compositions of precursors and alkaline liquids. For each of the paste mixtures, the mass of alkali activator solution was 40% of total binder. The ratios of SS/SH solutions were 1.5, 2.0 and 2.5. In the mixture ID of Table 3.2, the number after GFNS represents the percentage of GFNS and the number after R shows the ratio of SS/SH solutions. For instance, the mix designation GFNS-50-R-2.0 indicates a mixture with 50% GFNS as a replacement of fly ash and the ratio of SS/SH is 2.0.

Table 3.2 Mix proportions of geopolymer pastes

Mix ID	GFNS (%)	Fly ash (%)	SS[a]/SH[b] (R)	Molar ratio					
				$SiO_2/$ Al_2O_3	$Na_2O/$ SiO_2	$Na_2O/$ Al_2O_3	$H_2O/$ Na_2O	$MgO/$ SiO_2	$MgO/$ Al_2O_3
GFNS-0-R-1.5	0	100	1.5	5.004	0.106	0.529	12.306	0.029	0.143
GFNS-25-R-1.5	25	75	1.5	6.197	0.108	0.666	12.502	0.198	1.225
GFNS-50-R-1.5	50	50	1.5	8.313	0.109	0.910	12.705	0.378	3.146
GFNS-75-R-1.5	75	25	1.5	13.111	0.111	1.461	12.915	0.572	7.497
GFNS-100-R-1.5	100	0	1.5	34.456	0.114	3.916	13.131	0.780	26.861
GFNS-0-R-2.0	0	100	2.0	5.063	0.102	0.518	12.257	0.028	0.143
GFNS-25-R-2.0	25	75	2.0	6.271	0.104	0.652	12.457	0.195	1.225
GFNS-50-R-2.0	50	50	2.0	8.417	0.106	0.890	12.664	0.374	3.146
GFNS-75-R-2.0	75	25	2.0	13.280	0.108	1.430	12.877	0.565	7.497
GFNS-100-R-2.0	100	0	2.0	34.917	0.110	3.830	13.098	0.769	26.861
GFNS-0-R-2.5	0	100	2.5	5.104	0.100	0.511	12.222	0.028	0.143
GFNS-25-R-2.5	25	75	2.5	6.325	0.102	0.642	12.424	0.194	1.225
GFNS-50-R-2.5	50	50	2.5	8.491	0.103	0.877	12.633	0.370	3.146
GFNS-75-R-2.5	75	25	2.5	13.401	0.105	1.408	12.850	0.559	7.497
GFNS-100-R-2.5	100	0	2.5	35.247	0.107	3.770	13.074	0.762	26.861

[a]Sodium silicate solution.

[b]Sodium hydroxide solution.

3.2.3 Casting and curing

Fifteen geopolymer paste mixtures were prepared using different proportions of precursors and alkaline liquids as denoted in Table 3.2. The NaOH and Na_2SiO_3

solutions were mixed together at the desired ratio about half an hour before mixing with the solid precursors to enhance the reactivity of the activator liquid. The desired amount of GFNS and fly ash were dry mixed in a Hobart mixer first. After that the alkaline solution was added slowly as the mixing was continued. The fresh paste mixture was used for setting time, workability and soundness tests. The 50 mm cube moulds were filled up with geopolymer paste and compacted by a vibration table. To compare the effect of curing conditions on geopolymer, ambient curing and heat curing were applied on geopolymer specimens. The ambient condition consisted of a controlled temperature of 20 ± 3 °C with relative humidity of $65 \pm 5\%$. The samples were demoulded after 24 hours of casting and left in that controlled room till testing. For heat curing, after casting, the samples with moulds were kept in an oven at 60 °C for 24 hours. After completion of heat curing, the hardened samples were demolded and kept in room temperature till the time of testing.

3.2.4 Test methods

The studied fresh properties were setting times and workability of geopolymer paste. The setting time test was conducted at 23 °C using a Vicat apparatus following ASTM C191 [49]. To determine workability of fresh geopolymer paste, the flow time was measured using a flow cone according to ASTM C939 [50]. The flow cone was filled with geopolymer paste and allowed to discharge through a tube. The time for the first break of continuous flow is taken as the flow time, which is a measure of the fluidity and is related to the workability of the mixture. In addition, the flow value was determined by flow table test in accordance with ASTM C1437 [51].

Unsoundness of a binder may cause excessive volume change leading to cracks and strength loss. Since GFNS has a relatively high magnesium content as shown in Table 3.1, it is important to determine the soundness of geopolymer, although the reactivity of Mg depends on its chemical bonding in the slag. Therefore, in order to investigate the effect of high Mg on soundness of GFNS, the Le-Chatelier soundness test was performed following AS2350.5 [52].

Compressive strength of hardened geopolymer paste was tested at an axial loading rate of 18 MPa/min with a Matest machine as per AS 1012.9 [53]. The compressive strength of ambient cured specimens was determined at 7, 28, 56 and 90 days of room

temperature curing. On the other side, the compressive strength of heat cured geopolymer was determined after 1 day of cooling at room temperature (2 days after casting).

SEM and EDS analysis were used to investigate the microstructure of geopolymer products. The geopolymer paste cube specimen was cut by a diamond saw and the sectioned surface was coated with 10 nm carbon. After that, SEM images were obtained using a Neon 40EsB (Zeiss) microscope and elemental composition at various locations were investigated by EDS (Oxford Instruments) fitted with SEM instrument.

Quantitative X-ray diffraction (QXRD) analysis was performed to investigate the mineralogical contents of the raw binder and geopolymer paste. Geopolymer pastes were ground (dry grinding) by a ring mill to make the powder sample where particle size was less than 75 µm. Then 3 g powder sample was mixed with 0.3 g (10% of the original sample) corundum powder. Corundum powder was applied as a standard reference substance to perform quantitative analysis. Eight ml ethanol was then added to the powder mixture and ground (slurry grinding) by the McCrone micronizing mill where particle size was reduced to less than 5 µm. After that, the slurry specimen was dried, ground and packed into a clean specimen holder. A D8 Advance powder diffractometer (Bruker AXS, Germany) was used to collect the XRD patterns. The analysis was performed for 2 theta values of 7-120 degrees where step size was 0.015 degrees and collection time was 0.7 Sec/step. ICDD (International Centre for Diffraction Data) PDF4+ database and EVA 11.0 software were used to identify the phases. Then Rietveld [54] full pattern analysis was conducted by TOPAS [55] to find the relative weight proportion of the phases. Finally, the internal standard method [56] was applied using TOPAS software to determine the absolute proportion of amorphous and crystalline phases from the relative Rietveld weight proportion.

3.3 Results and Discussion

3.3.1 Setting time

Fig. 3.3 presents the effect of GFNS on setting time of geopolymer paste for the ratios of SS/SH of 1.5 (R-1.5) and 2.0 (R-2.0). It can be seen that for all the mixtures, initial and final setting times of geopolymer paste decreased with the increase of GFNS

content. In case of R-1.5, the control paste without GFNS showed longer initial (250 min) and final (405 min) setting times compared to the mixtures with GFNS. The setting time of neat fly ash geopolymer was long because of the slow reaction at room temperature. However, the initial setting time of geopolymer paste reduced to 165, 133, 100 and 60 minutes due to the use of 25, 50, 75 and 100% GFNS, respectively. It is seen that the difference between initial and final setting times of the geopolymer pastes using GFNS were very small as compared to neat fly ash paste and the difference decreased with the increase of GFNS content. For instance, in the R-1.5 mixtures, the difference between initial and final setting times of the neat fly ash geopolymer paste was 155 minutes and those of the pastes using 25, 50, 75 and 100% GFNS were 33, 27, 23 and 15 minutes, respectively. A similar trend was observed in the R-2.0 mixtures where the use of 0, 25, 50, 75 and 100% GFNS gave initial setting times of 410, 270, 240, 192 and 188 minutes, respectively. The corresponding final setting times were 640, 310, 276, 226 and 208 minutes, respectively.
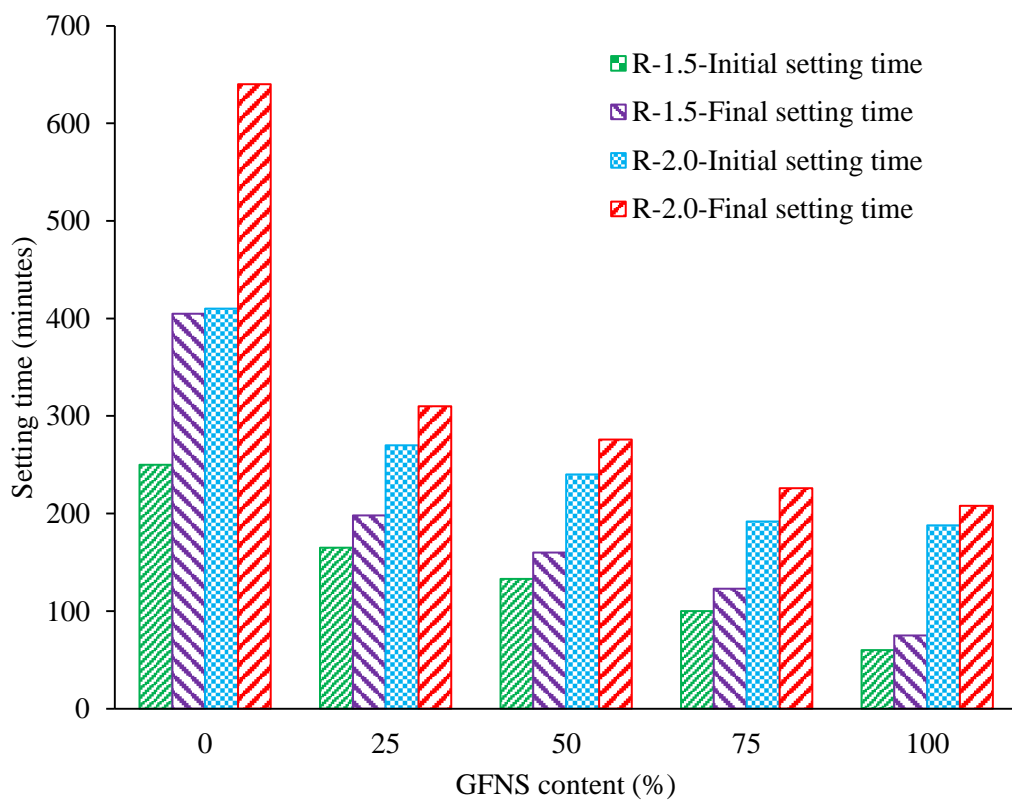
Fig. 3.3 Relationship between setting time and GFNS content in geopolymer paste.

It can be noticed from the Table 3.2 that an increase of GFNS content increased the SiO_2/Al_2O_3 ratio of the mixtures. In other words, the setting times of geopolymer paste decreased with the increase of SiO_2/Al_2O_3 ratio. The silica species ($[SiO_2(OH)_3]^-$ or $[SiO_2(OH)_2]^{2-}$) increased with the increase of SiO_2/Al_2O_3 ratio and successively accelerated the polycondensation between the silica species and $[Al(OH)_4]^-$, which in turn produced more alkaline aluminosilicate gel that reduced the setting times [57]. Moreover, setting time is also influenced by the Na_2O/Al_2O_3 ratio. It is noticed from Table 3.2 that the Na_2O/Al_2O_3 ratio increased with the increase of GFNS content that reduced the setting time of geopolymer paste. A similar trend of setting time results was reported by Balczár et al. [58]. Besides, GFNS contained a relatively higher proportion of MgO as compared to fly ash (Table 3.1). This increased the MgO/SiO_2 ratio and the MgO/Al_2O_3 ratio with the increase of GFNS (Table 3.2). It can be observed that setting time of geopolymer paste decreased with the increase of MgO/SiO_2 ratio and MgO/Al_2O_3 ratio. This is consistent with the finding of Fang et al. [59] reporting a decrease of setting time with the increase of MgO content.

Furthermore, it is seen from Fig. 3.3 that the geopolymer pastes having a SS/SH ratio of 2.0 (R-2.0) showed longer setting time for a particular GFNS content than the SS/SH ratio of 1.5 (R-1.5), though the paste of R-2.0 has a higher SiO_2/Al_2O_3 ratio than the paste of R-1.5. For instance, for 50% GFNS, mixtures with R-1.5 gave initial setting time of 133 minutes and final setting time of 160 minutes. On the other hand, for the same GFNS content (50%), the paste having R-2.0 gave initial setting time of 240 minutes and final setting time of 276 minutes. It can be noticed from Table 3.2 that for a particular GFNS content, the mixture having R-1.5 provided a higher molar ratio of Na_2O/SiO_2 and Na_2O/Al_2O_3 as compared to the R-2.0 mixtures. The increase of the Na_2O increased pH of the solution which resulted in a faster polycondensation and eventual faster setting of the mixtures having a SS/SH ratio of 1.5 as compared to those having SS/SH ratio of 2.0 [60]. As the mixture with SS/SH ratio of 2.5 took much longer time to set, the setting time test was not completed for that mixture. However, the similar trend was not observed by some researchers, where setting time decreased due to the increase of the SS/SH ratio. A higher SS/SH ratio increased the soluble silica, which accelerated the geopolymerization process and decreased the setting time [13].

3.3.2 Workability

The flow time and flow diameter were measured to determine workability of fresh geopolymer pastes. Flow time of the fresh paste mixture was measured using the flow cone method. Fig. 3.4 presents the influence of GFNS on flow time of paste for the R-2 mixtures. It can be noticed that flow time of geopolymer paste increased due to the increase of GFNS content by 25 and 50%. The control paste without GFNS showed a flow time of 1044 s, whereas 50% GFNS content showed the highest flow time of 1295 s. Flow time of 1112 s was measured for 25% GFNS contents. It was not possible to complete the flow cone test for the pastes containing 75 and 100% GFNS since the paste did not fully pass through the cone for these percentages of GFNS due to low workability, though the mixture was uniform and homogenous. For this reason, additional flow table test was conducted for all the mixtures to determine workability.
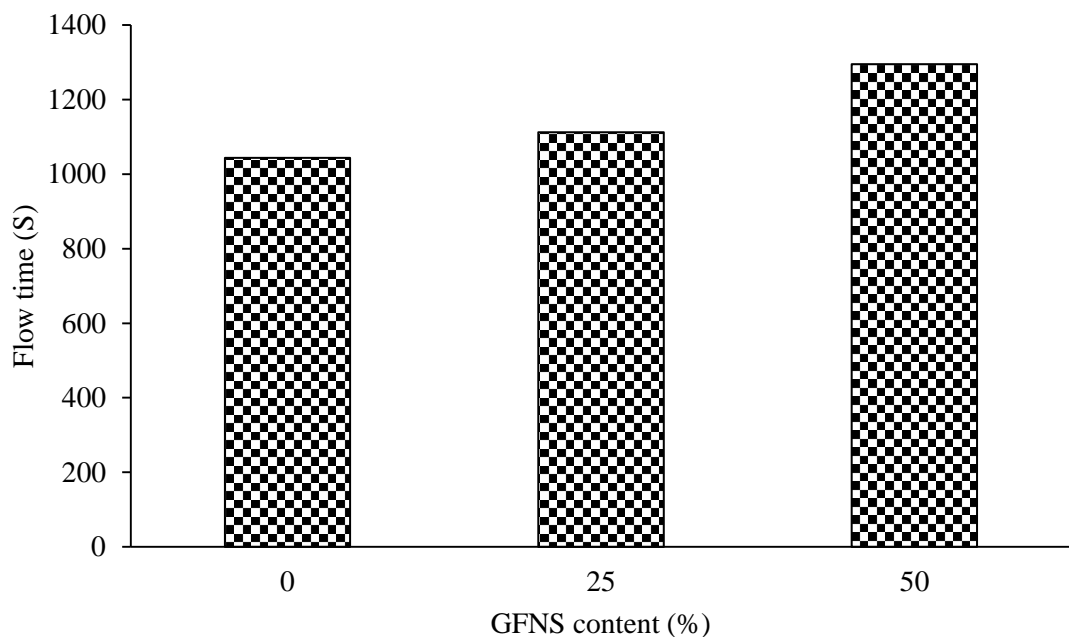
Fig. 3.4 Relationship between flow time and GFNS content in geopolymer paste (R-2.0 mixtures).
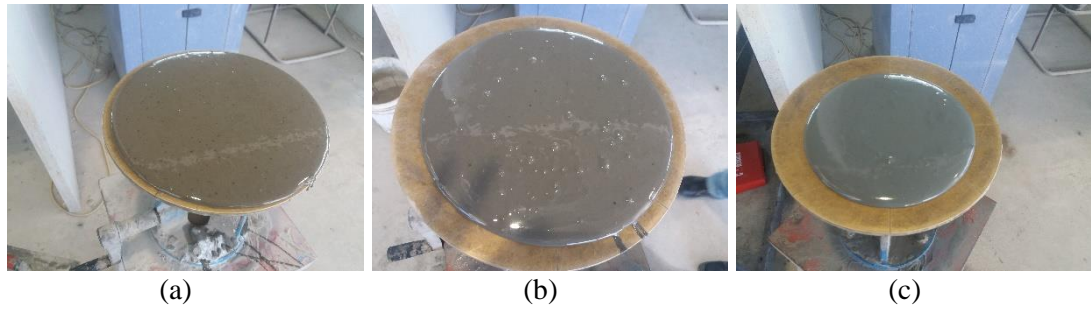
Fig. 3.5 Flow of geopolymer pastes (a) GFNS-0-R-2.0; (b) GFNS-50-R-2.0; and (c) GFNS-100-R-2.0.

Fig. 3.5 shows typical spreads of geopolymer pastes in the flow table test. It is noticed that an increase of GFNS content reduced the flow of geopolymer paste. Fig. 3.6 presents the effect of GFNS content on the flow of paste for SS/SH ratio of 1.5 (R-1.5), 2.0 (R-2.0) and 2.5 (R-2.5). For R-2.0 mixture, the control paste (without GFNS) provided the maximum flow of 140%, while the paste mixture with 100% GFNS exhibited the minimum flow of 110%. The flow values of 130, 129 and 125% were found for using 25, 50 and 75% GFNS, respectively. A similar trend can be seen for R-1.5 and R-2.5 mixtures. The increase of flow time and the reduction of flow value with the increase of GFNS are ascribed to the angular shape of GFNS particles as compared to the spherical fly ash particles (Fig. 3.1). Replacement of fly ash by GFNS increased the angular particles in the paste matrix. Therefore, the mobility of the paste decreased due to the increase of inter-particle friction by the angular shaped GFNS particles. The viscosity of the geopolymer reduced due to the ball-bearing mechanism of the spherical shaped fly ash particles and thus flow value of geopolymer was higher for the higher fly ash content [61]. Besides, the reaction of GFNS may also have contributed to the decrease of workability. Furthermore, the higher specific surface area of the GFNS than fly ash leads to the higher demand of liquid and in consequence, workability decreased.

Also, it can be seen from Fig. 3.6 that for the same GFNS content, in most of the cases, flow of geopolymer paste slightly decreased with the increase of the SS/SH ratio. For instance, for 50% GFNS content, the flow of the geopolymer paste were 135, 129 and 128% for using SS/SH ratio of 1.5, 2.0 and 2.5, respectively. Mixtures with higher amount of sodium silicate increased viscosity which decreased mobility for the particles and thus decreased the flow of paste [62].
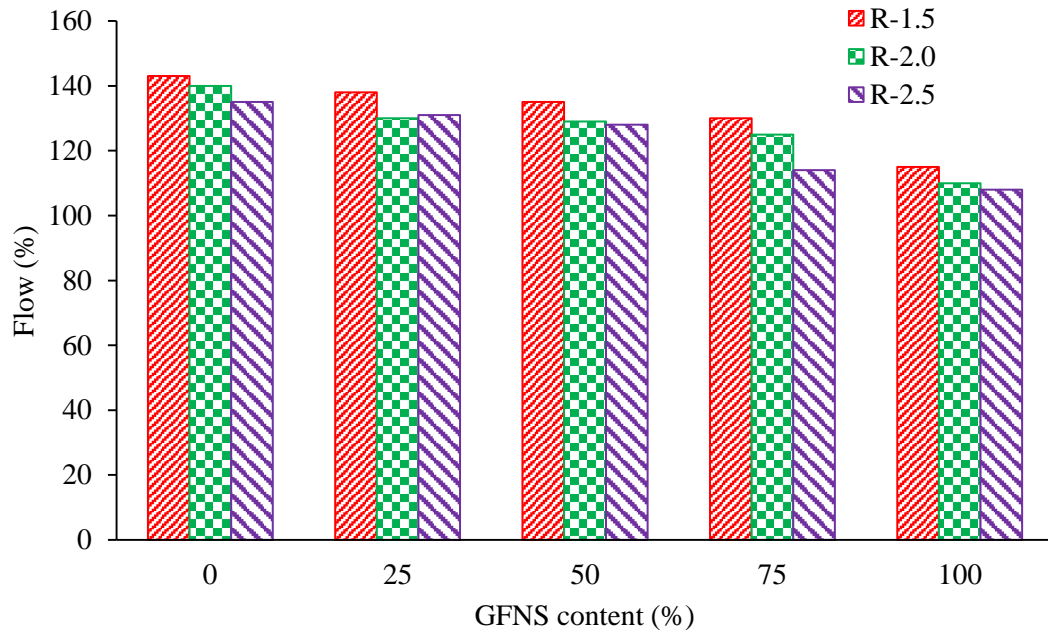
Fig. 3.6 Relationship between flow and GFNS content in geopolymer paste.

Moreover, water content plays a significant role on the workability of the mixtures. The molar ratio of H_2O/Na_2O of the mixtures varied from 12.22 to 13.13, which were within the range of 10 to 14, as reported by Hardjito [63] to produce workable fly ash geopolymers.

3.3.3 Soundness

Table 3.3 presents the influence of GFNS on the Le-Chatelier expansion of geopolymer paste for R-2.0 mixtures. It is seen that the expansion values varied between 0.13 and 0.18% where there was no definite trend for the increase of GFNS content (0-50%).

Table 3.3 Le-Chatelier expansions of geopolymer pastes

Sample ID	Expansion (%)
GFNS-0-R-2.0	0.18
GFNS-25-R-2.0	0.13
GFNS-50-R-2.0	0.15
GFNS-75-R-2.0	---
GFNS-100-R-2.0	---
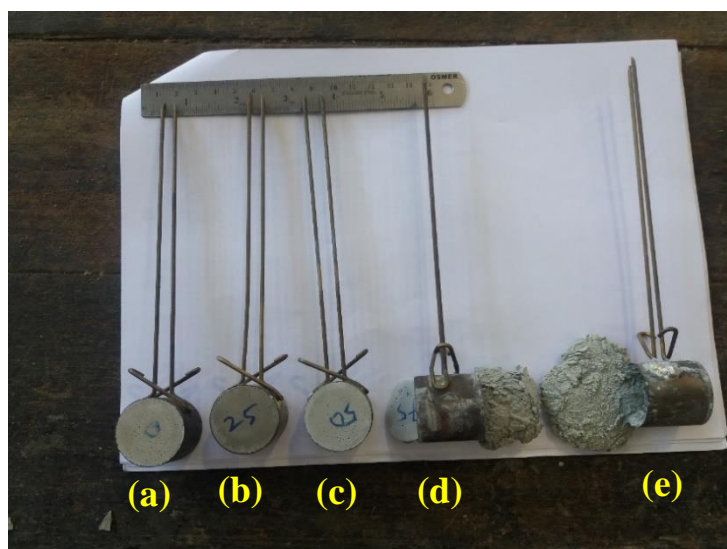
Fig. 3.7 Visual appearance of the samples after soundness test (a) GFNS-0-R-2.0, (b) GFNS-25-R-2.0, (c) GFNS-50-R-2.0, (d) GFNS-75-R-2.0, (e) GFNS-100-R-2.0.

It is also observed that expansions of all the mixtures were well below 5%, which is the limit of expansion of the Le-Chatelier test specified by Australian standard [64]. Therefore, although GFNS has a high magnesium content (Table 3.1), there was no significant effect of it on the expansion of geopolymer paste. From the XRD analysis of raw GFNS and GFNS-based paste, it was observed that the Mg content of GFNS exists in a crystalline forsterite form which will be discussed in the section 3.3.6. Magnesium is usually found to cause deleterious expansion by hydration if it exists in the form of mineral periclase [65]. Soundness test for using 75 and 100% GFNS was not possible due to deterioration of the specimen as shown in Fig. 3.7(d) and (e). This deterioration is attributed to the low early-age strength of the samples using 75 and 100% GFNS content as discussed in the compressive strength section. The low early strength of the samples using 75 and 100% GFNS were not capable to withstand at high water pressure of the soundness test.

3.3.4 Compressive strength

Compressive strength of the hardened geopolymar paste was determined after ambient curing and heat curing regimes. Fig. 3.8(a) shows the compressive strength of ambient cured geopolymer paste with age for SS/SH ratio of 2.0 (R-2.0) mixtures. Though setting time decreased with the increase of GFNS, compressive strength of the geopolymer paste slightly decreased with the increase of GFNS at the early age of 7

days. A similar observation of decreasing setting time and decreasing early strength with the increase of MgO was also reported by Fang et al. [59]. Since only a part of the magnesium content of GFNS reacted at the early period, compressive strength of the geopolymer paste decreased with the increase of GFNS. On the other hand, at 28 days and thereafter, the compressive strength significantly increased due to the rise of GFNS content of up to 75%. At 28 days, the paste mixtures having 0, 25, 50, 75 and 100% GFNS resulted in the compressive strengths of 33, 34, 37, 45 and 16 MPa, respectively. At 56 days, compressive strength increased by 17, 25 and 60% compared to that of the control (100% fly ash) paste sample for using 25, 50 and 75% GFNS, respectively. It can be seen that for all samples, compressive strength increased with the increase of age. However, in most cases, strength development rate slowed down after 56 days. At 28 days and thereafter, the use of 75% GFNS provided the maximum strength as compared to the other proportions of GFNS. Thus, 75% GFNS can be considered as the optimal content which gave the highest strength for ambient curing condition.
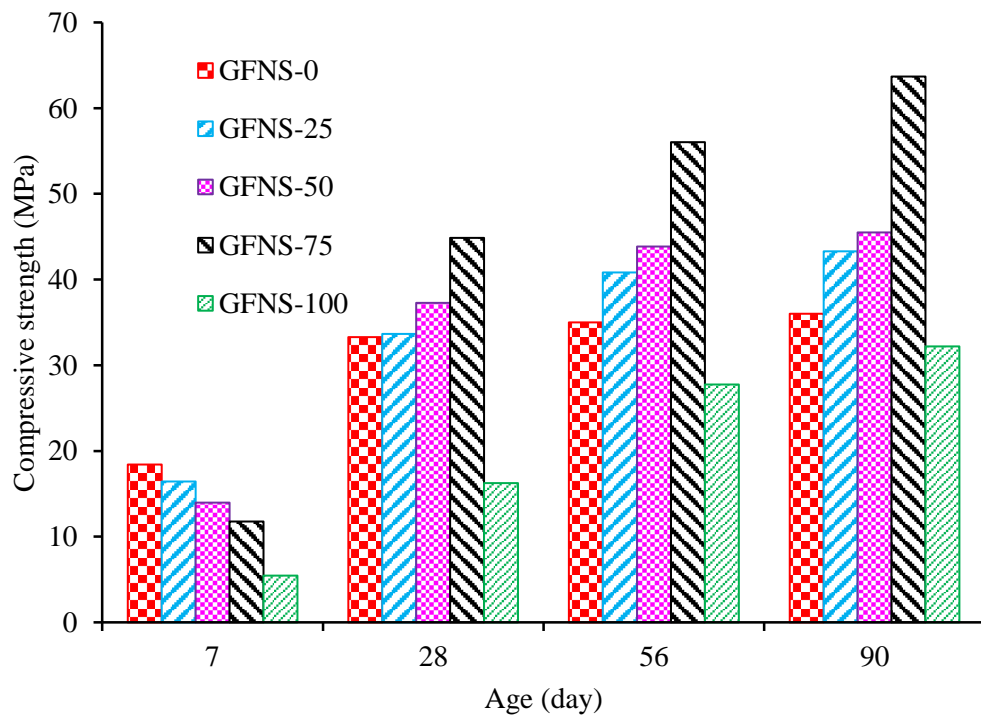
(a)
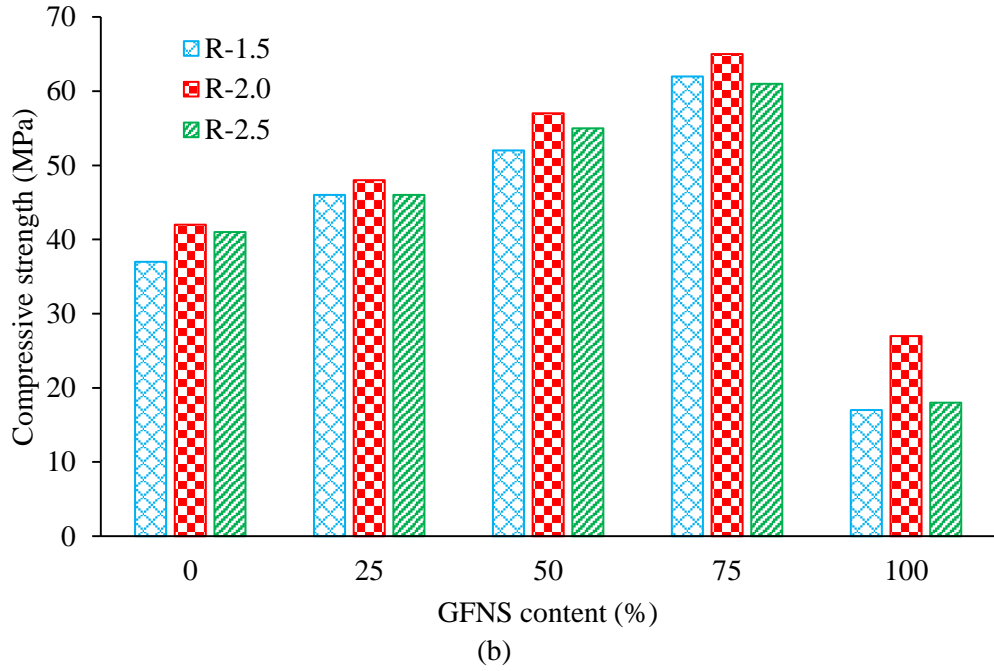
Fig. 3.8 Compressive strength of geopolymer paste (a) ambient curing (R-2.0 mixtures); and (b) heat curing at 60 °C for 24 hours.

At 28 days and afterwards, the increase of compressive strength due to the use of GFNS is ascribed to the development of alkaline aluminosilicate gel. Formation of the aluminosilicate gel is highly influenced by the alkaline solution and chemical constituents of the source materials. It can be observed from Table 3.2 that increase in GFNS content increased the SiO_2/Al_2O_3 ratio of the paste mixtures. In other words, the compressive strength of the geopolymer paste increased with the increase of SiO_2/Al_2O_3 ratio from 5.004 (GFNS-0-R-1.5) to 13.111 (GFNS-75-R-1.5) for SS/SH ratio of 1.5, from 5.063 (GFNS-0-R-2.0) to 13.280 (GFNS-75-R-2.0) for SS/SH ratio of 2.0 and from 5.104 (GFNS-0-R-2.5) to 13.401 (GFNS-75-R-2.5) for SS/SH ratio of 2.5. A higher percentage of Si enhances the formation of silicate oligomers as well as effective involvement of Al and thus, increased compressive strength of geopolymer [57]. In addition, compressive strength of geopolymer also increased with the increase of MgO/SiO_2 ratio and MgO/Al_2O_3 ratio for the use of up to 75% GFNS (Table 3.2). This is because the dissolved Mg^{2+} ions can react with Si-O-Si or Al-O-Si bonds and form M-(A)-S-H gel or hydrotalcite-like phases, subsequently hindering the precipitation of brucite [21]. Therefore, in the FA-GFNS geopolymerization process, Mg reacted with Si-O-Si, Al-O-Al or Al-O-Si bonds and developed sodium magnesium aluminosilicate hydrate (N-M-A-S-H) gel as described in Eqs. 3.1 and 3.2,

and hence increased compressive strength. The EDS results confirmed formation of N-M-A-S-H gel as discussed later in the section 3.3.5.

The N-M-A-S-H gel also hindered the precipitation of the brucite, thereby did not increase expansion in the Le-chatelier test as presented in the section 3.3.3. Winnefeld et al. [19] reported that sodium metasilicate activated slag with higher MgO content increased the hydration products and thus, reduced porosity and increased compressive strength. It was shown that in WG ($Na_2SiO_3.5H_2O$) activated slag paste, as the MgO content of the slag increased from 8% to 13%, the volume of hydrates increased by 9% and compressive strength increased by 50% to 80% at 28-days and later [18]. Besides, the compressive strength of the geopolymer increased with the increase of the Na_2O/SiO_2 ratio from 0.106 (GFNS-0-R-1.5) to 0.111 (GFNS-75-R-1.5) for SS/SH ratio of 1.5, from 0.102 (GFNS-0-R-2.0) to 0.108 (GFNS-75-R-2.0) for SS/SH ratio of 2.0 and from 0.100 (GFNS-0-R-2.5) to 0.105 (GFNS-75-R-2.5) for SS/SH ratio of 2.5. A higher Na_2O content can result in higher strength development in the long term [66]. The binding mechanism of geopolymer improved with the increase of Na_2O and hence, higher molar ratio of Na_2O/SiO_2 provided higher compressive strength [67]. Though the increase of Na_2O/SiO_2 ratio was very small, the increases of SiO_2/Al_2O_3, MgO/SiO_2 and MgO/Al_2O_3 ratios were significant due to the use of GFNS. Therefore, SiO_2/Al_2O_3, MgO/SiO_2 and MgO/Al_2O_3 ratios, increased by the increase of GFNS which played a significant role to produce alkaline aluminosilicate gel.

Fig. 3.8(b) shows compressive strength of the heat cured geopolymer paste. It can be noticed that for all SS/SH ratios, the compressive strength significantly increased due to the rise of GFNS content of up to 75%. For instance, compressive strengths of the pastes using SS/SH ratio of 2.0 (R-2.0) were 42, 48, 57, 65 and 27 MPa for 0, 25, 50, 75 and 100% GFNS, respectively. Thus, compressive strength increased by 14, 36 and 55% as compared to the control mixture for using 25, 50 and 75% GFNS, respectively. The increase of compressive strength is ascribed to the increase of the ratio of the SiO_2/Al_2O_3, Na_2O/SiO_2, MgO/SiO_2 and MgO/Al_2O_3 as discussed above.

Moreover, it can be seen from Fig. 3.8(b) that for the same GFNS content, compressive strength of geopolymer paste slightly increased as the SS/SH ratio increased from 1.5 to 2.0. For instance, for 75% GFNS content, compressive strength of the geopolymer

paste increased from 62 MPa to 65 MPa as the SS/SH ratio increased from 1.5 to 2.0. This increase of strength is also attributed to the increase of SiO_2/Al_2O_3 ratio of R-2.0 mixture compared to R-1.5 mixture as discussed before. On the other side, mixtures having a SS/SH ratio of 2.5 showed slightly lower strength as compared to the mixture with SS/SH ratio of 2.0, though the mixtures of SS/SH ratio of 2.5 have high SiO_2/Al_2O_3 ratio as compared to the corresponding mixtures of SS/SH ratio of 2.0. As the SS/SH ratio increased, sodium hydroxide decreased as compared to sodium silicate content. The low amount of sodium hydroxide made the mixture less alkaline, which reduced the polymerization rate as well as the strength of the geopolymer paste [68]. Therefore, the SS/SH ratio of 2.0 can be considered as optimum SS/SH ratio which provided the maximum strength.

It can be noticed from Fig. 3.8(a) and (b) that up to 75% GFNS content, the heat cured samples gave higher strength than the ambient cured samples. Compressive strength of the heat cured samples using SS/SH ratio of 2.0 were 27, 41, 54 and 44% higher than that of the 28-day ambient cured samples for using 0, 25, 50 and 75% GFNS, respectively. This is attributed to the high degree of geopolymerization at high temperature, which increased the reaction products, precipitation and compactness of the geopolymer [22]. However, after 56 days of ambient curing, the compressive strengths of ambient cured samples were comparable to those of the heat cured samples.
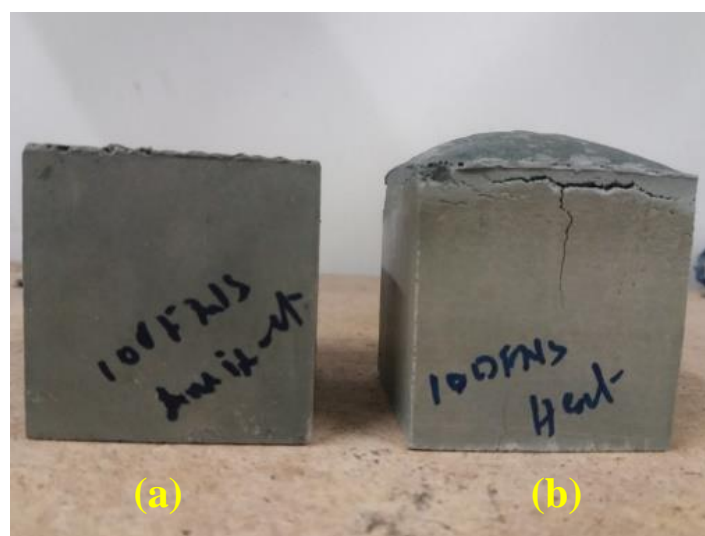
Fig. 3.9 GFNS-100-R-2.0 sample (a) ambient curing; and (b) heat curing at 60 °C for 24 hours.

Furthermore, it is seen from Fig. 3.8(a) and (b) that compressive strength of the geopolymer of 100% GFNS decreased as compared to the other mixtures for both ambient and heat curing, although the samples having 100% GFNS had the highest ratio of the SiO_2/Al_2O_3, Na_2O/SiO_2, MgO/SiO_2 and MgO/Al_2O_3 (Table 3.2). As GFNS has very low content of Al than Si, 100% GFNS sample without fly ash provided very high Si/Al ratio and Mg/Al ratio. The excess Si and Mg may cause development of unreactive silicate oligomers [57]. Besides, 100% GFNS samples with the highest Si/Al and Mg/Al had fast setting as compared to the other samples (Fig. 3.3). This fast setting may lead to the development of an incomplete geopolymer bond. The geopolymer products set quickly before the transformation of homogeneous structure as well as alumina silicate networking was low [69]. As a result, compressive strength of the sample using 100% GFNS was low. Moreover, Fletcher et al. [70] and Tho-In et al. [71] suggested that low-crosslinked aluminosilicate materials are formed at high Si/Al ratio leading to reduction of strength. It is also seen from Fig. 3.8(a) and (b) that for 100% GFNS, 56 and 90-day ambient cured strengths were higher than the strength of heat cured samples. This is attributed to the formation of cracks and bulging of the sample at high temperature using 100% GFNS, as shown in Fig. 3.9(b). At high temperature, the sample using 100% GFNS set very quickly, which caused the formation of cracks and consequently compressive strength reduced significantly. Therefore, for both ambient and heat curing, 75% GFNS can be considered as an optimal GFNS content which provided the highest compressive strength.

3.3.5 SEM and EDS analysis

The microstructures of GFNS-0-R-2.0 and GFNS-75-R-2.0 specimens were investigated after 56 days of ambient curing and heat curing at 60 °C for 24 hours. Fig. 3.10(a) and (b) presents the SEM images of the microstructure of GFNS-0-R-2.0 sample after ambient and heat curing, respectively, and the respective SEM images of GFNS-75-R-2.0 samples are shown in Fig. 3.11(a) and (b). It can be seen from the SEM images that the GFNS-75-R-2.0 sample having 75% GFNS content was less porous as compared to the GFNS-0-R-2.0 (control) sample. It is also seen that both heat cured samples showed higher cracks compared to the ambient cured samples. These cracks appeared due to shrinkage of the heat curing sample.
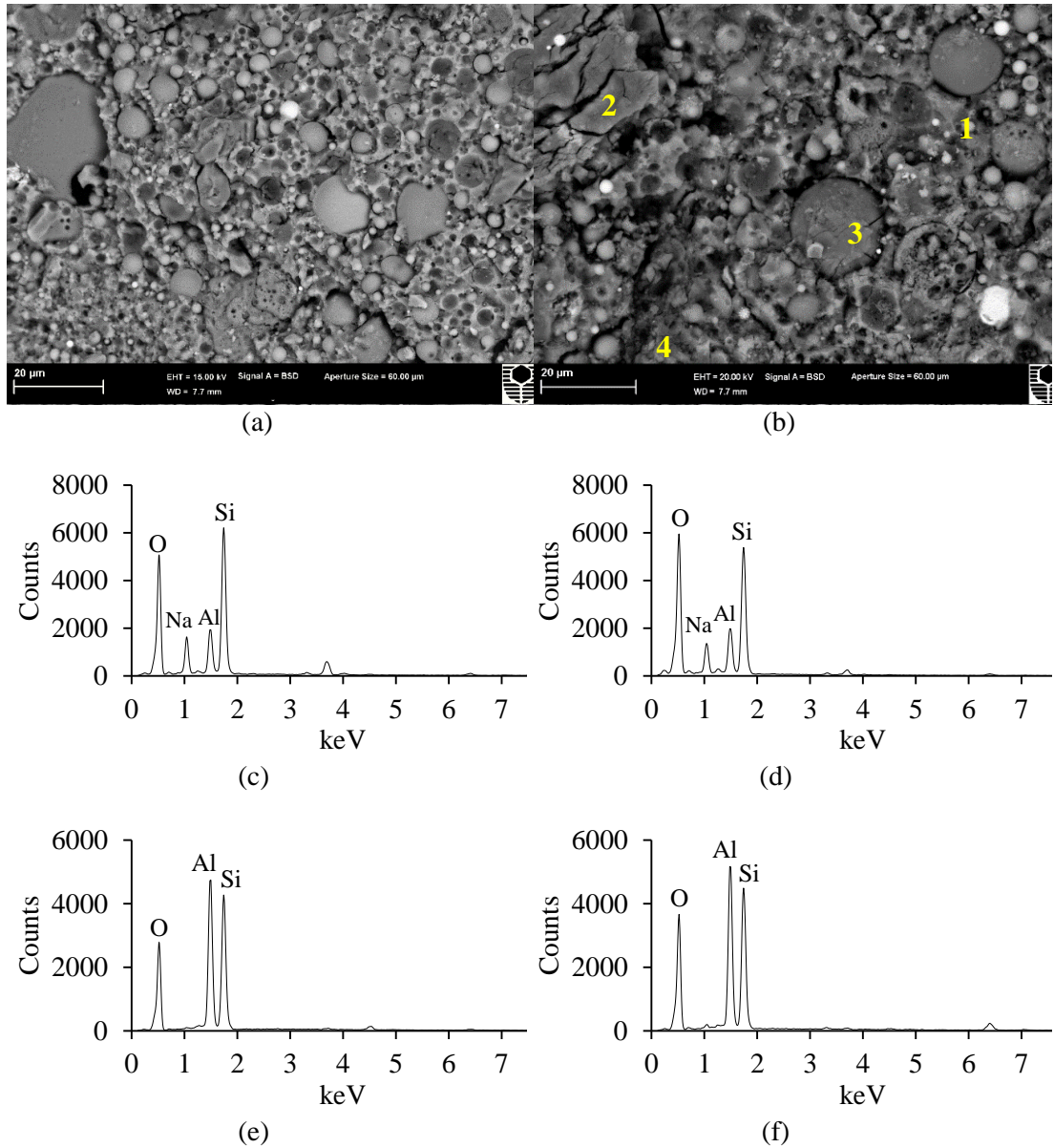
Fig. 3.10 SEM image and EDS spectra of GFNS-0-R-2.0 paste: (a) SEM image of ambient cured sample; (b) SEM image of heat cured sample, where 1 and 2 = N-A-S-H gel, 3 and 4 = unreacted or partially reacted fly ash; (c) EDS spectrum of point-1; (d) EDS spectrum of point-2; (e) EDS spectrum of point-3; (f) EDS spectrum of point-4.
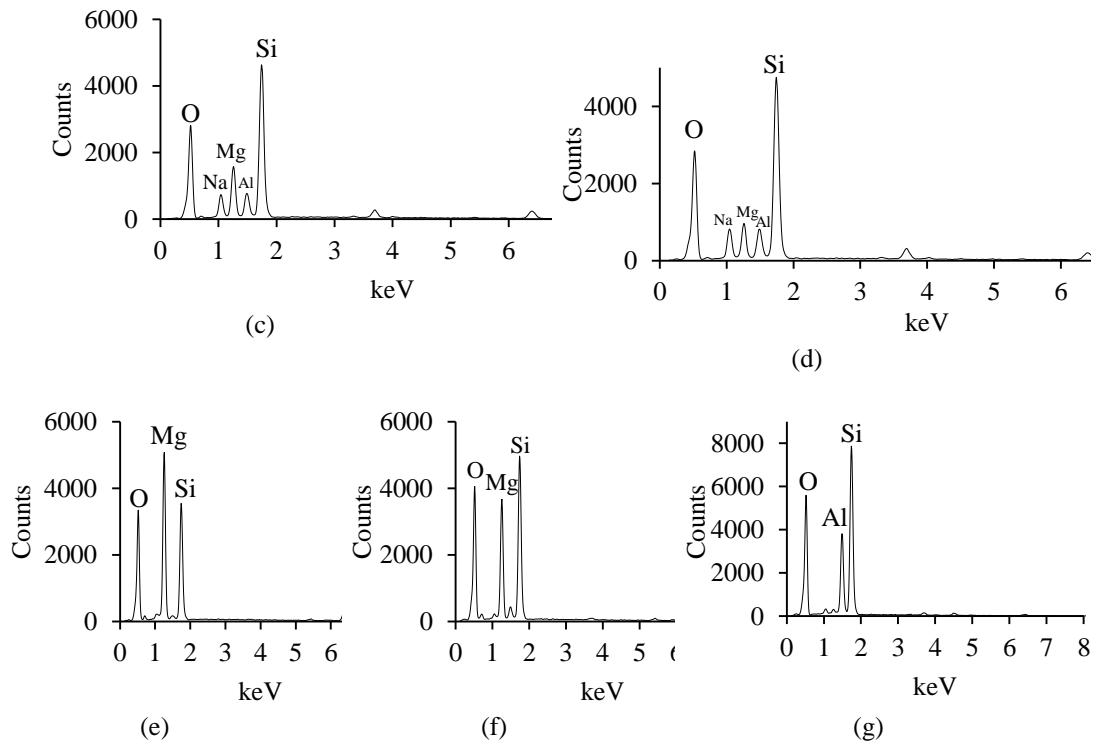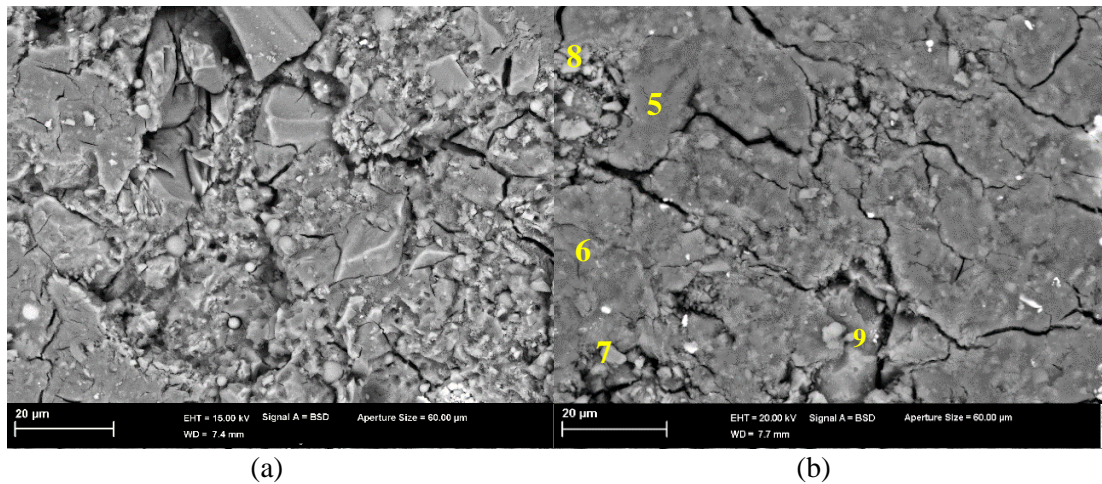
Fig. 3.11 SEM image and EDS spectra of GFNS-75-R-2.0 paste: (a) SEM image of ambient cured sample; (b) SEM image of heat cured sample, where 5 and 6 = N-M-A-S-H gel, 7 and 8 = unreacted or partially reacted GFNS, 9 = unreacted or partially reacted fly ash; (c) EDS spectrum of point-5; (d) EDS spectrum of point-6; (e) EDS spectrum of point-7; (f) EDS spectrum of point-8; (g) EDS spectrum of point-9.

Table 3.4 Chemical composition (atomic %) of the gel phase from EDS analysis

Sample ID	EDS point	Si	Al	Mg	Na	Si/Al	Mg/Al	Average Si/Al	Average Mg/Al
GFNS-0-R-2.0	1	16.5	5.3	0.4	7.5	3.113	0.075	2.945	0.085
	2	17.5	6.3	0.6	6.3	2.778	0.095		
GFNS-75-R-2.0	5	20.4	3.5	8.7	5.2	5.829	2.486	5.843	2.000
	6	20.5	3.5	5.3	6.1	5.857	1.514		

The EDS spectra of some selected points are also given in Figs. 3.10 and 3.11. The EDS spectra of point-1 and 2 show higher peaks of Na, Al and Si, which suggests the production of sodium aluminosilicate hydrate (N-A-S-H) gel in the GFNS-0-R-2.0 sample. Besides, the GFNS-0-R-2.0 sample has some unreacted or partially reacted fly ash particles (point-3 and 4), the shape of which is alike raw fly ash particles as shown in Fig. 3.1(b). Moreover, the EDS spectra of point-3 and 4 contain higher peaks of Si and Al.

On the other hand, the EDS spectrum of point-5 and 6 indicates higher peaks of Na, Mg, Al and Si, which indicates the formation of sodium magnesium aluminosilicate hydrate (N-M-A-S-H) gel in the GFNS-75-R-2.0 sample [42, 46]. The new gel phase is different from other alkali activated low magnesium or blast-furnace slags. In general, blast-furnace slag contained a higher proportion of calcium, which enhances the formation of calcium aluminosilicate hydrate (C-A-S-H) gel. For instance, in case of alkali activated GGBFS, which contains low magnesium and high calcium, usually C-A-S-H gel formed as a reaction product [13, 46].

The major chemical compositions of the gel phases, determined from EDS analysis are also given in Table 3.4. Two EDS points from the gel phase of each specimen were selected and the average value was recorded for Si/Al and Mg/Al ratio. It can be seen that Si/Al ratio of the gel phase increased from 2.945 to 5.843 and Mg/Al ratio increased from 0.085 to 2.000 for 75% substitution of fly ash by GFNS. This indicates the active participation of Si and Mg of GFNS to produce N-M-A-S-H gel in the geopolymerization process. Therefore, high Si/Al and Mg/Al ratios influenced the formation of sodium magnesium aluminosilicate hydrate (N-M-A-S-H) gel in the fly ash-GFNS based geopolymer, which yielded the denser microstructure and higher

strength as compared to the 100% fly ash geopolymer. Moreover, the GFNS-75-R-2.0 sample has some unreacted or partially reacted GFNS (point-7 and 8) and fly ash (point-9) particles, the shapes of which are same as those of the raw GFNS and fly ash particles. Besides, the unreacted GFNS particles of geopolymer may perform as micro-aggregates in the fly ash based system, thus also contributed to a denser structure and enhanced strength [71].

3.3.6 XRD analysis

The mineral contents of raw binder and heat cured geopolymer pastes having SS/SH ratio of 2.0 were determined by the quantitative X-ray diffraction (QXRD) method. Fig. 3.12(a) shows the XRD spectrum of all raw binders and paste samples of R-2.0 mixtures. For a better comparison of the XRD hump and peaks, the XRD spectrum of raw fly ash, raw GFNS, control paste (GFNS-0-R-2.0) and GFNS-75-R-2.0 paste are shown with the actual intensities in Fig. 3.12(b)-(e), respectively. The Corundum peaks of Fig. 3.12 are not associated with the original sample. It came from the corundum powder that was used as a standard reference substance for quantitative analysis. The results of QXRD analysis are shown in Table 3.5.
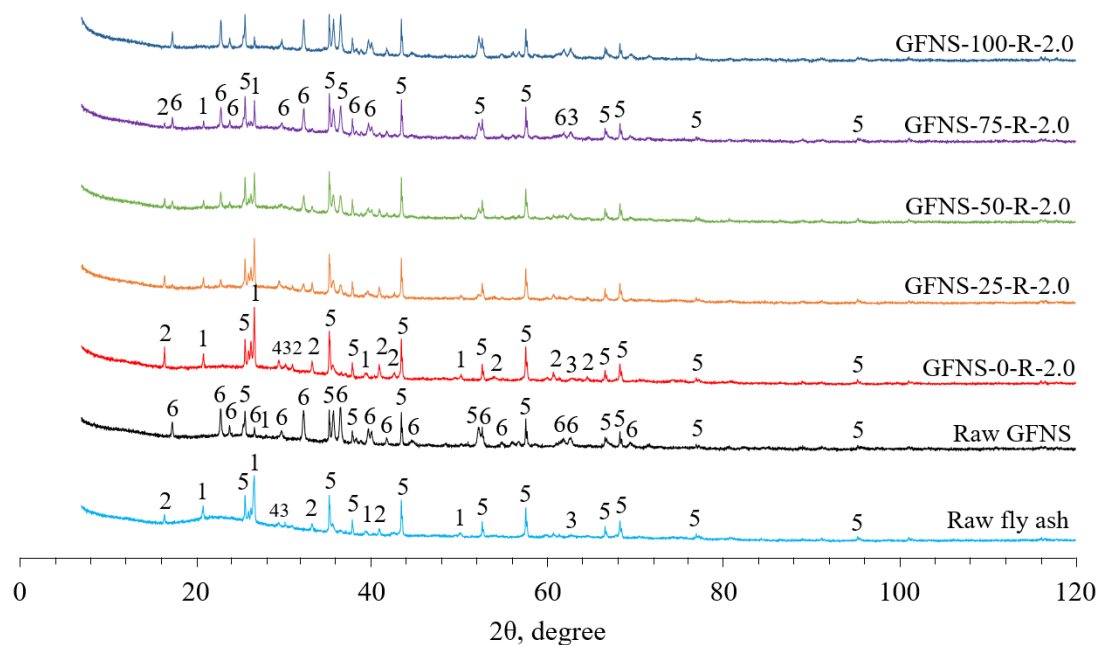
(a)
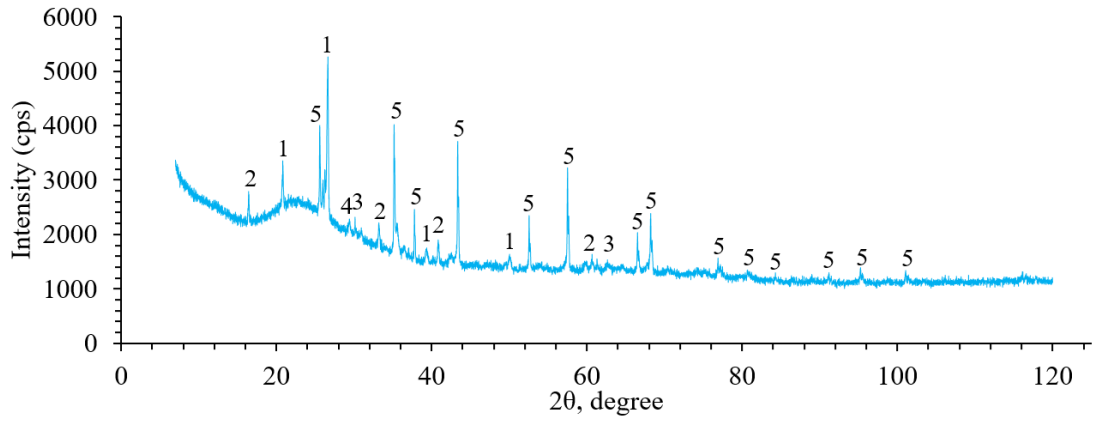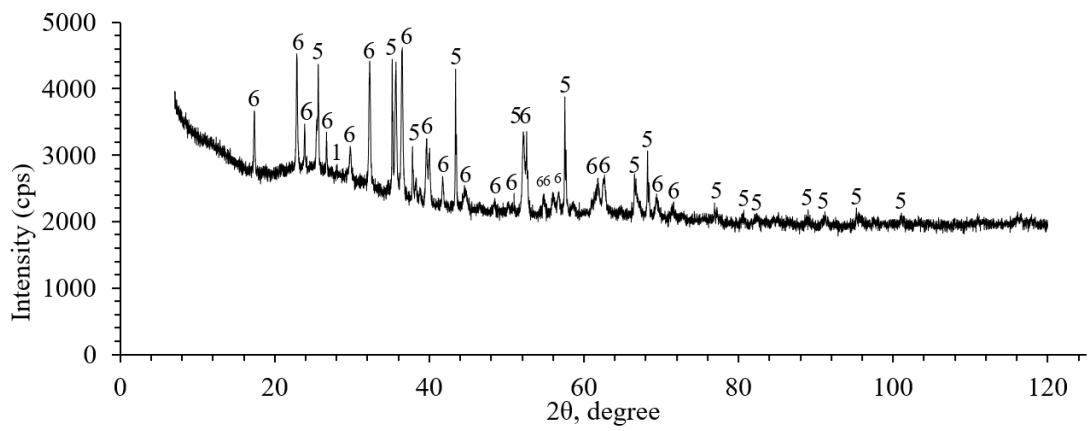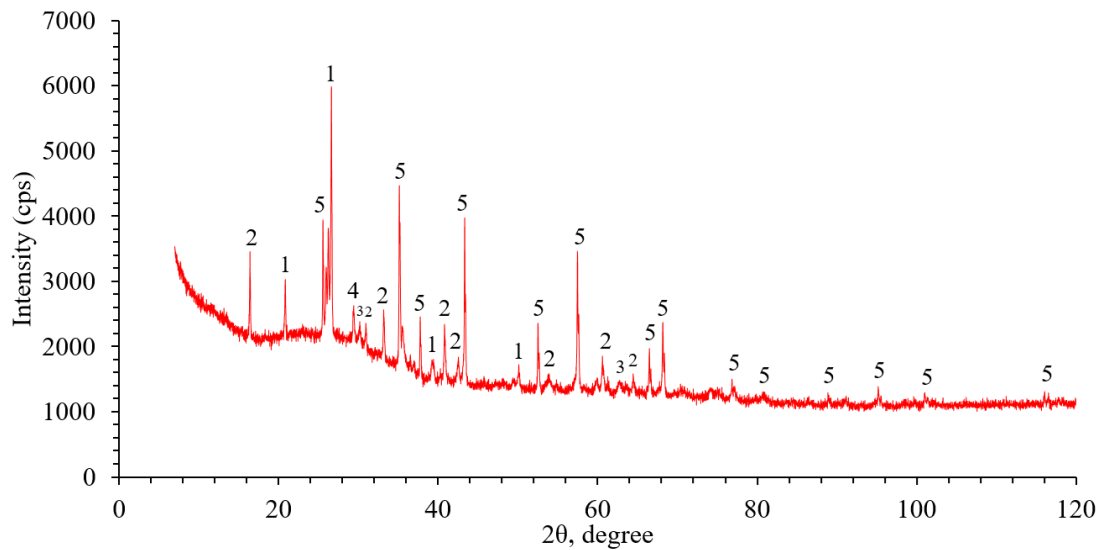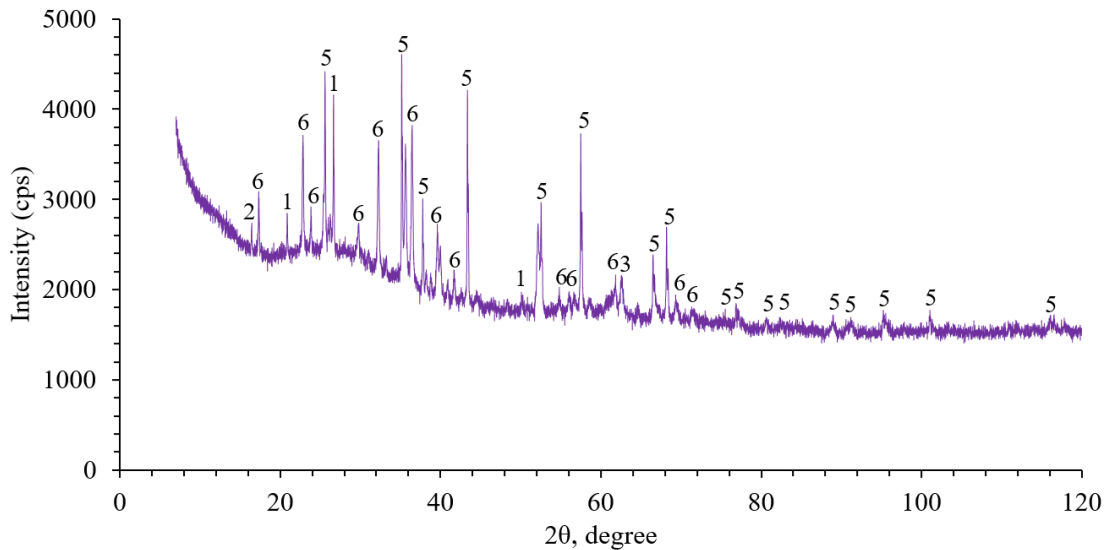
47

(b)

(c)

(d)

Legend
1-Quartz (SiO_2)
2-Mullite ($Al_6Si_2O_{13}$)
3-Magnetite [$Fe(Fe_{1.17}Ti_{0.54})O_4$)]
4-Calcite ($CaCO_3$)
5-Corundum (Al_2O_3)
6-Forsterite [$2(Mg_{0.90}Fe_{0.10})O.SiO_2$]

(e)

Fig. 3.12 XRD pattern (a) all raw binder and all geopolymer paste of R-2.0 mixtures; (b) raw fly ash; (c) raw GFNS; (d) GFNS-0-R-2.0; and (e) GFNS-75-R-2.0.

Table 3.5 Results of QXRD analysis

	Quartz (%)	Mullite (%)	Magnetite (%)	Calcite (%)	Forsterite (%)	Amorphous (%)
Raw FA	5.03	6.82	1.52	0.62	---	86.02
Raw GFNS	0.68	---	---	---	37.99	61.33
GFNS-0-R-2.0	5.00	12.33	2.24	1.23	---	79.20
GFNS-25-R-2.0	3.76	8.94	1.69	0.92	7.63	77.06
GFNS-50-R-2.0	2.44	5.87	1.29	0.04	14.29	76.06
GFNS-75-R-2.0	1.61	3.32	1.21	0.00	21.42	72.43
GFNS-100-R-2.0	0.52	---	---	0.00	28.02	71.46

It is seen from Fig. 3.12(b) and (c) that the XRD spectra of fly ash and GFNS have broad bands at $2\theta = 15°\text{-}30°$ and $2\theta = 20°\text{-}30°$, respectively. These broad bands indicate the presence of amorphous phase in the raw binder materials. The QXRD analysis reveals that the amorphous content of fly ash and GFNS were 86.02% and 61.33%, respectively (Table 3.5). The crystalline phases of fly ash comprised 5.03% quartz, 6.82% mullite, 1.52% magnetite and 0.62% calcite. On the other hand, the crystalline phases of GFNS included 37.99% forsterite and 0.62% quartz.

It can be noticed from Fig. 3.12(d) that a broad band existed in the XRD spectrum of GFNS-0-R-2.0 (control) paste sample, which indicates the presence of amorphous N-A-S-H gel as identified in the SEM images and EDS spectra. It is seen from Table 3.5 that the amorphous content of the GFNS-0-R-2.0 sample is 79.20%, whereas 5.00% quartz, 12.33% mullite, 2.24% magnetite and 1.23% calcite were present as the crystalline phases. It is also seen from the XRD spectrum of geopolymer paste that the peak intensity of mullite, quartz and magnetite decreased with the increase of GFNS due to the decrease of fly ash, as shown in Fig. 3.12(a). A similar phenomenon was also found in QXRD results, where the proportion of mullite, quartz and magnetite decreased with the increase of GFNS (Table 3.5). For instance, the quartz contents of the paste were 5.00, 3.76, 2.44, 1.61 and 0.52% for using 0, 25, 50, 75 and 100% GFNS, respectively. The peaks of calcite disappeared in the GFNS-75-R-2.0 sample which indicates that the crystalline contents were dissoluted by the highly alkaline solutions.

On the other hand, it is seen that the peak intensity as well as the proportion of forsterite increased with the increase of GFNS. However, though the geopolymer pastes having GFNS contained high crystalline phases, they had notable amounts of amorphous contents as well. The amorphous contents of the geopolymers were 77.06, 76.06, 72.43 and 71.46% for using 25, 50, 75 and 100% GFNS, respectively. The amorphous content of the geopolymer paste using GFNS are higher than that of the raw GFNS, which suggests the presence of N-M-A-S-H gel as identified in the section 3.3.5. Furthermore, it can be noticed from Fig. 3.12 that expansive brucite peak was not present in the geopolymer. This shows hindering of the precipitation of brucite by N-M-A-S-H gel as discussed in the section 3.3.4.

3.4 Summary

The effect of using GFNS with fly ash in geopolymer paste was investigated by setting time, workability, soundness, compressive strength and microstructure analysis. On the basis of acquired results, the following conclusions are drawn:

- Increase in GFNS content as a partial substitution of fly ash decreased the setting time of geopolymer paste. The decrease of SS/SH ratio from 2.0 to 1.5 increased the molar ratio of Na_2O/SiO_2 and Na_2O/Al_2O_3, which accelerated polycondensation resulting in a faster setting.

- Workability of geopolymer paste decreased due to the use of GFNS as a partial substitution of fly ash. The decrease of workability with the increase of GFNS is ascribed to the angular shape of GFNS particles as compared to the spherical shape of fly ash particles. Geopolymer pastes with less sodium silicate are less viscous which allowed more mobility for the particles and thus increased flow of the paste for a lower SS/SH ratio.

- The use of GFNS showed no adverse effect on the expansion of geopolymer despite its high magnesium content. This is because the Mg was found to be incorporated in the reaction product sodium magnesium aluminosilicate hydrate (N-M-A-S-H) gel.

- For both ambient and heat curing conditions, 75% GFNS can be considered as an optimal GFNS content which provided the highest compressive strength.

- The SEM images, EDS and XRD analysis revealed that the main reaction product of fly ash-GFNS geopolymer is amorphous sodium magnesium aluminosilicate hydrate gel, which improved the density of microstructure and contributed to the strength development by GFNS.

3.5 References

[1] E. Nimwinya, W. Arjharn, S. Horpibulsuk, T. Phoo-Ngernkham, A. Poowancum, A sustainable calcined water treatment sludge and rice husk ash geopolymer, J. Clean. Prod. 119 (2016) 128–134.

[2] M.S. Reddy, P. Dinakar, B.H. Rao, A review of the influence of source material's oxide composition on the compressive strength of geopolymer concrete, Microporous Mesoporous Mater. 234 (2016) 12–23.

[3] A. Fernández-Jiménez, J.G. Palomo, F. Puertas, Alkali-activated slag mortarsMechanical strength behaviour, Cem. Concr. Res. 33 (1999) 1313–1321.

[4] P. Duan, C. Yan, W. Zhou, D. Ren, Fresh properties, compressive strength and microstructure of fly ashgeopolymer paste blended with iron ore tailing under thermal cycle, Constr. Build. Mater. 118 (2016) 76-88.

[5] X. Liu, J. Jiang, H. Zhang, M. Li, Y. Wu, L. Guo, W. Wang, P. Duan, W. Zhang, Z. Zhang, 2020. Thermal stability and microstructure of metakaolin-based geopolymerblended with rice husk ash. Appl. Clay Sci. 196, 105769.

[6] S.K. Shill, S. Al-Deen, M. Ashraf, W. Hutchison, 2020. Resistance of fly ash based geopolymer mortar to both chemicals and high thermal cycles simultaneously. Constr. Build. Mater. 239, 117886.

[7] A. Mehta, R. Siddique, Sustainable geopolymer concrete using ground granulated blast furnace slag and rice husk ash: Strength and permeability properties, J. Clean. Prod. 205 (2018) 49-57.

[8] T. Bakharev, J.G. Sanjayan, Y.B. Cheng, Resistance of alkali-activated slag concrete to acid attack, Cem. Concr. Res. 33 (2003) 1607–1611.

[9] F. Puertas, T. Amat, A. Fernández-Jiménez, T. Vaˊzquez, Mechanical and durable behaviour of alkaline cement mortars reinforcedwith polypropylene fibres, Cem. Concr. Res. 33 (2003) 2031–2036.

[10] C. Ruiz-Santaquiteria, J. Skibsted, A. Fernández-Jiménez, A. Palomo, Alkaline solution/binder ratio as a determining factor in the alkaline activation of aluminosilicates, Cem. Concr. Res. 42 (2012) 1242–1251.

[11] K. Gao, K.L. Lin, D. Wang, C.L. Hwang, H.S. Shiu, Y.M. Chang, T.W. Cheng, Effects SiO_2/Na_2O molar ratio on mechanical properties and the microstructure of nano-SiO_2 metakaolin-based geopolymers, Constr. Build. Mater. 53 (2014) 503–510.

[12] P. Chindaprasirt, P. De Silva, K. Sagoe-Crentsil, S. Hanjitsuwan, Effect of SiO_2 and Al_2O_3 on the setting and hardening of high calcium fly ash-based geopolymer systems, J. Mater. Sci. 47 (2012) 4876–4883.

[13] P. Nath, P.K. Sarker, Effect of GGBFS on setting, workability and early strength properties of fly ash geopolymer concrete cured in ambient condition, Constr. Build. Mater. 66 (2014) 163–171.

[14] P. Nath, P.K. Sarker, Use of OPC to improve setting and early strength properties of low calcium fly ash geopolymer concrete cured at room temperature, Cem. Concr. Compos. 55 (2015) 205–214.

[15] E. Mohseni, Assessment of Na_2SiO_3 to NaOH ratio impact on the performance of polypropylene fiber-reinforced geopolymer composites, Constr. Build. Mater. 186 (2018) 904–911.

[16] P. Chindaprasirt, T. Chareerat, V. Sirivivatnanon, Workability and strength of coarse high calcium fly ash geopolymer, Cem. Concr. Compos. 29 (2007) 224–229.

[17] I. Ozer, S. Soyer-Uzun, Relations between the structural characteristics and compressive strength in metakaolin based geopolymers with different molar Si/Al ratios, Ceram. Int. 41 (2015) 10192–10198.

[18] M.B. Haha, B. Lothenbach, G. Le Saout, F. Winnefeld, Influence of slag chemistry on the hydration of alkali-activated blast-furnace slag - Part I: Effect of MgO, Cem. Concr. Res. 41 (2011) 955–963.

[19] F. Winnefeld, M. B. Haha, G. Le Saout, M. Costoya, S.C. Ko, B. Lothenbach, Influence of slag composition on the hydration of alkali-activated slags, J. Sustain. Cem. Mater. 4 (2014) 85–100.

[20] S.A. Bernal, N.R. San, R.J. Myers, R. Mejía De Gutiérrez, F. Puertas, J.S.G. Van Deventer, J.L. Provis, MgO content of slag controls phase evolution and structural changes induced by accelerated carbonation in alkali-activated binders, Cem. Concr. Res. 57 (2014) 33–43.

[21] A.F. Abdalqader, F. Jin, A. Al-Tabbaa, Characterisation of reactive magnesia and sodium carbonate-activated fly ash/slag paste blends, Constr. Build. Mater. 93 (2015) 506–513.

[22] P. Rovnaník, Effect of curing temperature on the development of hard structure of metakaolin-based geopolymer, Constr. Build. Mater. 24 (2010) 1176–1183.

[23] Y.C. Choi, S. Choi, 2015, Alkali-silica reactivity of cementitious materials using ferro-nickel slag fine aggregates produced in different cooling conditions, Constr. Build. Mater. 99 (2015) 279–287.

[24] Y. Huang, Q. Wang, M. Shi, Characteristics and reactivity of ferronickel slag powder, Constr. Build. Mater. 156 (2017) 773–789.

[25] Q.D. Nguyen, M.S.H Khan, A. Castel, T. Kim, 2019. Durability and microstructure properties of low-carbon concrete incorporating ferronickel slag sand and fly ash. J. Mater. Civ. Eng. 31(8), 04019152.

[26] J. Sun, J. Feng, Z. Chen, Effect of ferronickel slag as fine aggregate on properties of concrete, Constr. Build. Mater. 206 (2019) 201–209.

[27] N. Lemonis, P.E. Tsakiridis, N.S. Katsiotis, S. Antiohos, D. Papageorgiou, M.S. Katsiotis, M. Beazi-Katsioti, Hydration study of ternary blended cements containing ferronickel slag and natural pozzolan, Constr. Build. Mater. 81 (2015) 130–139.

[28] M.A. Rahman, P.K. Sarker, F.U.A. Shaikh, A.K. Saha, Soundness and compressive strength of Portland cement blended with ground granulated ferronickel slag, Constr. Build. Mater. 140 (2017) 194–202.

[29] B. Li, B. Huo, R. Cao, S. Wang, Y. Zhang, Sulfate resistance of steam cured ferronickel slag blended cement mortar, Cem. Concr. Compos. 96 (2019) 204–211.

[30] M. Zhai, H. Zhu, G. Liang, Q. Wu, C. Zhang, S. Hua, Z. Zhang, 2020. Enhancing the recyclability of air-cooled high-magnesium ferronickelslag in cement-based materials: A study of assessing soundness through modifying method. Constr. Build. Mater. 261, 120523.

[31] T. Yang, Z. Zhang, H. Zhu, X. Gao, C. Dai, Q. Wu, Re-examining the suitability of high magnesium nickel slag as precursors for alkali-activated materials, Constr. Build. Mater. 213 (2019) 109–120.

[32] R. Cao, Z. Jia, Z. Zhang, Y. Zhang, N. Banthia, Leaching kinetics and reactivity evaluation of ferronickel slag in alkaline conditions, Cem. Concr. Res. 137 (2020), 106202.

[33] K. Komnitsas, L. Yurramendi, G. Bartzas, V. Karmali, E. Petrakis, Factors affecting co-valorization of fayalitic and ferronickel slags for the production of alkali activated materials. Sci. Total Environ. 721 (2020), 137753.

[34] K. Komnitsas, D. Zaharaki, V. Perdikatsis, Geopolymerisation of low calcium ferronickel slags, J. Mater. Sci. 42 (2007) 3073–3082.

[35] K. Komnitsas, D. Zaharaki, G. Bartzas, Effect of sulphate and nitrate anions on heavy metal immobilisation in ferronickel slag geopolymers, Appl. Clay Sci. 73 (2013) 103–109.

[36] K. Komnitsas, D. Zaharaki, V. Perdikatsis, Effect of synthesis parameters on the compressive strength of low-calcium ferronickel slag inorganic polymers, J. Hazard. Mater. 161 (2009) 760–768.

[37] H. Xu, J.S.J.V. Deventer, The geopolymerisation of alumino-silicate minerals." Int. J. Miner. Process. 59 (2000) 247–266.

[38] I. Maragkos, I.P. Giannopoulou, D. Panias, Synthesis of ferronickel slag-based geopolymers, Miner. Eng. 22 (2009) 196–203.

[39] Z. Hu, M. Wyrzykowski, P. Lura, 2020. Estimation of reaction kinetics of geopolymers at early ages. Cem. Concr. Res. 129, 105971.

[40] D. Dimas, I. Giannopoulou, D. Panias, Polymerization in sodium silicate solutions: a fundamental process in geopolymerization technology, J. Mater. Sci. 44 (2009) 3719–3730.

[41] J. Sefcik, A.V. McCormick, Thermochemistry of aqueous silicate solution precursors to ceramics. AIChE J. 43 (1997), 2773–2784.

[42] Z. Zhang, Y. Zhu, T. Yang, L. Li, H. Zhu, H. Wang, Conversion of local industrial wastes into greener cement through geopolymer technology: A case study of high-magnesium nickel slag, J. Clean. Prod. 141 (2017) 463–471.

[43] T. Yang, X. Yao, Z. Zhang, Geopolymer prepared with high-magnesium nickel slag: Characterization of properties and microstructure, Constr. Build. Mater. 59 (2014) 188–194.

[44] T. Yang, Q. Wu, H. Zhu, Z. Zhang, Geopolymer with improved thermal stability by incorporating high-magnesium nickel slag, Constr. Build. Mater. 155 (2017) 475–484.

[45] K. Sakkas, P. Nomikos, A. Sofianos, D. Panias, Utilisation of FeNi-Slag for the production of inorganic polymeric materials for construction or for passive fire protection, Waste and Biomass Valorization 5 (2014) 403–410.

[46] A. Bouaissi, L. Li, M.M.A.B. Abdullah, Q. Bui, Mechanical properties and microstructure analysis of FA-GGBS-HMNS based geopolymer concrete, Constr. Build. Mater. 210 (2019) 198–209.

[47] G. Springer, Compositional and structural variations in garnierites, Canadian Mineralogist, 12 (1974), 381-388.

[48] A.K. Saha, P.K. Sarker, Sustainable use of ferronickel slag fine aggregate and fly ash in structural concrete: Mechanical properties and leaching study, J. Clean. Prod. 162 (2017) 438–448.

[49] ASTM C191, Standard test methods for time of setting of hydraulic cement by Vicat needle, ASTM International, West Conshohocken, PA, 2008.

[50] ASTM C939, Standard test Method for flow of grout for preplaced-aggregate concrete (flow cone method), ASTM International, West Conshohocken, PA, 2010.

[51] ASTM C1437, Standard test method for flow of hydraulic cement mortar. ASTM International, West Conshohocken, PA, 2007.

[52] AS2350.5, Methods of testing Portland, blended and masonry cements-Method 5: Determination of soundness, Standards Australia, 2016.

[53] AS1012.9, Methods of testing concrete - compressive strength tests - concrete , mortar and grout specimens, Standards Australia, 2014.

[54] H.M. Rietveld, A profile refinement method for nuclear and magnetic structures, J. Appl. Crystallogr. 2 (1969) 65–71.

[55] A.A. Coelho, TOPAS and TOPAS-Academic: An optimization program integrating computer algebra and crystallographic objects written in C++, J. Appl. Crystallogr. 51 (2018) 210–218.

[56] R.J Hill, C.J. Howard, Quantitative phase analysis from neutron powder diffraction data using the Rietveld method, J. Appl. Crystallogr. 20 (1987) 467–474.

[57] S. Yaseri, G. Hajiaghaei, F. Mohammadi, M. Mahdikhani, R. Farokhzad, The role of synthesis parameters on the workability, setting and strength properties of binary binder based geopolymer paste, Constr. Build. Mater. 157 (2017) 534–545.

[58] I. Balczár, T. Korim, A. Dobrádi, Correlation of strength to apparent porosity of geopolymers - Understanding through variations of setting time, Constr. Build. Mater. 93 (2015) 983–988.

[59] Y.H. Fang, J.F. Liu, Y.Q. Chen, Effect of magnesia on properties and microstructure of alkali-activated slag cement, Water Sci. Eng. 4 (2011) 463–469.

[60] C.R. Kaze, J.N.Y. Djobo, A. Nana, H.K. Tchakoute, E. Kamseu, U.C. Melo, C. Leonelli, H. Rahier, Effect of silicate modulus on the setting, mechanical strength and microstructure of iron-rich aluminosilicate (laterite) based-geopolymer cured at room temperature, Ceram. Int. 44 (2018) 21442–21450.

[61] J.L. Provis, P. Duxson, J.S.J. van Deventer, The role of particle technology in developing sustainable construction materials, Adv. Powder Technol. 21 (2010) 2–7.

[62] S.M. Laskar, S. Talukdar, 2017. Development of ultrafine slag-based geopolymer mortar for use as repairing mortar. J. Mater. Civ. Eng. 29 (5), 04016292.

[63] D. Hardjito, Studies of fly ash-based geopolymer concrete, Dissertation, Curtin University, 2005. http://hdl.handle.net/20.500.11937/634.

[64] AS3972, General purpose and blended cements, Standards Australia, 2010.

[65] AS3582.2, Supplementary cementitious materials Part 2: Slag - Ground granulated blast- furnace, Standards Australia. 2016.

[66] K. Yang, J. Song, A.F. Ashour, E. Lee, Properties of cementless mortars activated by sodium silicate, Constr. Build. Mater. 22 (2008) 1981–1989.

[67] M. Chi, R. Huang, Binding mechanism and properties of alkali-activated fly ash/slag mortars, Constr. Build. Mater. 40 (2013) 291–298.

[68] Y. Cheng, M. Hongqiang, C. Hongyu, W. Jiaxin, S. Jing, L. Zonghui, Y. Mingkai, Preparation and characterization of coal gangue geopolymers, Constr. Build. Mater. 187 (2018) 318–326.

[69] R.H.A. Rahim, K.A. Azizli, Z. Man, T. Rahmiati, L. Ismail, Effect of solid to liquid ratio on the mechanical and physical properties of fly ash geopolymer without sodium silicate, Appl. Mech. Mater. 625 (2014) 46–49.

[70] R.A. Fletcher, K.J.D. MacKenzie, C.L. Nicholson, S. Shimada, The composition range of aluminosilicate geopolymers, J. Eur. Ceram. Soc. 25 (2005) 1471–1477.

[71] T. Tho-In, V. Sata, K. Boonserm, P. Chindaprasirt, Compressive strength and microstructure analysis of geopolymer paste using waste glass powder and fly ash, J. Clean. Prod. 172 (2016) 2892–2898.

CHAPTER 4: WORKABILITY, STRENGTH AND MICROSTRUCTURAL PROPERTIES OF GFNS BLENDED FLY ASH GEOPOLYMER MORTAR

The contents presented in this chapter were published in the following paper:

Kuri, J. C., Khan, M. N. N., & Sarker, P. K. (2020). Workability, strength and microstructural properties of ground ferronickel slag blended fly ash geopolymer mortar. Journal of Sustainable Cement-Based Materials, https://doi.org/10.1080/21650373.2020.1823905.

This chapter evaluates the workability, strength and microstructure of ambient cured geopolymer mortar using GFNS with fly ash. The fresh and hardened properties of geopolymer paste using GFNS with fly ash were presented in the previous chapter (Chapter-3). It is important to investigate the interaction of GFNS binder with aggregates. Therefore, fresh and mechanical properties and durability performance of geopolymer mortar made with sand, different percentages of ground ferronickel slag and fly ash were investigated in this chapter.

4.1 Overview

The production of Portland cement is considered as an energy intensive and greenhouse gas emitting process due to the decomposition of limestone and flaming of fossil fuels in the manufacturing process [1-3]. Geopolymer binders are developed as potential alternatives in order to decrease the environmental effect of Portland cement [4-6]. Geopolymers are inorganic polymers where a chemical reaction occur between the alkaline liquids and aluminosilicate solid precursors [7-9].

Ferronickel slag (FNS) is an industrial residue discharged as a by-product of the manufacturing process of ferronickel alloys [10]. The main sources of nickel are pentlandite, garnierite and laterite ores. The ore is usually smelted in an electric arc furnace to produce ferronickel. After completion of the primary reduction operation at a temperature between 700 °C and 800 °C, the nickel ore is melted at temperatures ranging from 1500 °C to 1600 °C. The molten by-product known as ferronickel slag is cooled by air or water [11]. The principal constituents of FNS are Si, Fe and Mg, in a combination of crystalline and non-crystalline minerals [12]. The physical characteristics of water-cooled FNS are suitable to utilize as fine aggregate in concrete

[13, 14]. Furthermore, since FNS has a notable content of amorphous silica, ground FNS (GFNS) shows reactivity when mixed with cement or an alkaline liquid [15-18]. Komnitsas et al. [19] investigated the reactivity of GFNS by leaching test. The authors found that high amounts of Si and Al dissolute in the leached solution, which indicated a higher reactivity of GFNS. Yang et al. [20] investigated the reactivity of different types of air-cooled and water-cooled GFNS by using the dissolution experiments. It was reported that the air-cooled GFNS shows lower reactivity compared to the commonly used source materials, such as fly ash and blast furnace slag. On the other hand, water-cooled GFNS showed high reactivity.

Komnitsas et al. [21-23] investigated the suitability of using low-Ca electric arc furnace GFNS for geopolymer synthesis. Yang et al. [24, 25] reported sodium magnesium aluminosilicate gel as the prime constituent of high magnesium nickel slag (HMNS) geopolymer. In another study, Yang et al. [20] showed magnesium silicate hydrate, calcium silicate hydrate, hydrotalcite and brucite as the reaction products of the NaOH activated HMNS geopolymer. Production of fly ash and GFNS blended geopolymer can decrease around 60% energy and CO_2 emission compared to conventional cement paste production [26].

The properties of geopolymer are highly dependent on the solid precursors [27, 28]. A substantial amount of by-product ferronickel slag is available for sustainable use in construction [29]. The GFNS used in this study was produced by the smelting of garnierite ore found in New Caledonia which possesses a substantial part of the world's FNS accumulation. Most of the previous studies were conducted for heat curing condition which is associated with high energy and cost. However, it is important to understand the effects of the GFNS content, other mix design variables and curing conditions on different properties of the product. Therefore, this study focused on determination of the workability, strength and sorptivity of ambient-cured geopolymer mortars using up to a large percentage of GFNS as an alternative precursor with fly ash and varying alkali activator contents. SEM, EDS and quantitative XRD analysis were conducted to investigate the reaction products of the produced geopolymer. The SEM images were analysed by ImageJ software to determine the volume of micro pores. Thus, the reaction products and microstructure were used to understand the macro properties of FA-GFNS mortars.

4.2 Experimental Work

4.2.1 Materials and mix proportions

Class F fly ash (FA) and GFNS were used as the solid precursors to produce geopolymer mortar. The granulated FNS was ground to fine powder using a laboratory ball mill. The density of the GFNS was 2.95 g/cm^3 and that of fly ash was 2.40 g/cm^3. It was found that the particle size of approximately 70% GFNS and 70% fly ash was almost same (less than 30 μm). However, the particle size of the remaining GFNS was lower as compared to remaining fly ash. This indicates the higher fineness of GFNS than fly ash. The Blaine's specific surface area of the GFNS and fly ash were 420 m^2/kg and 380 m^2/kg, respectively.

Local sand with a fineness modulus of 1.94 was used as fine aggregate for the geopolymer mortars. A mixture of liquid sodium silicate and 8M sodium hydroxide solution at the mass ratio of 2:1 was used as the alkali activator solution (AAS). The sodium silicate solution consisted of 29.4% SiO_2, 14.7% Na_2O and 55.9% water. The amount of alkaline activator solution was 40% or 45% of the mass of solid precursors.

The mixture proportions, adopted from Nath and Sarker [30], along with the oxide molar ratio, atomic molar ratio and water/binder ratio are given in Table 4.1. The molar ratio and water/binder ratio were calculated using the chemical constituents of precursors and alkaline activator solution. GFNS was used as 0, 25, 50 and 75% replacement of fly ash in the binder. Substitution of fly ash by 100% GFNS was not studied due to very low workability of this mortar. In Table 4.1, the mixtures are designated by a number representing the percentage of GFNS and A for 40% alkaline liquid or B for 45% alkaline liquid. For instance, GFNS-25-A denotes a mixture with 25% GFNS as a replacement of fly ash and 40% alkaline liquid.

The microstructure of geopolymer was investigated on the corresponding paste mixtures having the same percentages of precursors and the alkaline solution of mortar mixtures without the fine aggregate.

Table 4.1 Mix proportions of geopolymer mortars

Mix ID	Mortar mixture quantity (kg/m³)					Oxide molar ratio, (atomic molar ratio)						Water/ binder
	Fly ash	GFNS	Sand	SH[a]	SS[b]	Na$_2$O/ SiO$_2$, (Na/Si)	Na$_2$O/ Al$_2$O$_3$, (Na/Al)	H$_2$O/ Na$_2$O, (H/Na)	SiO$_2$/ Al$_2$O$_3$, (Si/Al)	MgO/ SiO$_2$, (Mg/Si)	MgO/ Al$_2$O$_3$, (Mg/Al)	
GFNS -0-A	733	0	1173	98	196	0.102, (0.204)	0.518, (0.518)	12.257, (12.257)	5.063, (2.531)	0.028 (0.028)	0.144 (0.072)	0.247
GFNS -25-A	550	183	117	98	196	0.104, (0.208)	0.652, (0.652)	12.457, (12.457)	6.271, (3.136)	0.195 (0.195)	1.226 (0.613)	0.247
GFNS -50-A	367	367	1173	98	196	0.106, (0.212)	0.890, (0.890)	12.664, (12.664)	8.417, (4.209)	0.374 (0.374)	3.146 (1.573)	0.247
GFNS -75-A	183	550	117	98	196	0.108, (0.216)	1.430, (1.430)	12.877, (12.877)	13.280, (6.640)	0.565 (0.565)	7.498 (3.749)	0.247
GFNS -0-B	733	0	113	110	220	0.113, (0.226)	0.578, (0.578)	12.361, (12.361)	5.136, (2.568)	0.027 (0.027)	0.144 (0.072)	0.279
GFNS -25-B	550	183	113	110	220	0.115, (0.230)	0.729, (0.729)	12.541, (12.541)	6.365, (3.182)	0.192 (0.192)	1.226 (0.613)	0.279
GFNS -50-B	367	367	1137	110	220	0.117, (0.234)	0.997, (0.997)	12.727, (12.727)	8.547, (4.274)	0.368 (0.368)	3.146 (1.573)	0.279
GFNS -75-B	183	550	1137	110	220	0.119, (0.238)	1.604, (1.604)	12.918, (12.918)	13.492, (6.746)	0.556 (0.556)	7.498 (3.749)	0.279

[a]Sodium hydroxide solution
[b]Sodium silicate solution

4.2.2 Specimen preparation and testing

To make geopolymer mortars, the solid precursors and saturated surface dry (SSD) sand were first dry-mixed in a Hobart mixer and then the premixed alkaline activator solution was added while mixing was continued till attainment of a uniform mixture. The fresh mortar mix was used for flow test to determine workability and to cast 50 mm cube specimens with compaction using a vibrating table. The specimens were demoulded at 24 hours after casting and cured at 20 ± 3 °C and 65 ± 5% relative humidity till testing.

To measure the workability of fresh mortar, flow test was conducted according to ASTM C1437 [31]. Compressive strength of hardened mortar was determined following AS 1012.9 [32] at the ages of 7, 28, 56 and 90 days.

To determine the porosity of mortar, the volume of permeable voids (VPV) test was performed according to ASTM C642 [33]. Discs of 50 mm thick were cut from 100

mm diameter cylindrical mortar samples after 56 days of curing. The oven-dry mass after drying at 110 °C for 24 hours, SSD mass after immersion in water for 48 hours, SSD mass after boiling for 5 hours and immersed apparent mass of the samples were recorded successively to determine VPV.

To measure the capillary suction of geopolymer mortar, sorptivity test was carried out following ASTM C1585 [34]. After 56 days of curing, 50 mm thick cylindrical discs were cut from 100 mm diameter cylindrical mortar specimens. The side surface of the cylindrical disc was sealed by a duct tape and the top surface was covered with a plastic sheet so that only bottom surface was exposed to water. The mass of the specimen was recorded before and after contact with water at selected time intervals. The rate of water absorption was taken as the sorptivity coefficient.

SEM images and EDS analysis were conducted in order to obtain insights of the reaction products. The SEM images were used to investigate the morphology, bonding between reaction product and the particles, micro cracks and pores. The SEM images were also used to determine the porosity of the specimen by using ImageJ software [35]. The porous portion was extracted from the SEM image by thresholding the image on the basis of the grey level histogram. The EDS results provided elemental compositions at various locations of the specimen. Dual-beam field emission scanning electron microscope (ZEISS NEON 40EsB FIB-SEM) was used for microstructure analysis which combined high resolution imaging with EDS and electron backscattered diffraction (EBSD).

The mineralogical analysis of the raw fly ash, GFNS and geopolymer were determined by the quantitative X-ray diffraction (QXRD) method. The XRD patterns of the specimens were collected by using the powder diffractometer D8 Advance (Bruker AXS, Germany). The analysis was conducted at 2 theta values of 7-120 degrees with a step size 0.015 degrees and measuring time of 0.7 Sec/step. The phases were identified by EVA 11.0 software using ICDD PDF4+ database. Then the relative weight proportion of the phases were determined by TOPAS [36] using Rietveld [37] full pattern analysis. Afterwards, the relative Rietveld weight proportions of the phases were converted to the absolute proportions by internal standard method [38] using TOPAS software.

4.3 Results and Discussion

4.3.1 Workability

The workability of fresh geopolymer mortar was measured by flow test as shown in Fig. 4.1. The influences of GFNS on the flow of mortars for 40% and 45% alkali activator liquid are plotted in Fig. 4.2. It is seen that the increase of GFNS has reduced the flow value of the mortar. In case of 40% alkaline liquid, the control mortar without GFNS showed the highest flow of 83%, whereas the flow decreased to 54% for using 75% GFNS. The flow values of mortars using 25% and 50% GFNS were 78% and 65%, respectively. A similar trend was noticed for 45% alkaline liquid, where 0%, 25%, 50% and 75% GFNS showed flow values of 110%, 93%, 85% and 73%, respectively. The reduction of flow due to the increase of GFNS is ascribed to the angular shape of GFNS particles. The angular shaped GFNS particles increased inter-particle friction and reduced the flow of mortar. On the other hand, the spherical shape of fly ash particles reduced the viscosity of the geopolymer by ball-bearings mechanism and increased the flow value [39]. Besides, the higher fineness of GFNS compared to that of fly ash increased the demand of liquid [40, 41] and consequently, flow of the mortar reduced with the increase of GFNS.

| (a) | (b) |

Fig. 4.1 Flow: (a) 100% fly ash (GFNS-0-B), (b) 75% GFNS with 25% fly ash (GFNS-75-B)
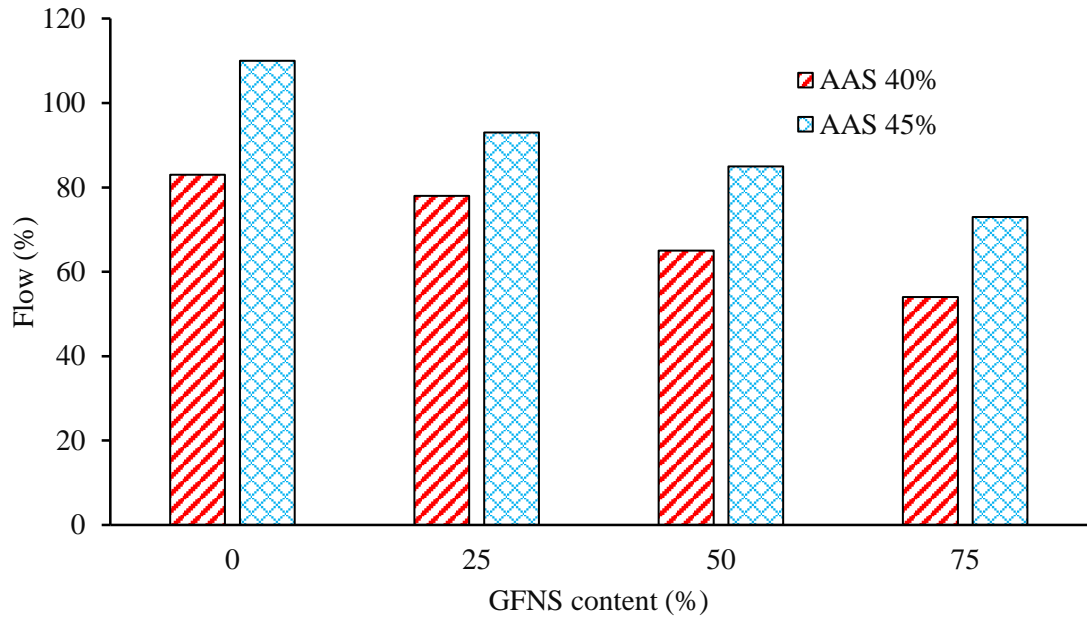
Fig. 4.2 Relationship between flow and GFNS content in geopolymer mortar

Moreover, it is noticed from Fig. 4.2 that the liquid content has a notable influence on the workability of geopolymer mortar. For the same GFNS content, flow of mortar increased as the liquid content increased from 40% to 45%. The increase of workability is ascribed to the increase of water to binder ratio as the liquid content increased. A similar trend of increase in flow with the increase of alkaline liquid was reported in literature [42, 43]. Furthermore, the H_2O/Na_2O molar ratio has a considerable influence on the workability of geopolymer. It can be noticed from Table 4.1 that the molar ratio of H_2O/Na_2O was within the range of 10 to 14 which is usually found to produce workable fly ash geopolymers, as reported by Hardjito [44].

4.3.2 Compressive strength

Fig. 4.3 presents the compressive strength development of geopolymer mortars with age. It was observed that the increasing of GFNS has decreased the compressive strength at the early age of 7 days. However, at 28 days and beyond, compressive strength of geopolymer mortar significantly increased due to the increase of GFNS of up to 75%. For instance, the 28-day compressive strengths of mortars using 40% alkaline liquid were 57 MPa, 65 MPa, 68 MPa and 75 MPa for using 0, 25, 50 and 75% GFNS, respectively. The corresponding 90-day strengths were 80 MPa, 86 MPa, 91 MPa and 96 MPa, respectively. It is seen that the use of 75% GFNS increased the compressive strength of mortar by 31%, 28% and 20% compared to that of the control

mortar at 28, 56 and 90 days, respectively. A similar trend was noticed for the mortars using 45% alkaline liquid, as shown in Fig. 4.3(b). It is observed that, for all the samples, compressive strength increased with the increase of age. However, the rate of strength increase slowed down after 56 days. It can be noticed from Fig. 4.3(a) that, for 40% alkaline liquid, the 90-day compressive strength increased by 8%, 13% and 20% compared to that of the control geopolymer mortar for using 25%, 50% and 75% GFNS, respectively. Besides, in the case of 45% alkaline liquid and same curing period of 90 days, compressive strength increased by 24%, 34% and 41% for using 25%, 50% and 75% GFNS, respectively. It is seen that, for both the liquid contents, 50% and 75% GFNS provided almost the same strength at 56 days. Furthermore, for 45% alkaline liquid, strength at a particular age for 75% GFNS was almost same as that for 50% GFNS. However, for both the liquid contents, 75% GFNS provided the maximum strength at 90 days of age. Therefore, GFNS contents of 75% can be considered as optimum which provided the maximum strength for 40% and 45%

(a)
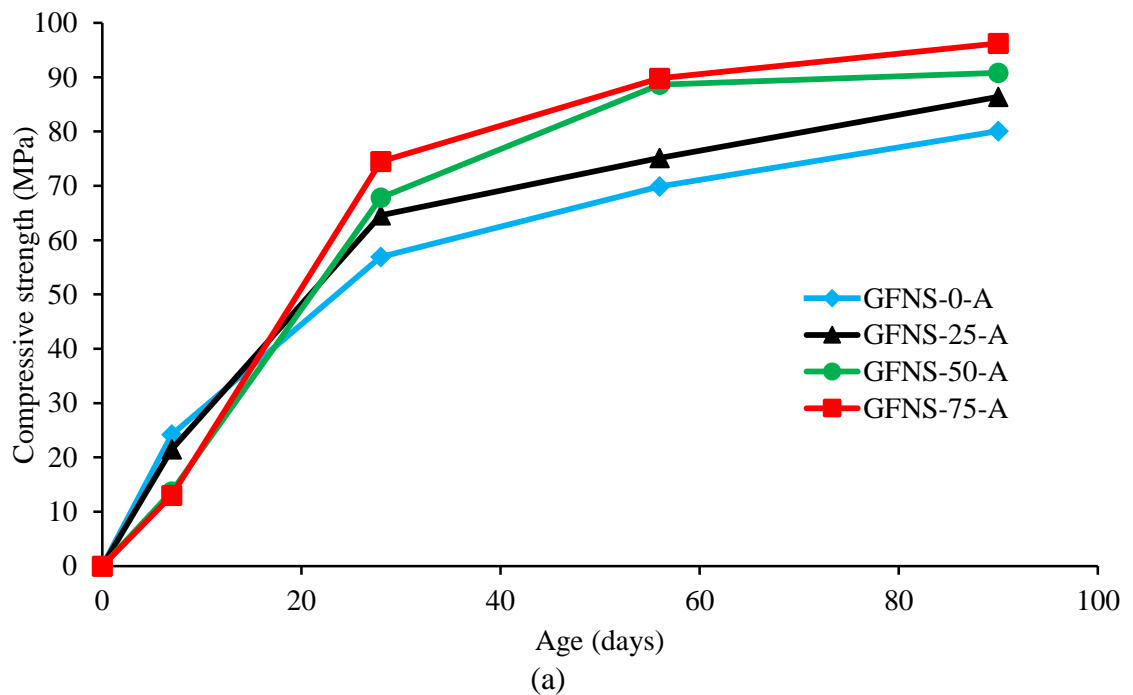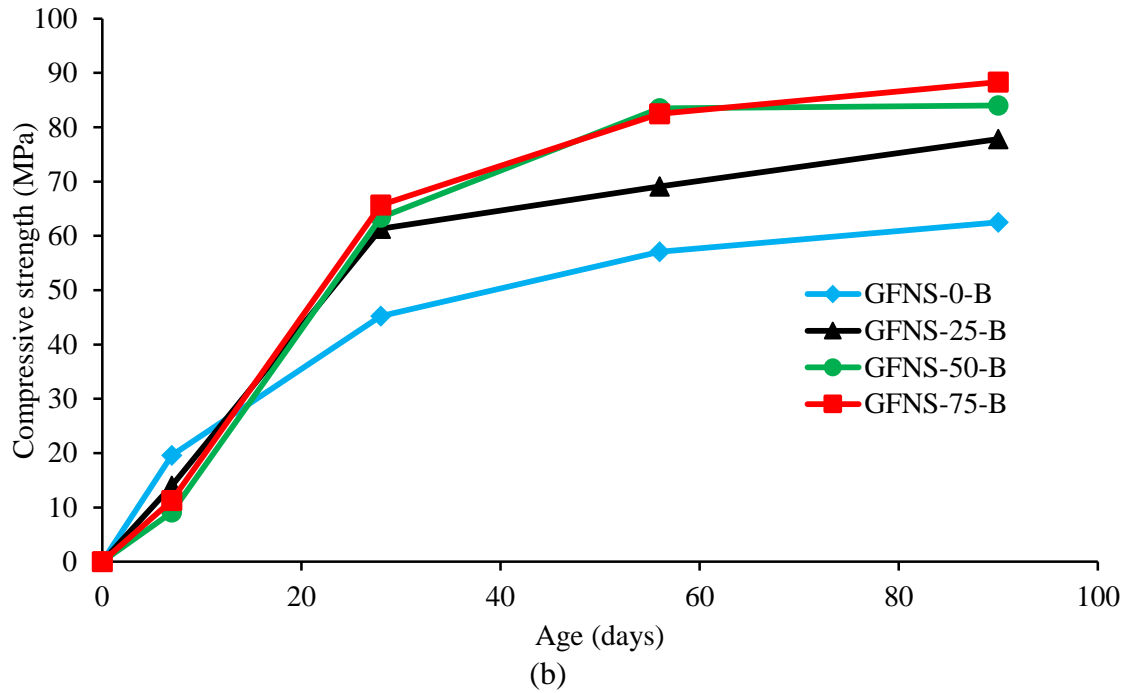
Fig. 4.3 Compressive strength of geopolymer mortar with different GFNS contents:

(a) 40% AAS, (b) 45% AAS

alkaline activator liquid. Furthermore, the density of the geopolymer mortar was determined at 56 days of age. Generally, the increasing trend of compressive strength correlated with the increasing trend of density of the mortar as the GFNS content increased. The density of mortars using 40% alkaline liquid were 2165, 2215, 2240 and 2280 kg/m^3 for the use of 0, 25, 50 and 75% GFNS, respectively. In case of 45% alkaline solution, the density were 2134, 2174, 2201 and 2254 kg/m^3 for using 0, 25, 50 and 75% GFNS, respectively. The rise of density of mortar due to the use of GFNS is ascribed to the higher density of GFNS as compared to fly ash. The significant increase of compressive strength of the mortar containing GFNS at 28 days and thereafter is ascribed to the formation of alkaline aluminosilicate gel which will be discussed further in the SEM and EDS analysis section. Moreover, chemical constituents of the precursor and alkaline liquid have significant effects on the production of aluminosilicate gel. It is noticed from Table 4.1 that the increasing of GFNS in the mixture has increased the SiO_2/Al_2O_3 ratio. Accordingly, compressive strength increased with the increase of Si/Al ratio from 2.531 (GFNS-0-A) to 6.640 (GFNS-75-A) for 40% alkaline liquid and from 2.568 (GFNS-0-B) to 6.746 (GFNS-75-B) for 45% alkaline liquid. In geopolymerization, the alkaline activator solution

dissolves the GFNS and fly ash particles completely or partially. After dissolution, Si and Al contents create the bonds of Si-O-Si and Si-O-Al and develop silicate oligomers as well as $Al(OH)_4^-$. A higher amount of silica increases silicate oligomers development and enhances effective involvement of Al in the process to develop three dimensional networks which increased the compressive strength [43]. Moreover, the increase of GFNS in the mixture has increased the MgO/SiO_2 ratio and MgO/Al_2O_3 ratio. In consequence, compressive strength increased with the increase of Mg/Si ratio and Mg/Al ratio for both the alkaline liquid contents. Dissolved Mg^{2+} can react with the broken bonds of Si-O-Si and Si-O-Al and develop magnesium alumino-silicate hydrate (M-A-S-H) [45]. However, in the case of fly ash-GFNS geopolymerization, Na^+ (mostly coming from alkaline solution) and Mg^{2+} (mostly come from GFNS) reacted with broken bonds of Si-O-Si and Si-O-Al to form sodium magnesium alumino-silicate hydrate (N-M-A-S-H) gel. The EDS results confirmed the formation of N-M-A-S-H gel as discussed later in the sections on SEM and EDS analysis.

It can be noticed from Table 4.1 that the molar ratio Na_2O/SiO_2 increased due to the increase of GFNS. The compressive strength of geopolymer increased with the increase of Na_2O/SiO_2 ratio from 0.102 (GFNS-0-A) to 0.108 (GFNS-75-A) for 40% alkaline liquid and from 0.113 (GFNS-0-B) to 0.119 (GFNS-75-B) for 45% alkaline liquid. Besides, the molar ratio of Na_2O/Al_2O_3 increased due to the increase of GFNS, which also increased the compressive strength of geopolymer mortar. The increase of Na_2O improved the binding mechanism of geopolymer and hence higher compressive strength was found for the higher Na_2O/SiO_2 and Na_2O/Al_2O_3 ratios [46, 47]. Pimraksa et al. [48] observed that the geopolymer with a high Na_2O/Al_2O_3 ratio provided a compact amorphous geopolymer matrix compared to that with a lower Na_2O/Al_2O_3 ratio. However, after a certain limit, a higher molar ratio of Na_2O/Al_2O_3 decreased strength due to the excess Na^+ ions, which weaken the bond in sialate network [49, 50].

It can be noticed from Fig. 4.3 that 40% alkaline activator solution resulted in higher compressive strength at a particular age as compared to 45% alkaline solution, though the mixtures of 45% solution have higher Si/Al and Na/Si ratios compared to the corresponding mixtures of 40% solution. The mixtures of 40% alkaline solution had a water/binder ratio of 0.247 whereas those of 45% solution had a water/binder ratio of

0.279 (Table 4.1). Lower water/binder ratio gives a more compact structure, whereas higher water/binder ratio leads to more porous structures and more evaporation of water [51]. Therefore, compressive strengths of the mixtures with higher water/binder ratio were less than those of the mixtures with lower water/binder ratio. A similar trend was reported by Maragkos et al. [7]. Furthermore, excessive water diluted the alkaline liquid which slows down the dissolution and geopolymer reaction resulting in reduction of strength [42]. Excess alkaline solution not only increases the amount of water, but also the OH^- ions and alkaline cations content in the system which fosters an increase of poorly polymerized reactive species as well as hindering polymerization [52]. However, there is a limit of water to binder ratio below which the mixture will be too dry and unworkable.

4.3.3 Porosity

The porosity of geopolymar mortar was determined by measuring the volume of permeable voids (VPV). Fig. 4.4 shows the effect of GFNS on the VPV of geopolymer mortars for 40% and 45% alkaline liquid contents.
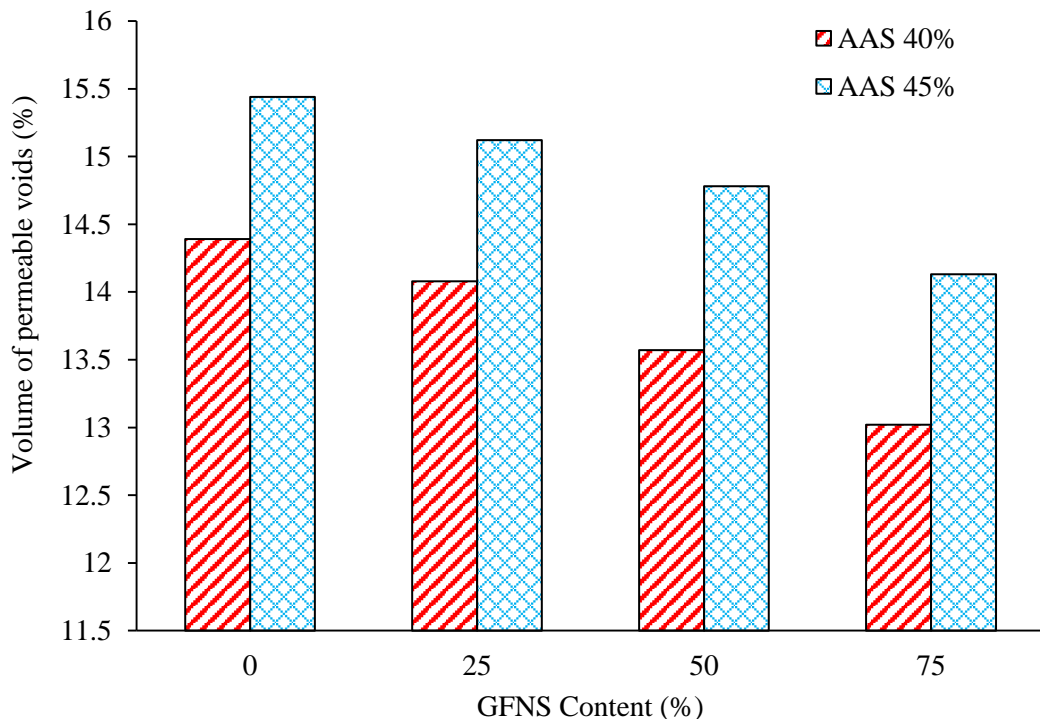
Fig. 4.4 Volume of permeable voids of geopolymer mortars with different GFNS contents

It is noticed that porosity of mortar decreased with the increase of GFNS content. The VPV values of mortars using 40% alkaline liquid were 14.39, 14.08, 13.57 and 13.02% for using 0, 25, 50 and 75% GFNS, respectively. A similar trend can be observed for 45% alkaline solution, where VPV values of 15.44, 15.12, 14.78 and 14.13% were found for using 0, 25, 50 and 75% GFNS, respectively. The decrease of porosity with the increase of GFNS content is attributed to the presence of more compact structures due to the formation of new aluminosilicate gel which is consistent with the discussions in sections 4.3.2. Furthermore, it is seen from Fig. 4.4 that for the same GFNS content, the porosity of mortar increased as the alkaline liquid increased from 40% to 45%. The mixtures of 40% alkaline liquid had lower water/binder ratios compared to those of 45% alkaline liquid (Table 4.1). A higher water to binder ratio leads to higher evaporation of water resulting in more porosity of the mortar, as discussed in the compressive strength section. Therefore, VPV values of the mixtures with a higher water to binder ratio were higher than those of the mixtures with lower water to binder ratio and consequently lower strength developed in mortars with a higher water to binder ratio (Fig. 4.3).

4.3.4 Sorptivity

The effect of GFNS on the sorptivity coefficient of geopolymer mortars with 40% and 45% alkaline liquid are shown in Fig. 4.5. It is seen that for both the liquid contents, sorptivity coefficient decreased due to the increase of GFNS content. The sorptivity coefficients of mortars using 40% alkaline liquid were 4.52×10^{-2}, 4.41×10^{-2}, 3.78×10^{-2} and 3.35×10^{-2} mm/s$^{1/2}$ for the use of 0, 25, 50 and 75% GFNS, respectively. In case of 45% alkaline solution, the sorptivity coefficients were 5.54×10^{-2}, 5.44×10^{-2}, 4.54×10^{-2} and 4.28×10^{-2} mm/s$^{1/2}$ for using 0, 25, 50 and 75% GFNS, respectively. The decrease of sorptivity coefficient by the use of GFNS indicates the reduction of porosity. Therefore, the newly formed aluminosilicate gel due to the use of GFNS provided denser matrix which reduced the sorptivity as well as porosity and increased compressive strength as discussed in sections 4.3.2 and 4.3.3.
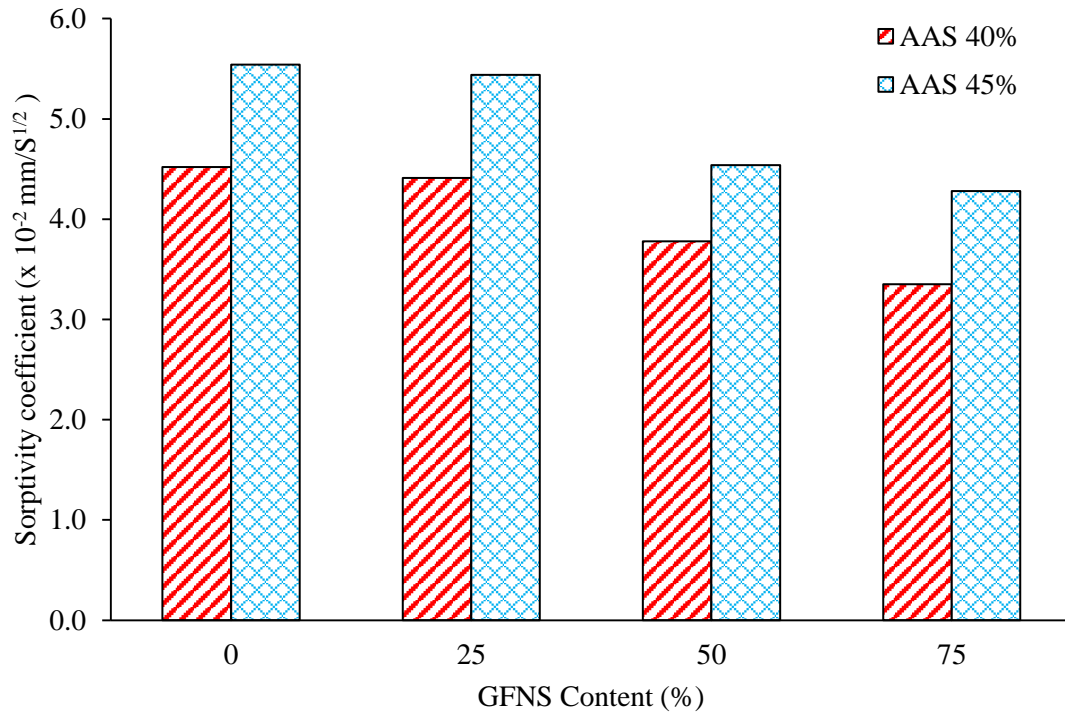
Fig. 4.5 Sorptivity of geopolymer mortars with different GFNS contents

Moreover, the sorptivity coefficients of geopolymer mortar increased as the alkaline activator solution increased from 40% to 45%. A higher alkaline solution provided higher water to binder ratio, which increased the porosity and thus gave higher sorptivity and lower strength as discussed in the earlier sections.

4.3.5 SEM and EDS analysis

The reaction products of two geopolymer pastes having 0% GFNS (control sample with 100% fly ash) and 75% GFNS with 40% alkaline activator solution were investigated at 56 days of age. Figs. 4.6 and 4.7 show the SEM images of the control specimen and that with 75% GFNS content, respectively. The EDS spectra of selected points with chemical compositions (atomic %) are also shown in the figures.
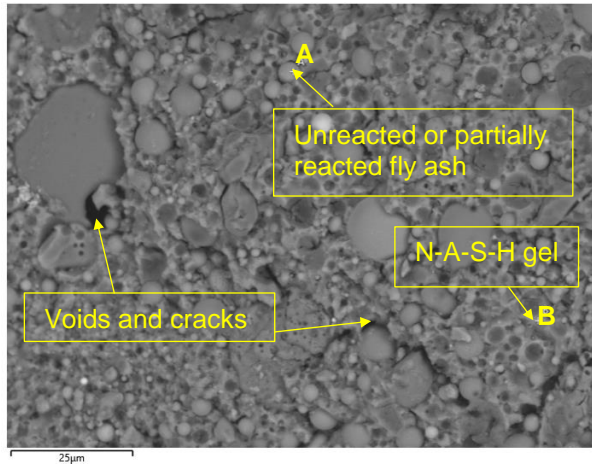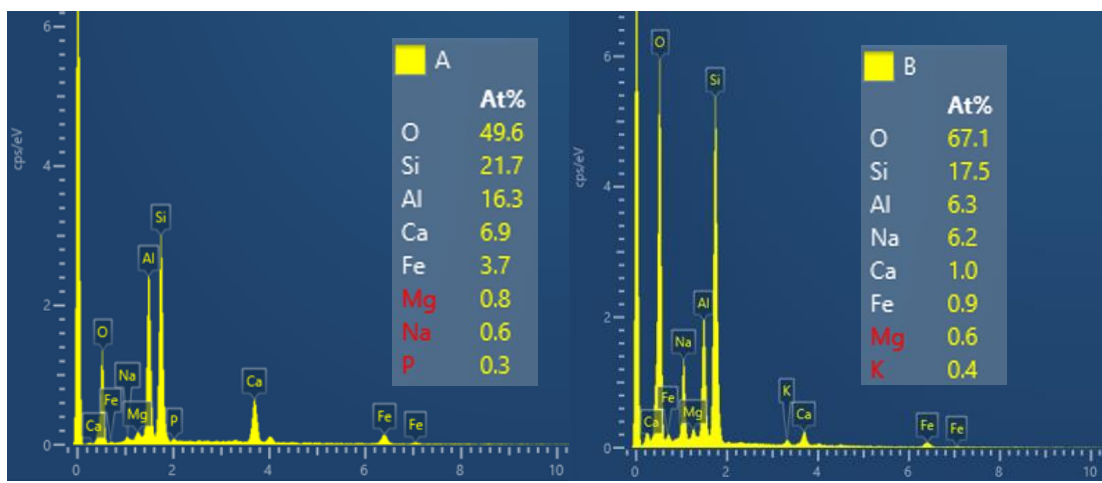
Fig. 4.6 SEM image and EDS spectra of geopolymer using 100% fly ash: (a) SEM, (b) EDS spectrum A, (c) EDS spectrum B
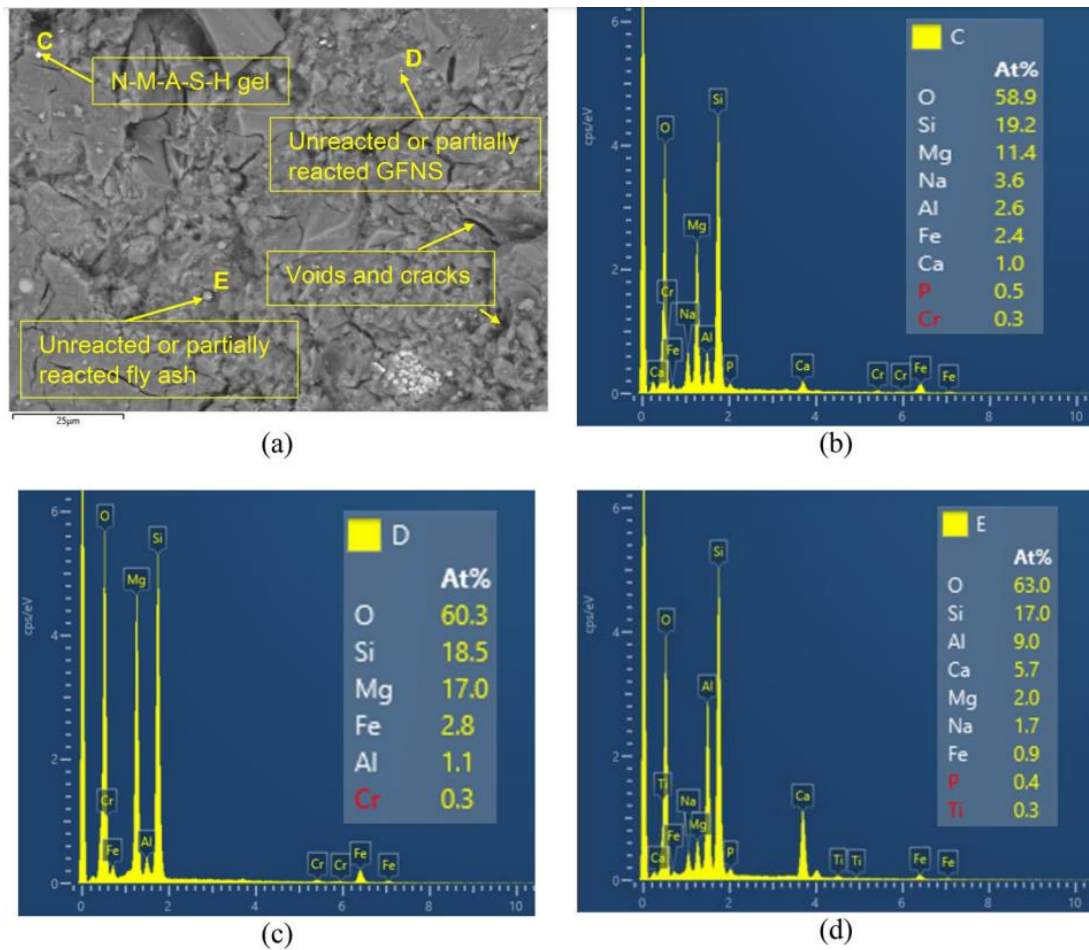
Fig. 4.7 SEM image and EDS spectra of geopolymer using 75% GFNS with 25% fly ash: (a) SEM, (b) EDS spectrum C, (c) EDS spectrum D, (d) EDS spectrum E

It can be seen from Fig. 4.6(a) that the 0% GFNS sample has some partially reacted or unreacted fly ash particles (A). The 0% GFNS sample contains geopolymer product (B) which provided the strength of the sample. The EDS spectrum of point B (Fig. 4.6(c)) shows that the geopolymer product of 0% GFNS contains higher peaks as well as a higher proportion of O, Si, Al and Na compared to the other elements, which indicates the presence of sodium alumino-silicate hydrate (N-A-S-H) gel. It is to be noted that the other elements (Ca, Fe, Mg, k) may be incorporated in the geopolymer product. For instance, Ca may develop calcium silicate hydrate (C-S-H) or calcium alumino-silicate hydrate (C-A-S-H). However, as the geopolymer product contains trace amounts of Ca, Fe, Mg, k and higher proportion of O, Si, Al and Na, sodium alumino-silicate hydrate (N-A-S-H) gel can be considered as the main reaction product of fly ash geopolymer.
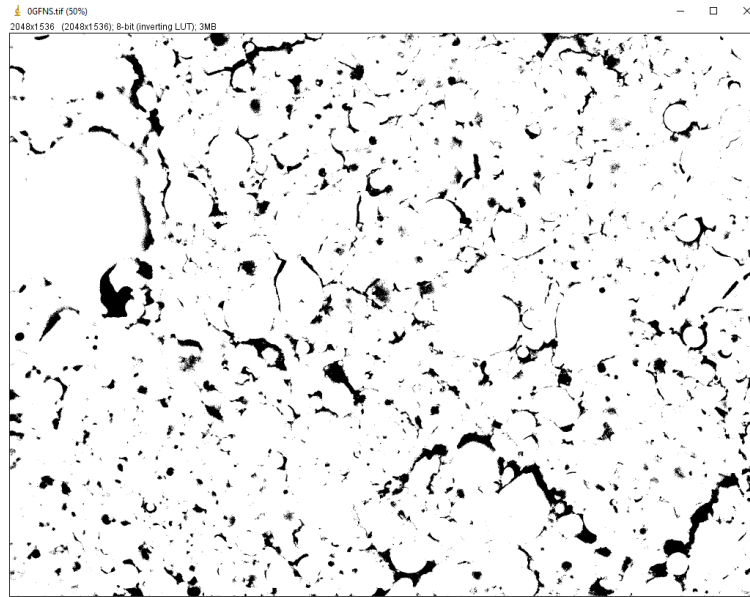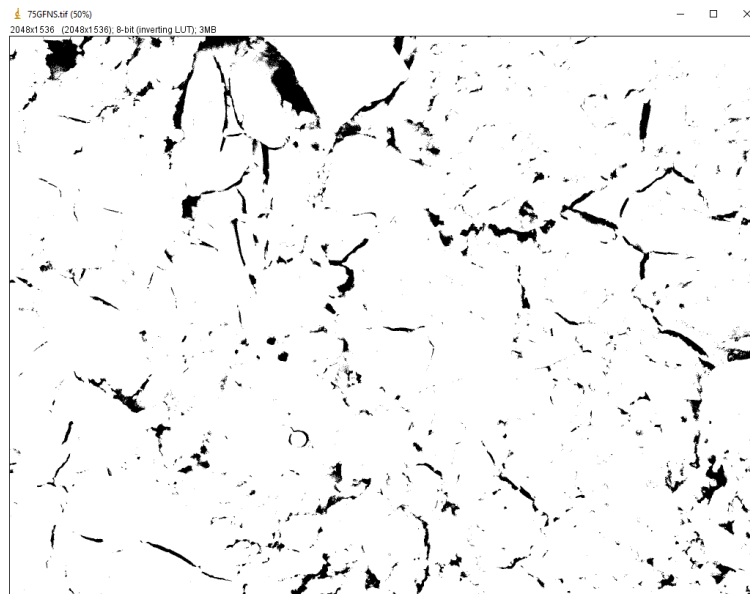
Fig. 4.8 Porosity of geopolymer (a) using 100% fly ash, (b) using 75% GFNS with 25% fly ash

On the other hand, the product (C in Fig. 4.7(a)) of 75% GFNS sample is different from that of the 0% GFNS sample. It is seen from the EDS spectrum (Fig. 4.7(b)) that the product of 75% GFNS contains higher proportion of O, Si, Mg, Na and Al, which indicates the presence of sodium-magnesium-alumino-silicate hydrate (N-M-A-S-H) gel, providing the higher strength of FA-GFNS geopolymers compared to the neat fly ash based geopolymer. In addition, the specimen contained some partially reacted or

unreacted GFNS (D) and fly ash (E) particles. The unreacted or partially reacted GFNS particles may act as micro-aggregate covered by the reaction product and provide a dense structure by filling effect which can also contribute to the strength [53]. Fig. 4.8 shows the porous portion of specimens which was extracted from the SEM images by ImageJ software. It is seen that the microstructure of the specimen with 75% GFNS was more compact than that of the specimen with 0% GFNS. Porosity of the geopolymer paste was determined from eight images of each specimen and the average value is reported as the porosity. It was found that porosity of the 75% GFNS sample was 4.62%, whereas porosity of the 0% GFNS sample was 6.85%. Therefore, lower porosity of 75% GFNS sample was associated with a more compact microstructure. It is established that a higher strength can be expected for a matrix with more compact microstructure [54].

4.3.6 XRD analysis

Fig. 4.9 presents the XRD spectrum of raw binder materials and geopolymer pastes with different proportions of fly ash and GFNS. The main crystalline phases of fly ash were quartz and mullite. Small amounts of magnetite and calcite were present in the fly ash. On the other hand, forsterite and a small amount of quartz were present in the ferronickel slag. It can be seen from the XRD spectra that fly ash based geopolymer (without GFNS) contained the crystalline phases of quartz, mullite and magnetite which came from the fly ash. Trace amount of calcite was identified due to the carbonation of exposed surface under ambient conditions. A broad hump can be seen between 2θ of 18° and 40° in the 0% GFNS sample, which was between 15° and 30° in the raw fly ash. This is an indication of the development of amorphous content as a result of the geopolymerisation reaction [55, 56].

Besides, QXRD analysis was performed on raw fly ash, GFNS and all geopolymer specimens using TOPAS software. The results of QXRD analysis are shown in Table 4.2. It is noticed that fly ash and GFNS mainly comprised of amorphous phases and the amorphous contents were 86.02% and 61.33%, respectively. It can be observed from Table 4.2 that the amorphous content of the 0% GFNS geopolymer (GFNS-0-A) increased compared to that in raw fly ash. This amorphous phase indicates the presence of geopolymer product (N-A-S-H gel). It is found that the 0% GFNS geopolymer contained 89% amorphous content and the remaining crystalline phases

74
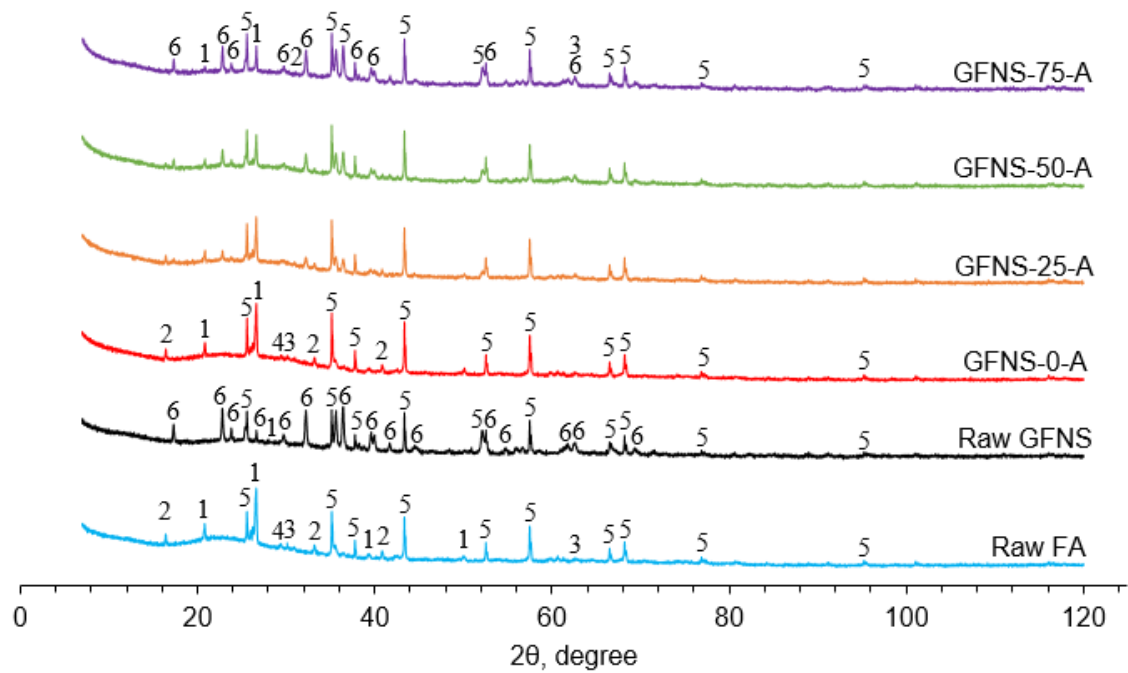
Legend
1 PDF 00-005-0490 SiO_2 Quartz, low
2 PDF 00-015-0776 $Al_6Si_2O_{13}$ Mullite, syn
3 PDF 01-071-6449 $Fe(Fe_{1.17}Ti_{0.54})O_4$ Magnetite, titanian
4 PDF 00-047-1743 $CaCO_3$ Calcite
5 PDF 00-010-0173 Al_2O_3 Corundum, syn
6 PDF 00-007-0075 $2(Mg_{0.90}Fe_{0.10})O.SiO_2$ Forsterite

Fig. 4.9 X-ray diffraction (XRD) patterns of precursors and geopolymer samples

Table 4.2 Results of quantitative XRD analysis (mass %)

	Quartz	Mullite	Magnetite	Calcite	Forsterite	Amorphous
	(%)	(%)	(%)	(%)	(%)	(%)
Raw fly ash	5.03	6.81	1.52	0.62	---	86.02
Raw GFNS	0.68	---	---	---	38.0	61.30
GFNS-0-A	4.02	5.40	1.28	0.30	---	89.00
GFNS-25-A	2.80	4.23	1.11	0.16	7.58	84.12
GFNS-50-A	2.09	2.69	0.67	0.002	13.46	79.60
GFNS-75-A	1.31	2.86	0.29	0.00	22.58	72.96

75

included 5.40% mullite, 4.02% quartz, 1.28% magnetite and 0.30% calcite (Table 4.2). It is also observed that the peak intensity (Fig. 4.9) as well as the amount of quartz, mullite and magnetite (Table 4.2) decreased with the increase of GFNS content due to the decrease of fly ash content. The peak of minor calcite disappeared in the sample with 75% fly ash replacement by GFNS. This indicates that the crystalline phase dissolute under a great extent of alkaline environments [57]. On the other hand, the peak intensity and amount of forsterite, contributed by the GFNS, increased due to the increase of GFNS. This suggests that the crystalline phase is comparatively stable during the geopolymerization process. It can be noticed from Table 4.2 and Fig. 4.9 that, though the geopolymers using GFNS has high crystalline phases, they had significant proportions of amorphous contents. The amorphous contents were 84.12%, 79.60% and 72.96% for using 25%, 50% and 75% GFNS, respectively. These are higher than the amorphous content of raw GFNS (61.30%). Therefore, the amorphous content of the geopolymer using GFNS indicates the presence of sodium magnesium alumino-silicate hydrate (N-M-A-S-H) gel, which was identified in the SEM and EDS presented in the previous section.

4.4 Summary

The effects of using GFNS with a class F fly ash on the workability, strength development, and sorptivity of geopolymer mortar were investigated. GFNS was used to replace fly ash by 25%, 50% and 75% in geopolymer mortars. The alkali liquid content was 40% or 45% of the solid geopolymer precursor. The reaction products of geopolymers were evaluated by using SEM, EDS and XRD. Porosity of the microstructure was determined by ImageJ software. On the basis of acquired results, the following conclusions are drawn:

- Workability of geopolymer mortar reduced due to the increase of GFNS as a substitute of fly ash. Flow of the mortar with 45% alkaline liquid decreased from 110% for no GFNS to 73% for using 75% GFNS. As expected, flow of the mortars using 40% alkaline liquid were less than those with 45% alkaline liquid. However, all the geopolymer mortars using up to 75% GFNS were workable. The reduction of workability due to the increase of GFNS is ascribed to the angular shape and higher fineness of GFNS particles.

- Inclusion of GFNS reduced the compressive strength of geopolymer mortar at the early age of 7 days. However, at 28 days and beyond, compressive strength significantly increased due to the use of GFNS. The GFNS content of 75% provided the maximum compressive strength of geopolymer mortar. The 28-day and 90-day compressive strengths of geopolymer mortar using 40% alkaline liquid were 75 MPa and 96 MPa, respectively. The corresponding strengths decreased to 66 MPa and 84 MPa, respectively, for using 45% alkaline liquid. This shows a potential use of GFNS as a replacement of fly ash by up to 75% for the production of high strength geopolymers.

- The use of GFNS decreased the porosity and sorptivity of the geopolymer mortar by providing denser structures due to the improvement of reaction mechanism.

- SEM images showed more compact microstructure of geopolymers using GFNS compared to that using 100% fly ash. The XRD results showed increase of crystalline phases with the increase of GFNS content. The EDS revealed that the main reaction product of FA-GFNS geopolymer is sodium-magnesium-alumino-silicate hydrate (N-M-Al-Si-H) gel, which is related to the denser microstructure and the resulting strength increase by GFNS.

4.5 References

[1] N. Lemonis, P.E. Tsakiridis, N.S. Katsiotis, S. Antiohos, D. Papageorgiou, M.S. Katsiotis, M. Beazi-Katsioti, Hydration study of ternary blended cements containing ferronickel slag and natural pozzolan, Constr. Build. Mater. 81 (2015) 130–139.

[2] A. Wongsa, A. Wongkvanklom, D. Tanangteerapong, P. Chindaprasirt, Comparative study of fire-resistant behaviors of high-calcium fly ash geopolymer mortar containing zeolite and mullite, J. Sustain. Cem. Mater. 9 (2020) 307-321.

[3] M. Khalifeh, A. Saasen, T. Vrålstad, H.B. Larsen, H. Hodne, Experimental study on the synthesis and characterization of aplite rock-based geopolymers, J. Sustain. Cem. Mater. 5 (2016) 233-246.

[4]   H. El-Hassan, N. Ismail, Effect of process parameters on the performance of fly ash/GGBS blended geopolymer composites, J. Sustain. Cem. Mater. 7 (2018) 122-140.

[5]   J. Ye, W. Zhang, D. Shi, Performance evolutions of tailing-slag-based geopolymer under severe conditions, J. Sustain. Cem. Mater. 4 (2015) 101-115.

[6]   A.M.A. Aboshia, R.A. Rahmat, M.F.M. Zain, A. Ismail, Early age shrinkage cracking of restrained metakaolin-slag-palm oil fuel ash binder geopolymer mortars, J. Sustain. Cem. Mater. 7 (2018) 271-295.

[7]   I. Maragkos, I.P. Giannopoulou, D. Panias, Synthesis of ferronickel slag based geopolymers, Minerals Eng. 22 (2) (2009) 196–203.

[8]   Z. Zhang, H. Wang, J.L. Provis, Quantitative study of the reactivity of fly ash in geopolymerization by FTIR, J. Sustain. Cem. Mater. 1 (2012) 154-166.

[9]   E. Alvarez-Ayuso, X. Querol, F. Plana, A. Alastuey, N. Moreno, M. Izquierdo, O. Font, T. Moreno, S. Diez, E. Vazquez, M. Barra, Environmental, physical and structural characterisation of geopolymer matrixes synthesised from coal (co-)combustion fly ashes, J Hazard Mater. 154 (2008) 175-183.

[10] Y. Huang, Q. Wang, M. Shi, Characteristics and reactivity of ferronickel slag powder, Constr. Build. Mater. 156 (2017) 773–789.

[11] Y.C. Choi, S. Choi, Alkali-silica reactivity of cementitious materials using ferro-nickel slag fine aggregates produced in different cooling conditions, Constr. Build. Mater. 99 (2015) 279–287.

[12] A.K. Saha, P.K. Sarker, Expansion due to alkali-silica reaction of ferronickel slag fine aggregate in OPC and blended cement mortars, Constr. Build. Mater. 123 (2016) 135–142.

[13] A.K. Saha, P.K. Sarker, Durability characteristics of concrete using ferronickel slag fine aggregate and fly ash, Mag. Concr. Res. 70 (2018) 865–874.

[14] J. Sun, J. Feng, Z. Chen, Effect of ferronickel slag as fine aggregate on properties of concrete, Constr. Build. Mater. 206 (2019) 201–209.

[15] A.K. Saha, P.K. Sarker, Mechanical properties of concrete using ferronickel slag and fine aggregate and supplementary cementitious material, Concrete in Australia. 44 (2018) 40-44.

[16] D. Wang, Q. Wang, S. Zhuang, J. Yang, Evaluation of alkali-activated blast furnace ferronickel slag as a cementitious material: Reaction mechanism,

engineering properties and leaching behaviors, Constr. Build. Mater. 188 (2019) 860–873.

[17] H. Kim, C.H. Lee, K.Y. Ann, Feasibility of ferronickel slag powder for cementitious binder in concrete mix, Constr. Build. Mater. 207 (2019) 693–705.

[18] Y. Chen, T. Ji, Z. Yang, W. Zhan, Y. Zhang, Sustainable use of ferronickel slag in cementitious composites and the effect on chloride penetration resistance, Constr. Build. Mater. 240 (2020) 117969.

[19] K. Komnitsas, L. Yurramendi, G. Bartzas, V. Karmali, E. Petrakis, Factors affecting co-valorization of fayalitic and ferronickel slags for the production of alkali activated materials, Sci. Total Environ. 721 (2020), 137753.

[20] T. Yang, Z. Zhang, H. Zhu, X. Gao, C. Dai, Q. Wu, Re-examining the suitability of high magnesium nickel slag as precursors for alkali-activated materials, Constr. Build. Mater. 213 (2019) 109–120.

[21] K. Komnitsas, D. Zaharaki, V. Perdikatsis, Geopolymerisation of low calcium ferronickel slags, J. Mater. Sci. 42 (2007) 3073–3082.

[22] K. Komnitsas, D. Zaharaki, V. Perdikatsis, Effect of synthesis parameters on the compressive strength of low-calcium ferronickel slag inorganic polymers, J. Hazard. Mater. 161 (2009) 760–768.

[23] K. Komnitsas, D. Zaharaki, G. Bartzas, Effect of sulphate and nitrate anions on heavy metal immobilisation in ferronickel slag geopolymers, Appl. Clay Sci. 73 (2013) 103–109.

[24] T. Yang, X. Yao, Z. Zhang, Geopolymer prepared with high-magnesium nickel slag: Characterization of properties and microstructure, Constr. Build. Mater. 59 (2014) 188–194.

[25] T. Yang, Q. Wu, H. Zhu, Z. Zhang, Geopolymer with improved thermal stability by incorporating high-magnesium nickel slag, Constr. Build. Mater. 155 (2017) 475–484.

[26] Z. Zhang, Y. Zhu, T. Yang, L. Li, H. Zhu, H. Wang, Conversion of local industrial wastes into greener cement through geopolymer technology: A case study of high-magnesium nickel slag, J. Clean. Prod. 141 (2017) 463–471.

[27] K. Sakkas, P. Nomikos, A. Sofianos, D. Panias, Utilisation of FeNi-Slag for the production of inorganic polymeric materials for construction or for passive fire protection, Waste and Biomass Valorization 5 (2014) 403–410.

[28] A. Bouaissi, L. Li, M.M.A.B. Abdullah, Q. Bui, Mechanical properties and microstructure analysis of FA-GGBS-HMNS based geopolymer concrete, Constr. Build. Mater. 210 (2019) 198–209.

[29] A.K. Saha, P.K. Sarker, Sustainable use of ferronickel slag fine aggregate and fly ash in structural concrete: Mechanical properties and leaching study, J. Clean. Prod. 162 (2017) 438–448.

[30] P. Nath, P.K. Sarker, Use of OPC to improve setting and early strength properties of low calcium fly ash geopolymer concrete cured at room temperature, Cem. Concr. Compos. 55 (2015) 205–214.

[31] ASTM C1437, Standard test method for flow of hydraulic cement mortar, ASTM International, West Conshohocken, PA, 2007.

[32] AS1012.9, Methods of testing concrete - compressive strength tests – concrete, mortar and grout specimens, Standards Australia, 2014.

[33] ASTM C642, Standard test method for density, absorption, and voids in hardened concrete, ASTM International, West Conshohocken, PA, 2006.

[34] ASTM C1585, Standard test method for measurement of rate of absorption of water by hydraulic-cement concretes, ASTM International, West Conshohocken, PA, 2004.

[35] M.D. Abràmofff, P.J. Magalhães, S.J. Ram, Image processing with ImageJ, Biophotonics Int. 11 (2005) 36–43.

[36] A.A. Coelho, TOPAS and TOPAS-Academic: An optimization program integrating computer algebra and crystallographic objects written in C++, J. Appl. Crystallogr. 51 (2018) 210–218.

[37] H.M. Rietveld, A profile refinement method for nuclear and magnetic structures, J. Appl. Crystallogr. 2 (1969) 65–71.

[38] R.J Hill, C.J. Howard, Quantitative phase analysis from neutron powder diffraction data using the Rietveld method, J. Appl. Crystallogr. 20 (1987) 467–474.

[39] J.L. Provis, P. Duxson, J.S.J. van Deventer, The role of particle technology in developing sustainable construction materials, Adv. Powder Technol. 21 (2010) 2–7.

[40] M. Khodr, D.W. Law, C. Gunasekara, S. Setunge, R. Brkljaca, Compressive strength and microstructure evolution of low calcium brown coal fly ash-based geopolymer, J. Sustain. Cem. Mater. 9 (2020) 17-34.

[41] S. Yan, K. Sagoe-Crentsil, Evaluation of fly ash geopolymer mortar incorporating calcined wastepaper sludge, J. Sustain. Cem. Mater. 5 (2016) 370-380.

[42] A. Sathonsaowaphak, P. Chindaprasirt, K. Pimraksa, Workability and strength of lignite bottom ash geopolymer mortar, J Hazard Mater. 168 (2009) 44–50.

[43] S. Yaseri, G. Hajiaghaei, F. Mohammadi, M. Mahdikhani, R. Farokhzad, The role of synthesis parameters on the workability, setting and strength properties of binary binder based geopolymer paste, Constr. Build. Mater. 157 (2017) 534–545.

[44] D. Hardjito, Studies of fly ash-based geopolymer concrete, Dissertation, Curtin University, 2005. http://hdl.handle.net/20.500.11937/634.

[45] A.F. Abdalqader, F. Jin, A. Al-Tabbaa, Characterisation of reactive magnesia and sodium carbonate-activated fly ash/slag paste blends, Constr. Build. Mater. 93 (2015) 506–513.

[46] M. Chi, R. Huang, Binding mechanism and properties of alkali-activated fly ash/slag mortars, Constr. Build. Mater. 40 (2013) 291–298.

[47] G.V.P.B. Singh, K.V.L. Subramaniam, Effect of active components on strength development in alkali-activated low calcium fly ash cements, J. Sustain. Cem. Mater. 8 (2019) 1-19.

[48] K. Pimraksa, P. Chindaprasirt, A. Rungchet, K. Sagoe-Crentsil, T. Sato, Lightweight geopolymer made of highly porous siliceous materials with various Na_2O/Al_2O_3 and SiO_2/Al_2O_3 ratios, Mater. Sci. Eng. A. 528 (2011) 6616–6623.

[49] J.W. Phair, J.S.J. Van Deventer, Effect of the silicate activator pH on the microstructural characteristics of waste-based geopolymers, Int. J. Miner. Process. 66 (2002) 121–143.

[50] K. Juengsuwattananon, F. Winnefeld, P. Chindaprasirt, K. Pimraksa, Correlation between initial SiO_2/Al_2O_3, Na_2O/Al_2O_3, Na_2O/SiO_2 and H_2O/Na_2O ratios on phase and microstructure of reaction products of metakaolin-rice husk ash geopolymer, Constr. Build. Mater. 226 (2019) 406–417.

[51] Y. Cheng, M. Hongqiang, C. Hongyu, W. Jiaxin, S. Jing, L. Zonghui, Y. Mingkai, Preparation and characterization of coal gangue geopolymers, Constr. Build. Mater. 187 (2018) 318–326.

[52] C. Ruiz-Santaquiteria, J. Skibsted, A. Fernández-Jiménez, A. Palomo, Alkaline solution/binder ratio as a determining factor in the alkaline activation of aluminosilicates, Cem. Concr. Res. 42 (2012) 1242–1251.

[53] T. Tho-In, V. Sata, K. Boonserm, P. Chindaprasirt, Compressive strength and microstructure analysis of geopolymer paste using waste glass powder and fly ash, J. Clean. Prod. 172 (2016) 2892–2898.

[54] M. Steveson, K. Sagoe-Crentsil, Relationships between composition, structure and strength of inorganic polymers : Part 2 Fly ash-derived inorganic polymers, J. Mater. Sci. 40 (2005) 4247–4259.

[55] J.L. Provis, G.C. Lukey, J.S.J. Van Deventer, Do geopolymers actually contain nanocrystalline zeolites? a reexamination of existing results, Chem. Mater. 17 (2005) 3075–3085.

[56] P. Duxson, A. Fernández-Jiménez, J.L. Provis, G.C. Lukey, A. Palomo, J.S.J. Van Deventer, Geopolymer technology: The current state of the art, J. Mater. Sci. 42 (2007) 2917–2933.

[57] D. Zaharaki, K. Komnitsas, V. Perdikatsis, Use of analytical techniques for identification of inorganic polymer gel composition, J Mater Sci. 45 (2010) 2715–2724.

CHAPTER 5: EFFECT OF HIGH TEMPERATURE EXPOSURE ON GFNS BLENDED FLY ASH GEOPOLYMER MORTARS

The contents presented in this chapter were published in the following paper:

Kuri, J. C., Majhi, S., Sarker, P. K., & Mukherjee A. (2021). Microstructural and non-destructive investigation of the effect of high temperature exposure on ground ferronickel slag blended fly ash geopolymer mortars. Journal of Building Engineering, 43, 103099.

This chapter evaluates the elevated temperature exposure effect on ambient-cured geopolymer mortar using ground ferronickel slag with fly ash. It is important to understand the high temperature response of a newly developed construction material in order to assess the effect of fire exposures. The effects of different percentages of ground ferronickel slag with fly ash and different temperature exposures on geopolymer mortars were evaluated by the changes in mass, cracking behaviour, compressive strength, microstructure and ultrasonic pulse velocity after exposure to temperatures up to 1000 °C.

5.1 Overview

Ordinary Portland cement (OPC) concrete can be considered as a non-combustible material with low thermal conductivity [1]. Incidences of accidental fire in structures is not uncommon. The temperature rises rapidly during the incidence of fire, which leads to the degradation of concrete structures [2, 3]. Although OPC concrete has high resistance to elevated temperatures, cracks, spalling and loss of strength may be unavoidable. Calcium hydroxide is one of the important hydration products of OPC binder and it decomposes at around 400 °C. For this reason, the strength of OPC concrete significantly decreases at temperatures above 400 °C [4]. Geopolymers are being developed as alternative binders that have different reaction products and they have also been reported to possess good resistance to elevated temperatures [5-7].

Geopolymers are inorganic binders, synthesized by aluminosilicate source materials and alkaline activators. In recent years, geopolymers have gained significant interest on account of their physical and mechanical properties [8-11]. Moreover, they are eco-friendly and durable. Field-scale applications of geopolymer concrete include an aircraft pavement at the Wellcamp Airport, Australia; a four-story building at Global

83

Change Research Institute, Queensland University, Australia; and a bridge at Qionglai Airport, China [1,12].

Geopolymers have been reported to maintain their amorphous nature at high temperatures up to 1300 °C [13, 14]. Crystallization in geopolymers highly depends on the ratio of Si/Al and alkaline cation. After exposure to high temperature, dehydration and dihydroxylation take place before crystallization [15, 16]. Visible cracks are noticed in geopolymer paste after 800 °C exposure as a result of this process [17, 18]. Further, the characteristics of geopolymer at elevated temperature highly depends on the produced aluminosilicate gel, which is associated with the chemical composition of the precursors and the alkali activator [19, 20].

Ferronickel slag (FNS) is an industrial by-product of the nickel production process [21-23]. The principal chemical constituents of FNS are SiO_2, MgO, and Fe_2O_3, which are present in crystalline and non-crystalline mineral forms [24-26]. FNS has a high proportion of amorphous silica. Thus, it shows reactivity when it is ground to powder (GFNS) and used as a supplementary cementitious material with OPC [27-30]. GFNS can be introduced as a supplementary cementitious material by mixing it with an alkali [31-34]. Thus, GFNS can be potentially synthesized to produce geopolymer [35-38].

Scant information is available on the thermal performance of GFNS based geopolymers. Sakkas et al. [39-41] found that the compressive strength and thermal conductivity of GFNS geopolymers are comparable to existing fire-resistant materials. In another study, Sakkas et al. [42] subjected potassium-based GFNS geopolymer to elevated temperatures to assess its application as a thermal barrier. It was observed that GFNS geopolymer maintained its structural integrity without any visible damage. As per Zaharaki et al. [43] after exposure to 800 °C, the residual strength of GFNS geopolymer was suitable for application as passive fire protection material. Geopolymers with high magnesium nickel slag (HMNS) showed an improvement in thermal stability by improving the residual strength and reduction in mass loss and shrinkage compared to neat fly ash geopolymer [44]. The physical changes by the exposure to elevated temperatures on geopolymer mortars using different proportions of GFNS with fly ash need investigation through a non-destructive paradigm.

Ultrasonics is an effective non-destructive method to understand the integrity of

construction materials [45]. These ultrasonic waves are usually generated and received through a piezo transducer. Traditionally, the time taken by an incident ultrasonic wave to traverse through the specimen is recorded and correlated with its compressive strength [46]. The response of these piezo transducers can be better understood by including frequency spectra to the time signal [47]. The frequency spectra are devoid of information from the temporal spectra of the signal. Thus, time-frequency analysis of the acquired ultrasonic signals is warranted. Challenges in the localization of time-frequency spectra can lead to uncertainty in establishing the arrival times of ultrasonic signals. An improved S-Transforms shall improve localization of time-frequency spectra leading to improved reliability in the determination of arrival time of ultrasonic waves.

The feasibility of GFNS as a precursor for geopolymers has been established in terms of fresh and mechanical properties [36, 48]. However, their responses to high temperatures need to be studied in order to assess their performance against accidental fire. The present study investigated the effect of elevated temperatures up to 1000 °C on the geopolymer mortar synthesized from GFNS blended fly ash. The effect of temperature gradient on this geoploymer was studied through a series of macro and micro level investigations. The effect of elevated temperature on geopolymer mortar specimens was determined first by the extent of cracks and changes in mass. Destructive compression tests were undertaken to find the variation of strength on a macro scale. Microstructural changes at various levels of temperature exposure was determined through thermogravimetric analysis (TGA), scanning electron microscopy (SEM), energy dispersive X-ray spectra (EDS) and quantitative X-ray diffraction (QXRD) analysis. The macro and micro level studies were further explored through a novel wave based non-destructive technique. The time-frequency spectra from the ultrasonic tests were used to understand the overall condition of the specimen upon exposure to high temperatures.

5.2 Experimental Work

5.2.1 Materials and mix proportions

Fly ash and GFNS were used as the precursors for the production of geopolymer mortar. According to ASTM C618-19 [49], the fly ash was classified as class F. The alkaline activator was a blend of sodium hydroxide (8M) and sodium silicate (Na_2O =

14.7%, $SiO_2 = 29.4\%$, and $H_2O = 55.9\%$) solutions in the mass ratio of 1:2. The fine aggregate used was local sand with fineness modulus of 1.94.

Table 5.1 Mix proportions of geopolymer mortars

Mix ID	Ingredients (kg/m^3)				
	GFNS	Fly ash	Sand	SH[1]	SS[2]
GFNS-0	0	733	1137	110	220
GFNS-25	183	550	1137	110	220
GFNS-50	367	367	1137	110	220
GFNS-75	550	183	1137	110	220

[1]Sodium hydroxide solution

[2]Sodium silicate solution

The mixture proportions of geopolymer mortars and are given in Table 5.1 which were selected based on the previous studies [48, 50, 51]. Fly ash was substituted by 0, 25, 50 and 75% GFNS. In the mix ID of Table 5.1, the mixtures containing 0, 25, 50 and 75% GFNS were designated as GFNS-0, GFNS-25, GFNS-50 and GFNS-75, respectively. The quantity of activator liquid was 45% by mass of the total solid precursor.

5.2.2 Sample preparation and testing

The GFNS, fly ash and saturated surface dry (SSD) sand were dry mixed and then the alkali activator (mixture of SH and SS) liquid was added gradually to obtain a uniform mortar mixture. The mortar mixtures were then cast into 50 mm × 50 mm × 50 mm moulds, compacted, sealed and kept in ambient environment (20 °C temperature and 60% relative humidity) for 24 hours. Afterwards, the samples were demoulded and cured in the ambient condition till testing.

It was found from the previous studies [36, 48] that the strength of fly ash-GFNS geopolymers continued to increase considerably beyond 28 days when subjected to curing in ambient condition. However, the rate of strength gain slowed down after 56 days. Therefore, to evaluate the effect of high temperature, geopolymer mortar samples were exposed to temperatures of 200 to 1000 °C after 56 days of curing in ambient condition. A locally built electric furnace was used to apply the heat on

geopolymer mortar samples with a heating rate of 5 °C/min, which is compatible with the RILEM standard heating rate [52, 53]. Once the target temperature was reached, it was kept constant for 2 hours. The visual appearance, mass change, ultrasonic pulse velocity, compressive strength and microstructure were investigated after exposure to high temperature.

Compressive strength of geopolymer mortar samples was tested in accordance with AS 1012.9 [54] using a Controls MCC8 machine at an axial loading rate of 0.30 MPa/sec.

QXRD analysis was conducted to evaluate the mineralogical changes of the specimen after high temperature exposure. To evaluate the mineralogical phases accurately, QXRD analysis was conducted on corresponding paste samples exposed to same elevated temperature. Geopolymer samples were ground and mixed with 10% corundum powder as an internal standard. The XRD patterns were recorded by D8 advance diffractometer, operated at 40kV and 40mA, with LynxEye detector. The XRD patterns were acquired in the 5-120° 2θ range, with a step size of 0.015° and scanning speed of 0.7 Sec/step. The EVA 11.0 software with ICDD powder diffraction file (PDF) database was used to identify the phases. Rietveld [55] analysis was then performed using TOPAS [56] to determine the relative weight proportions of the phases. After that, the relative Rietveld weight proportions were converted to the absolute fractions using the internal standard method [57].

SEM and EDS analysis was conducted on geopolymer mortar samples to find the microstructural changes due to the elevated temperature. The sample was cut carefully with a thin saw. The sectioned surface of the specimen was covered by 10 nm carbon and attached with the stub using carbon tape. SEM images and EDS data were acquired by a Mira3 XMU (Tescan) microscope fitted with Oxford instruments.

Thermogravimetric analysis (TGA) was performed to detect the phase changes due to the high temperatures using a Mettler Toledo TGA instrument. TGA was conducted on corresponding paste samples to determine the heat flow and loss of mass at different temperatures.

Ultrasonic tests were conducted for non-destructive investigation of the mortar specimen upon exposure to elevated temperatures. The schematic diagram of

experimental setup for the acquisition of ultrasonic waves is shown in Fig. 5.1.
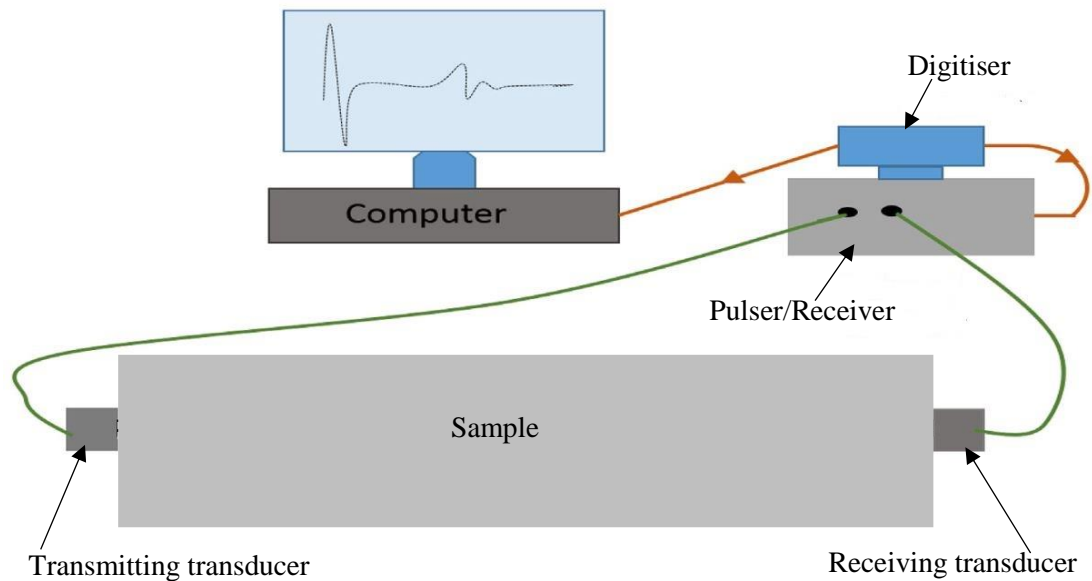
Fig. 5.1 Experimental setup for the acquisition of ultrasonic waves [47]

The mortar samples were placed between transmitting and receiving transducers. The lead zirconate titanate (PZT) transducers of 100 kHz central frequency was used to transmit the signal through the mortar samples. A DPR 300 model (JSR ultrasonics) pulser-receiver system was used. A Picoscope 6 version 6.4.64.0 modular oscilloscope was used to digitize the ultrasonic data.

5.3 Results and Discussion

5.3.1 Visual inspection

After exposure to high temperature, visual inspection of geopolymer samples was conducted to monitor the changes of colour, cracking pattern and spalling behaviour. The physical appearance of the neat fly ash and fly ash-GFNS blended geopolymer mortars after exposure to elevated temperatures are shown in Fig. 5.2. It was noticed that after exposure to 200 °C, no significant change was observed on the outer surface as well as in the colour of the samples. A significant change in colour were observed after exposure to 600 °C. The change in colour is ascribed to the loss of water and phase transformation of geopolymer [58]. The presence of red colouration at high temperature is ascribed to the oxidation of mineral constituents [59, 60]. After 800 °C, eye visible cracks were observed in the samples. Evaporation and migration of water

at high temperature led to the formation of cracks.
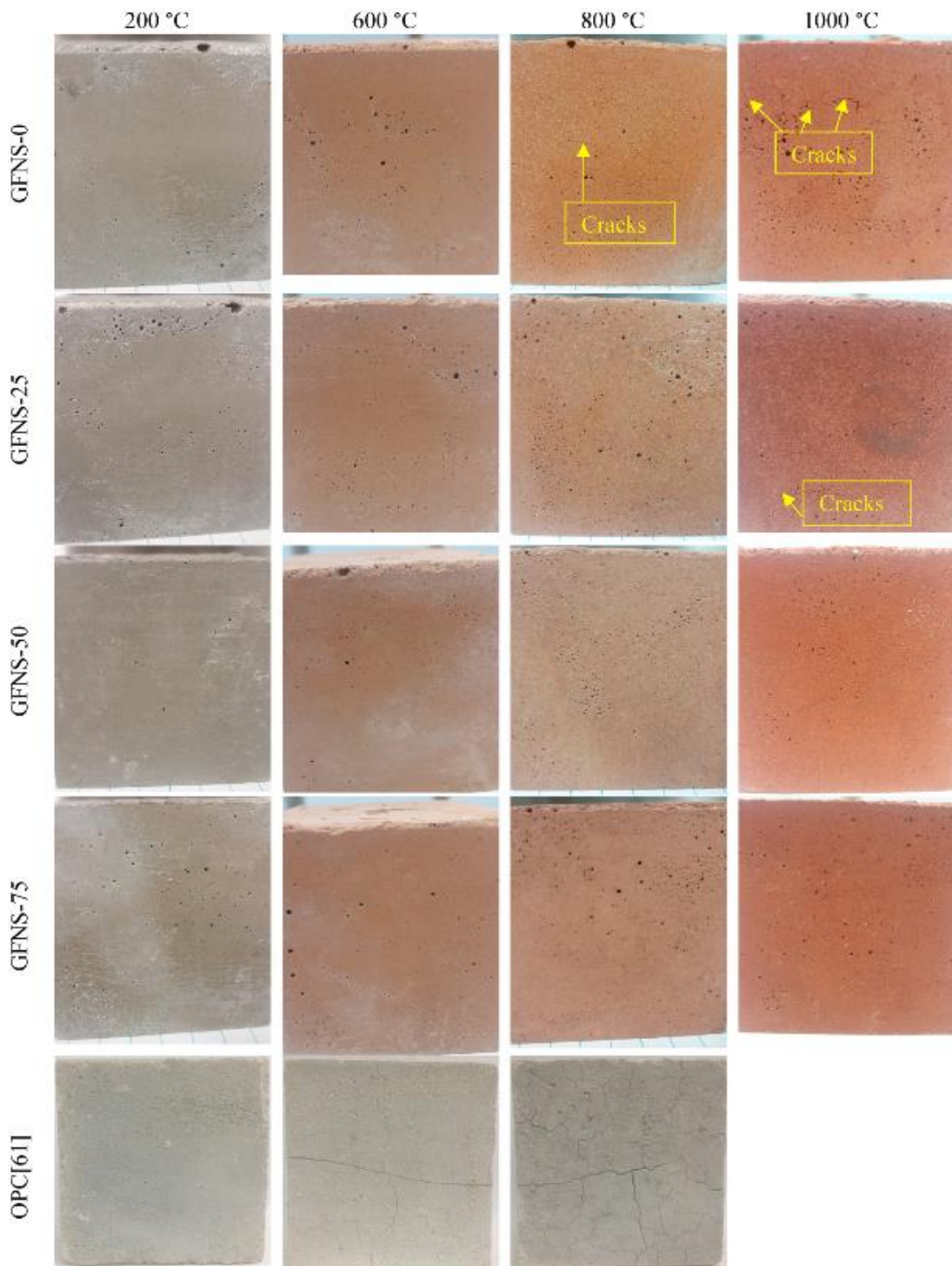
Fig. 5.2 Physical appearance of the geopolymer and OPC mortars after exposure to high temperatures

Besides, the cracks were also contributed by the decomposition of geopolymer matrix and transformation of phases at elevated temperatures, as discussed in section 5.3.4.

However, spalling was not noticed due to the high temperature exposure up to 1000 °C. It is noticed that more cracks were formed in the GFNS-0 (neat fly ash) sample compared to the fly ash-GFNS mortar samples, which is consistent with the finding of the SEM images and ultrasonic investigations as discussed in sections 5.3.5 and 5.3.7, respectively. This indicates that the incorporation of GFNS makes the geopolymer mortar more stable against the elevated temperature exposures.

To compare the thermal stability of geopolymer mortar with OPC mortar, physical appearance of OPC mortars at elevated temperatures reported in a previous study [61] are also shown in Fig. 5.2. Unlike the geopolymer mortar, the colour of OPC mortar did not change significantly. It can be clearly observed from Fig. 5.2 that at the same temperature, OPC mortar showed more eye visible cracks than geopolymer mortar which leads to low residual compressive strength of OPC mortar. It was reported that after 400 °C, eye visible cracks were noticed in OPC mortar and it increased at higher temperature [61].

5.3.2 Residual compressive strengths

Fig. 5.3 presents the residual compressive strength of geopolymer mortar after exposure to different temperatures. After ambient curing of 56 days, compressive strengths of the mortars were 56, 64, 68 and 71 MPa for using 0, 25, 50 and 75% GFNS, respectively. The compressive strength of neat fly ash (GFNS-0) geopolymer is mainly associated with sodium alumiosilicate hydrate (N-A-S-H) gel as identified in SEM and EDS investigation. The increase of strength of geopolymer on account of the use of GFNS is associated with the development of N-M-A-S-H gel as detected in SEM and EDS analysis. The details about the reaction mechanism and associated strength gaining process due to the use of GFNS are described in the previous studies [38, 48]. For all the geopolymer mixtures, compressive strength slightly increased as the temperature increased to 200 °C (Fig. 5.3). The increase of strength during the loss of free water is ascribed to the continuation of geopolymerization as reported by several researchers [62-64].
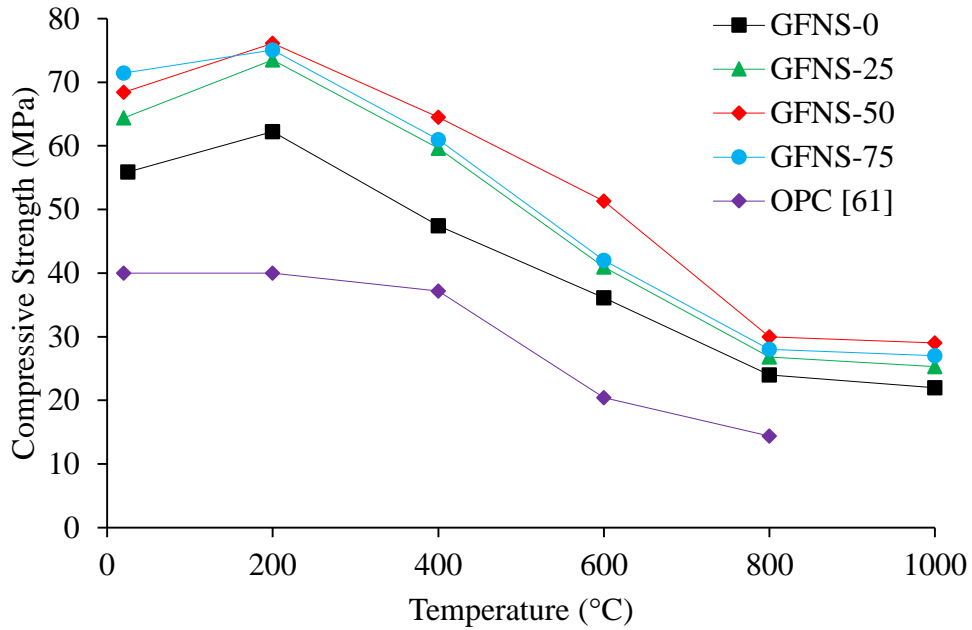
Fig. 5.3 Residual compressive strength at different temperatures

The further increase of temperature reduced strength of the mortar. Above 400 °C, compressive strength of mortar significantly decreased as compared to the unexposed samples. This is ascribed to the movement of physically bonded water, chemically bonded water and OH groups, phase transformation of geopolymers, development of anhydrous products and sintering process [65, 66]. At 600 °C, compressive strength of mortar reduced by 35.33, 36.40, 25.02 and 41.22% as compared to the unexposed specimens containing 0, 25, 50 and 75% GFNS, respectively. The amorphousness of geopolymer matrix started to transfer to crystalline structure beyond 600 °C [64]. A similar trend of the formation of new crystalline structures at high temperature were found in XRD analysis as discussed later in section 5.3.4. At elevated temperatures, non-uniform recrystallization occurred which resulted in the formation of large cracks that consequently reduced strength [64, 67].

Overall, fly ash-GFNS geopolymer provided higher residual compressive strength than neat fly ash geopolymer. GFNS improved the residual strength by producing N-M-A-S-H gel. Yang et al. [44] reported a similar observation of higher residual strength in GFNS incorporated geopolymers than neat fly ash geopolymer. In general, up to the use of 50% GFNS, the trend of compressive strength reduction of the samples after exposure to elevated temperatures is similar to that of the sample before

exposure. The samples with 50% GFNS showed maximum residual strength throughout the exposure period. The residual compressive strengths of geopolymer mortar with 50% GFNS were 76, 65, 51, 30 and 29 MPa at 200, 400, 600, 800 and 1000 °C, respectively. Therefore, geopolymer mortar with 50% GFNS provided the highest thermal stability throughout the high temperature exposure periods. Though the mixture with 75% GFNS provided highest compressive strength before heat exposure, it did not show the highest strength after exposure to elevated temperature. High temperature and high GFNS content may increase the hydration reaction but can make a weak interface in the 75% GFNS sample than the 50% GFNS sample. Thus less residual strength was found in the 75% GFNS sample than the 50% GFNS sample. A similar observation was found in literature where the influence of GGBFS content with fly ash was studied and 20% GGBFS was found as optimum for the highest residual strength after high temperature exposures [68].

The variation of compressive strength at high temperature in OPC mortar reported by Saha et al. [61], is also plotted in Fig. 5.3. It is observed that at high temperature exposure, OPC mortar showed the lowest residual strength. The residual compressive strengths of OPC mortar were 40, 37, 20 and 14 MPa at 200, 400, 600 and 800 °C, respectively. Decomposition of portlandite at high temperature is the primary reason for this significant strength reduction in OPC mortar [61].

5.3.3 Weight loss

The weights of the mortar samples were measured before and after exposure to elevated temperatures. It was noticed that the weight of the all geopolymer mortar samples decreased with the increase of temperature. The percentage of weight loss of mortar samples at different high temperatures are shown in Fig. 5.4. When the temperature increased, dehydration occurred and moisture escaped the mortar. In consequence, internal damage and weight loss of the specimens occurred [17, 69]. It is observed that for all the mixtures, significant weight loss occurred up to 600 °C and then it became stable. For instance, weight losses of the GFNS-50 samples were 2.83, 6.26, 7.87, 7.85 and 7.52% at 200, 400, 600, 800 and 1000 °C, respectively. The significant weight loss before 600 °C is ascribed to the evaporation of free water and OH groups. At the early stage of heating (less than 100 °C), evaporation of physically bonded water occurred. The chemically bonded water evaporated when the

temperature increased to 400 °C. The weight loss after 400 °C is ascribed to dehydroxylation of hydroxyl groups. The weight loss beyond 600 °C is ascribed to the decomposition of compounds in the geopolymer [17, 70].
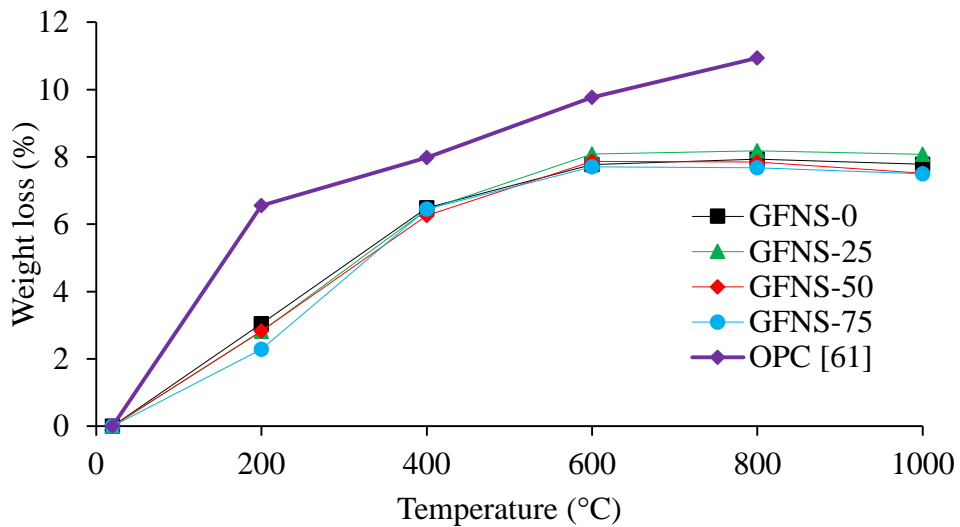
Fig. 5.4 Weight loss at high temperatures

In general, the variation of weight loss at a particular temperature was very small for 0, 25, 50 and 75% GFNS contents. For instance, at 200 °C, the weight loss varied from 2.29% to 3.05 % in the samples with 0, 25, 50 and 75% GFNS. The weight loss variations were 6.26-6.49%, 7.71-8.09%, 7.93-8.18% and 7.50-8.08% at 400, 600, 800 and 1000 °C, respectively.

It can be noticed from Fig. 5.4 that the OPC mortar samples showed significant weight loss at 200 °C. Afterwards, the weight loss increased at smaller rates. However, OPC mortars exhibited more weight loss compared to all geopolymer samples throughout the high temperature exposure. The significant mass loss of OPC mortar at 200 °C temperature associates to the reduction of physically bound water. Subsequently, decomposition of portlandite took place after 400 °C and thus further weight loss occurred beyond 400 °C [61].

5.3.4 XRD analysis

The XRD patterns of geopolymers before and after exposure to elevated temperatures are shown in Fig. 5.5. It is noticed from Fig. 5.5(a) that before heat exposure, the XRD pattern of neat fly ash geopolymer (GFNS-0) contained a broad hump between 18° and 40° of 2θ. This broad hump shows the existence of amorphous N-A-S-H gel as detected in SEM and EDS investigation discussed in section 5.3.5. The produced N-A-S-H gel is associated with the strength of the neat fly ash geopolymer. Besides, the XRD spectra of neat fly ash geopolymer contained crystalline mullite, quartz, magnetite and calcite phases. Table 5.2 shows the results of the QXRD analysis of neat fly ash and fly ash-GFNS geopolymers. It can be noticed from Table 5.2 that before heat exposure, the neat fly ash geopolymer (GFNS-0) contained 5.4% mullite, 4.0% quartz, 1.3% magnetite, 0.3% calcite and 89.0% amorphous content. Before exposure, a broad hump is also noticed in all the fly ash-GFNS geopolymers which indicates the presence of amorphous N-M-A-S-H gel as identified in section 5.3.5. This gel provides a dense microstructure of fly ash-GFNS blended geopolymer and thus higher compressive strength was found in fly ash-GFNS blended geopolymer compared to neat fly ash geopolymer. The amorphous proportions of the fly ash-GFNS geopolymers were 84.1, 79.6 and 72.9% on account of the use of 25, 50 and 75% GFNS, respectively. The crystalline phase of the fly ash-GFNS blended geopolymers contained mullite, quartz, magnetite and forsterite, where the intensity (Fig. 5.5) as well as the amount (Table 5.2) of mullite, quartz and magnetite reduced with the decrease of fly ash. The peak intensity and the amount of forsterite increased with the increase of GFNS. Before exposure to high temperature, forsterite contents were 7.6, 13.5 and 22.6% on account of the use of 25, 50 and 75% GFNS, respectively.

(a)

(b)

95

Legend
1 Quartz (SiO_2)
2 Mullite ($Al_6Si_2O_{13}$)
3 Magnetite ($Fe(Fe_{1.17}Ti_{0.54})O_4$)
4 Calcite ($CaCO_3$)
5 Corundum (Al_2O_3)

6 Forsterite ($2(Mg_{0.90}Fe_{0.10})O.SiO_2$)
7 Albite ($Na_{0.84}Ca_{0.16})Al_{1.16}Si_{2.84}O_8$)
8 Omphacite ($Na_{0.33}Ca_{0.59}Mg_{0.59}Fe_{0.24}Al_{0.24}Si_2O_6$)
9 Nepheline ($Na_{3.205}Al_{3.205}Si_{4.795}O_{16}$)
H Hematite ($Fe_{1.984}O_3$)

Fig. 5.5 XRD patterns of geopolymer before [48] and after exposure to high temperature (a) GFNS-0, (b) GFNS-25, (c) GFNS-50, (d) GFNS-75

It is observed from Fig. 5.5 that up to 600 °C, for all sample groups, crystalline phases of the geopolymer were almost same as those before the heat exposure. However, the intensity and amount of crystalline phases and amorphous phases were changed by the elevated temperature. For instance, the GFNS-50 samples had the amorphous contents of 79.6, 75.5 and 73.7% at 20, 200 and 600 °C, respectively. When the temperature increased to 600 °C, for all mixtures, the intensity (Fig. 5.5) and amount (Table 5.2) of quartz and mullite increased compared to those of the samples before heat exposure. The QXRD results revealed that the amount of quartz increased from 4.0% to 5.2% at 600 °C. The corresponding mullite contents were 5.4% and 13.0% for the neat fly ash geopolymer sample. A similar trend can be noticed for the fly ash-GFNS geopolymers. This increase of quartz and mullite contents indicates the decomposition of aluminosilicate structures [1]. The decomposition of geopolymer structure leads to a significant increase of porosity and consequently, compressive strength of the mortar significantly reduced due to high temperature exposures.

Table 5.2 Results of QXRD analysis

Sample ID	Temperature (°C)	Quartz (%)	Mullite (%)	Magnetite (%)	Calcite (%)	Forsterite (%)	Albite (%)	Omphacite (%)	Hematite (%)	Nepheline (%)	Amorphous (%)
GFNS-0	B*	4.0	5.4	1.3	0.3	---	---	---	---	---	89.0
	200	4.9	11.6	1.7	0.5	---	---	---	---	---	81.3
	600	5.2	13.0	1.8	0.3	---	---	---	---	---	79.7
	1000	4.2	15.0	6.3	0.5	---	11.0	---	---	---	62.9
GFNS-25	B*	2.8	4.2	1.1	0.2	7.6	---	---	---	---	84.1
	200	3.7	8.7	1.7	0.1	7.3	---	---	---	---	78.4
	600	4.1	9.4	1.6	0.0	7.7	---	---	---	---	77.2
	1000	2.3	15.0	4.8	0.0	6.3	13.8	3.2	1.8	2.4	50.4
GFNS-50	B*	2.1	2.7	0.7	0.0	13.5	---	---	---	---	79.6
	200	2.9	5.6	1.0	0.0	14.8	---	---	---	---	75.5
	600	2.8	6.3	1.2	0.0	16.0	---	---	---	---	73.7
	1000	1.4	8.2	6.3	0.0	15.5	5.9	4.2	1.6	3.9	53.1
GFNS-75	B*	1.3	2.9	0.3	0.0	22.6	---	---	---	---	72.9
	200	1.6	3.7	0.9	0.0	23.5	---	---	---	---	70.3
	600	1.5	3.7	1.3	0.0	24.2	---	---	---	---	69.3
	1000	0.5	2.4	8.0	0.0	28.1	1.1	3.4	1.6	2.5	52.5

*Before exposure to high temperature [48]

It is also seen for all the samples that the number of crystalline peaks increased and amorphous content decreased significantly as the temperature further increased to 1000 °C. Ye et al. [71] reported a similar observation of new crystalline peaks on ore-dressing tailing of bauxite and GGBFS blended geopolymer at 1000°C. In case of neat fly ash geopolymer, the intensity of quartz peak decreased and a new crystalline phase of albite was found (Fig. 5.5). The new type of crystal albite (11.0%) produced due to the phase transformation of N-A-S-H gel of the neat fly ash geopolymer at high temperature [1, 44]. Some amounts of SiO_2 were consumed during the phase transformation and thus the intensity as well as the amount of quartz decreased at 1000 °C. On the other hand, in addition to albite, several new phases namely omphacite, hematite and nepheline phases were also observed in fly ash-GFNS blended geopolymers (Fig. 5.5, Table 5.2). At high temperature, N-M-A-S-H gel of fly ash-GFNS blended geopolymer decomposed or transformed to Na-Silicate (albite, nepheline) and Mg-Silicate (omphacite) based crystalline phases. Moreover, the iron content of GFNS and fly ash increased the magnetite content and formed new phase of hematite at high temperature. This non-uniform phase transformation resulted in disintegration of the geopolymer matrix at elevated temperature and thus changed the microstructure and strength. However, N-M-A-S-H gel of fly ash-GFNS geopolymer provided higher thermal stability and thus higher residual strength and less cracks and voids was found in fly ash-GFNS geopolymer compared to neat fly ash geopolymer.

5.3.5 SEM and EDS analysis

The SEM images of the geopolymer mortars before and after exposure to 400 and 1000 °C are shown in Fig. 5.6. From the EDS spectrum 1 it can be seen that before exposure, the principal components of neat fly ash (GFNS-0) geopolymer contained Na, Al, Si and O, which indicates the presence of N-A-S-H gel. On the other hand, the major components of reaction product in fly ash-GFNS blended geopolymer are Na, Mg, Al, Si and O (spectrum 2, 3 and 4), which indicates the presence of N-M-A-S-H gel in fly ash-GFNS blended geopolymer mortar. The details about the produced aluminosilicate gel is discussed in the previous studies [36, 48]. Before heat exposure, the mortar with GFNS had a denser microstructure compared to the neat fly ash geopolymer mortar. The compactness increased with the increase of GFNS content and in consequence, the GFNS-75 sample showed higher compressive strength than the other mixtures. The denser structure and higher strengths (Fig. 5.3) of the fly ash-

GFNS blended geopolymer mortars is associated with the reaction product of N-M-A-S-H gel as reported in the previous studies [36, 38].
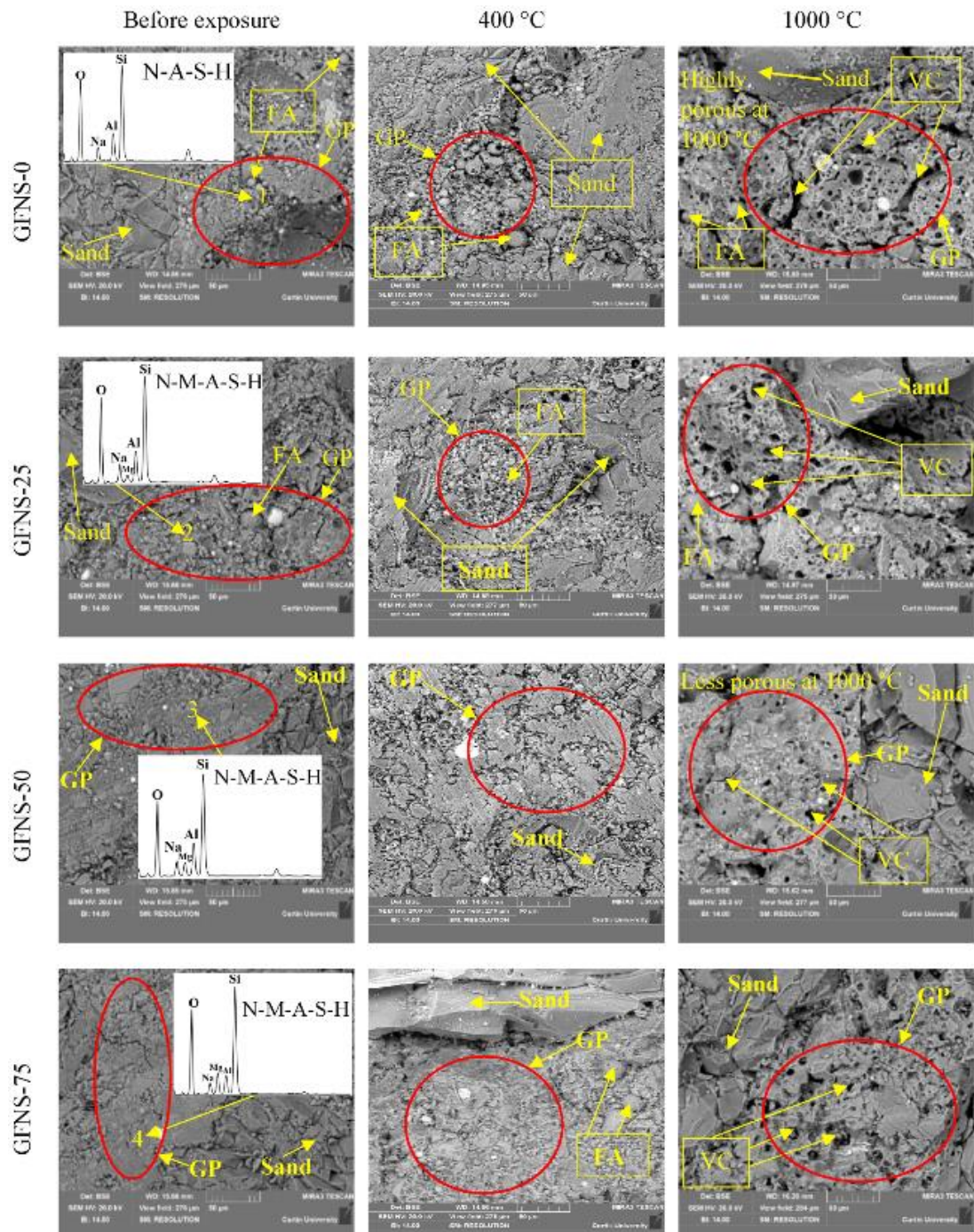
Fig. 5.6 SEM images of geopolymer mortar at different temperatures (GP = geopolymer matrix, FA = unreacted or partially reacted fly ash, VC = voids and cracks)

It is noticed from Fig. 5.6 that at high temperature, all geopolymer samples have more voids and cracks compared to the samples before heat exposure and these voids and cracks increased with the increase of temperature. The presence of porous structure occurred due to the loss of weight, decomposition of geopolymer matrix and transformation of phases at high temperature as described in the previous sections. It is also noticed that geopolymer mortar with GFNS showed lower microstructural deterioration compared to the neat fly ash geopolymer mortar and thus resulted in less strength losses. The improvement is ascribed to the presence of N-M-A-S-H in fly ash-GFNS geopolymer. The result indicates that the development of a compact microstructure by GFNS provided higher thermal stability. Particularly, at high temperature, the GFNS-50 sample provided denser microstructure and thus provided better thermal performance at high temperature.

5.3.6 Thermogravimetric analysis (TGA)

Fig. 5.7 shows the TGA results of neat fly ash and fly ash-GFNS geopolymers. The changes of mass and heat flow with the increase of temperatures are shown in the figure. It can be seen that mass loss increased with the increase of temperature in all the samples. The heat flow plot shows the presence of several endothermic peaks. The initial endothermic peak can be seen between 130 and 140 °C in all the samples. The initial peak corresponds to the evaporation of free and physically bonded water within the N-A-S-H or N-M-A-S-H products [15, 72, 73]. Thus, a substantial mass loss was found in this temperature range, as noticed in Fig. 5.7.
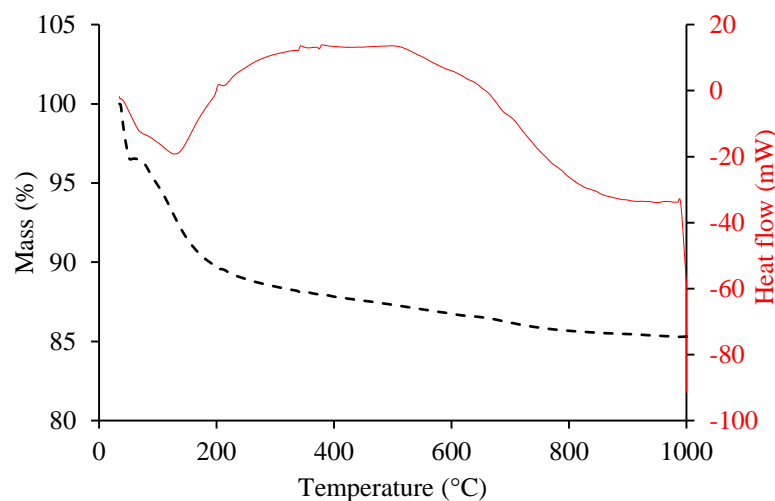
(a)
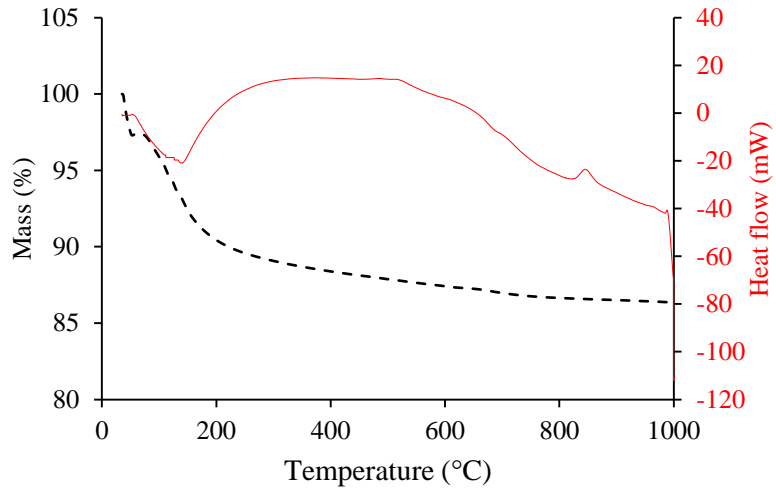
(b)
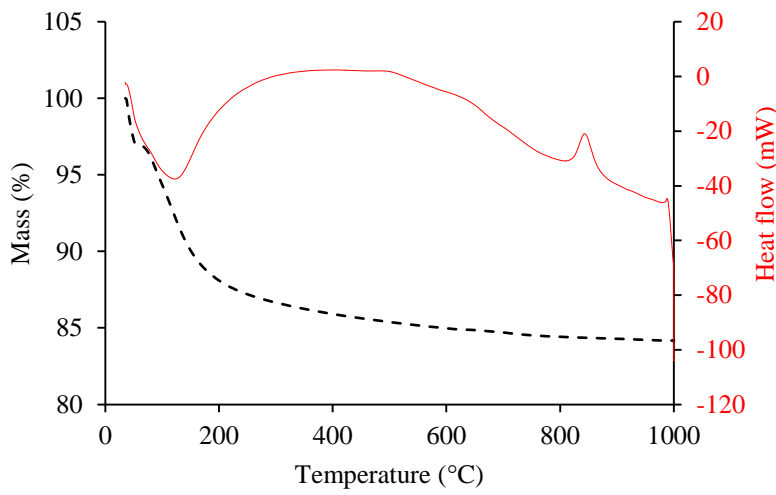
(c)
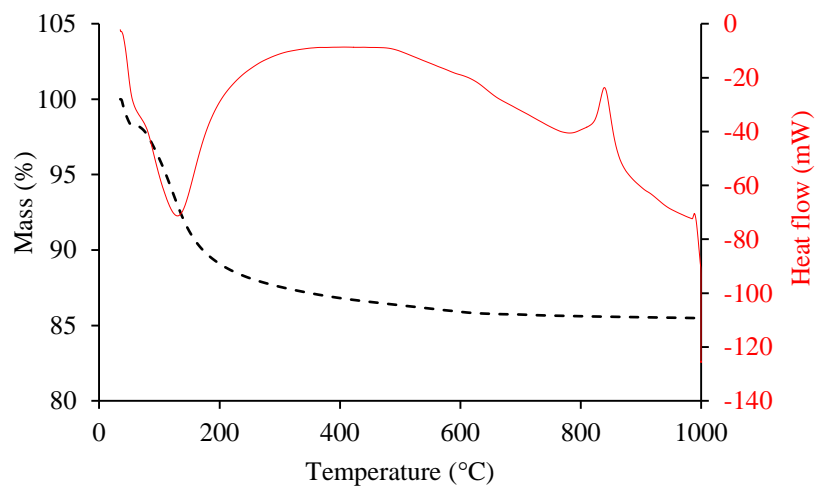
(d)

Fig. 5.7 TGA results of geopolymer (a) GFNS-0, (b) GFNS-25, (c) GFNS-50, (d)

GFNS-75

Further increase of temperature increased the mass loss due to the dehydroxylation of hydroxyl groups [74, 75]. However, the variation of mass loss was almost similar for all the samples (GFNS-0, GFNS-25, GFNS-50 and GFNS-75) which is consistent with mass loss of mortar samples discussed in section 5.3.3. The endothermic peaks beyond 800 °C were correlated with the decomposition of compounds from the N-A-S-H and N-M-A-S-H products [17, 69, 76]. The decomposition of aluminosilicate gel significantly reduced the amorphous content and increased the crystalline contents at 1000 °C as found in XRD analysis. Further investigations into physical properties of various specimen were undertaken through ultrasonics based non-destructive testing.

5.3.7 Ultrasonic investigation

Ultrasonics based non-destructive testing was used to evaluate the condition of the specimens subject to elevated temperature. First the time-signals from the ultrasonic testing were acquired as A-Scans and subsequently their frequency content was understood. As the frequency spectra do not contain any temporal information regarding the acquired signal, a time-frequency analysis was undertaken to understand the variation in temporal characteristics of the signal vis-à-vis their frequency content. The variation in the temporal and frequency content on GFNS-50 specimens subject to elevated temperatures were undertaken hereby. This will be extended towards understanding the changes in other specimen.

5.3.7.1 Time: A-Scan

The Time of flight (ToF) is a popular method to investigate the material properties [45]. It is the travelling time of the wave from the incidence point to the reception point based on the wave's interaction with the material under investigation. Fig. 5.8 shows a typical time-signal measured on a GFNS-50 specimen at different exposure conditions. Clearly, there exists an ambiguity with regards to the identification of arrival peak for ToF calculation.

(a)

(b)

1

0.5

0

-0.5

-1

Normalised amplitude

0   20   40   60   80

Time (μs)
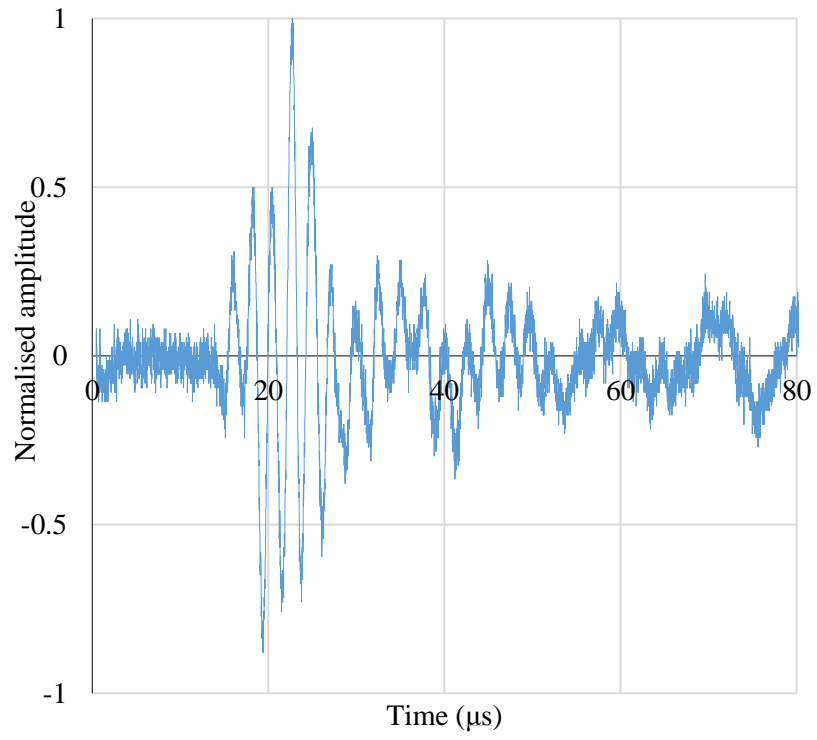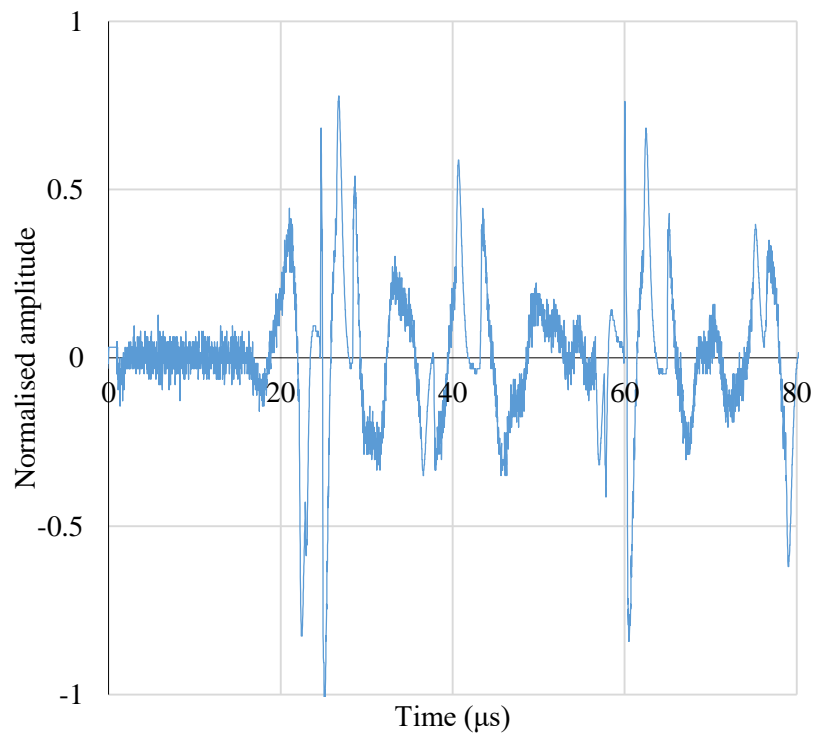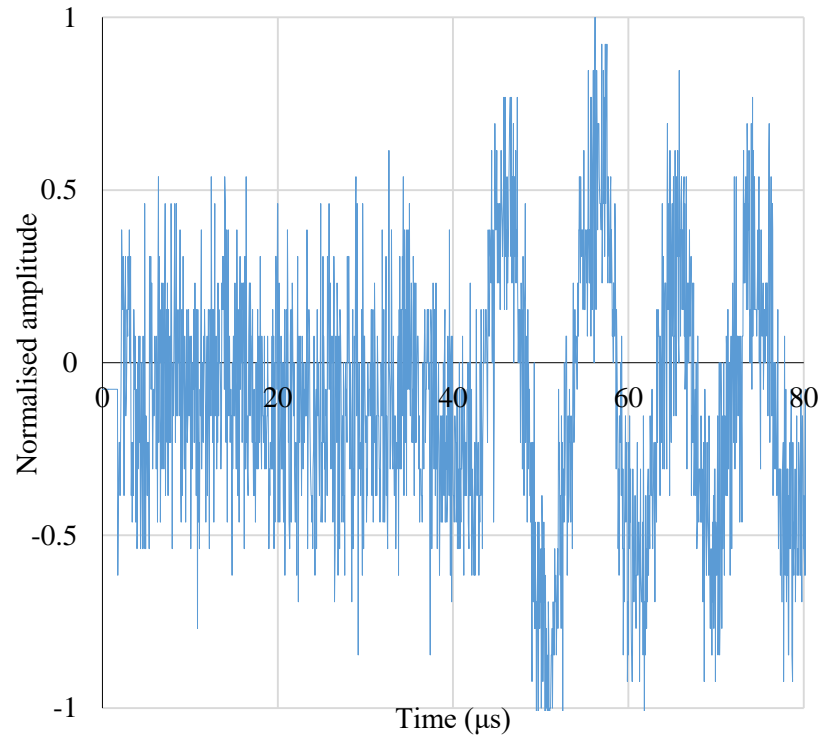
(C)

Fig. 5.8 Variation in ToF in GFNS-50 specimen at (a) ambient temperature, (b) 400 °C and (c) 800 °C

ToF is the first step towards understanding the changes of the GFNS-50 specimen due to the exposure to elevated temperature. An overall increase in the arrival time after its exposure to elevated temperature was observed in the specimen (Fig. 5.8). To establish the causality underlying this increase in ToF, the time-signals warrant analysis in the frequency domain.

5.3.7.2 Frequency: Additional information in case of including frequency data

Inclusion of frequency information to the temporal data shall add additional information with regards to the physical condition of the specimen. Fig. 5.9 shows the variation in the frequency response after the GFNS-50 specimen was exposed to different temperatures. It can be seen that at ambient conditions, along with the frequency peaks between 100 and 150 kHz, additional peaks between 400 and 450 kHz can also be observed.

104
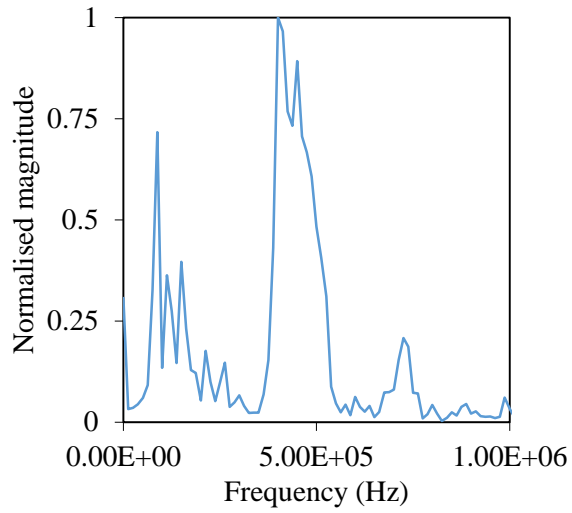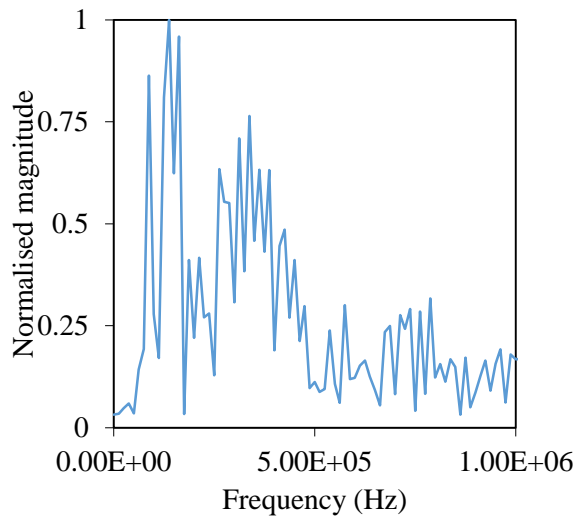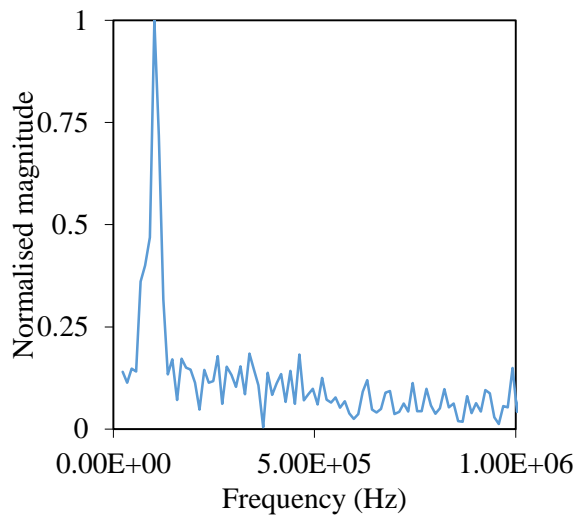
Fig. 5.9 Variation in frequency response in GFNS-50 specimen at (a) ambient temperature, (b) 400 °C and (c) 800 °C

These peaks can be attributed to the response of the transducer to the input excitation. Clearly, the higher frequency components were affected once the specimen was exposed to higher temperatures. The higher frequency components are associated with a smaller wavelength. The attenuation of the higher frequency component is possibly on account of their interaction with the developing cracks that are proportional to the wavelength of higher frequency waves. The frequency spectra plots are devoid of any temporal information associated with the acquired signal. Thus, temporal information is to be added in terms of time-frequency analysis.

5.3.7.3 Time-frequency

The incorporation of temporal details to the frequency spectra shall enhance the overall interpretation of the acquired signal [47, 77]. The temporal location of the dominant frequencies as identified in Fig. 5.8 needs to be established. An improved S-Transforms has revealed the location of these dominant frequencies (Fig. 5.10). Improvement in the temporal locations of discrete frequency components are achieved by introducing a Gaussian window to localize these frequencies. The standard deviation of this Gaussian window is varied linearly as per the particular frequency being localized. The parameters 'a' and 'b' modulate this standard deviation. Thus, a judicious selection of the parameters 'a' and 'b' is warranted [47, 77]. In the present case, a = 10; b = 0.02 was used to localize the time-frequency spectra of the acquired ultrasonic signals.

(a)
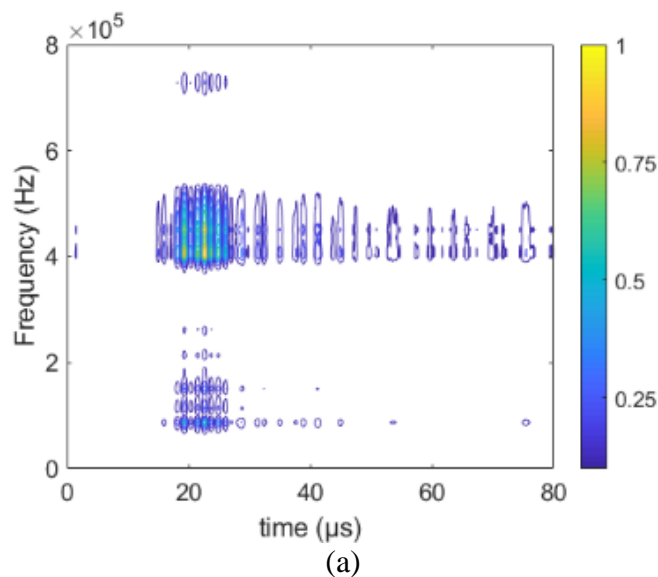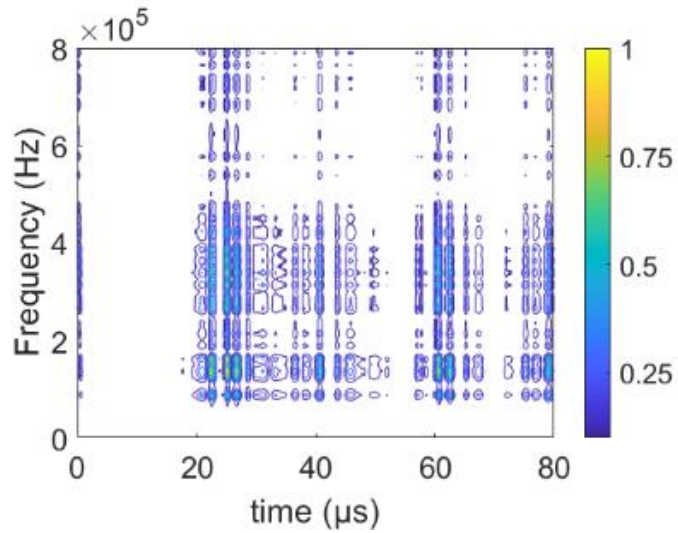
(b)
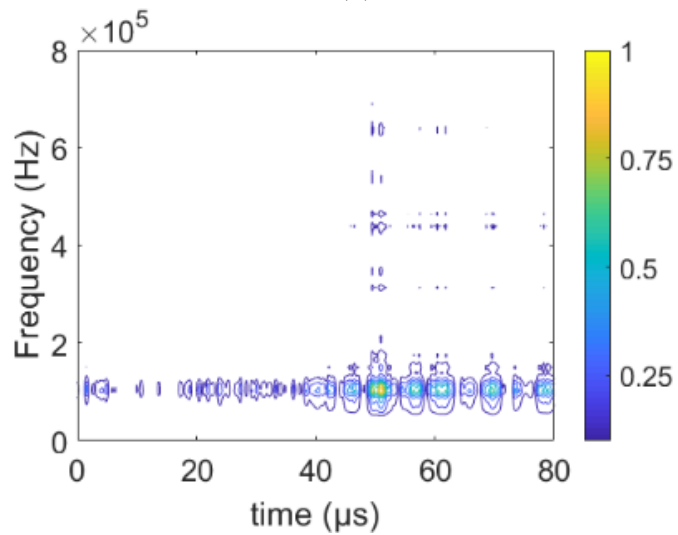
(c)

Fig. 5.10 Variation in time-frequency response in GFNS-50 specimen at (a) ambient temperature, (b) 400 °C and (c) 800 °C

Variation in the acquired signal in terms of a shift in the temporal and frequency spectra was observed. Overall, a shift in higher frequencies towards the lower frequencies along with a decrease in the arrival time was observed. This trend is to be now investigated and quantified for GFNS-0, GFNS-25, GFNS-50 and GFNS-75 specimens. A spectral index is to be developed.

5.3.7.4 Spectra index

A spectral index (I) is hereby introduced to correlate the variation in time-frequency spectra as established in section 5.3.6.3 with the physical condition of the specimen. This index is computed from the time-frequency spectral content as per Eq. 5.1 [47, 77]. In the specified frequency zones as per Table 5.3, the spectral content up to 80 μs is used in the spectral index calculation. Subsequently, this index is plotted in time-frequency-exposure temperature domain (Fig. 5.11).

$$I = \sum_{f=f_1}^{f_2} S(t,f) \dots\dots\dots\dots\dots\dots\dots\dots\dots\dots\dots\dots\dots\dots\dots\dots (5.1)$$

Table 5.3 Selection criteria in the frequency domain for lower and higher frequencies in Eq. 5.1

	f_1	f_2
Lower frequency	90 kHz	110 kHz
Higher frequency	390 kHz	450 kHz
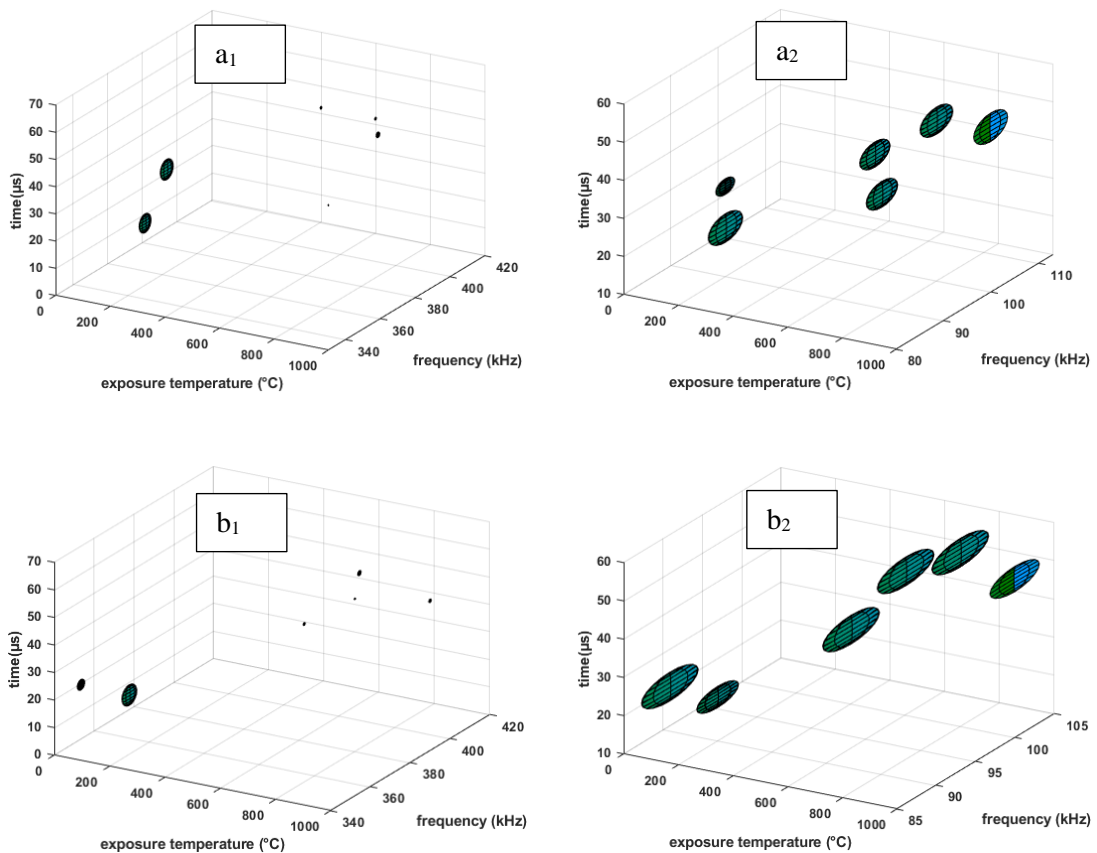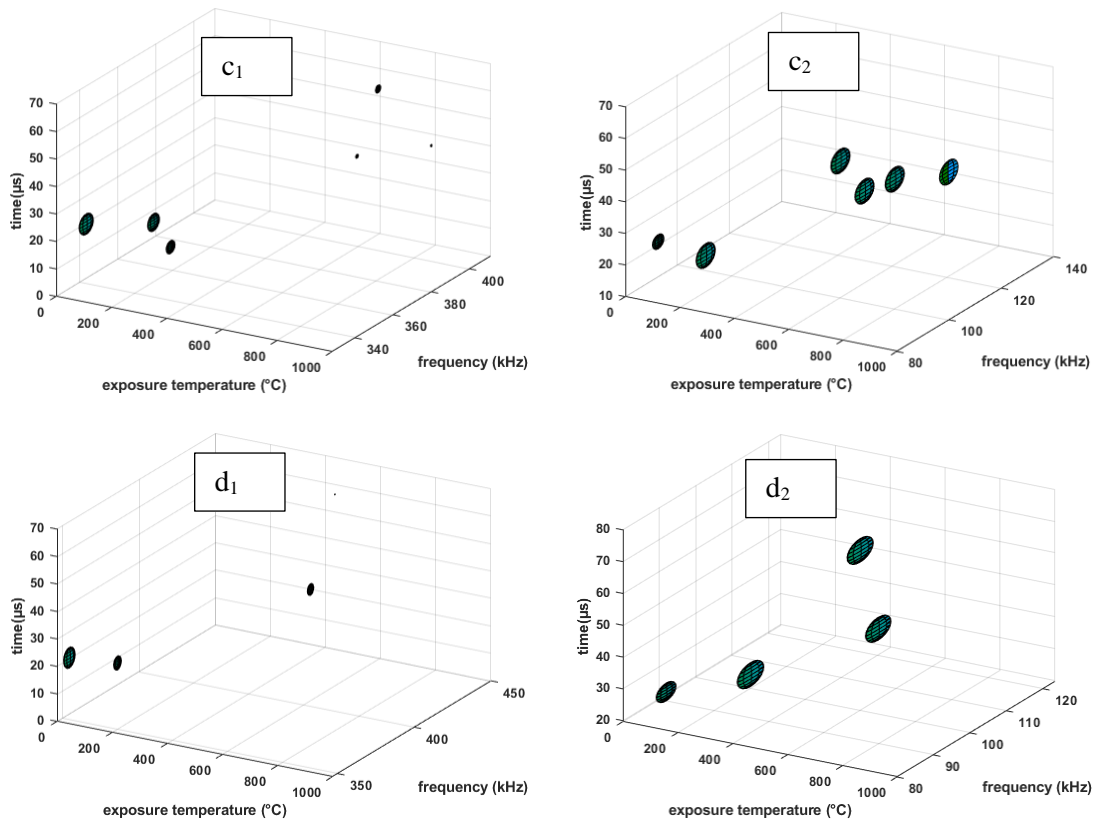
Fig. 5.11 Variation in time-frequency based spectral index for exposure conditions as per Table 5.4

Table 5.4 Nomenclature for specimens exposed to various temperatures

Specimen	Higher frequency	Lower frequency
GFNS-0	a_1	a_2
GFNS-25	b_1	b_2
GFNS-50	c_1	c_2
GFNS-75	d_1	d_2

The variation in the spectral content of the acquired signal reveals the dominant frequency components between 90 kHz and 110 kHz represent the lower frequency components. Understandably this frequency range is close to the resonant frequency of the transducer which is 100 kHz. Alongside the lower frequencies, higher frequency components between 390 kHz and 450 kHz were also generated. These higher frequencies were generated on account of the response of the piezo transducers to the input excitation. The differential variation in frequency components shall reveal details about the physical condition of the specimen on account of exposure to elevated

temperature. In GFNS-0, the lower frequency component dominates across all temperature exposures. This was on account of the presence of voids and cracks in the specimen at ambient temperature which expanded with exposure to temperature as discussed in sections 5.3.1 and 5.3.5.

For GFNS-0 specimens, after the specimen was exposed to 200 °C, the higher frequency components dropped below the noise level as observed in Fig. $5.11a_1$. A similar trend in GFNS-25 was observed as per Fig. $5.11b_1$. This can be attributed to the development of cracks in the specimen as observed from the micrographs (Fig. 5.6). During this instance, the contribution of the lower frequency components remains unaffected (Fig. $5.11a_2$ and $5.11b_2$). Thus, the combined contribution of higher and lower frequency components governs the ToF calculations (Fig. $5.11a_1$-$5.11b_2$).

For GFNS-50, the least amount of pores translated to the dominance of higher frequency components in the spectra (Fig. $5.11c_1$ and $5.11c_2$). Significant higher frequency components persisted till 400 °C before eventually decreasing from then. Thus, up to 400 °C, the ToF calculations are governed by a combination of higher and lower frequency components. The lower frequency components persisted across all temperature exposure ranges as observed in Fig. $5.11c_2$. Beyond 400 °C, the lower frequency components govern the ToF calculations. Overall, the GFNS-50 mix developed the least amount of voids compared to other specimens across various ranges of exposure to high temperatures. The micrographs in Fig. 5.6 support the findings in Fig. $5.11c_1$ and $5.11c_2$.

In the case of GFNS-75, the higher frequency components diminished quickly once it was exposed to a higher temperature. This indicates the development of profound cracks for this particular mix (Fig. $5.11d_1$). After 600 °C reliable signals couldn't be acquired in this specimen as profound cracking in the specimen lead to the signal being diminished past noise level (Fig. $5.11d_1$). The lower frequency components persisted across all temperature exposure ranges (Fig. $5.11d_2$). Thus, their contribution was the prime factor governing ToF in this specimen. Overall, GFNS-50 was the most compact specimen that exhibited the highest compressive strength.

5.3.7.5 Velocity measurement

Fig. 5.12 presents the variation in ultrasonic pulse velocity due to exposure to elevated temperature. A slight decrease in the overall travel time has increased corresponding ultrasonic pulse velocity for GFNS-0, GFNS-25, and GFNS-50 up to a temperature of 200 °C. The velocity increased slightly between 1.28% and 3.19% across the specimen. In the same range, the residual compressive strength of these specimens increased between 5.07 % and 14.14 % (Fig. 5.3). Thus, at 200 °C the temperature gradient did not cause any significant evolution of cracks in the mortar matrix. However, the ultrasonic velocity for GFNS-75 was an outlier to this trend. Past 200°C, there was an overall monotonous decrease in the travel velocity across all specimens except for GFNS-75.
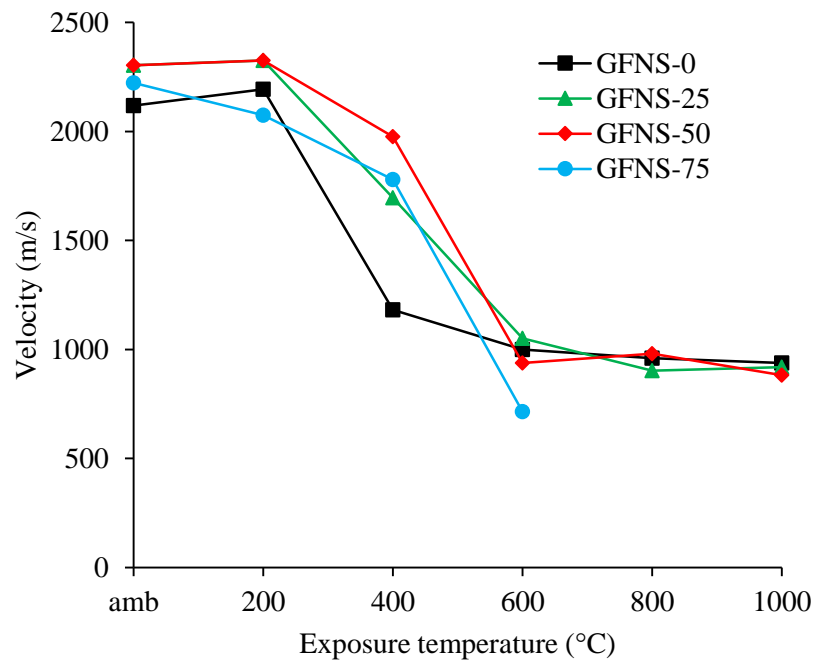
Fig. 5.12 Variation in velocity due to exposure to elevated temperature

It is worth observing that the decrease in velocity in GFNS-25 and GFNS-50 remained the least indicating these mixes developed the least cracks. This fairs well with the results of compressive strength (Fig. 5.3). Between 200 °C and 400 °C, the highest decrease in ultrasonic velocity of 46.11% was observed in GFNS-0. This was on account of profound cracks due to the development of temperature gradient. For GFNS-0, the compressive strength was reduced by 23.72%. In this exposure region, the velocity decreased by 17.67 % for GFNS-50, which was the least amongst all the

111

specimens. The compressive strength decreased by 15.30% between 200 °C and 400 °C. Thus, GFNS-50 exhibited the least decrease in compressive strength and velocity. This shows GFNS-50 developed the least amount of cracks amongst all other specimens at 400 °C.

This trend changed significantly between 400 °C and 600 °C. The velocity decreased by 52.26% and 59.88% in the case of GFNS-50 and GFNS-75. The evolution of voids and the development of profound cracking in the mortar paste on account of the formation of a temperature gradient were responsible for the same. This can be observed clearly in Figs. 5.2 and 5.6. The compressive strength for these specimens dropped by 20.46% and 31.15%, respectively (Fig. 5.3). In the case of GFNS-0 and GFNS-25, the velocity dropped by 15.25% and 37.86% respectively for GFNS-0 and GFNS-25. Their compressive strengths decreased by 23.87% and 31.28%, respectively. Thus, the overall decrease in ultrasonic velocity establishes their sensitivity towards incipient cracks. Manifestation of these cracks has decreased the compressive strength of these specimens.

The compressive strength dropped between 25.02% and 41.22% at 600 °C across the specimens. The biggest drop of 41.22% was observed for GFNS-75 indicating a large majority of cracks had developed at 600 °C. For GFNS-75, the highest drop in ultrasonic velocity was observed at 600 °C compared to ambient temperature. The ultrasonic velocity remained mostly unchanged past 600 °C for all the specimens. Though the specimens had developed significant cracks by this temperature, the weight lost in the specimens past 600 °C due to exposure to temperature was not significant (Fig. 5.4). Thus, the higher frequency component in ultrasonic waves is considerably attenuated due to these propagating cracks. But, due to the insignificant weight loss, the overall ultrasonic velocity did not vary considerably past 600 °C. However, due to the developing temperature gradient, the compressive strength continued to decrease across all the specimens past 600 °C. Thus, after 600 °C, the trend in residual compressive strength across the specimens is not accurately represented by variation in ultrasonic pulse velocity. Overall, it can be concluded that GFNS-50 exhibited better resistance against exposure to elevated temperatures especially between 200 °C and 600 °C.

5.4 Summary

The effect of elevated temperature ranging from 200 °C to 1000 °C on fly ash-GFNS blended geopolymer mortar was investigated by evaluating the compressive strength, weight loss, visual appearance, ultrasonic investigation and microstructural analysis. Based on the results, the following conclusions are drawn:

- The residual compressive strength of fly ash-GFNS blended geopolymer mortar is higher than that of neat fly ash geopolymer mortar after exposure to high temperatures. The specimens of mixture GFNS-50 provided maximum compressive strength after the high-temperature exposures.

- The visual observations and SEM images showed that the voids and cracks of the geopolymer mortar increased with the increase of temperature. However, at elevated temperature, fly ash-GFNS blended geopolymer maintained a better-compacted structure than the neat fly ash geopolymer mortar. The N-M-A-S-H gel developed in fly ash-GFNS blended geopolymer mortar made it denser and stable against high-temperature exposure compared to neat fly ash geopolymer mortar.

- The XRD results indicated that up to 600 °C, crystalline phases of all the geopolymer samples were almost the same as those before the heat exposure. As the temperature further increased to 1000 °C, the number of crystalline peaks increased and amorphous content decreased significantly. A new type of crystal albite was found due to the phase transformation of N-A-S-H gel of the neat fly ash geopolymer at 1000 °C. On the other hand, at 1000 °C, N-M-A-S-H gel of fly ash-GFNS blended geopolymer decomposed or transformed to Na-Silicate (albite, nepheline) and Mg-Silicate (omphacite) based crystalline phases.

- An ultrasonics-based non-destructive test was used to understand the development of voids and cracks in the mortar matrix. The contribution of lower and higher frequency and their differential variation with the evolution of voids were quantified. Overall, the evolution of cracks and voids has a greater diminishing effect on the higher frequencies compared to the lower frequencies. Thus, non-destructive tests have revealed that the GFNS-50 mix had better resistance to the evolution of cracks on account of exposure to

elevated temperatures. The dominance of higher frequency components in the signal spectra indicates the same.

5.5 References

[1] H.Y. Zhang, G.H. Qiu, V. Kodur, Z.S. Yuan, Spalling behavior of metakaolin-fly ash based geopolymer concrete under elevated temperature exposure, Cem. Concr. Compos. 106 (2020) 103483.

[2] N.F. Abushawashi, V. Vimonsatit, F.U.A. Shaikh, Flexural behavior of hybrid PVA fibers reinforced ferrocement panels at elevated temperatures, Fire Mater. 42 (2018) 782–793.

[3] U. Schneider, Concrete at high temperatures - a general review, Fire Saf. J. 13 (1988) 55–68.

[4] A. Mendes, J.G. Sanjayan, W.P. Gates, F. Collins, The influence of water absorption and porosity on the deterioration of cement paste and concrete exposed to elevated temperatures, as in a fire event, Cem. Concr. Compos. 34 (2012) 1067–1074.

[5] D.L. Y Kong, J.G. Sanjayan, Effect of elevated temperatures on geopolymer paste, mortar and concrete, Cem. Concr. Res. 40 (2010) 334–339.

[6] P.N. Lemougna, A. Adediran, J. Yliniemi, A. Ismailov, E. Levanen, P. Tanskanen, P. Kinnunen, J. Roning, M. Illikainen, Thermal stability of one-part metakaolin geopolymer composites containing high volume of spodumene tailings and glass wool, Cem. Concr. Compos. 114 (2020) 103792.

[7] H.Y. Zhang, V. Kodur, B. Wu, L. Cao, F. Wang, Thermal behavior and mechanical properties of geopolymer mortar after exposure to elevated temperatures, Constr. Build. Mater. 109 (2016) 17–24.

[8] Y. Chen, T. Ji, Z. Yang, W. Zhan, Y. Zhang, Sustainable use of ferronickel slag in cementitious composites and the effect on chloride penetration resistance, Constr. Build. Mater. 240 (2020) 117969.

[9] N.S. Katsiotis, P.E. Tsakiridis, D. Velissariou, M.S. Katsiotis, S.M. Alhassan, M. Beazi, Utilization of ferronickel slag as additive in Portland cement: a hydration leaching study, Waste and Biomass Valorization 6 (2015) 177–189.

[10] H. Kim, C.H. Lee, K.Y. Ann, Feasibility of ferronickel slag powder for cementitious binder in concrete mix, Constr. Build. Mater. 207 (2019) 693–705.

[11] S. Majhi, A. Mukherjee, A.F. Spadaccini, Thermal performance of an alkali-activated paste for bonding fibre sheets with concrete, Compos. B Eng. 162 (2019) 43–53.

[12] R. Bligh, T. Glasby, Development of Geopolymer Precast Floor Panels for the Global Change, Institute at University of Queensland, Concr. (2013) 1–8.

[13] A. Buchwald, M. Vicent, R. Kriegel, C. Kaps, M. Monz´o, A. Barba, Geopolymeric binders with different fine fillers - phase transformations at high temperatures, Appl. Clay Sci. 46 (2009) 190–195.

[14] K. Zheng, L. Chen, M. Gbozee, Thermal stability of geopolymers used as supporting materials for TiO2 film coating through sol-gel process: feasibility and improvement, Constr. Build. Mater. 125 (2016) 1114–1126.

[15] P. Duxson, G.C. Lukey, J.S.J. van Deventer, Physical evolution of Na-geopolymer derived from metakaolin up to 1000 °C, J. Mater. Sci. 42 (2007) 3044–3054.

[16] A. van Riessen Subaer, Thermo-mechanical and microstructural characterisation of sodium-poly(sialate-siloxo) (Na-PSS) geopolymers, J. Mater. Sci. 42 (2007) 3117–3123.

[17] Y. Ayg¨ormez, O. Canpolat, M.M. Al-mashhadani, M. Uysal, Elevated temperature, freezing-thawing and wetting-drying effects on polypropylene fiber reinforced metakaolin based geopolymer composites, Constr. Build. Mater. 235 (2020) 117502.

[18] T. Bakharev, Thermal behaviour of geopolymers prepared using class F fly ash and elevated temperature curing, Cem. Concr. Res. 36 (2006) 1134–1147.

[19] N.K. Lee, K.T. Koh, G.H. An, G.S. Ryu, Influence of binder composition on the gel structure in alkali activated fly ash/slag pastes exposed to elevated temperatures, Ceram. Int. 43 (2017) 2471–2480.

[20] S.M. Park, J.G. Jang, N.K. Lee, H.K. Lee, Physicochemical properties of binder gel in alkali-activated fly ash/slag exposed to high temperatures, Cem. Concr. Res. 89 (2016) 72–79.

[21] M. Bouasria, L. Babouri, F. Khadraoui, D. Chateigner, S. Gascoin, V. Pralong, M. Benzaama, B. Orberger, Y.E. Mendili, Insight into the partial replacement of cement by ferronickel slags from New Caledonia, Eur. J. Environ. Civ. Eng. (2020), https://doi.org/10.1080/19648189.2020.1814421.

[22] Y.C. Choi, S. Choi, Alkali-silica reactivity of cementitious materials using ferro- nickel slag fine aggregates produced in different cooling conditions, Constr. Build. Mater. 99 (2015) 279–287.

[23] A.K. Saha, M.N.N. Khan, P.K. Sarker, Value added utilization of by-product electric furnace ferronickel slag as construction materials: a review, Resour. Conserv. Recycl. 134 (2018) 10–24.

[24] Y. Huang, Q. Wang, M. Shi, Characteristics and reactivity of ferronickel slag powder, Constr. Build. Mater. 156 (2017) 773–789.

[25] D. Wang, Q. Wang, S. Zhuang, J. Yang, Evaluation of alkali-activated blast furnace ferronickel slag as a cementitious material: reaction mechanism, engineering properties and leaching behaviors, Constr. Build. Mater. 188 (2018) 860–873.

[26] Q. Wu, S. Wang, T. Yang, H. Zhu, S. Li, Effect of high-magnesium nickel slag on hydration characteristics of Portland cement, J. Mater. Civ. Eng. 31 (2019) 04019051.

[27] N. Lemonis, P.E. Tsakiridis, N.S. Katsiotis, S. Antiohos, D. Papageorgiou, M. S. Katsiotis, M. Beazi-Katsioti, Hydration study of ternary blended cements containing ferronickel slag and natural pozzolan, Constr. Build. Mater. 81 (2015) 130–139.

[28] B. Li, B. Huo, R. Cao, S. Wang, Y. Zhang, Sulfate resistance of steam cured ferronickel slag blended cement mortar, Cem. Concr. Compos. 96 (2019) 204–211.

[29] M.A. Rahman, P.K. Sarker, F.U.A. Shaikh, A.K. Saha, Soundness and compressive strength of Portland cement blended with ground granulated ferronickel slag, Constr. Build. Mater. 140 (2017) 194–202.

[30] M. Zhai, H. Zhu, G. Liang, Q. Wu, C. Zhang, S. Hua, Z. Zhang, Enhancing the recyclability of air-cooled high-magnesium ferronickel slag in cement-based materials: a study of assessing soundness through modifying method, Constr. Build. Mater. 261 (2020) 120523.

[31] R. Cao, Z. Jia, Z. Zhang, Y. Zhang, N. Banthia, Leaching kinetics and reactivity evaluation of ferronickel slag in alkaline conditions, Cem. Concr. Res. 137 (2020) 106202.

[32] K. Komnitsas, L. Yurramendi, G. Bartzas, V. Karmali, E. Petrakis, Factors affecting co-valorization of fayalitic and ferronickel slags for the production of alkali activated materials, Sci. Total Environ. 721 (2020) 137753.

[33] K. Komnitsas, D. Zaharaki, V. Perdikatsis, Effect of synthesis parameters on the compressive strength of low-calcium ferronickel slag inorganic polymers, J. Hazard Mater. 161 (2009) 760–768.

[34] N. You, B. Li, R. Cao, J. Shi, C. Chen, Y. Zhang, The influence of steel slag and ferronickel slag on the properties of alkali-activated slag mortar, Constr. Build. Mater. 227 (2019) 116614.

[35] K. Komnitsas, D. Zaharaki, V. Perdikatsis, Geopolymerisation of low calcium ferronickel slags, J. Mater. Sci. 42 (2007) 3073–3082.

[36] J.C. Kuri, M.N.N. Khan, P.K. Sarker, Fresh and hardened properties of geopolymer binder using ground high magnesium ferronickel slag with fly ash, Constr. Build. Mater. 272 (2021) 121877.

[37] I. Maragkos, I.P. Giannopoulou, D. Panias, Synthesis of ferronickel slag-based geopolymers, Miner. Eng. 22 (2009) 196–203.

[38] T. Yang, X. Yao, Z. Zhang, Geopolymer prepared with high-magnesium nickel slag: Characterization of properties and microstructure, Constr. Build. Mater. 59 (2014) 188–194.

[39] K. Sakkas, P. Nomikos, A. Sofianos, D. Panias, Sodium-based fire resistant geopolymer for passive fire protection, Fire Mater. 39 (2015) 259–270.

[40] K. Sakkas, P. Nomikos, A. Sofianos, D. Panias, Utilisation of FeNi-Slag for the production of inorganic polymeric materials for construction or for passive fire protection, Waste and Biomass Valorization 5 (2014) 403–410.

[41] K. Sakkas, P. Nomikos, A. Sofianos, D. Panias, Inorganic polymeric materials for passive fire protection of underground constructions, Fire Mater. 37 (2013) 140–150.

[42] K. Sakkas, D. Panias, P.P. Nomikos, A.I. Sofianos, Potassium based geopolymer for passive fire protection of concrete tunnels linings, Tunn. Undergr. Space Technol. 43 (2014) 148–156.

[43] D. Zaharaki, M. Galetakis, K. Komnitsas, Valorization of construction and demolition (C&D) and industrial wastes through alkali activation, Constr. Build. Mater. 121 (2016) 686–693.

[44] T. Yang, Q. Wu, H. Zhu, Z. Zhang, Geopolymer with improved thermal stability by incorporating high-magnesium nickel slag, Constr. Build. Mater. 155 (2017) 475–484.

[45] A.K. Saha, P.K. Sarker, S. Majhi, Effect of elevated temperatures on concrete incorporating ferronickel slag as fine aggregate, Fire Mater. 43 (2019) 8–21.

[46] A.K. Saha, S. Majhi, P.K. Sarker, A. Mukherjee, A. Siddika, F. Aslani, Y. Zhuge, Non- destructive prediction of strength of concrete made by lightweight recycled aggregates and nickel slag, J. Build. Eng. 33 (2021) 101614.

[47] S. Majhi, A. Mukherjee, N.V. George, B. Uy, Corrosion detection in steel bar: a time- frequency approach, NDT E Int. 107 (2019) 102150.

[48] J.C. Kuri, M.N.N. Khan, P.K. Sarker, Workability, strength and microstructural properties of ground ferronickel slag blended fly ash geopolymer mortar, J. Sustain. Cem. Mater. (2020), https://doi.org/10.1080/ 21650373.2020.1823905.

[49] ASTM C618-19, Standard Specification for Coal Fly Ash and Raw or Calcined Natural Pozzolan for Use in Concrete, ASTM International, West Conshohocken, PA, 2019.

[50] J.C. Kuri, M.N.N. Khan, P.K. Sarker, Compressive strength of geopolymer mortar using ground ferronickel slag and fly ash, 2644-108X, Proceedings of International Structural Engineering and Construction 7 (1) (August 2020), https://doi.org/ 10.14455/isec.res.2020.7(1).mat-05.

[51] P. Nath, P.K. Sarker, Use of OPC to improve setting and early strength properties of low calcium fly ash geopolymer concrete cured at room temperature, Cem. Concr. Compos. 55 (2015) 205–214.

[52] A. Hosan, S. Haque, F. Shaikh, Compressive behaviour of sodium and potassium activators synthetized fly ash geopolymer at elevated temperatures: a comparative study, J. Build. Eng. 8 (2016) 123–130.

[53] RILEM TC 129-MHT, Test methods for mechanical properties of concrete at high temperatures - compressive strength for service and accident conditions, Mater. Struct. 28 (1995) 410–414.

[54] AS 1012.9, Methods of Testing Concrete Method 9: Compressive Strength Tests — Concrete , Mortar and Grout Specimens, Standards Australia, Sydney, 2014.

[55] H.M. Rietveld, A profile refinement method for nuclear and magnetic structures, J. Appl. Crystallogr. 2 (1969) 65–71.

[56] A.A. Coelho, TOPAS and TOPAS-Academic: an optimization program integrating computer algebra and crystallographic objects written in C++, J. Appl. Crystallogr. 51 (2018) 210–218.

[57] R.J. Hill, C.J. Howard, Quantitative phase analysis from neutron powder diffraction data using the Rietveld method, J. Appl. Crystallogr. 20 (1987) 467–474.

[58] N.R. Short, J.A. Purkiss, S.E. Guise, Assessment of fire damaged concrete using colour image analysis, Constr. Build. Mater. 15 (2001) 9–15.

[59] I. Hager, Colour change in heated concrete, Fire Technol. 50 (2014) 945–958.

[60] W.D.A. Rickard, A.V. Riessen, P. Walls, Thermal character of geopolymers synthesized from class F fly ash containing high concentrations of Iron and a-Quartz, Int. J. Appl. Ceram. Technol. 7 (2010) 81–88.

[61] A.K. Saha, P.K. Sarker, V. Golovanevskiy, Thermal properties and residual strength after high temperature exposure of cement mortar using ferronickel slag aggregate, Constr. Build. Mater. 199 (2019) 601–612.

[62] M.N.N. Khan, P.K. Sarker, Effect of waste glass fine aggregate on the strength, durability and high temperature resistance of alkali-activated fly ash and GGBFS blended mortar, Constr. Build. Mater. 263 (2020) 120177.

[63] N. Ranjbar, M. Mehrali, U.J. Alengaram, H.S.C. Metselaar, M.Z. Jumaat, Compressive strength and microstructural analysis of fly ash/palm oil fuel ash based geopolymer mortar under elevated temperatures, Constr. Build. Mater. 65 (2014) 114–121.

[64] Z. Yang, R. Mocadlo, M. Zhao, R.D. Sisson, M. Tao, J. Liang, Preparation of a geopolymer from red mud slurry and class F fly ash and its behavior at elevated temperatures, Constr. Build. Mater. 221 (2019) 308–317.

[65] P. Behera, V. Baheti, J. Militky, P. Louda, Elevated temperature properties of basalt microfibril filled geopolymer composites, Constr. Build. Mater. 163 (2018) 850–860.

[66] S.A. Omer, R. Demirboga, W.H. Khushefati, Relationship between compressive strength and UPV of GGBFS based geopolymer mortars exposed to elevated temperatures, Constr. Build. Mater. 94 (2015) 189–195.

[67] S. Luhar, S. Chaudhary, I. Luhar, Thermal resistance of fly ash based rubberized geopolymer concrete, J. Build. Eng. 19 (2018) 420–428.

[68] F. Qu, W. Li, Z. Tao, A. Castel, K. Wang, High temperature resistance of fly ash/ GGBFS-based geopolymer mortar with load-induced damage, Mater. Struct. 53 (2020) 111.

[69] A. Celik, K. Yilmaz, O. Canpolat, M.M. Al-mashhadani, Y. Ayg̈ormez, M. Uysal, High-temperature behavior and mechanical characteristics of boron waste additive metakaolin based geopolymer composites reinforced with synthetic fibers, Constr. Build. Mater. 187 (2018) 1190–1203.

[70] X. Jiang, Y. Zhang, R. Xiao, P. Polaczyk, M. Zhang, W. Hu, Y. Bai, B. Huang, A comparative study on geopolymers synthesized by different classes of fly ash after exposure to elevated temperatures, J. Clean. Prod. 270 (2020) 122500.

[71] J. Ye, W. Zhang, D. Shi, Effect of elevated temperature on the properties of geopolymer synthesized from calcined ore-dressing tailing of bauxite and ground- granulated blast furnace slag, Constr. Build. Mater. 69 (2014) 41–48.

[72] M.B. Haha, B. Lothenbach, G.L. Saout, F. Winnefeld, Influence of slag chemistry on the hydration of alkali-activated blast-furnace slag—part II: effect of Al2O3, Cem. Concr. Res. 42 (2012) 74–83.

[73] S. Zhang, A. Keulen, K. Arbi, G. Ye, Waste glass as partial mineral precursor in alkali-activated slag/fly ash system, Cem. Concr. Res. 102 (2017) 29–40.

[74] T. Bakharev, Thermal behavior of geopolymers prepared using class F fly ash and elevated temperature curing, Cem. Concr. Res. 36 (2006) 1134–1137.

[75] K. Valdiviés-Cruz, A. Lam, C.M. Zicovich-Wilson, Chemical interaction of water molecules with framework Al in acid zeolites: a periodic ab initio study on H- clinoptilolite, Phys. Chem. Chem. Phys. 17 (2015) 23657–23666.

[76] P. Duan, C. Yan, W. Zhou, Compressive strength and microstructure of fly ash based geopolymer blended with silica fume under thermal cycle, Cem. Concr. Res. 78 (2017) 108–119.

[77] S. Majhi, A. Mukherjee, N.V. George, V. Karaganov, B. Uy, Corrosion monitoring in steel bars using Laser ultrasonic guided waves and advanced signal processing, Mech. Syst. Signal Process. 149 (2021), 107176.

CHAPTER 6: SULPHURIC ACID RESISTANCE OF GFNS BLENDED FLY ASH GEOPOLYMER MORTAR

The contents presented in this chapter were published in the following paper:

Kuri, J. C., Sarker, P. K., & Shaikh, F.U.A. (2021). Sulphuric acid resistance of ground ferronickel slag blended fly ash geopolymer mortar. Construction and Building Materials, 313, 125505.

This chapter presents an investigation on the sulphuric acid resistance of geopolymer mortar made using different proportions of ground ferronickel slag (GFNS) with fly ash. The changes in mass, visual appearance, compressive strength and microstructure of the geopolymer mortars were evaluated after immersion in 3% sulphuric acid solution for up to 1 year.

6.1 Overview

Durability performance is an important design consideration of concrete structures. High durability of concrete is desired to achieve long service life of a structure and minimize the requirement of maintenance [1]. The deterioration of concrete structures is usually accelerated when they are exposed to aggressive environment, such as acid exposures. The sulphuric acid attack is a common deterioration mechanism that is used to investigate the acid resistance of concrete. A structure can be exposed to aggressive sulphuric acid in different ways. Industrial effluent, ground water and acid rains are the major sources of sulphuric acid that can cause deterioration of concrete structures [2, 3]. Apart from the industries producing sulphuric acid, others that use the acid in their production process include the producers of chemicals, fertilizers, metals, battery, electronics and petroleum. In the process of acid attack in OPC concrete, calcium ions are leached from the hydrated product to form calcium salt of the acid which leads to increase the porosity resulting in decreases of strength and durability [4, 5]. The recently developed geopolymer binders are generally shown to have a very good resistance against acid attack when compared to OPC concrete [6–8].

Geopolymers are ceramic-like materials with three-dimensional silica aluminate structures, produced by chemical reaction between alkali liquids and aluminosilicate materials [9, 10]. Recently, geopolymers have attracted notable interests due to its

environmental benefit of using wastes and by-products as well as their good mechanical properties and durability performances [11–14].

Several studies reported favourable performance of geopolymer in the sulphuric acid environment [15-18]. Fernando and Said [19] found that the mine waste mud based geopolymer concrete provided higher stability than OPC concrete in sulphuric acid solution. Lee and Lee [20] evaluated the influence of the proportion of GGBFS to fly ash on the sulphuric acid resistance of geopolymer paste. The authors reported that as the N-A-S-H gel is less susceptible to sulphuric acid than C-(A)-S-H gel, better resistance to sulphuric acid was found in geopolymers containing less amount of GGBFS. In contrast, Lloyd et al. [24] found that corrosion resistance of geopolymer increased with the increase of GGBFS content after 100 days of exposure to highly concentrated (pH = 1.0) sulphuric acid. The GGBFS content increased the denseness of the microstructure by producing C-(A)-S-H gel which reduced the depth of corrosion. A better performance was found in fly ash geopolymer when exposed to 5% sulphuric acid solutions as compared to OPC paste [5]. Ariffin et al. [21] found that pulverized fuel ash and palm oil fuel ash blended geopolymer concrete had better resistance than OPC concrete. Allahverdi and Škvára [22, 23] studied the corrosion mechanism of geopolymer at high, medium and low concentrations of sulphuric acid. The authors reported that deposition of gypsum was found in the corroded layer due to the use of highly concentrated (pH = 1) sulphuric acid. On the other hand, only ions were leached in a solution of low concentration (pH = 3) without the deposition of gypsum. Recently, Gu et al. [25] suggested a multiscale approach to investigate the deterioration mechanism of alkali activated and conventional cementitious materials after the sulphuric acid attack. The authors found that durability highly depends on the scale of the maturity of the products such as paste, mortar or concrete.

The resistance of geopolymers against acidic attack is highly dependent on the properties of aluminosilicate gel products. The characteristics of aluminosilicate gel greatly depends on the chemical constituents of the precursor and alkaline liquid. Ferronickel slag is an industrial metallurgical slag, discharged during the manufacturing of ferronickel alloys [26–29]. Ferronickel slag contains a considerable proportion of Si, Fe and Mg, which exist in crystalline and non-crystalline mineral forms [30–33]. Due to its high proportion of amorphous silica, ground ferronickel slag

(GFNS) showed reactivity when mixed with OPC as a supplementary binder [34–37] or with an alkaline solution to produce geopolymers as a precursor material [38–42]. The feasibility of using GFNS to produce geopolymer is reported in some previous studies [10, 43–46]. The use of GFNS in OPC mortars showed an improvement in terms of sulphuric acid resistance [47]. However, there is a lack of detailed results in literature on the sulphuric acid attack of geopolymers containing GFNS as a precursor. Therefore, the effect of sulphuric acid exposure on geopolymer mortars applying various percentages of GFNS with fly ash needs to be investigated.

The resistance of geopolymer mortar synthesized by GFNS and fly ash was investigated after exposure to the sulphuric acid solution for up to 12 months. The changes in mass, compressive strength and visual appearance of the geopolymer mortars after exposure to sulphuric acid were evaluated. The microstructural and mineralogical changes were investigated by SEM, EDX and QXRD (quantitative X-ray diffraction) analysis to gain an insight into the deterioration process.

6.2 Experimental Work

6.2.1 Materials and mix proportions

The GFNS and fly ash were used as the precursor to make geopolymer mortar [48]. As the principal oxide (SiO_2 + Al_2O_3 + Fe_2O_3) of fly ash is greater than 70%, it is categorized as class F based on ASTM C618-05 [49]. A mixture of Na_2SiO_3 solution with 14.7% Na_2O, 29.4% SiO_2 and 55.9% H_2O, and 8 molar sodium hydroxide solution was used as the alkali activator. Natural sand with fineness modulus of 1.95 was used as the fine aggregate. The sand was prepared to saturated surface dry (SSD) condition following ASTM C128 [50].

Table 6.1 Mixture proportions of geopolymer mortars [48]

Mixture ID	Ingredients (kg/m^3)				
	GFNS	Fly ash	Sand	SH[*]	SS[**]
GFNS0	0	733	1137	110	220
GFNS25	183	550	1137	110	220
GFNS50	367	367	1137	110	220
GFNS75	550	183	1137	110	220

[*]Sodium hydroxide liquid
[**]Sodium silicate liquid

123

Table 6.1 shows the mixture proportions of geopolymer mortar. The mortar mixtures are selected on the basis of the previous works [48, 51, 52]. Fly ash was partially replaced by 0, 25, 50 and 75% mass of GFNS and the corresponding mixtures are referred as GFNS0, GFNS25, GFNS50 and GFNS75, respectively. The alkali liquid was 45% mass of the precursors and the mass ratio of Na_2SiO_3 to NaOH liquids was 2.0. Some geopolymer paste samples were cast according to the previous study [44] for microstructural analysis.

6.2.2 Sample preparation and testing

To cast the geopolymer mortar samples, the GFNS-fly ash blend and SSD sand were first dry mixed and then the alkaline liquid was mixed slowly to get a uniform fresh mixture. The $50 \times 50 \times 50$ mm^3 moulds were then filled with geopolymer mortar and compaction was done by a vibrating table. The samples were cured at 60 °C for 24 hours. The samples were demolded after heat curing and stored in ambient condition (20 ± 3 °C temperature, 65 ± 5% relative humidity) till testing.

The sulphuric acid resistance test of geopolymer mortars was conducted according to the modified test method B of ASTM C 267 [53]. After heat curing at 60 °C for 24 hours, the mortar specimens were cooled down to room temperature and then submerged in 3% sulphuric acid solution for up to one year. The sulphuric acid solution was refreshed monthly in order to maintain the strength of the acid. The visual appearance, weight, compressive strength and microstructure of the samples were examined at various exposure periods. After a certain exposure period, the samples were taken out from the liquid and loose particles of the surface were removed carefully by a soft brush.

The loss of alkalinity of the sample was determined by splitting the exposed samples and applying a 1% phenolphthalein solution on the cut surface. After applying the phenolphthalein solution, the surface area that shows pink or purple colour indicates the regions of high alkalinity, where pH is more than about 9.0. On the other hand, the colourless region was considered as the alkalinity lost area due to the penetration of acid, where the pH value is lower than 9.0 [54, 55].

Before and after acid exposure, compressive strength test of the samples was conducted by a Controls MCC8 machine according to AS 1012.9 [56].

The SEM and EDX analysis were conducted to investigate the microstructure and elemental compositions of the acid-exposed samples using a scanning electron microscope (Mira3 XMU Tescan) equipped with Oxford Instruments.

The QXRD analysis was conducted to evaluate the change of mineralogical phase and amorphous content of the acid-exposed samples. For accurate mineralogical analysis, QXRD analysis was performed on paste specimens exposed to same exposure condition of mortar. The XRD data was acquired by a D8 Advance diffractometer with operating conditions of 40kV and 40mA. The XRD patterns were collected at 2θ values of $7°$-$120°$ where step size was $0.015°$ and measuring time was 0.7 sec/step. The EVA 11.0 software was used to determine the phases. After that, a quantitative phase analysis was performed by Rietveld [57] full pattern analysis using TOPAS [58]. The relative Rietveld weight percentages were converted to the absolute proportions by the internal standard method [59].

6.3 Results and Discussion

6.3.1 Visual inspection

Fig. 6.1 presents the visual appearance of geopolymer mortar and paste specimens at different sulphuric acid exposure periods. It is seen that all the geopolymer mortar samples were structurally intact with only minor damages at the surface after the acid exposures. For all the mixtures, the surface deterioration of specimens increased with the increase of exposure duration. However, it can be noticed that the most visible deterioration occurred on the neat fly ash (GFNS0) geopolymer mortar where sand particles came exposed due to the loss of geopolymer paste from the surface. On the other hand, many visible cracks were observed in all the geopolymer paste samples after immersion in sulphuric acid solution. However, significant scaling and spalling was observed in the GFNS0 paste sample after one month of acid exposure. Therefore, it was not possible to continue further acid exposure of the GFNS0 paste samples due to the severe damages.
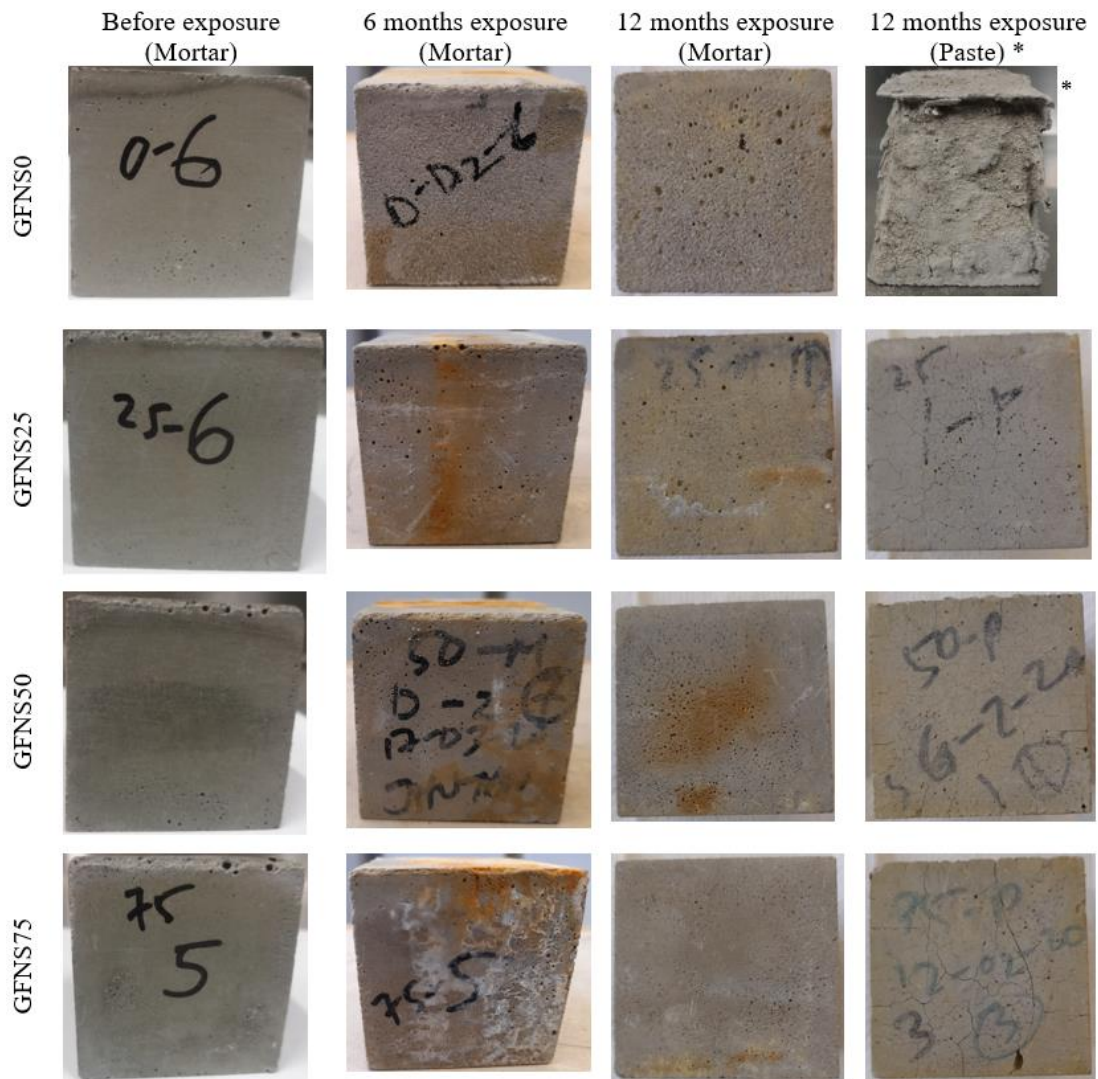
Fig. 6.1 Visual appearance of the geopolymer mortars and pastes at different H_2SO_4 exposure periods (*One month exposure for GFNS0 paste sample)

Fig. 6.2 presents the photographs of cross-sections of geopolymer mortar specimens after spraying the phenolphthalein solution. It is seen that all the samples showed a purple/pink colour throughout the surfaces before acid exposure which indicates the high alkalinity of the samples. After immersion in the acid solution, the outer layer of all the samples remained colourless and core became light pink. This indicates the loss of alkalinity of the samples after immersion in acid solution. It can be noticed that the colourless area of all samples increased with the exposure period and thus the loss of alkalinity of the sample increased with the exposure period. The depth of sulphuric acid penetration or ion exchange area of the sample is related to the loss of alkalinity [1].
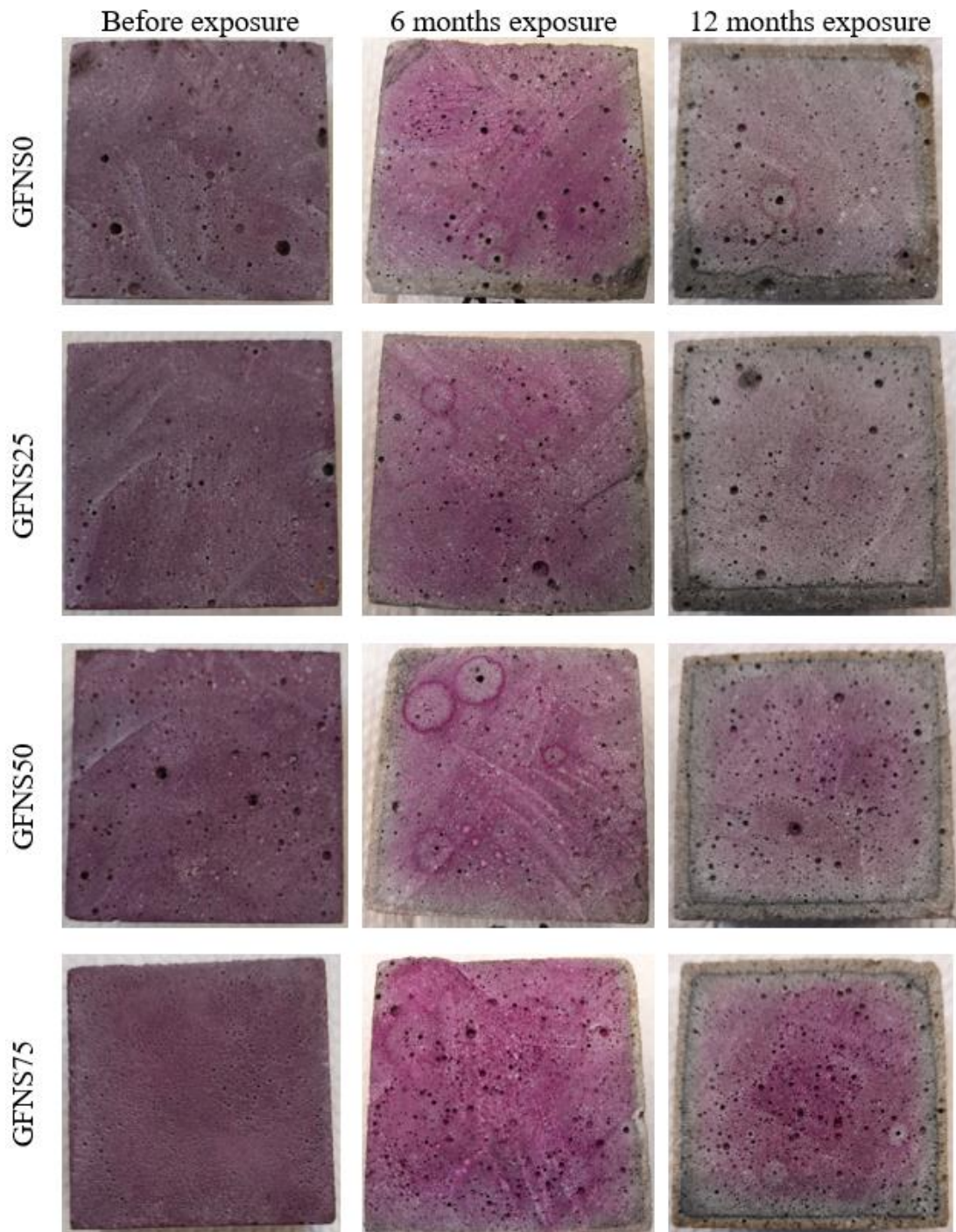
Fig. 6.2 Visual appearance of the cross section of geopolymer mortars sprayed with phenolphthalein solution

It can be noticed that after exposure to the sulphuric acid solution, sample GFNS0 showed a less pink core with a larger colourless area compared to the other samples. This indicates the higher loss of alkalinity due to the ingress of higher amount of sulphuric acid in the neat fly ash (GFNS0) geopolymer mortar. On the other hand,

inclusion of GFNS provided a more compact structure and reduced the ingress of sulphuric acid. Thus, the fly ash-GFNS blended samples showed less colourless areas and large pink core areas. However, the lowest alkalinity loss area with highest pink core area was observed in sample GFNS75 due to the more compact structure as identified in the SEM image and EDX analysis, which are discussed in section 6.3.4.

6.3.2 Residual compressive strength

The residual compressive strengths of the geopolymer mortars after sulphuric acid exposures are shown in Fig. 6.3. Before immersion in sulphuric acid solution, compressive strengths of the mortar samples of mixtures GFNS0, GFNS25, GFNS50 and GFNS75 were 54, 63, 66 and 71 MPa, respectively. The strength of GFNS0 sample is primarily associated with N-A-S-H gel as recognized in SEM and EDX analysis discussed in section 6.3.4. The rise of strength due to the use of GFNS is correlated with the formation of sodium magnesium alumiosilicate hydrate (N-M-A-S-H) gel [44, 45] as found in SEM and EDX analysis. It can be noticed that loss of strength occurred in all the samples, and it increased gradually with the increase of acid exposure period. The strength loss after 12 months of sulphuric acid exposure of samples GFNS0, GFNS25, GFNS50 and GFNS75 were 43.67, 31.05, 24.15 and 22.54%, respectively with respect to the corresponding compressive strengths before acid exposure.
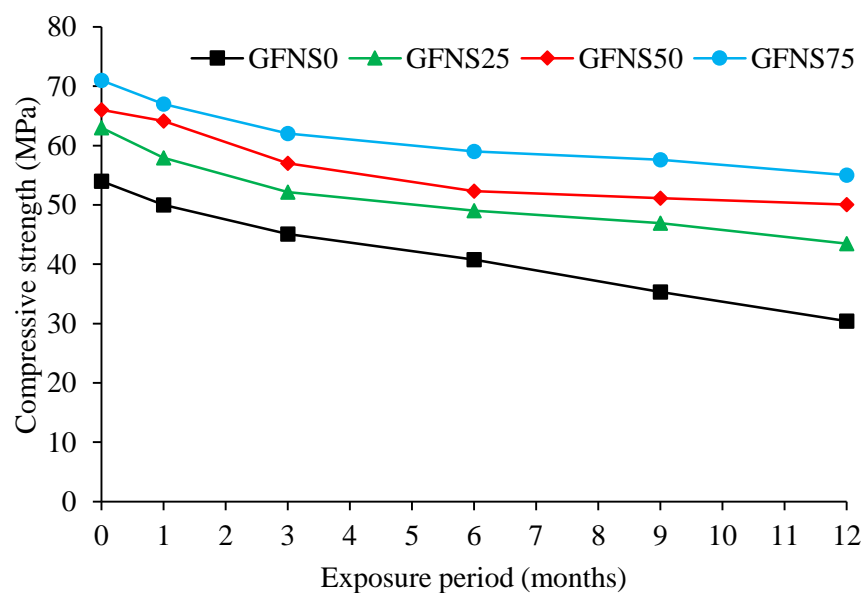
Fig. 6.3 Residual compressive strength of mortars exposed to sulphuric acid solution

The strength loss is attributed to the breakdown of aluminosilicate network of geopolymer by the sulphuric acid [21]. The aluminosilicate network of geopolymer product is broken by the H^+ of H_2SO_4 and yields ($Si(OH)_4$) and Al^{3+} [2, 5, 60]. Thus, the oxy-aluminium bridge (-Al…O-Si-O) of geopolymer is destroyed by sulphuric acid which leads to reduce the strength of the geopolymer [60].

Moreover, the deterioration of geopolymer is ascribed to the formation of gypsum due to the reaction of calcium and sulphuric acid [61, 62]. The gypsum induces expansive pressure, which increased cracks and consequently the loss of strength [13, 60]. The presence of gypsum was identified in SEM, EDX and XRD results discussed in sections 6.3.4 and 6.3.5.

It can be observed that fly ash-GFNS geopolymer mortars (GFNS25, GFNS50, GFNS75) showed lower losses of strength than the neat fly ash (GFNS0) geopolymer mortar. The lower loss of strength of the fly ash-GFNS geopolymers is attributed to the existence of more stable N-M-A-S-H gel compared to N-A-S-H gel of the neat fly ash geopolymer as discussed in section 6.3.4. Furthermore, fly ash contained a higher percentage of calcium than GFNS. Therefore, after exposure to sulfuric acid solution, higher calcium content of fly ash reacted with sulphur ions of sulphuric acid and formed higher amount of gypsum in neat fly ash geopolymer mortar as determined in the QXRD analysis presented in section 6.3.5. The deposition of higher amount of gypsum in neat fly ash geopolymer matrix induced higher stresses which increased the expansive microcracks and consequently more deterioration occurred in neat fly ash geopolymer mortar than the fly ash-GFNS geopolymer mortars. It is also seen that GFNS75 with the highest GFNS content showed highest residual strength compared to other mixtures throughout the exposure periods. Incorporation of GFNS made a dense structure by developing N-M-A-S-H gel as found in section 6.3.4. Thus, lower ingress of sulphuric acid occurred in GFNS75 due to the lower porosity and consequently highest residual strength found in the samples of this mix. A similar observation was found in previous studies [2, 63, 64], where lower porosity improved the sulphuric acid resistance by reducing the ingress of acid. Besides, higher amount of GFNS content reduced the calcium content in the mixture. In consequence, less gypsum is formed in GFNS75 and thus, less cracks and higher residual strength found in GFNS75 compared to the other mixtures.

6.3.3 Mass change

Fig. 6.4 presents the mass loss of the mortar specimens after exposure to acid solution. The mass losses after different exposure periods were calculated with respect to initial mass before acid exposure. It is seen that the mass loss of the samples increased gradually with the increase of acid exposure period. After 12 months of exposure to the sulphuric acid solution, 2.95, 2.15, 1.36 and 1.50% mass losses were found in GFNS0, GFNS25, GFNS50 and GFNS75, respectively.
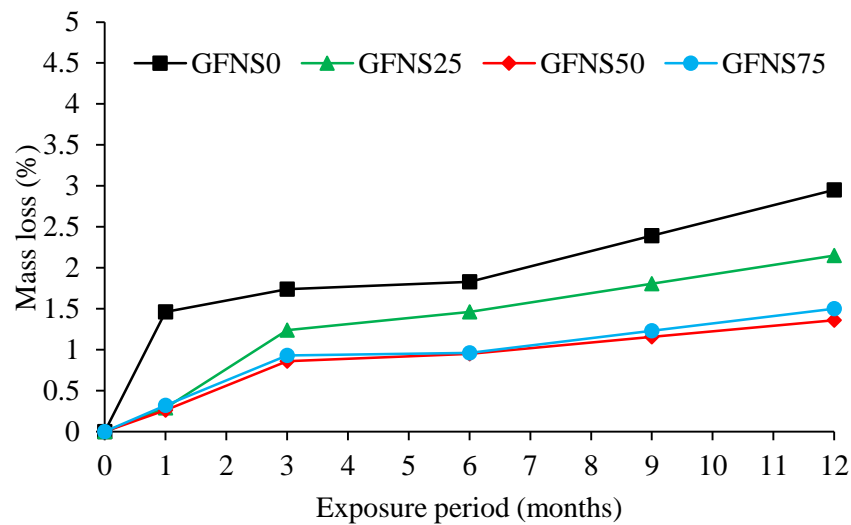
Fig. 6.4 Mass loss of mortars after immersion in sulphuric acid solution

The loss of mass is attributed to the depolymerisation of the aluminosilicate gel and leaching of ions from the matrix. Besides, the mass loss is attributed to the formation of gypsum as identified in SEM, EDX and XRD analysis discussed in section 6.3.4 and 6.3.5. The gypsum induced internal stresses which caused expansion and dimensional instability in the matrix [20]. Thus, microcracks formed in the geopolymer matrix and consequently scaling and spalling occurred in the surface layers which leads to reduce the mass of the sample [4, 13]. However, it can be observed that low mass losses were found in fly ash-GFNS blended mortars than in the neat fly ash geopolymer mortar. The less mass loss of the fly ash-GFNS blended geopolymer is ascribed to the low calcium content of GFNS and more stable N-M-A-S-H gel.

6.3.4 SEM and EDX analysis

Fig. 6.5 presents the SEM micrographs and EDX spectrums of geopolymer mortars at different acid exposure periods. It can be noted that the specimens for SEM and EDX were collected from the outer layer of the samples.

131
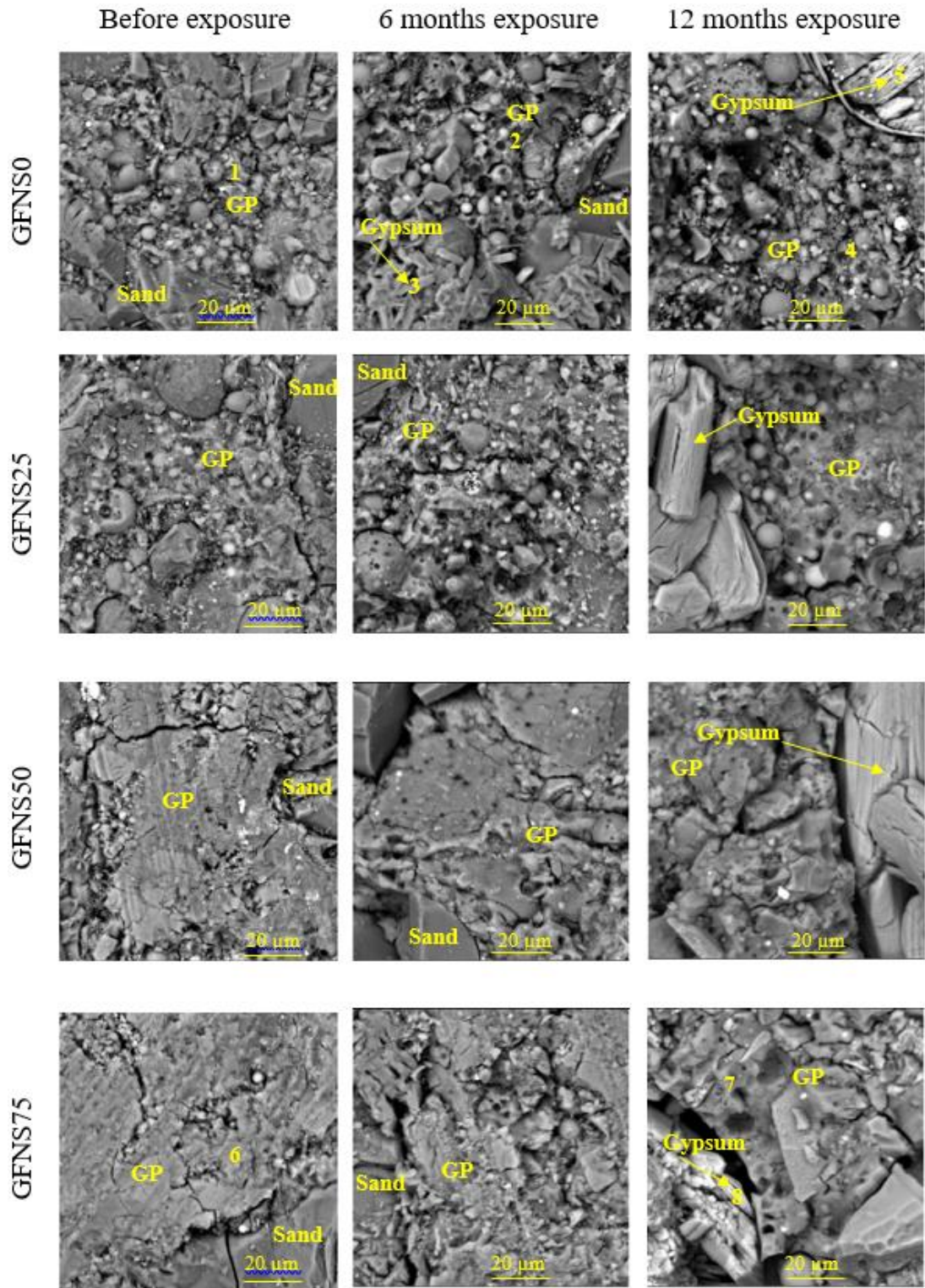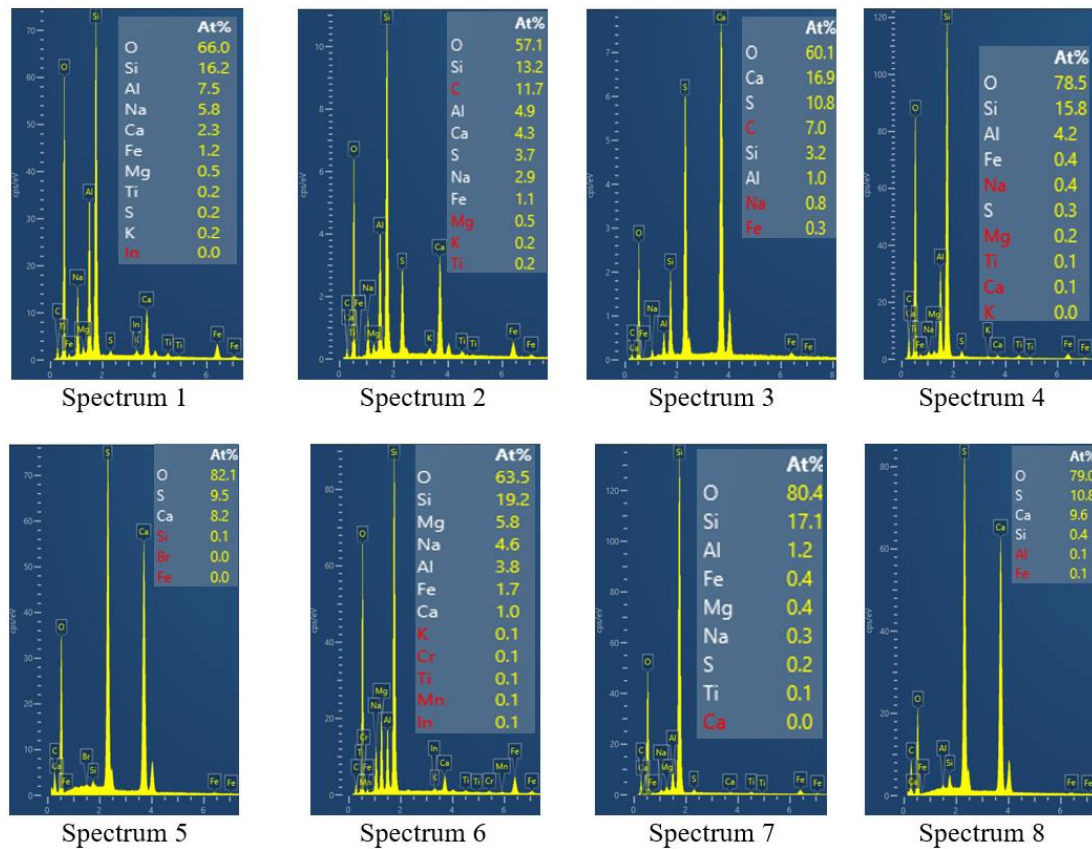
**Fig. 6.5** SEM images and EDX spectra of geopolymer mortars at different acid exposure periods (GP indicates geopolymer matrix)

Before immersion, a homogenous and compact microstructure was noticed for all the samples. It can be seen from the EDX spectrum 1 that before exposure, the main constituents of GFNS0 specimen were sodium (Na), aluminium (Al), silicon (Si) and oxygen (O), indicating the existence of N-A-S-H gel [44, 65]. It can be noticed that after exposure, the dense microstructure of the pre-exposure mortar changed to more porous microstructure. The deterioration of geopolymer mortar is associated with the depolymerisation of the aluminosilicate gel in acid solution. After exposure to acid solution, Na and Al contents of the gel leached to acid solution and thus the Na and Al content of the geopolymer matrix reduced (spectra 2 and 4). The geopolymer matrix deteriorated due to the gradual depletion of Na and Al [1, 8]. Moreover, after 6 months and 12 months of exposure to acid solution, rod shaped crystal substances are also seen in the neat fly ash geopolymer mortar. The EDX spectra of those substances confirmed the presence of gypsum crystal as indicated by the major proportions of calcium, sulphur and oxygen (spectra 3 and 5).

In contrast, GFNS25, GFNS50 and GFNS75 geopolymer mortars showed more compact microstructure than the GFNS0 geopolymer mortar. Before the acid exposure, the prime compositions of the GFNS25, GFNS50 and GFNS75 geopolymer matrix were sodium (Na), magnesium (Mg), aluminium (Al), silicon (Si) and oxygen (O) (spectrum 6), indicating the existence of N-M-A-S-H gel in the fly ash-GFNS geopolymer [44, 65]. The less porous structure and high strength (Fig. 6.3) of fly ash-GFNS blended geopolymers is correlated with the produced N-M-A-S-H gel described in the earlier studies [45, 48]. After the acid exposure, these components are also reduced (spectrum 7) in the deteriorated area which was similar to that of the neat fly ash geopolymer mortar. However, the mortar sample with GFNS exhibited less deterioration than the neat fly ash mortar. The N-M-A-S-H gel provided a dense structure which reduced the penetration of acid solution and in consequence, less deterioration occurred in the fly ash-GFNS mortars. The denseness increased with the increase of GFNS, and thus lower deterioration occurred in the GFNS75 specimen compared to the other specimens. Furthermore, though expansive gypsum (spectrum 8) crystals were found in the fly ash-GFNS mortars after 12 months of exposure, it was not found after 6 months of exposure.

Although the EDX point analysis is helpful to get an idea of the reaction product, an EDX mapping can be further helpful to get an overall trend of increase or decrease of a particular element in an area. Therefore, after acid exposure, the EDX map of geopolymer paste covering a region including high and low deteriorated areas is shown in Fig. 6.6. From the EDX map, it can be seen that the concentrations of Na, Mg and Al in the outer surface (highly deteriorated area) are lower than those of the inner surface (less deteriorated area). This indicates the leaching of Na, Mg and Al from the matrix due to the acid penetration. On the other hand, it is noticed that the concentration of Si is higher in the highly deteriorated area than in the less deteriorated area for all the samples. Leaching of Na, Mg and Al into the sulphuric acid solution enriched the geopolymer matrix in Si and thus showed higher concentrations of Si [4]. Higher Si can cause shrinkage and thus cracks were formed in the deteriorated layer.

GFNS0   GFNS25   GFNS50   GFNS75
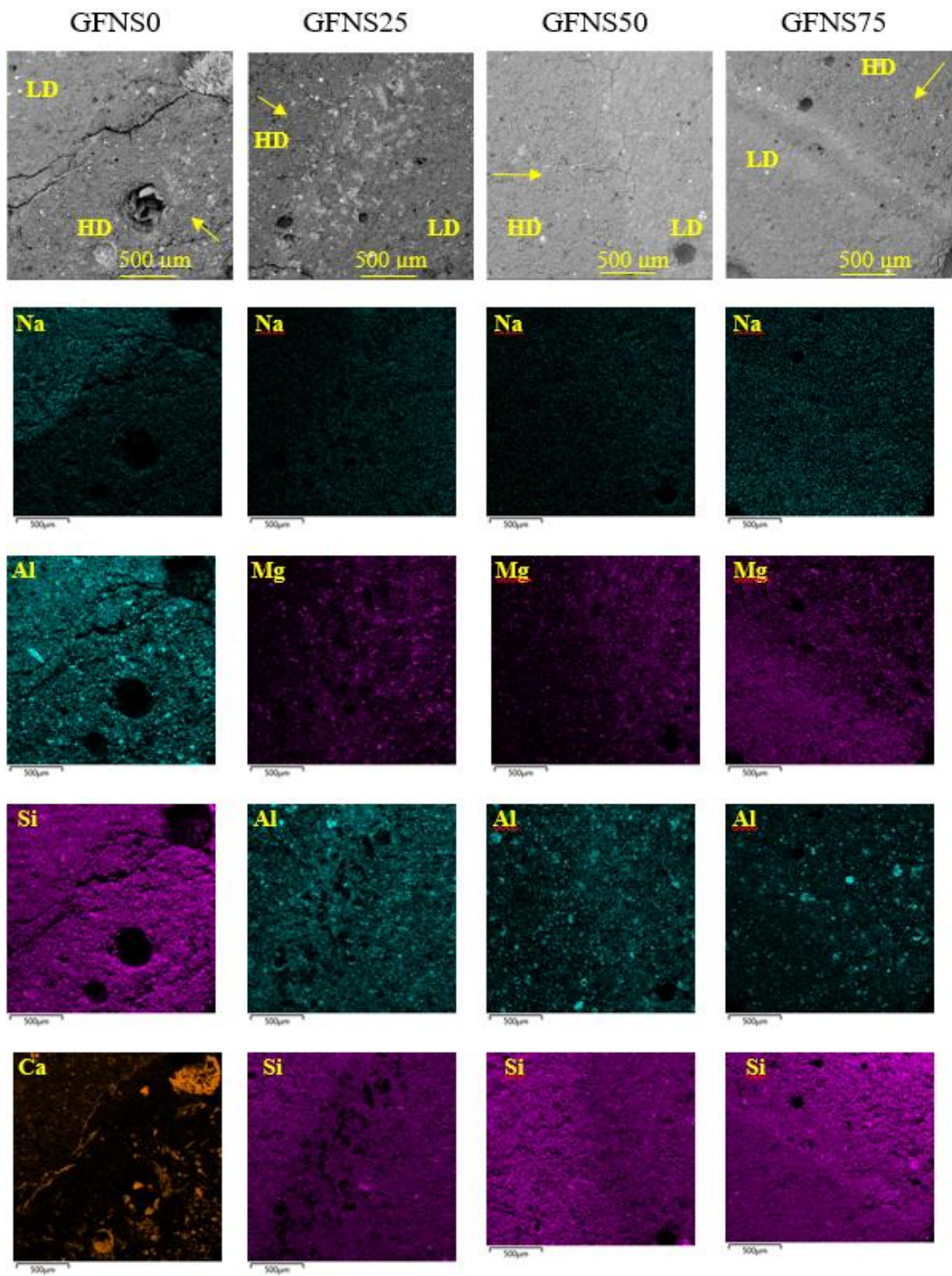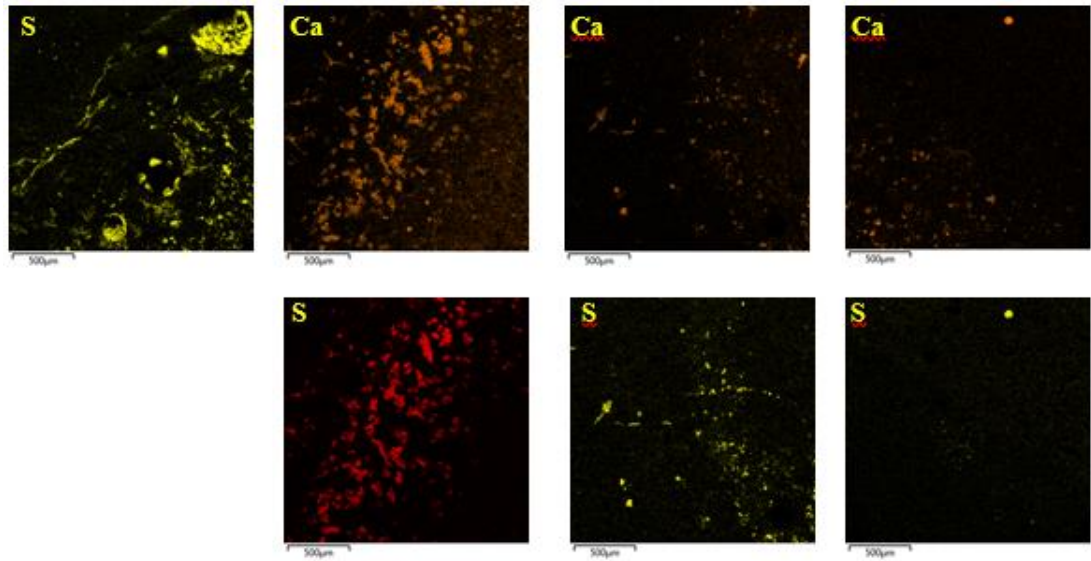
Fig. 6.6 SEM images and EDX mapping of geopolymer pastes after sulphuric acid exposures (GFNS-0 exposed for 1 month and GFNS-25, GFNS-50 and GFNS-75 exposed for 12 months; Arrow indicates the direction of acid penetration; LD and HD denote the low and high deteriorated areas, respectively)

It is also observed that the high concentrations Ca and S present in the deteriorated region of GFNS0 and GFNS25 specimens, which indicates the presence of gypsum in those specimens. It can be noticed that low concentrations of Ca and S present in the deteriorated region of GFNS50 and GFNS75 paste specimens, which indicates the presence of trace amount of gypsum in these specimens. This observation fairs well with XRD results presented discussed in section 6.3.5.

6.3.5 XRD analysis

Fig. 6.7 presents the XRD patterns of geopolymer pastes before and after acid exposure (1 month for GFNS0, 12 months for GFNS25, GFNS50 and GFNS75). The XRD patterns of the specimens before acid exposure are reproduced here from the previous work [44] for comparison with the patterns after acid exposure. It is seen that before the exposure to sulphuric acid solution, a broad band existed at 18°-40° 2θ in the neat fly ash (GFNS0) geopolymer [Fig. 6.7]. This broad band denotes the existence of amorphous N-A-S-H gel found in section 6.3.4. Further, crystalline quartz, mullite, magnetite and carbonate phases existed in GFNS0 specimen. A broad band also existed in the fly ash-GFNS geopolymers (GFNS25, GFNS50, GFNS75), which denotes the existence of amorphous N-M-A-S-H gel found in section 6.3.4.

135
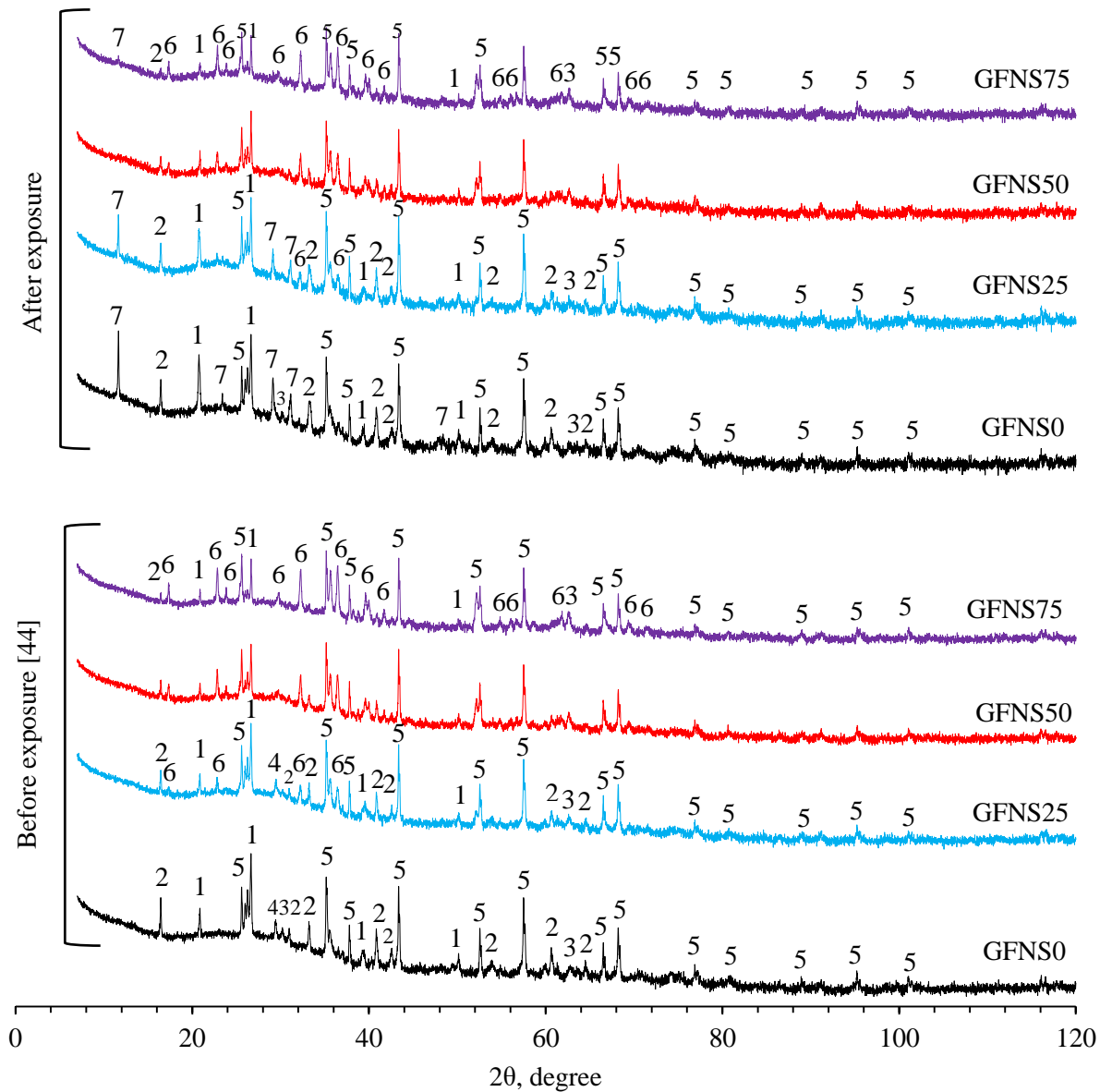
Legend

1 PDF 00-005-0490 SiO_2 Quartz, low	**5** PDF 00-010-0173 Al_2O_3 Corundum, syn
2 PDF 00-015-0776 $Al_6Si_2O_{13}$ Mullite, syn	**6** PDF 00-007-0075 $2(Mg_{0.90}Fe_{0.10})O.SiO_2$
3 PDF 01-071-6449 $Fe(Fe_{1.17}Ti_{0.54})O_4$	Forsterite
Magnetite, titanian	**7** PDF 00-033-0311 $CaSO_4.2H_2O$ Gypsum, syn
4 PDF 00-047-1743 $CaCO_3$ Calcite	

Fig. 6.7 X-ray diffraction (XRD) patterns of geopolymer paste before and after exposure to sulphuric acid solution

Table 6.2 Results of QXRD analysis

Sample ID	Exposure conditions	Quartz (%)	Mullite (%)	Magnetite (%)	Calcite (%)	Forsterite (%)	Gypsum (%)	Amorphous (%)
GFNS0	B[1]	5.0	12.3	2.2	1.2	---	---	79.3
	A[2]	5.4	13.8	2.8	0.6	---	6.9	70.5
GFNS25	B[1]	3.8	8.9	1.7	0.9	7.6	---	77.1
	A[2]	3.7	10.0	2.0	0.0	4.3	3.4	76.6
GFNS50	B[1]	2.4	5.9	1.3	---	14.3	---	76.1
	A[2]	2.6	6.7	1.4	---	13.9	0.4	75.0
GFNS75	B[1]	1.6	3.3	1.2	---	21.4	---	72.5
	A[2]	1.6	3.7	5.5	---	19.0	0.6	69.6

[1]Before acid exposure [44]

[2]After acid exposure

In addition to quartz, mullite, magnetite and carbonate, forsterite phase also existed in fly ash-GFNS geopolymer. It is seen that the intensity of quartz, mullite, magnetite and carbonate peaks decreased, and forsterite peaks increased on account of the reduction of fly ash and increase of GFNS. The QXRD analysis was conducted to determine the actual quantities of crystalline and amorphous contents. Table 6.2 presents the summary of the QXRD results of geopolymer specimens. It is seen that before acid exposure, the quartz content reduced from 5.0% in GFNS0 specimen to 3.8, 2.4 and 1.6% in GFNS25, GFNS50 and GFNS75, respectively (Table 6.2). The amounts of mullite, magnetite and carbonate also decreased with the decrease of fly ash and increase of GFNS (Table 6.2). On the other hand, the forsterite content increased from 7.6% in GFNS25 to 14.3 and 21.4% in GFNS50 and GFNS75, respectively. Before acid exposure, the amorphous contents were 79.3, 77.1, 76.1 and 72.5% in GFNS0, GFNS25, GFNS50 and GFNS75, respectively [44].

It can be observed from the XRD pattern of GFNS0 specimen that after immersion in sulphuric acid, the intensity of quartz and mullite slightly increased than in the original

specimen. Besides, a new crystalline phase of gypsum was noticed in specimen GFNS0, which supports the observations in SEM images. The QXRD results showed that specimen GFNS0 contained 5.4% quartz, 13.8% mullite, 2.8% magnetite, 0.6% calcite and 6.9% gypsum after exposure to the sulphuric acid solution (Table 6.2). The increases of quartz and mullite contents are attributed to the decomposition of aluminosilicate gel after sulphuric acid exposure.

The amorphous contents of specimen GFNS0 is reduced from 79.3% before acid exposure to 70.5% after exposure. On the other hand, the amorphous contents of GFNS25, GFNS50 and GFNS75 slightly decreased from 77.1% to 76.6%, from 76.1% to 75.0% and from 72.5% to 69.6%, respectively. The new phase of gypsum was also observed in fly ash-GFNS geopolymer. However, lower amounts of gypsum were found in the fly ash-GFNS geopolymers than in the neat fly ash geopolymer. The gypsum contents of GFNS25, GFNS50 and GFNS75 were 3.4, 0.4 and 0.6%, respectively. This suggests that the inclusion of GFNS reduced the formation of expansive gypsum. In consequence, less cracks and voids with higher residual strength were found in the fly ash-GFNS geopolymer mortars compared to neat fly ash geopolymer mortar as discussed in the previous sections.

6.4 Summary

The sulphuric acid resistance of GFNS blended fly ash geopolymer mortar was evaluated in this study. The following conclusions are drawn from the experimental results:

- The use of GFNS as a partial replacement of fly ash was found to enhance the resistance of geopolymer mortar against sulphuric acid attack. After exposure to 3% sulphuric acid solution, the losses of compressive strength and mass of fly ash-GFNS geopolymer mortars were less than those of the neat fly ash geopolymer mortar. The lowest strength loss was found in GFNS75 specimens after the acid exposures up to one year. The strength losses after one year of sulphuric acid exposure were 43.67, 31.05, 24.15 and 22.54% in the mortar specimens of mixtures GFNS0, GFNS25, GFNS50 and GFNS75, respectively.

- The lower strength loss of the fly ash-GFNS geopolymer mortar is attributed to the presence of more stable N-M-A-S-H gel compared to N-A-S-H gel of

neat fly ash geopolymer. Incorporation of GFNS made a dense structure by the production of N-M-A-S-H gel. Thus, lower ingress of acid occurred in the sample of GFNS75 mortar due to the lower porosity. Consequently, the lowest strength loss was observed in the mortar containing 75% GFNS.

- The QXRD results showed that the gypsum contents of GFNS0, GFNS25, GFNS50 and GFNS75 were 6.9, 3.4, 0.4 and 0.6%, respectively. The higher amount of gypsum after acid exposure in the neat fly ash geopolymer may have induced higher stresses that led to increased cracks. Consequently, less deterioration occurred in the fly ash-GFNS geopolymer mortar than in the neat fly ash geopolymer mortar.

6.5 References

[1] T.A. Aiken, J. Kwasny, W. Sha, M.N. Soutsos, Effect of slag content and activator dosage on the resistance of fly ash geopolymer binders to sulfuric acid attack, Cem. Concr. Res. 111 (2018) 23–40.

[2] P.S. Deb, P.K. Sarker, S. Barbhuiya, Sorptivity and acid resistance of ambient-cured geopolymer mortars containing nano-silica, Cem. Concr. Compos. 72 (2016) 235–245.

[3] R. Alzeebaree, A. Çevik, B. Nematollahi, J. Sanjayan, A. Mohammedameen, M.E. Gülşan, Mechanical properties and durability of unconfined and confined geopolymer concrete with fiber reinforced polymers exposed to sulfuric acid, Constr. Build. Mater. 215 (2019) 1015–1032.

[4] M. Vafaei, A. Allahverdi, P. Dong, N. Bassim, Acid attack on geopolymer cement mortar based on waste-glass powder and calcium aluminate cement at mild concentration, Constr. Build. Mater. 193 (2018) 363–372.

[5] T. Bakharev, Resistance of geopolymer materials to acid attack, Cem. Concr. Res. 35 (2005) 658–670.

[6] P. Duxson, A. Fernández-Jiménez, J.L. Provis, G.C. Lukey, A. Palomo, J.S.J. Van Deventer, Geopolymer technology: The current state of the art, J. Mater. Sci. 42 (2007) 2917–2933.

[7] T. Bakharev, J.G. Sanjayan, Y.B. Cheng, Resistance of alkali-activated slag concrete to acid attack, Cem. Concr. Res. 33 (2003) 1607–1611.

[8] V. Sata, A. Sathonsaowaphak, P. Chindaprasirt, Resistance of lignite bottom ash geopolymer mortar to sulfate and sulfuric acid attack, Cem. Concr. Compos. 34 (2012) 700–708.

[9] P. Zhang, K. Wang, Q. Li, J. Wang, Y. Ling, Fabrication and engineering properties of concretes based on geopolymers/alkali-activated binders - A review, J. Clean. Prod. 258 (2020) 120896.

[10] I. Maragkos, I.P. Giannopoulou, D. Panias, Synthesis of ferronickel slag-based geopolymers, Miner. Eng. 22 (2009) 196–203.

[11] W.G. Valencia-Saavedra, R. Mejía de Gutiérrez, F. Puertas, Performance of FA-based geopolymer concretes exposed to acetic and sulfuric acids, Constr. Build. Mater. 257 (2020) 119503.

[12] E. Hewayde, M. Nehdi, E. Allouche, G. Nakhla, Effect of geopolymer cement on microstructure, compressive strength and sulphuric acid resistance of concrete, Mag. Concr. Res. 58 (2006) 321–331.

[13] M. Vafaei, A. Allahverdi, Durability of Geopolymer Mortar Based on Waste-Glass Powder and Calcium Aluminate Cement in Acid Solutions, J. Mater. Civ. Eng. 29 (2017) 04017196.

[14] P. Sturm, G.J.G. Gluth, C. Jäger, H.J.H. Brouwers, H.C. Kühne, Sulfuric acid resistance of one-part alkali-activated mortars, Cem. Concr. Res. 109 (2018) 54–63.

[15] W. Zhang, X. Yao, T. Yang, C. Liu, Z. Zhang, Increasing mechanical strength and acid resistance of geopolymers by incorporating different siliceous materials, Constr. Build. Mater. 175 (2018) 411–421.

[16] H.A. Khan, A. Castel, M.S.H. Khan, Corrosion investigation of fly ash based geopolymer mortar in natural sewer environment and sulphuric acid solution, Corros. Sci. 168 (2020) 108586.

[17] S.A. Bernal, E.D. Rodrígueza, R.M. de Gutiérrez, J.L. Provis, Performance of alkali-activated slag mortars exposed to acids, J. Sustain. Cem. Mater. 1 (2012) 138–151.

[18] T. Suresh, G. Partha, G. Somnath, Acid Resistance of Fly ash based Geopolymer mortars, Int. J. Recent Trends Eng. 1 (2009) 36–40.

[19] P.T. Fernando, J. Said, Resistance to acid attack, abrasion and leaching behavior of alkali-activated mine waste binders, Mater. Struct. Constr. 44 (2011) 487–498.

[20] N.K. Lee, H.K. Lee, Influence of the slag content on the chloride and sulfuric acid resistances of alkali-activated fly ash/slag paste, Cem. Concr. Compos. 72 (2016) 168–179.

[21] M.A.M. Ariffin, M.A.R. Bhutta, M.W. Hussin, M. Mohd Tahir, N. Aziah, Sulfuric acid resistance of blended ash geopolymer concrete, Constr. Build. Mater. 43 (2013) 80–86.

[22] A. Allahverdi, F. Škvára, Sulfuric acid attack on hardened paste of geopolymer cements part 1. Mechanism of corrosion at relatively high concentrations, Ceram. - Silikaty. 49 (2005) 225–229.

[23] A. Allahverdi, F. Škvára, Sulfuric acid attack on hardened paste of geopolymer cements Part 2. Corrosion mechanism at mild and relatively low concentrations, Ceram. - Silikaty. 50 (2006) 1–4.

[24] R.R. Lloyd, J.L. Provis, J.S.J. Van Deventer, Acid resistance of inorganic polymer binders. 1. Corrosion rate, Mater. Struct. Constr. 45 (2012) 1–14.

[25] L. Gu, P. Visintin, T. Bennett, Sulphuric Acid Resistance of Cementitious Materials: Multiscale Approach to Assessing the Degradation, J. Mater. Civ. Eng. 32 (2020) 04020171.

[26] Y. Huang, Q. Wang, M. Shi, Characteristics and reactivity of ferronickel slag powder, Constr. Build. Mater. 156 (2017) 773–789.

[27] A.K. Saha, M.N.N. Khan, P.K. Sarker, Value added utilization of by-product electric furnace ferronickel slag as construction materials: A review, Resour. Conserv. Recycl. 134 (2018) 10–24.

[28] N.S. Katsiotis, P.E. Tsakiridis, D. Velissariou, M.S. Katsiotis, S.M. Alhassan, M. Beazi, Utilization of Ferronickel Slag as Additive in Portland Cement: A Hydration Leaching Study, Waste and Biomass Valorization. 6 (2015) 177–189.

[29] Q.D. Nguyen, M.S.H. Khan, A. Castel, T. Kim, Durability and Microstructure Properties of Low-Carbon Concrete Incorporating Ferronickel Slag Sand and Fly Ash, J. Mater. Civ. Eng. 31 (2019) 04019152.

[30] Y.C. Choi, S. Choi, Alkali-silica reactivity of cementitious materials using ferro-nickel slag fine aggregates produced in different cooling conditions, Constr. Build. Mater. 99 (2015) 279–287.

[31] H. Kim, C.H. Lee, K.Y. Ann, Feasibility of ferronickel slag powder for cementitious binder in concrete mix, Constr. Build. Mater. 207 (2019) 693–705.

[32] Y. Chen, T. Ji, Z. Yang, W. Zhan, Y. Zhang, Sustainable use of ferronickel slag in cementitious composites and the effect on chloride penetration resistance, Constr. Build. Mater. 240 (2020) 117969.

[33] Q.D. Nguyen, A. Castel, T. Kim, M.S.H. Khan, Performance of fly ash concrete with ferronickel slag fine aggregate against alkali-silica reaction and chloride diffusion, Cem. Concr. Res. 139 (2021) 106265.

[34] N. Lemonis, P.E. Tsakiridis, N.S. Katsiotis, S. Antiohos, D. Papageorgiou, M.S. Katsiotis, M. Beazi-Katsioti, Hydration study of ternary blended cements containing ferronickel slag and natural pozzolan, Constr. Build. Mater. 81 (2015) 130–139.

[35] B. Li, B. Huo, R. Cao, S. Wang, Y. Zhang, Sulfate resistance of steam cured ferronickel slag blended cement mortar, Cem. Concr. Compos. 96 (2019) 204–211.

[36] M.A. Rahman, P.K. Sarker, F.U.A. Shaikh, A.K. Saha, Soundness and compressive strength of Portland cement blended with ground granulated ferronickel slag, Constr. Build. Mater. 140 (2017) 194–202.

[37] M. Zhai, H. Zhu, G. Liang, Q. Wu, C. Zhang, S. Hua, Z. Zhang, Enhancing the recyclability of air-cooled high-magnesium ferronickel slag in cement-based materials: A study of assessing soundness through modifying method, Constr. Build. Mater. 261 (2020) 120523.

[38] R. Cao, Z. Jia, Z. Zhang, Y. Zhang, N. Banthia, Leaching kinetics and reactivity evaluation of ferronickel slag in alkaline conditions, Cem. Concr. Res. 137 (2020) 106202.

[39] K. Komnitsas, L. Yurramendi, G. Bartzas, V. Karmali, E. Petrakis, Factors affecting co-valorization of fayalitic and ferronickel slags for the production of alkali activated materials, Sci. Total Environ. 721 (2020) 137753.

[40] K. Komnitsas, D. Zaharaki, V. Perdikatsis, Effect of synthesis parameters on the compressive strength of low-calcium ferronickel slag inorganic polymers, J. Hazard. Mater. 161 (2009) 760–768.

[41] N. You, B. Li, R. Cao, J. Shi, C. Chen, Y. Zhang, The influence of steel slag and ferronickel slag on the properties of alkali-activated slag mortar, Constr. Build. Mater. 227 (2019) 116614.

[42] Z. Zhang, Y. Zhu, T. Yang, L. Li, H. Zhu, H. Wang, Conversion of local industrial wastes into greener cement through geopolymer technology: A case study of high-magnesium nickel slag, J. Clean. Prod. 141 (2017) 463–471.

[43] K. Komnitsas, D. Zaharaki, V. Perdikatsis, Geopolymerisation of low calcium ferronickel slags, J. Mater. Sci. 42 (2007) 3073–3082.

[44] J.C. Kuri, M.N.N. Khan, P.K. Sarker, Fresh and hardened properties of geopolymer binder using ground high magnesium ferronickel slag with fly ash, Constr. Build. Mater. 272 (2021) 121877.

[45] T. Yang, X. Yao, Z. Zhang, Geopolymer prepared with high-magnesium nickel slag: Characterization of properties and microstructure, Constr. Build. Mater. 59 (2014) 188–194.

[46] K. Sakkas, P. Nomikos, A. Sofianos, D. Panias, Utilisation of FeNi-Slag for the production of inorganic polymeric materials for construction or for passive fire protection, Waste and Biomass Valorization. 5 (2014) 403–410.

[47] A.K. Saha, P.K. Sarker, Acid resistance of mortar using Ferronickel slag (FNS) aggregate and ground FNS as supplementary cementitious material, ACI Mater. J. 116 (2019) 65–76.

[48] J.C. Kuri, M.N.N. Khan, P.K. Sarker, Workability, strength and microstructural properties of ground ferronickel slag blended fly ash geopolymer mortar, J. Sustain. Cem. Mater. 0 (2020) 1–18.

[49] ASTM C618-05. Standard Specification for Coal Fly Ash and Raw or Calcined Natural Pozzolan for Use in Concrete. West Conshohocken, PA: ASTM International, 2005.

[50] ASTM C618-15. Standard Test Method for Relative Density (Specific Gravity) and Absorption of Fine Aggregate. West Conshohocken, PA: ASTM International, 2015.

[51] P. Nath, P.K. Sarker, Use of OPC to improve setting and early strength properties of low calcium fly ash geopolymer concrete cured at room temperature, Cem. Concr. Compos. 55 (2015) 205–214.

[52] J.C. Kuri, M.N.N. Khan, P.K. Sarker, Compressive strength of geopolymer mortar using ground ferronickel slag and fly ash, 3rd Eur. Mediterr. Struct. Eng. Constr. Conf. 2020, Euro-Med-Sec 2020. (2020) 1–6.

[53] ASTM C267, Standard Test Methods for Chemical Resistance of Mortars, Grouts, and Monolithic Surfacings and Polymer Concretes, ASTM International, West Conshohocken, PA, 2012.

[54] C.F. Chang, J.W. Chen, The experimental investigation of concrete carbonation depth, Cem. Concr. Res. 36 (2006) 1760–1767.

[55] E. Liu, M. Ghandehari, C. Brückner, G. Khalil, J. Worlinsky, W. Jin, A. Sidelev, M.A. Hyland, Mapping high pH levels in hydrated calcium silicates, Cem. Concr. Res. 95 (2017) 232–239.

[56] Standards Australia, AS1012.9:2014 Methods of testing concrete Method 9: Compressive strength tests — Concrete , mortar and grout specimens, Stand. Aust. Int. Ltd, Sydney. (2014) 1–13.

[57] H.M. Rietveld, A profile refinement method for nuclear and magnetic structures, J. Appl. Crystallogr. 2 (1969) 65–71.

[58] A.A. Coelho, TOPAS and TOPAS-Academic: An optimization program integrating computer algebra and crystallographic objects written in C++: An, J. Appl. Crystallogr. 51 (2018) 210–218.

[59] R.J. Hill, C.J. Howard, Quantitative phase analysis from neutron powder diffraction data using the Rietveld method, J. Appl. Crystallogr. 20 (1987) 467–474.

[60] P. Chindaprasirt, U. Rattanasak, S. Taebuanhuad, Resistance to acid and sulfate solutions of microwave-assisted high calcium fly ash geopolymer, Mater. Struct. Constr. 46 (2013) 375–381.

[61] L. Gu, P. Visintin, T. Bennett, Evaluation of accelerated degradation test methods for cementitious composites subject to sulfuric acid attack; application to conventional and alkali-activated concretes, Cem. Concr. Compos. 87 (2018) 187–204.

[62] M. Nasir, M.A. Megat Johari, M. Maslehuddin, M.O. Yusuf, Sulfuric acid resistance of alkali/slag activated silico-manganese fume-based mortars, Struct. Concr. 22 (2021) E400–E414.

[63] N.I. Fattuhi, and B.P. Hughes, The performance of cement paste and concrete subjected to sulphuric acid attack, Cem. Concr. Res. 18 (1988) 545–553.

[64] D. Israel, D.E. Macphee, E.E. Lachowski, Acid attack on pore-reduced cements, J. Mater. Sci. 32 (1997) 4109–4116.

[65] J.C. Kuri, S. Majhi, P.K. Sarker, A. Mukherjee, Microstructural and non-destructive investigation of the effect of high temperature exposure on ground ferronickel slag blended fly ash geopolymer mortars, J. Build. Eng. 43 (2021) 103099.

CHAPTER 7: SULPHATE RESISTANCE OF GFNS BLENDED FLY ASH GEOPOLYMER MORTAR

The content presented in this chapter is submitted to the Structural Concrete journal for possible publication.

Kuri, J. C., Nuruzzaman, M., & Sarker, P. K. (2022). Sulphate resistance of geopolymer mortar produced using ground ferronickel slag with fly ash. Structural Concrete for possible publication (*Under review*).

This chapter presents an investigation on the durability of geopolymer mortar made from ground ferronickel slag (GFNS) with fly ash (FA) after immersion in 5% sodium sulphate solution for 1.5 years. The changes of compressive strength, mass, length, visual appearance and microstructures of the geopolymer mortars were investigated.

7.1 Overview

Ordinary Portland cement (OPC) is the most common binder for conventional concrete productions. However, the production of OPC requires high energy and it emits significantly high amounts of greenhouse gases [1]. Around 0.9 tonnes of CO2 is discharged during the manufacturing of one tonne of cement [2]. In this regard, geopolymer is being developed as an environmentally friendly alternative binder to OPC. Substituting OPC by geopolymer binder can potentially reduce up to 80% CO_2 emission [3]. In addition to environmental friendliness, geopolymers show good mechanical properties and durability performance [4-7].

In regards to durability and serviceability, sulphate attack is a very common way of deterioration of concrete structures. Based on the sources of sulphate environment, two types of sulphate attack can be experienced by concrete structure, namely external and internal sulphate attacks. A concrete structure can experience an internal sulphate attack by sulphate ions of the binder [8, 9]. The external sulphate attack is caused by sulphate exposure in the surrounding of concrete such as sea water, industrial effluent, ground water or contaminated soil [9, 10]. In most of the cases, sulphate ions react with calcium hydroxide and aluminium containing phases (monosulphate and tricalcium aluminate) to form expansive ettringite and gypsum [11, 12]. In consequence, expansion, cracking, spalling and losses of strength and mass can occur in concrete structures.

In general, the sulphate resistance of geopolymer concrete is reported as superior to that of OPC concrete [13, 14]. The higher resistance is attributed to the less amount of calcium phases in geopolymers [15, 16]. Khan et al. [17] reported that alkali activated GGBFS showed high sulphate resistance by producing hydrotalcite. However, Gopalakrishnan and Chinnaraju [18] found that though 100% GGBFS geopolymer concrete performed better in a normal environment, geopolymer concrete with 60% GGBFS and 40% fly ash provided better sulphate resistance than 100% GGBFS geopolymer concrete. The stability of geopolymer against sulphate environment depends on the activator type and concentration and cation type of sulphate solution [19]. Elyamany et al. [20] found that the sulphate resistance of geopolymers increased with the increase of NaOH solution's concentration and curing temperature and decrease of the alkali solution to precursor ratio. The authors reported that geopolymer with 15% silica fume, 35% GGBFS and 50% fly ash provided the highest resistance against magnesium sulphate exposure. Beltrame et al. [21] found that alkali activated slag from charcoal showed higher sodium sulphate resistance than sulphate-resistant blended Portland cement. The geopolymer containing lower water to binder ratio provided higher resistance to sulphate attack than the geopolymer with higher water to binder ratio [22]. Karakoç et al. [23] reported that strength of ferrochrome slag geopolymer concrete decreased with the increase of $MgSO_4$ content and exposure period. Kwasny et al. [11] found that the microstructure of lithomarge-based geopolymer was unaffected due to sulphate exposure. Ye et al. [24] reported that little compositional alteration and ettringite formation occurred due to the Na_2SO_4 attack on alkali-activated slag. Aliques-Granero et al. [25] found that alkali activated GGBFS showed very little expansion and alkali activated fly ash showed no expansion upon sodium sulphate exposure.

Ferronickel slag (FNS) is an industrial residue which is discharged in the manufacture process of ferronickel alloys [26-29]. About 150 million tonnes of FNS by-product is produced annually in the world, which makes it the fourth largest slag produced by smelting process [30]. The physical characteristics of FNS are competent for use as an aggregate in concrete [31-33]. Furthermore, as FNS has a notable percentage of amorphous silica, ground FNS (GFNS) has shown reactivity when utilized with conventional cement [34-37] or with an alkaline liquid in geopolymers [38-42]. The incorporation of GFNS as supplementary cementitious materials (SCM) improved the

sulphate resistance of OPC mortars as reported in previous studies [43, 44]. However, to the best of the author's knowledge, there is no study available on the sulphate resistance of geopolymers where GFNS is incorporated as a precursor material. Therefore, the influence of sulphate exposure on geopolymers containing different proportions of GFNS and fly ash needs to be investigated. This is essential to evaluate the durability of GFNS-fly ash geopolymers against sulphate exposures.

The sources of ore and cooling method greatly influences the reactivity of GFNS. This study used the water cooled FNS produced from garnierite ores of New Caledonia. Over two million tonnes of FNS is produced annually by SLN, New Caledonia and over 25 million tonnes of the by-product is stockpiled in that area [45]. Therefore, utilization of FNS as a binder in the construction sector will benefit the environment and pave the way of safe disposal of the by-products. The suitability of the GFNS as a source material was investigated in earlier studies focusing on the fresh and mechanical properties [46, 47]. However, durability of GFNS geopolymer in sulphate environment is also essential to ensure its long term stability in aggressive environment. Therefore, the effect of sodium sulphate exposure was investigated in terms of physical appearance, residual compressive strength, mass change, length change and microstructural changes of the geopolymer mortar.

7.2 Materials and methodology

7.2.1 Materials and mixture proportion

GFNS and fly ash (FA) were utilized as solid precursors and natural sand was utilized as aggregate to produce geopolymer mortars. The amorphous content of GFNS and fly ash were 61.33% and 86.02%, respectively. Furthermore, GFNS contained the crystal phases of 0.68% quartz and 38.00% forsterite ferroan. The crystalline contents of fly ash were quartz (5.03%), mullite (6.81%), magnetite (1.52%) and calcite (0.62%) [46]. A mixture of liquid Na_2SiO_3 with 29.40% SiO_2, 14.70% Na_2O and 55.90% water, and 8 molar NaOH solution was used as the alkali activator. The mass ratio of Na_2SiO_3 to NaOH solutions was 2. The mix proportions of mortars were adopted from the earlier studies [46, 48], shown in Table 7.1. The amount of activator solution was 45% of the solid precursors. Fly ash was substituted by 0, 25, 50 and 75% GFNS and the respective mixtures are denoted as 0-GFNS, 25-GFNS, 50-GFNS and 75-GFNS, respectively.

Table 7.1 Mix proportions of mortar [46]

Mix ID	Materials (kg/m^3)				
	Fly ash	GFNS	Sand	NaOH solution	Na$_2$SiO$_3$ solution
0-GFNS	733	0	1137	110	220
25-GFNS	550	183	1137	110	220
50-GFNS	367	367	1137	110	220
75-GFNS	183	550	1137	110	220

7.2.2 Preparation of samples and test procedures

The alkali activator was made by mixing the NaOH and Na$_2$SiO$_3$ solutions. To make the geopolymer mortar, the solid precursors and SSD sand were first mixed for 2 minutes. The alkali activator was then mixed to attain a uniform mortar mixture. The fresh mortar was poured into the mould and compacted. The specimens were cured in an oven at 60 °C for 24 hours. The specimens were demoulded after heat curing and left in ambient environment for cooling down. After one day of cooling (two days after casting), initial compressive strength of mortars was measured following AS 1012.9:2014 [49].

The sulphate resistances of geopolymer mortars were studied by immersion of the samples in 5% Na$_2$SO$_4$ solution for up to 1.5 years. The Na$_2$SO$_4$ solution was renewed monthly throughout the exposure period. After a certain immersion period, the change of length was measured from prism bar ($25 \times 25 \times 285$ mm) in accordance with ASTM C157-08 [50] and the changes of compressive strength, mass and microstructure were evaluated using the 50 mm cube samples. The SEM and EDX investigation of the specimens was conducted using a Tescan Mira3 microscope. The QXRD analysis was performed to determine the mineralogical phase changes of the immersed samples as described in the section 7.3.5.

7.3 Results and Discussion

7.3.1 *Physical appearance*

Fig. 7.1 presents the physical appearance of mortars before and after 1.5 years immersion in Na_2SO_4 solution. It is observed that all samples had no visual sign of degradation after 1.5 years of immersion in Na_2SO_4 solution. Similar observations of no sign of deterioration were found in previous studies [11, 19, 23]. The low calcium content of precursors and cross linked alumino silicate gel are considered to make geopolymers stable against Na_2SO_4 exposure. Expansive gypsum or ettringite were not found as products due to the low calcium contents of the precursors [15, 18]. Thus, cracking or spalling were not observed in the samples after immersion in Na_2SO_4 solution. Moreover, the sodium content of Na_2SO_4 solution is also considered to maintain the stability of geopolymer samples [22]. It is seen that the influence of GFNS has insignificant effect on the physical appearances of the mortars after immersion in Na_2SO_4 solution.
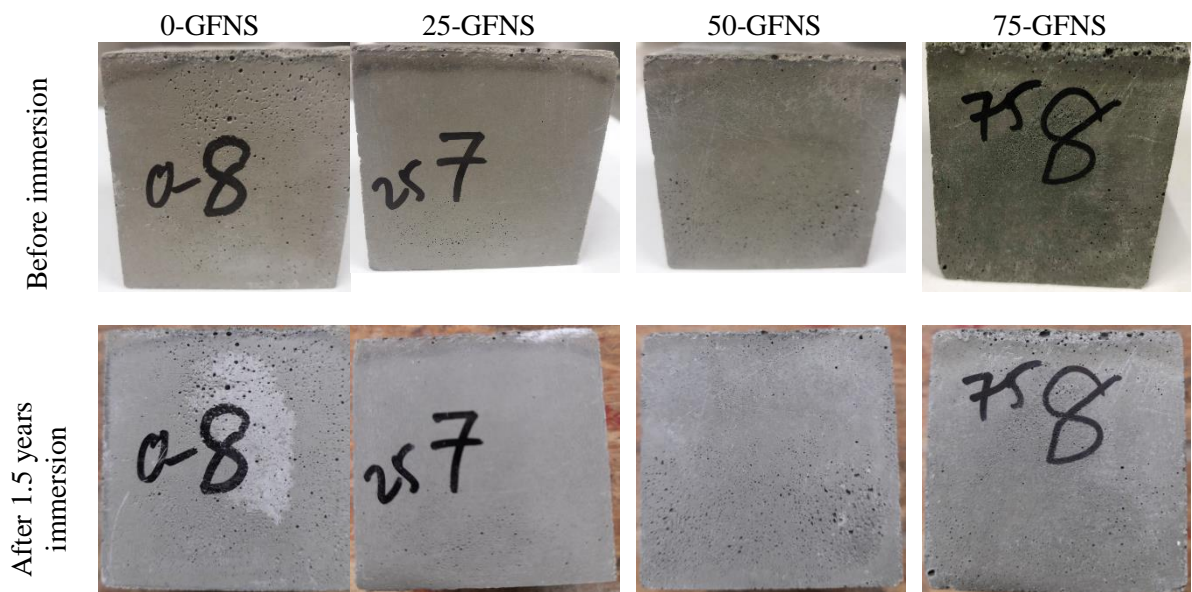
Fig. 7.1 Physical appearance of the mortars

7.3.2 *Compressive strength*

Fig. 7.2 presents the compressive strengths of geopolymer mortars before and after immersion in Na_2SO_4 solution. It can be seen that before exposure, FA-GFNS (25-GFNS, 50-GFNS and 75-GFNS) geopolymer mortar showed higher strength than the

100% FA (0-GFNS) mortar. Before exposure to Na_2SO_4 solution, the compressive strengths of the mixtures 0-GFNS, 25-GFNS, 50-GFNS and 75-GFNS were 53.5, 62.4, 65.8 and 71.9 MPa, respectively. The high strength of GFNS blended geopolymers are ascribed to the development of N-M-A-S-H gel as described in details in the earlier works [40, 47].
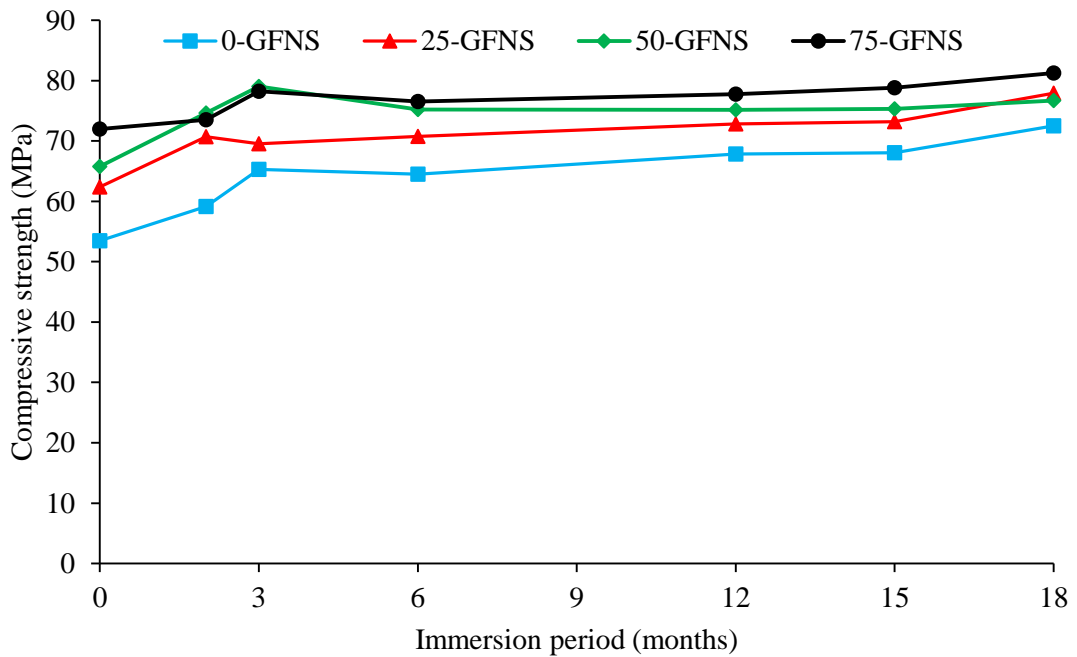
Fig. 7.2 Compressive strength of mortars immersed in Na_2SO_4 solution

It is observed from Fig. 7.2 that the compressive strengths of all the mixtures increased after immersion in Na_2SO_4 solution compared to their strengths before sulphate exposure. The increasing rate of strength was higher in first 3 months immersion than that after this period. At 3 months of immersion, the compressive strengths of the mixtures 0-GFNS, 25-GFNS, 50-GFNS and 75-GFNS were 65.3, 69.6, 79.0 and 78.2 MPa, respectively. On the other hand, between 3 months and 12 months of immersion periods, the increase of strength slowed down and in some samples, strength slightly reduced compared to the strength at 3 months of immersion. This might be happen due to the migration of alkaline ions from the sample to the solution. After 12 months of immersion, compressive strength of the samples showed an increasing rate of strength. The increase of compressive strength generally suggests a good performance of the geopolymer mortars against sodium sulphate exposure. A

similar trend of strength gain of fly ash geopolymers in sodium sulphate solution was found in several previous studies [15, 51, 52]. The good performance of geopolymer against sodium sulphate is attributed to the presence of neutralised cross-linked aluminosilicate structure [18, 53]. Besides, Bakharev et al. [13] reported that the gain of strength is correlated with the continued reaction in geopolymers by the Na^+ from sodium sulphate solution. Moreover, the low calcium content of precursors resisted to produce expansive gypsum and ettringite. Thus, the sample did not deteriorated in sodium sulphate solution.

It can be noticed that, though all samples have good sodium sulphate resistance, the residual strength of the 25-GFNS, 50-GFNS and 75-GFNS samples are higher than that of the 0-GFNS samples. It is also noticed that the 75-GFNS samples provided highest strength at most of the immersion periods. The higher strength of the 25-GFNS, 50-GFNS and 75-GFNS geopolymers are ascribed to the presence of stable N-M-A-S-H gel than the N-A-S-H gel of the 0-GFNS geopolymer, as further discussed in the section 7.3.6. Furthermore, calcium content of GFNS is lower than that of fly ash. Fernandez-Jimenez et al. [54] reported that calcium content has a significant role on durability of geopolymers. Thus, the lower calcium content of GFNS blended geopolymers provided higher stability compared to the neat fly ash geopolymers.

7.3.3 Weight change

Fig. 7.3 shows the weight change of the mortars immersed in Na_2SO_4 solution. It is observed that the weight of all specimens slightly rose with the rise of immersion period until 6 months of immersion. For instance, the weight of the 0-GFNS sample increased by 0.54%, 0.66% and 0.89% at 2, 3 and 6 months immersion periods, respectively compared to those before exposure. After 6 months, the weight of the all samples decreased until 12 months. After 12 months of immersion, weights of all the samples increased again. The gain in weight could be associated with the absorption of exposed liquid by the specimens [11, 23, 52].
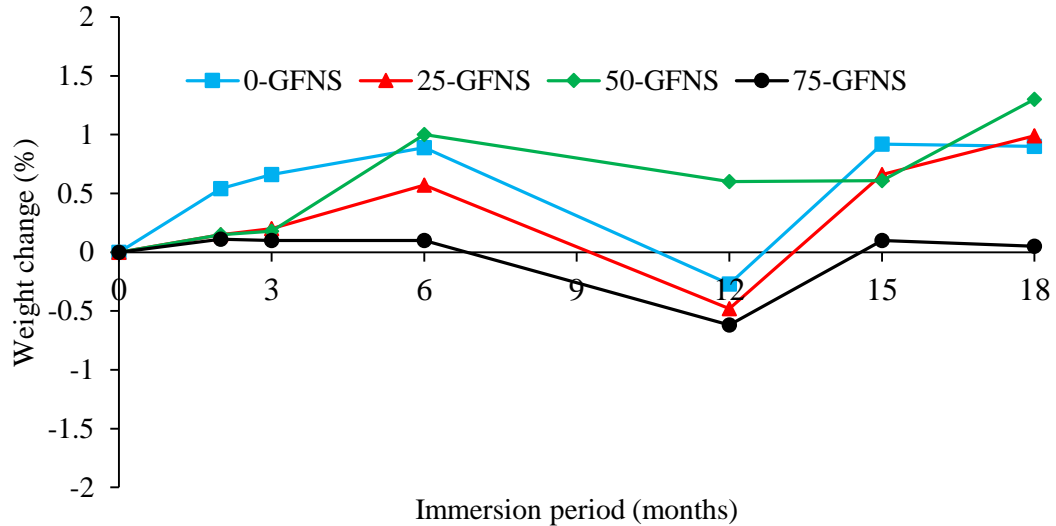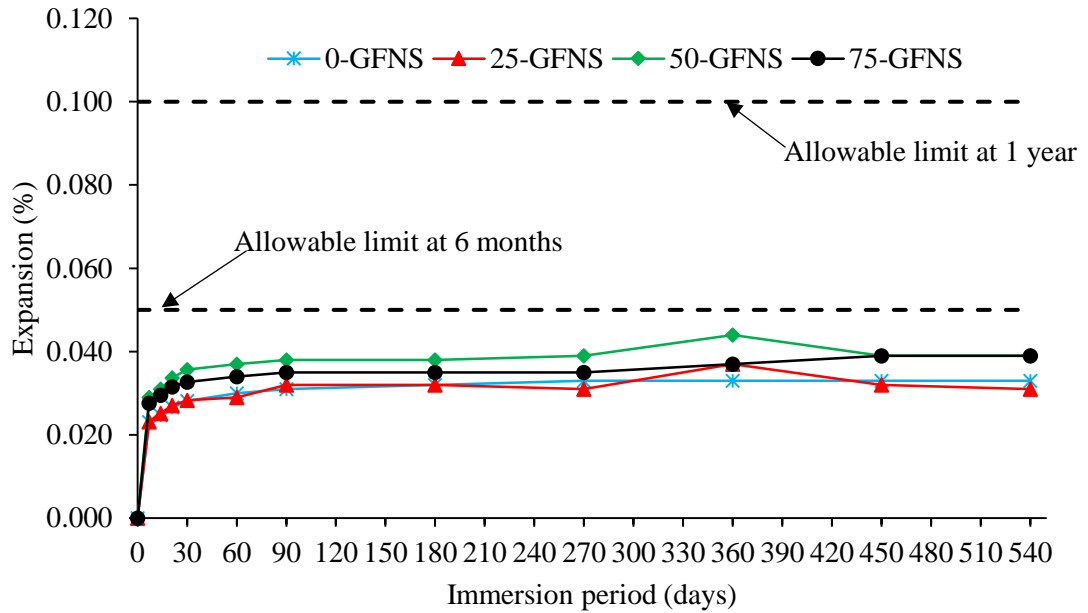
Fig. 7.3 Weight change of mortars immersed in Na_2SO_4 solution (positive values represent weight gain and negative values represent weight loss)

It is also seen that the initial weight gain of 0-GFNS sample is higher compared to the samples of other mixtures. This might be due to the absorption of higher amount of liquid by the micro pores of the 0-GFNS sample as shown in SEM images in section 7.3.6. On the other hand, the 75-GFNS samples showed the lowest weight gain throughout the exposure period due to the absorption of lowest liquid by the pore structure. The weight drop between 6 and 12 months may be ascribed to the leaching of alkaline ions from the samples to the solution [11, 20, 21]. However, the change of weight has insignificant influence on the strength of the mortars.

7.3.4 Length Change

Fig. 7.4 shows the changes of length of the geopolymer mortar bars after exposure to Na_2SO_4 solution. It can be seen that initially samples of all the mixtures expanded sharply. For instance, after 7 days of immersion, expansion of 0-GFNS, 25-GFNS, 50-GFNS and 75-GFNS samples were 0.023, 0.023, 0.029 and 0.028%, respectively. It should be noted that at different time intervals, the expansions of the samples were measured immediately after taking out from the solution and wiping the surface immediately. Therefore, initial expansion may have occurred due to the absorption of liquid by the micro pore of the samples, which induced slight pressure and thus, slight expansion occurred in the samples. However, after 7 days of immersion, the samples

153

expanded very slowly up to 1.5 years. After 540 days (1.5 years) of immersion, expansion of 0-GFNS, 25-GFNS, 50-GFNS and 75-GFNS samples were 0.033, 0.031, 0.039 and 0.039%, respectively.

Fig. 7.4 Length change of mortars immersed in Na_2SO_4 solution

**Fig. 7.5** The mortar prism bars after 1.5 years of immersion in Na_2SO_4 solution

It is also seen that the expansion of 50-GFNS and 75-GFNS samples were slightly higher compared to 0-GFNS and 25-GFNS samples. However, the expansions of all the samples were well below the acceptable limit (0.05% at 6 months and 0.10% at one year) as recommended by ACI guideline [55]. Moreover, no visible damage

except some white substances was noticed on all mortar prism bar after 1.5 years of immersion in the sodium sulphate solution, as shown in Fig. 7.5. It is noted that the pictures of Fig. 7.5 were taken after 1-day air drying and the white substance was not visible before drying. Therefore, the whitish substance may have produced due to efflorescence.

7.3.5 XRD analysis

The XRD analysis was conducted on paste samples which were exposed to similar environment of mortar bars. Specimens were collected from the exposed surface for the XRD investigation. Fig. 7.6 shows the XRD spectra of geopolymers. The XRD patterns of the geopolymers before immersion are reconstructed from the earlier study [47]. It is seen that before immersion, neat FA geopolymer (0-GFNS) comprised crystalline quartz, mullite, calcite and magnetite phases. On the other hand, FA-GFNS geopolymer (25-GFNS, 50-GFNS and 75-GFNS) contained quartz, mullite, calcite, magnetite and forsterite crystalline phases. A broad hump existed in all the samples, which showed the presence of amorphous contents [47]. Corundum peaks in XRD patterns come from the corundum powders which were used as standard material for QXRD analysis.

It can be seen that after 1.5 years immersion in sodium sulphate solution, the XRD patterns are almost same as before immersion for all samples. Though there is no new phase observed after 1.5 years exposure, the intensity of the peaks slightly changed. To evaluate the actual quantity of the phases, QXRD analysis was conducted by Rietveld [46, 56, 57] analysis using TOPAS [58] software. A typical Rietveld fitting plot for 50-GFNS after 1.5 years immersion is shown in Fig.7.7. It can be noticed that the calculated profile is superimposed on the observed pattern and the difference between observed and calculated profile is very low, which suggests a high accuracy of the QXRD results. The summary of XRD results are shown in Table 7.2.
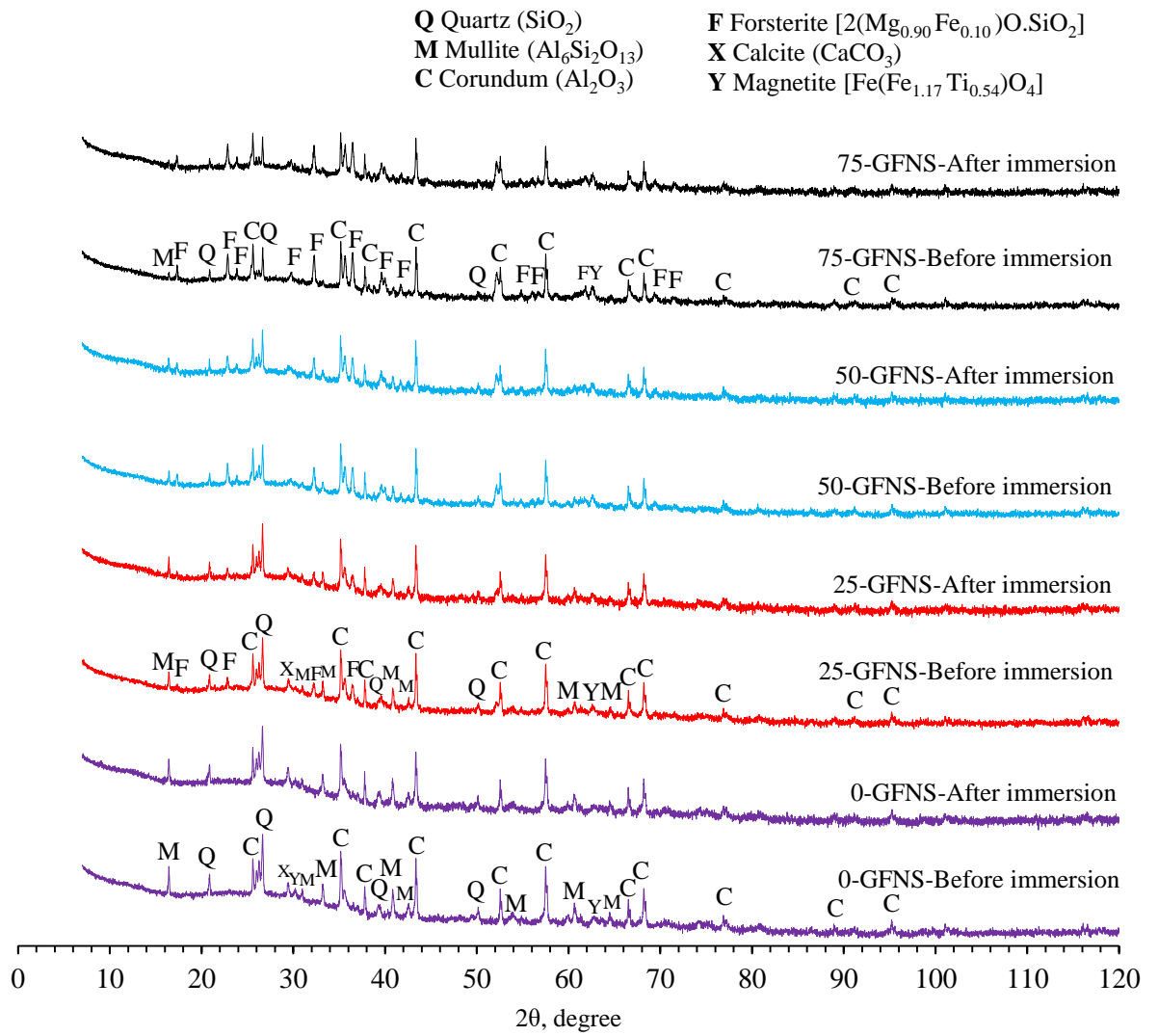
Fig. 7.6 XRD spectra of geopolymer samples before immersion [47] and after 1.5 years of immersion in Na_2SO_4 solution
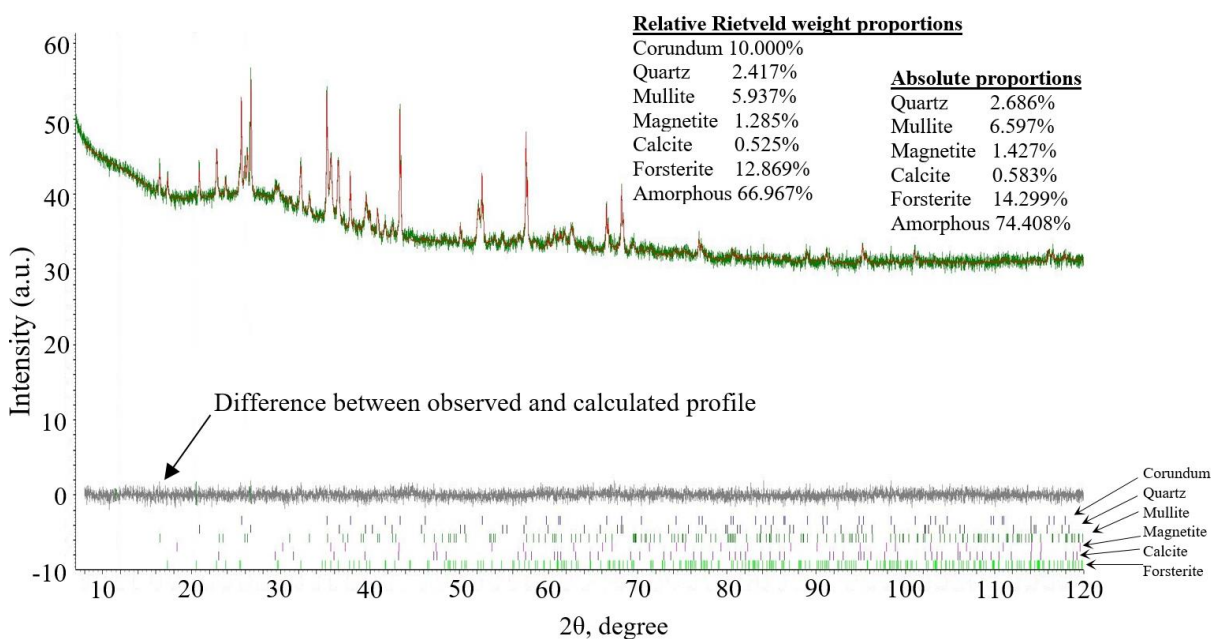
Fig. 7.7 Rietveld refinement plot of 50-GFNS (after 1.5 years immersion) sample using TOPAS software. (The green line pattern represents the observed XRD pattern and red line pattern represents the calculated profile).

Table 7.2 Summary of QXRD results

Specimen ID	Immersion periods	Quartz (%)	Mullite (%)	Magnetite (%)	Calcite (%)	Forsterite (%)	Amorphous (%)
0-GFNS	Before[*]	5.002	12.333	2.236	1.229	---	79.200
	After[**]	4.982	13.290	2.469	2.054	---	77.205
25-GFNS	Before[*]	3.758	8.940	1.692	0.917	7.628	77.064
	After[**]	3.840	9.537	1.870	1.054	7.531	76.168
50-GFNS	Before[*]	2.438	5.873	1.290	0.043	14.293	76.063
	After[**]	2.686	6.597	1.427	0.583	14.299	74.408
75-GFNS	Before[*]	1.611	3.320	1.214	0.003	21.423	72.429
	After[**]	1.636	3.686	3.311	0.529	21.739	69.100

[*]Before immersion [47]

[**]After 1.5 years immersion in sodium sulphate solution

It is noticed from Table 7.2 that after 1.5 years of immersion in sulphate solution, the quartz, mullite, magnetite and calcite contents of 0-GFNS sample changed from 5.002% to 4.982%, 12.333% to 13.290%, 2.236% to 2.469% and 1.229% to 2.054%, respectively. On the other hand, the amorphous content of 0-GFNS reduced from 79.200% in before immersion to 77.205% in after immersion. Almost same trend can be observed for fly ash-GFNS geopolymer (25-GFNS, 50-GFNS and 75-GFNS) where quartz, mullite, magnetite, calcite contents slightly increased and amorphous content slightly decreased (Table 7.2). Forsterite content slightly changed from 7.628% to 7.531%, from 14.293% to 14.299% and from 21.423% to 21.739% in the 25-GFNS, 50-GFNS and 75-GFNS samples, respectively. However, the change of crystalline content is very low for all samples, which showed the high stability of geopolymer against sodium sulphate exposure [11]. Moreover, after exposure to sodium sulphate, expansive products (gypsum or ettringite) were not found in XRD investigation. Similar observations in terms of the absence of gypsum or ettringite in sodium sulphate immersed specimens were reported in previous studies [15, 17, 22, 25]. The low amount of calcium content in the precursors prevented the formation of expansive gypsum or ettringite and thus, provided good stability against sulphate attack. Though all the samples showed good stability against sulphate attack, the fly ash-GFNS geopolymer was found less susceptible to damage in sulphate solution than the neat fly ash geopolymer due to the lower calcium content of GFNS than in fly ash.

7.3.6 Scanning electron microscopy with EDX

Fig. 7.8 presents the microscopic images and EDX spectra of mortar specimens. The specimens were collected from the outer surface for SEM and EDX investigation. Three EDX points of the gel phase were selected for each specimen as shown in Fig. 7.8. A typical EDX spectrum of aluminosilicate gel for each sample is shown in Fig. 7.8 and a summary of the change of chemical constituent of the aluminosilicate gel immersed in sodium sulphate solution is given in Table 7.3. It is observed that before exposure, 0-GFNS sample contained higher peaks of Na, Al, Si and O, which represents the existence of N-A-S-H product. Meanwhile, 25-GFNS, 50-GFNS and 75-GFNS samples contained higher peaks of Na, Mg, Al, Si and O, indicating N-M-A-S-H product [40, 47].

	Before immersion	After 1.5 years of immersion

0-GFNS

Before immersion (Spectrum-1):

	At%
O	66.0
Al	14.4
Si	13.8
Na	4.0
Ca	0.7
Fe	0.4
Cl	0.2
Mo	0.2
K	0.2
Ti	0.1

Spectrum-1

After 1.5 years of immersion (Spectrum-4):

	At%
O	69.9
Si	13.6
Na	5.6
Al	5.1
Ca	3.4
Fe	0.8
Mg	0.8
S	0.3
K	0.2
Cl	0.1
Ti	0.1

Spectrum-4

25-GFNS

Before immersion (Spectrum-7):

	At%
O	66.8
Si	13.3
Al	8.7
Mg	5.7
Na	3.4
Fe	1.1
Ca	0.7
Cr	0.1
Ti	0.1
Mn	0.0

Spectrum-7

After 1.5 years of immersion (Spectrum-11):

	At%
O	66.1
Si	15.2
Na	7.3
Al	5.7
Mg	2.5
Ca	1.2
Fe	1.0
S	0.7
Ti	0.1
K	0.1
Cr	0.0

Spectrum-11

Fig. 7.8 SEM images and EDX spectrum of geopolymer mortar immersed in sulphate solution

Table 7.3 Change of chemical composition (atomic %) of the aluminosilicate gel immersed in sodium sulphate solution

Sample ID	Immersion period	EDX point	Na	Mg	Al	Si	Avg. Na	Avg. Mg	Avg. Al	Avg. Si
0-GFNS	Before[*]	1	4.0	---	14.4	13.8	4.5	0.3	10.9	13.3
		2	3.9	0.4	8.9	12.4				
		3	5.6	0.5	9.3	13.6				
	After[**]	4	5.6	0.8	5.1	13.6	5.1	0.3	7.2	12.2
		5	3.8	---	10.8	11.4				
		6	5.8	---	5.8	11.5				
25-GFNS	Before[*]	7	3.4	5.7	8.7	13.3	4.6	3.1	6.5	14.3
		8	5.5	2	5.4	14.5				
		9	5	1.7	5.4	15.2				
	After[**]	10	7.8	1.6	5.1	13.2	6.9	2.9	5.3	14.8
		11	7.3	2.5	5.7	15.2				
		12	5.5	4.5	5.2	16.1				
50-GFNS	Before[*]	13	5.4	2	4.4	15.7	4.9	3.0	4.8	16.4
		14	5.7	2.4	6.5	14.3				
		15	3.5	4.7	3.5	19.2				
	After[**]	16	5.6	1.9	6.0	18.6	5.2	3.4	5.9	15.0
		17	5.8	1.9	8.9	11.9				
		18	4.2	6.5	2.9	14.6				
75-GFNS	Before[*]	19	4.6	6.5	3.3	15.4	3.5	8.0	3.4	17.9
		20	2.3	9.6	3.6	21.3				
		21	3.7	8	3.2	17.1				
	After[**]	22	6.7	5.8	2.9	13.5	6.4	4.7	4.4	13.3
		23	5.9	3.6	6.6	12.2				
		24	6.6	4.8	3.7	14.1				

[*]Before immersion
[**]After 1.5 years of immersion in sodium sulphate solution

Before exposure to sulphate solution, a homogenous and dense microstructure is observed for all the mixtures. However, FA-GFNS blended mortars provided more compact microstructures than the neat FA mortar. The dense microstructure and high strength (Fig. 7.2) of FA-GFNS geopolymer is related with the developed N-M-A-S-H gel as discussed in the earlier works [40, 47].

The SEM images suggested that there was no significant change of microstructure, especially no new distinct phase was observed after immersion in sodium sulphate solution. It is also seen that after immersion, the corresponding peaks of aluminosilicate gels were still present in the specimen, which indicates stability of the aluminosilicate gel after immersion in sodium sulphate solution. Sata et al. [54] reported similar results showing that geopolymer products were less susceptible to sulphate attack. However, the amount of some elements changed due to slight leaching after sodium sulphate exposure. The SEM image and EDX spectrum showed no existence of expansive gypsum or ettringite supporting the XRD results discussed in section 7.3.5.

From the EDX results, it can be noticed that for all the samples that Na content of most of the spectrum increased compared to the before exposure results. For instance, the average Na content of the 0-GFNS sample increased from 4.5% at before immersion to 5.1% after 1.5 years immersion in sodium sulphate solution. The corresponding values increased from 4.6% to 6.9%, 4.9% to 5.2% and 3.5% to 6.4% for 25-GFNS, 50-GFNS and 75-GFNS, respectively. This suggests the absorption of Na^+ ion by the geopolymer products, which were helpful to maintain good stability against sulphate solution. Thus, strength increased after exposure to sodium sulphate solution as discussed in section 7.3.2. It should be noted that Na_2SO_4 could be used as an activator in geopolymer [59]. Therefore, Na_2SO_4 could produce a beneficial condition by improving further alkali activation of the precursors [21]. However, a few micro pores were observed after immersion, which might have occurred due to the leaching of some elements as evidenced by EDX results (Table 7.3). It is also seen that the specimen 0-GFNS was more porous compared to the other specimens and thus, lower strength was observed in specimen 0-GFNS compared to the other GFNS blended geopolymer mortar specimens.

7.4 Summary

This study investigated the sodium sulphate resistance of FA-GFNS blended geopolymer mortar. The following conclusions are made from the study:

- The neat FA and FA-GFNS geopolymer mortar samples had no obvious visual sign of deterioration after 1.5 years immersion in Na_2SO_4 solution. The expansions of the mortar after exposure to Na_2SO_4 solution were well below the recommended limit of the expansion. The low calcium content of precursors and cross linked alumino-silicate gel made geopolymers stable against sulphate attack.

- After exposure to Na_2SO_4 solution for 1.5 years, the compressive strength of all geopolymer mortar samples increased compared to those before immersion. The highest strength was found in 75-GFNS samples after immersion in Na_2SO_4 solution for 1.5 years. The higher strength of FA-GFNS geopolymer is ascribed to the production of stable N-M-A-S-H gel than N-A-S-H gel of the neat FA geopolymer.

- The presence of alumionosilicate gel before and after exposure to Na_2SO_4 solution indicated good stability of the geopolymer mortar against sulphate attack. Moreover, the absorption of Na^+ ion by the geopolymer products were helpful to improve further alkali activation of the precursors. The SEM, EDX and XRD analysis also suggested the absence of expansive gypsum or ettringite in geopolymer mortar after immersion in Na_2SO_4 solution. All geopolymer samples had good stability against the sodium sulphate solution. However, the lower calcium content of GFNS made the FA-GFNS blended geopolymer less susceptible to damage in sulphate solution than the neat fly ash geopolymer.

7.5 References

[1] Bouaissi, L. yuan Li, M.M. Al Bakri Abdullah, Q.B. Bui, Mechanical properties and microstructure analysis of FA-GGBS-HMNS based geopolymer concrete, Constr. Build. Mater. 210 (2019) 198–209.

[2] N. Lemonis, P.E. Tsakiridis, N.S. Katsiotis, S. Antiohos, D. Papageorgiou, M.S. Katsiotis, M. Beazi-Katsioti, Hydration study of ternary blended cements

containing ferronickel slag and natural pozzolan, Constr. Build. Mater. 81 (2015) 130–139.

[3] P. Duxson, J.L. Provis, G.C. Lukey, J.S.J. van Deventer, The role of inorganic polymer technology in the development of "green concrete," Cem. Concr. Res. 37 (2007) 1590–1597.

[4] J.C. Kuri, M.N.N. Khan, P.K. Sarker, Compressive strength of geopolymer mortar using ground ferronickel slag and fly ash, 3rd Eur. Mediterr. Struct. Eng. Constr. Conf. 2020, Euro-Med-Sec 2020. (2020) 1–6. https://doi.org/10.14455/isec.res.2020.7(1).mat-05.

[5] W.J. Long, J. kai Peng, Y. cun Gu, J. lin Li, B. Dong, F. Xing, Y. Fang, Recycled use of municipal solid waste incinerator fly ash and ferronickel slag for eco-friendly mortar through geopolymer technology, J. Clean. Prod. 307 (2021) 127281.

[6] J.C. Kuri, P.K. Sarker, F.U.A. Shaikh, Sulphuric acid resistance of ground ferronickel slag blended fly ash geopolymer mortar, Constr. Build. Mater. 313 (2021) 125505.

[7] I. Maragkos, I.P. Giannopoulou, D. Panias, Synthesis of ferronickel slag-based geopolymers, Miner. Eng. 22 (2009) 196–203.

[8] B. Guirguis, M.H. Shehata, J. Duchesne, B. Fournier, B. Durand, P. Rivard, The application of a new oxidation mortar bar test to mixtures containing different cementing systems, Constr. Build. Mater. 173 (2018) 775–785.

[9] M. Santhanam, M.D. Cohen, J. Olek, Sulfate attack research, Cem. Concr. Res. 31 (2001) 845–851.

[10] T. Ikumi, S. Cavalaro, I. Segura, C. Goodier, S. Austin, Simplified Analytical Assessment of Damaged Induced by the External Sulphate Attack in Concrete Piles, in: D.A. Hordijk, M. Luković (Eds.), High Tech Concr. Where Technol. Eng. Meet, Springer International Publishing, Cham, 2018: pp. 2282–2289.

[11] J. Kwasny, T.A. Aiken, M.N. Soutsos, J.A. McIntosh, D.J. Cleland, Sulfate and acid resistance of lithomarge-based geopolymer mortars, Constr. Build. Mater. 166 (2018) 537–553.

[12] R. Tixier, B. Mobasher, Modeling of Damage in Cement-Based Materials Subjected to External Sulfate Attack. II: Comparison with Experiments, J. Mater. Civ. Eng. 15 (2003) 314–322.

[13] T. Bakharev, J.G. Sanjayan, Y.B. Cheng, Sulfate attack on alkali-activated slag concrete, Cem. Concr. Res. 32 (2002) 211–216.

[14] A.M. Rashad, Y. Bai, P.A.M. Basheer, N.B. Milestone, N.C. Collier, Hydration and properties of sodium sulfate activated slag, Cem. Concr. Compos. 37 (2013) 20–29.

[15] M.A.R. Bhutta, W.M. Hussin, M. Azreen, M.M. Tahir, Sulphate Resistance of Geopolymer Concrete Prepared from Blended Waste Fuel Ash, J. Mater. Civ. Eng. 26 (2014) 04014080.

[16] C. Villa, E.T. Pecina, R. Torres, L. Gómez, Geopolymer synthesis using alkaline activation of natural zeolite, Constr. Build. Mater. 24 (2010) 2084–2090.

[17] M.S.H. Khan, O. Kayali, U. Troitzsch, Effect of NaOH activation on sulphate resistance of GGBFS and binary blend pastes, Cem. Concr. Compos. 81 (2017) 49–58.

[18] R. Gopalakrishnan, K. Chinnaraju, Durability of ambient cured alumina silicate concrete based on slag/fly ash blends against sulfate environment, Constr. Build. Mater. 204 (2019) 70–83.

[19] T. Bakharev, Durability of geopolymer materials in sodium and magnesium sulfate solutions, Cem. Concr. Res. 35 (2005) 1233–1246.

[20] H.E. Elyamany, A.E.M. Abd Elmoaty, A.M. Elshaboury, Magnesium sulfate resistance of geopolymer mortar, Constr. Build. Mater. 184 (2018) 111–127.

[21] N.A.M. Beltrame, C. Angulski da Luz, M. Perardt, R.D. Hooton, Alkali activated cement made from blast furnace slag generated by charcoal: Resistance to attack by sodium and magnesium sulfates, Constr. Build. Mater. 238 (2020) 117710.

[22] I. Ismail, S.A. Bernal, J.L. Provis, S. Hamdan, J.S.J. Van Deventer, Microstructural changes in alkali activated fly ash/slag geopolymers with sulfate exposure, Mater. Struct. Constr. 46 (2013) 361–373.

[23] M.B. Karakoç, I. Türkmen, M.M. Maraş, F. Kantarci, R. Demirboła, Sulfate resistance of ferrochrome slag based geopolymer concrete, Ceram. Int. 42 (2016) 1254–1260.

[24] H. Ye, Z. Chen, L. Huang, Mechanism of sulfate attack on alkali-activated slag: The role of activator composition, Cem. Concr. Res. 125 (2019) 105868.

[25] J. Aliques-Granero, M.T. Tognonvi, A. Tagnit-Hamou, Durability study of AAMs: Sulfate attack resistance, Constr. Build. Mater. 229 (2019) 117100.

[26] Y. cun Gu, J.L. Li, J.K. Peng, F. Xing, W.J. Long, K.H. Khayat, Immobilization of hazardous ferronickel slag treated using ternary limestone calcined clay cement, Constr. Build. Mater. 250 (2020) 118837.

[27] X. Liu, T. Li, W. Tian, Y. Wang, Y. Chen, Study on the durability of concrete with FNS fine aggregate, J. Hazard. Mater. 381 (2020) 120936.

[28] Q.D. Nguyen, M.S.H. Khan, T. Xu, A. Castel, Mitigating the risk of early age cracking in fly ash blended cement-based concrete using ferronickel slag sand, J. Adv. Concr. Technol. 17 (2019) 295–308.

[29] A.K. Saha, P.K. Sarker, Expansion due to alkali-silica reaction of ferronickel slag fine aggregate in OPC and blended cement mortars, Constr. Build. Mater. 123 (2016) 135–142.

[30] B. Xi, R. Li, X. Zhao, Q. Dang, D. Zhang, W. Tan, Constraints and opportunities for the recycling of growing ferronickel slag in China, Resour. Conserv. Recycl. 139 (2018) 15–16.

[31] J. Sun, J. Feng, Z. Chen, Effect of ferronickel slag as fine aggregate on properties of concrete, Constr. Build. Mater. 206 (2019) 201–209.

[32] A.K. Saha, P.K. Sarker, Sustainable use of ferronickel slag fine aggregate and fly ash in structural concrete: Mechanical properties and leaching study, J. Clean. Prod. 162 (2017) 438–448.

[33] Y.C. Choi, S. Choi, Alkali-silica reactivity of cementitious materials using ferro-nickel slag fine aggregates produced in different cooling conditions, Constr. Build. Mater. 99 (2015) 279–287.

[34] A. Qi, X. Liu, Z. Wang, Z. Chen, Mechanical properties of the concrete containing ferronickel slag and blast furnace slag powder, Constr. Build. Mater. 231 (2020).

[35] H. Kim, C.H. Lee, K.Y. Ann, Feasibility of ferronickel slag powder for cementitious binder in concrete mix, Constr. Build. Mater. 207 (2019) 693–705.

[36] Y. Chen, T. Ji, Z. Yang, W. Zhan, Y. Zhang, Sustainable use of ferronickel slag in cementitious composites and the effect on chloride penetration resistance, Constr. Build. Mater. 240 (2020) 117969.

[37] M.A. Rahman, P.K. Sarker, F.U.A. Shaikh, A.K. Saha, Soundness and compressive strength of Portland cement blended with ground granulated ferronickel slag, Constr. Build. Mater. 140 (2017) 194–202.

[38] K. Komnitsas, D. Zaharaki, V. Perdikatsis, Geopolymerisation of low calcium ferronickel slags, J. Mater. Sci. 42 (2007) 3073–3082.

[39] K. Sakkas, P. Nomikos, A. Sofianos, D. Panias, Utilisation of FeNi-Slag for the production of inorganic polymeric materials for construction or for passive fire protection, Waste and Biomass Valorization. 5 (2014) 403–410.

[40] T. Yang, X. Yao, Z. Zhang, Geopolymer prepared with high-magnesium nickel slag: Characterization of properties and microstructure, Constr. Build. Mater. 59 (2014) 188–194.

[41] N. You, B. Li, R. Cao, J. Shi, C. Chen, Y. Zhang, The influence of steel slag and ferronickel slag on the properties of alkali-activated slag mortar, Constr. Build. Mater. 227 (2019) 116614.

[42] J.C. Kuri, S. Majhi, P.K. Sarker, A. Mukherjee, Microstructural and non-destructive investigation of the effect of high temperature exposure on ground ferronickel slag blended fly ash geopolymer mortars, J. Build. Eng. 43 (2021) 103099.

[43] B. Li, B. Huo, R. Cao, S. Wang, Y. Zhang, Sulfate resistance of steam cured ferronickel slag blended cement mortar, Cem. Concr. Compos. 96 (2019) 204–211.

[44] A.K. Saha, P.K. Sarker, Effect of sulphate exposure on mortar consisting of ferronickel slag aggregate and supplementary cementitious materials, J. Build. Eng. 28 (2020) 101012.

[45] Q.D. Nguyen, A. Castel, T. Kim, M.S.H. Khan, Performance of fly ash concrete with ferronickel slag fine aggregate against alkali-silica reaction and chloride diffusion, Cem. Concr. Res. 139 (2021) 106265.

[46] J.C. Kuri, M.N.N. Khan, P.K. Sarker, Workability, strength and microstructural properties of ground ferronickel slag blended fly ash geopolymer mortar, J. Sustain. Cem. Mater. 0 (2020) 1–18. https://doi.org/10.1080/21650373.2020.1823905.

[47] J.C. Kuri, M.N.N. Khan, P.K. Sarker, Fresh and hardened properties of geopolymer binder using ground high magnesium ferronickel slag with fly ash, Constr. Build. Mater. 272 (2021) 121877.

[48] P. Nath, P.K. Sarker, Use of OPC to improve setting and early strength properties of low calcium fly ash geopolymer concrete cured at room temperature, Cem. Concr. Compos. 55 (2015) 205–214.

[49] Standards Australia, AS1012.9:2014 Methods of testing concrete Method 9: Compressive strength tests — Concrete , mortar and grout specimens, Stand. Aust.

[50] ASTM C157, 2008. ASTM C157-08, Standard test method for length change of hardened hydraulic-cement mortar and concrete, ASTM International, West Conshohocken, PA.

[51] M.A.M. Ariffin, M.A.R. Bhutta, M.W. Hussin, M. Mohd Tahir, N. Aziah, Sulfuric acid resistance of blended ash geopolymer concrete, Constr. Build. Mater. 43 (2013) 80–86.

[52] G.C. Long-term, S.E. Wallah, B. V Rangan, LOW-CALCIUM FLY ASH-BASED By Curtin University of Technology, Concrete. (2006).

[53] V. Sata, A. Sathonsaowaphak, P. Chindaprasirt, Resistance of lignite bottom ash geopolymer mortar to sulfate and sulfuric acid attack, Cem. Concr. Compos. 34 (2012) 700–708.

[54] A. Fernandez-Jimenez, I. García-Lodeiro, A. Palomo, Durability of alkali-activated fly ash cementitious materials, J. Mater. Sci. 42 (2007) 3055–3065.

[55] ACI, 2008. ACI 201.2R-08, Guide to Durable Concrete, American Concrete Institute.

[56] H.M. Rietveld, A profile refinement method for nuclear and magnetic structures, J. Appl. Crystallogr. 2 (1969) 65–71.

[57] R.J. Hill, C.J. Howard, Quantitative phase analysis from neutron powder diffraction data using the Rietveld method, J. Appl. Crystallogr. 20 (1987) 467–474.

[58] A.A. Coelho, TOPAS and TOPAS-Academic: An optimization program integrating computer algebra and crystallographic objects written in C++: An, J. Appl. Crystallogr. 51 (2018) 210–218.

[59] A.M. Rashad, Y. Bai, P.A.M. Basheer, N.C. Collier, N.B. Milestone, Chemical and mechanical stability of sodium sulfate activated slag after exposure to elevated temperature, Cem. Concr. Res. 42 (2012) 333–343.

CHAPTER 8: CONCLUSIONS AND RECOMMENDATIONS

8.1 Overview

The focus of this study was to evaluate the effect of using ground ferronickel slag (GFNS) as a source material in geopolymer. The GFNS was used as 25, 50, 75 and 100% replacement of fly ash to produce geopolymer paste and mortar. The GFNS used in this study was produced by the smelting of garnierite ore found in New Caledonia which constitutes a substantial part of the world's FNS accumulation. A mixture of NaOH and Na_2SiO_3 liquids was used as the alkali activator solution (AAS). The amount of the alkali activator solution was 40% or 45% of the total binder and the ratio of sodium silicate to the sodium hydroxide solutions varied from 1.5 to 2.5. The effects of GFNS as a precursor on fresh and mechanical properties and durability performance of geopolymer paste and mortar were investigated. Microstructural investigation, such as SEM, EDS, XRD and TGA were applied in different stages of this study. The main outcomes of this research and some recommendations for future studies are presented in this chapter.

8.2 Conclusions

The following conclusions are drawn based on the obtained results:

Fresh and mechanical properties of geopolymer paste and mortar using GFNS as a precursor

- Setting time of geopolymer paste decreased with the increase of GFNS as a partial replacement of fly ash. Initial setting time of paste with SS/SH ratio of 2.0 decreased from 410 minutes for without GFNS to 188 minutes for using 100% GFNS. The decrease of setting time by the increase of GFNS is attributed to the increase of SiO_2/Al_2O_3 and MgO/Al_2O_3 ratios, which increased the geopolymerization reaction. Setting times of the geopolymer pastes using an alkaline solution with SS/SH ratio of 1.5 were less than those with SS/SH ratio of 2.0. The decrease of setting time by the decrease of SS/SH ratio is ascribed to the increase of Na_2O/Al_2O_3 and Na_2O/SiO_2 ratios, which accelerated the polycondensation process.

- The use of GFNS as replacement of fly ash reduced the workability geopolymer paste and mortar. Mixtures having a higher amount of GFNS

showed higher flow time and lower flow value. The flow of paste using SS/SH ratio of 2.0 decreased from 140% for using 100% fly ash to 110% for using 100% GFNS. The flow of the mortar with 45% alkaline solution reduced from 110% for without GFNS to 73% for using 75% GFNS. The decrease of flow due to the rise of GFNS is attributed to the angular GFNS particles than the spherical shape of fly ash. The flow of the geopolymer pastes using a SS/SH ratio of 1.5 were higher than those with ratios of 2.0 and 2.5. Viscosity of Na_2SiO_3 solution is higher than that of NaOH solution. Therefore, a higher proportion of Na_2SiO_3 solution reduced the mobility of particles and hence reduced the flow of geopolymer paste.

- As the magnesium was incorporated in the reaction product sodium magnesium alumino-silicate hydrate (N-M-A-S-H) gel, high magnesium content of GFNS has no adverse effect on the expansion of geopolymer. The Le-Chatelier expansions of the geopolymer pastes were well below 5%, which is the recommended limit of the expansion of determined by this test. Moreover, no expansive brucite was found in the XRD analysis.

- The compressive strength of the geopolymer pastes using SS/SH ratio of 2.0 were higher than those with SS/SH ratio of 1.5 and 2.5. At the early age of 7 days, compressive strength of the ambient-cured geopolymer paste decreased with the increase of GFNS. However, at 28 days and thereafter, strength significantly increased with the increase of GFNS content up to 75%. The 28-day, 56-day and 90-day compressive strengths of ambient cured geopolymer paste using 75% GFNS were 45 MPa, 56 MPa and 64 MPa, respectively. On the other hand, for the same GFNS content, compressive strength of 65 MPa was achieved by accelerated heat curing at 60 °C for 1 day. For using 75% GFNS, the 28-day and 90-day compressive strengths of mortar with 45% alkaline solution were 66 MPa and 84 MPa, respectively.

- The principal reaction product of fly ash-GFNS geopolymer was N-M-A-S-H gel, which provided denser microstructure and thus developed higher strength in fly ash-GFNS geopolymer than neat fly ash geopolymer.

- The inclusion of GFNS was found beneficial to decrease the sorptivilty and porosity of the geopolymer mortar.

Higher thermal resistance of GFNS blended fly ash geopolymer mortars

- Thermal resistance of fly ash-GFNS geopolymer mortar was higher compared to neat fly ash geopolymer mortar. Geopolymer mortar having 50% GFNS showed maximum residual compressive strength throughout the applied elevated temperature exposure up to 1000 °C.

- The cracks and voids of the geopolymer mortar rose with the rise of temperature. However, the N-M-A-S-H gel produced in fly ash-GFNS geopolymer provided a higher thermal stability than neat fly ash geopolymer. Thus, at high temperature, fly ash-GFNS geopolymer showed less porous structure compared to neat fly ash geopolymer.

- The crystalline phases of the geopolymer did not change significantly until 600 °C exposures. The number of crystalline peaks increased and amorphousity decreased significantly at 1000 °C exposure. At 1000 °C, a new phase of albite was observed in neat fly ash geopolymer due to the decomposition or transformation of N-A-S-H gel. On the other hand, albite, nepheline and omphacite phases were noticed in fly ash-GFNS geopolymer due to the decomposition or transformation of N-M-A-S-H gel at 1000 °C. The amorphous contents of GFNS-50 decreased from 79.6% for ambient temperature to 75.5, 73.7, and 53.1% for 200, 600 and 1000 °C exposures, respectively.

- Non-destructive ultrasonic test results revealed that the lower frequency component dominates across all temperature exposures in the neat fly ash (without GFNS) geopolymer mortar, which indicates the presence of more voids and cracks than other samples. On the other hand geopolymer mortar with 50% GFNS had the least amount of pores as indicated by the dominance of higher frequency components in the spectra.

Higher sulphuric acid resistance of GFNS blended fly ash geopolymer mortars

- The losses of compressive strength and mass of fly ash-GFNS blended geopolymer mortars were lower than those of the neat fly ash geopolymer mortar after immersion in 3% sulphuric acid solution. The lowest strength loss was found in the samples containing 75% GFNS throughout the exposure periods. The strength losses after 12 months of sulphuric acid exposure were

171

43.67, 31.05, 24.15 and 22.54% in the samples containing of 0, 25, 50 and 75% GFNS, respectively.

- Incorporation of GFNS made a dense structure by developing N-M-A-S-H gel and the denseness increased with the rise of GFNS content. Thus, lower ingress of sulphuric acid occurred in the sample containing 75% GFNS due to the lower porosity. Consequently, the lowest strength loss was found in the mortar with 75% GFNS.

- The visual observations and micrographs showed that the deterioration of neat fly ash geopolymer mortar was higher than that of the fly ash-GFNS geopolymer mortar specimens. The high calcium content of fly ash reacted with sulfuric acid and formed a higher amount of expansive gypsum in the neat fly ash geopolymer than in the fly ash-GFNS geopolymers. The QXRD results confirmed that the gypsum contents were 6.9, 3.4, 0.4 and 0.6% for the use of 0, 25, 50 and 75% GFNS, respectively. The deposition of higher amount of gypsum by acid in the neat fly ash geopolymer induced higher stresses that led to increased cracks. Consequently, more deterioration occurred in the neat fly ash geopolymer than fly ash-GFNS geopolymers.

Higher sulphate resistance of GFNS blended fly ash geopolymer mortars

- The neat FA and FA-GFNS geopolymer mortar samples had no significant visual sign of deterioration after 18 months immersion in 3% Na_2SO_4 solution. The expansions of the geopolymer mortars after immersion in Na_2SO_4 solution were well below the recommended limit of the expansion. The low calcium content of precursors and cross linked alumino-silicate gel made geopolymers stable against sulphate attack.

- After 1.5 years of immersion in Na_2SO_4 solution, the compressive strength of all geopolymer mortar increased compared to the before immersion samples. The highest strength was found in the sample containing 75% GFNS after 1.5 years of immersion in Na_2SO_4 solution. The higher strength of FA-GFNS geopolymer is ascribed to the production of stable N-M-A-S-H gel compared to N-A-S-H gel of the neat FA geopolymer.

- The presence of alumionosilicate gel before and after immersion in Na_2SO_4 solution indicated good stability of the geopolymer mortar against sulphate attack. Moreover, the absorption of Na^+ ion by the geopolymer products were

helpful to improve the further alkali activation of the precursors. SEM, EDX and XRD investigation also suggested the absence of expansive gypsum or ettringite in geopolymer mortar after immersion in Na_2SO_4 solution. All geopolymer samples had good stability against the sodium sulphate solution. However, the lower calcium content of GFNS made the fly ash-GFNS blended geopolymer less susceptible to damage in sulphate solution than neat fly ash geopolymer.

8.3 Recommendations for future study

- In this research, properties of GFNS-fly ash geopolymer were investigated where, fly ash was replaced by different proportions of GFNS. Further research can be conducted for GFNS-GGBFS and GFNS-metakaolin based geopolymers, where GGBFS and metakaolin will be partially replaced by GFNS.

- This study investigated the fresh, mechanical and durability performance of geopolymer containing GFNS as a precursor. The dynamic properties of this geopolymer can be investigated in future.

- Other durability tests such as carbonation, chloride attack, and half potential test could be studied in the future.

- The performance of composite geopolymer made with different fibers can be investigated.

- In this study, granulated FNS was transformed to ground FNS (GFNS) and used as a binder in alkali activated systems. Further studies can be conducted considering granulated FNS as fine aggregate in geopolymer mortar and concrete.

BIBLIOGRAPHY DISCLAIMER

Every reasonable effort has been made to acknowledge the owners of copyright material. I would be pleased to hear from any copyright owner who has been omitted or incorrectly acknowledged.

APPENDIX A: Images of experiments

Fig. A.1 Preparation of geopolymer pastes and mortars in Hobart mixer

Fig. A.2 Setting time test of geopolymer paste

Fig. A.3 Flow time test of geopolymer paste

Fig. A.4 Flow table test

Fig. A.5 Le-Chatelier Soundness test

Fig. A.6 Compressive strength test

Fig. A.7 Sorptivity test

Fig. A.8 Elevated temperature exposure test
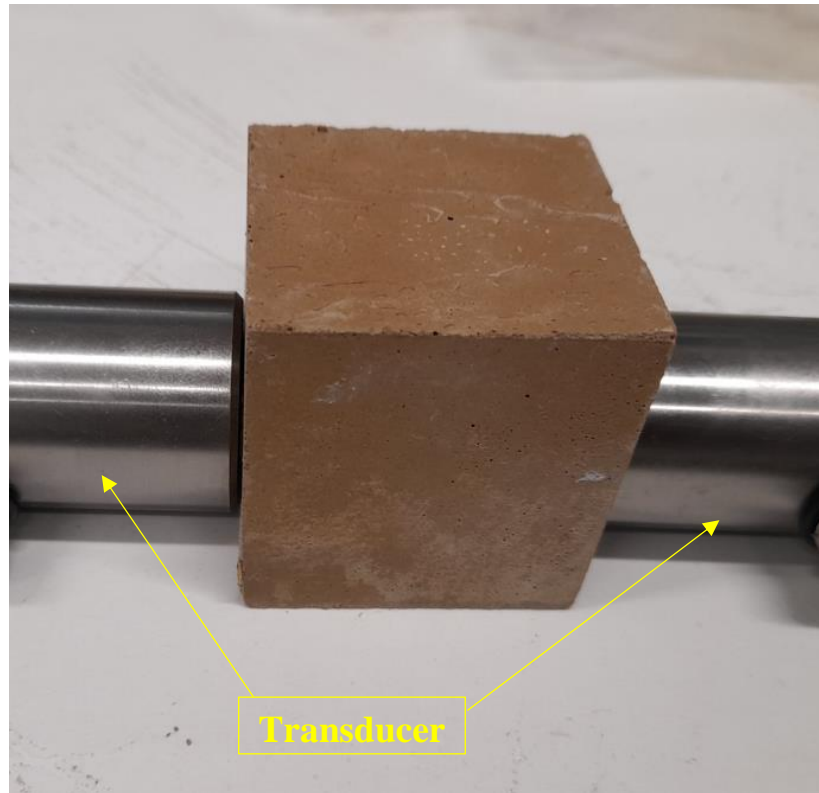
Fig. A.9 Placement of sample between transducers for ultrasonic tests

(a) Placing hardened geopolymer paste sample in the ring mill container

(b) Ring mill

(c) Powder sample after grinding in ring mill
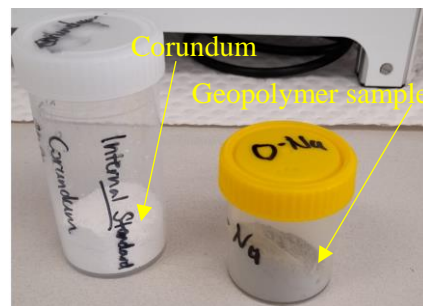
(d) Corundum (Internal standard) and geopolymer powder sample

(e) Corundum and sample powder in micronizing mill container

(f) McCrone micronizing mill

(g) Slurry specimen after grinding in micronizing mill
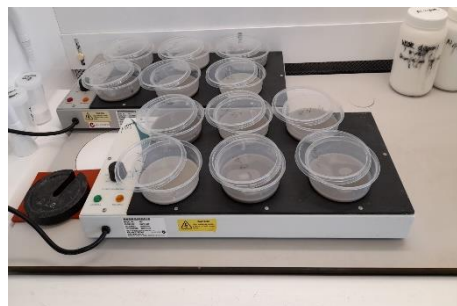
(h) Drying of slurry specimen

(i) Grinding of dried specimen

(j) Packing in specimen holder

(k) Placing of specimen holder for XRD measurement

(l) XRD measurement in D8 Advance powder diffractometer

Fig. A.10 QXRD sample preparation

Fig. A.11 Specimens for SEM and EDS analysis

Article 1

J. C. Kuri, M. N. N. Khan and P. K. Sarker. Fresh and hardened properties of geopolymer binder using ground high magnesium ferronickel slag with fly ash. Construction and Building Materials, 272 (2021) 121877.
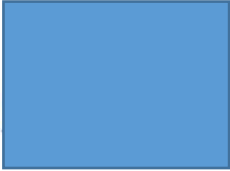
Authors and full affiliations:

J.C. Kuri, PhD student, School of Civil and Mechanical Engineering, Curtin University, WA.

M.N.N. Khan, Adjunct Research Associate, School of Civil and Mechanical Engineering, Curtin University, WA.

P.K. Sarker, Associate Professor, School of Civil and Mechanical Engineering, Curtin University, WA.

Co-author attribution: **M.N.N. Khan** and **P.K. Sarker**

Name of Co-author	Literature review	Experimental design/idea	Data collection	Data analysis	Discussion	Paper writing
M.N.N. Khan			√		√	
I acknowledge that these represent my contribution to the above research output. (Signature)						
P.K. Sarker		√		√	√	√
I acknowledge that these represent my contribution to the above research output. (Signature)						

Authors and full affiliations:

J.C. Kuri, PhD student, School of Civil and Mechanical Engineering, Curtin University, WA.

M.N.N. Khan, Adjunct Research Associate, School of Civil and Mechanical Engineering, Curtin University, WA.

P.K. Sarker, Associate Professor, School of Civil and Mechanical Engineering, Curtin University, WA.

Co-author attribution: **M.N.N. Khan** and **P.K. Sarker**

Name of Co-author	Literature review	Experimental design/idea	Data collection	Data analysis	Discussion	Paper writing
M.N.N. Khan			√		√	
I acknowledge that these represent my contribution to the above research output. (Signature)						
P.K. Sarker		√		√	√	√
I acknowledge that these represent my contribution to the above research output. (Signature)						

Article 3

J. C. Kuri, S. Majhi, P. K. Sarker and A. Mukherjee. Microstructural and non-destructive investigation of the effect of high temperature exposure on ground ferronickel slag blended fly ash geopolymer mortars. Journal of Building Engineering, 43 (2021) 103099.

Authors and full affiliations:

J.C. Kuri, PhD student, School of Civil and Mechanical Engineering, Curtin University, WA.

S. Majhi, Research Associate, School of Civil and Mechanical Engineering, Curtin University, WA.

P.K. Sarker, Associate Professor, School of Civil and Mechanical Engineering, Curtin University, WA.

A. Mukherjee, Professor, School of Civil and Mechanical Engineering, Curtin University, WA.

Co-author attribution: **S. Majhi, P.K. Sarker** and **A. Mukherjee**

Name of Co-author	Literature review	Experimental design/idea	Data collection	Data analysis	Discussion	Paper writing
S. Majhi			√	√		√
I acknowledge that these represent my contribution to the above research output. (Signature)						
P. K. Sarker		√		√	√	√
I acknowledge that these represent my contribution to the above research output. (Signature)						
A. Mukherjee					√	√
I acknowledge that these represent my contribution to the above research output. (Signature)						

Article 4

J. C. Kuri, P. K. Sarker and F. U. A. Shaikh. Sulphuric acid resistance of ground ferronickel slag blended fly ash geopolymer mortar. Construction and Building Materials, 313 (2021) 125505.

Authors and full affiliations:

J.C. Kuri, PhD student, School of Civil and Mechanical Engineering, Curtin University, WA.

P.K. Sarker, Associate Professor, School of Civil and Mechanical Engineering, Curtin University, WA.

F.U.A. Shaikh, Associate Professor, School of Civil and Mechanical Engineering, Curtin University, WA.

Co-author attribution: **P.K. Sarker** and **F.U.A. Shaikh**

Name of Co-author	Literature review	Experimental design/idea	Data collection	Data analysis	Discussion	Paper writing
P. K. Sarker		√		√	√	√
I acknowledge that these represent my contribution to the above research output. (Signature)						
F. U. A. Shaikh					√	√
I acknowledge that these represent my contribution to the above research output. (Signature)						

Article 5

J. C. Kuri, M. Nuruzzaman and P. K. Sarker. Sulphate resistance of geopolymer mortar produced using ground ferronickel slag with fly ash. Structural Concrete, 2022 (Under Review).

Authors and full affiliations:

J.C. Kuri, PhD student, School of Civil and Mechanical Engineering, Curtin University, WA.

M. Nuruzzaman, PhD student, School of Civil and Mechanical Engineering, Curtin University, WA.

P.K. Sarker, Associate Professor, School of Civil and Mechanical Engineering, Curtin University, WA.

Co-author attribution: **M. Nuruzzaman** and **P.K. Sarker**

Name of Co-author	Literature review	Experimental design/idea	Data collection	Data analysis	Discussion	Paper writing
M. Nuruzzaman					√	
I acknowledge that these represent my contribution to the above research output. (Signature)						
P.K. Sarker		√		√	√	√
I acknowledge that these represent my contribution to the above research output. (Signature)						

APPENDIX C: Copyright permission

Article 1

J. C. Kuri, M. N. N. Khan and P. K. Sarker. Fresh and hardened properties of geopolymer binder using ground high magnesium ferronickel slag with fly ash. Construction and Building Materials, 272 (2021) 121877.

Article 2

J. C. Kuri, M. N. N. Khan and P. K. Sarker. Workability, strength and microstructural properties of ground ferronickel slag blended fly ash geopolymer mortar. Journal of Sustainable Cement-Based Materials, 2020. https://doi.org/10.1080/21650373.2020.1823905.

Article 3

J. C. Kuri, S. Majhi, P. K. Sarker and A. Mukherjee. Microstructural and non-destructive investigation of the effect of high temperature exposure on ground ferronickel slag blended fly ash geopolymer mortars. Journal of Building Engineering, 43 (2021) 103099.

Article 4

J. C. Kuri, P. K. Sarker and F. U. A. Shaikh. Sulphuric acid resistance of ground ferronickel slag blended fly ash geopolymer mortar. Construction and Building Materials, 313 (2021) 125505.

Article 5

J. C. Kuri, M. Nuruzzaman and P. K. Sarker. Sulphate resistance of geopolymer mortar produced using ground ferronickel slag with fly ash. Structural Concrete, 2022 (Under Review).

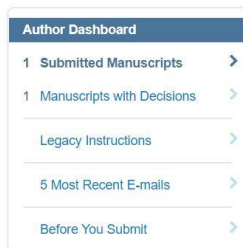**Author Dashboard**

1 Submitted Manuscripts >
1 Manuscripts with Decisions >
Legacy Instructions >
5 Most Recent E-mails >
Before You Submit >

Submitted Manuscripts

STATUS	ID	TITLE	CREATED	SUBMITTED
Under Review	suco.202200534 (REX-PROD-1-B5344E97-3FBE-4325-859E-1792B4893299-61123F5C-C330-400C-A413-47723F2AD35A-65007)	Sulphate resistance of geopolymer mortar produced using ground ferronickel slag with fly ash View Submission	29-May-2022	29-May-2022